1-1-2012

Exploring conformational variability of an rna domain in the ribosome: from structure and function to potential antibiotic targeting

Yogo Sakakibara
Wayne State University,

EXPLORING CONFORMATIONAL VARIABILITY OF AN RNA DOMAIN IN THE RIBOSOME: FROM STRUCTURE AND FUNCTION TO POTENTIAL ANTIBIOTIC TARGETING

by

YOGO SAKAKIBARA

DISSERTATION

Submitted to the Graduate School

of Wayne State University,

Detroit, Michigan

in partial fulfillment of the requirements

for the degree of

DOCTOR OF PHILOSOPHY

2012

MAJOR: CHEMISTRY (BIOCHEMISTRY)

Approved by:

_____

Advisor Date

_____

_____

_____

DEDICATION

To my father Dr. Toshiyuki Sakakibara, my mother Keiko Sakakibara, and in memory of my grandmother Fumie Okada, for their endless support.

ACKNOWLEDGEMENTS

I would like to thank my supervisor Dr. Christine S. Chow for her thorough support throughout my graduate career in Wayne State University. I would not have had even an opportunity to get my Ph.D. study done without her mentorship. Her attention and insightful suggestions to science always helped me to elicit my best work and to obtain proficient skills and knowledge as an independent researcher. She always guided me in the right direction as a scientist. Furthermore, she has been always unbelievably patient with my unskilled communication in English and tried to understand me and give thoughtful advices.

I would like to thank my committee members, Dr. Tamara L. Hendrickson, Dr. Stephanie L. Brock, and Dr. Philip R. Cunningham for their time and critical and valuable suggestions.

I would like to thank Dr. Hiroshi Sugiyama in Kyoto University, Japan, for his dedicated support even after I graduated from his laboratory. Without his teaching and education for being scientist during my master studies under his guidance, I would not have done these Ph.D. studies as the same level as I have done.

I would like to thank Dr. Kuniaki Tatsuta in Waseda University, Japan, for his mentorship. He taught me what is science and how interesting science is. I would not have been in the science field and I would not have known how exciting doing science is without obtaining chance to work under his guidance as an undergraduate researcher in his lab.

I would like to thank my co-workers in Dr. Chow's lab, particularly Sanjaya C. Abeysirigunawardena and Anne-Cécile E. Duc. Also, I would like to thank Mirjana Dimovska and Adhnan Mohamed for their patience to work with me under tough situations.

Finally, I would like to thank my family and friends in Japan and the United States for their support throughout my Ph.D. studies.

This work was supported by a grant from the National Institutes of Health.

TABLE OF CONTENTS

LIST OF TABLES

LIST OF FIGURES

Chapter 1
Introduction to the ribosome and the role of helix 69

1.1.The ribosome

According to the central dogma, genetic information coded in DNA is transcribed into messenger RNA (mRNA), which is in turn converted into protein information by a process called translation [1]. In all living organisms, translation of mRNA into protein is performed by the ribosome, which is a ribonucleoprotein complex (RNP). The bacterial ribosome is composed of two main subunits (Figure 1.1) [2], and has an overall mass of about 25 MDa and size around 20 nm in diameter [3, 4]. The large subunit (50S subunit) consists of 2904 nucleotides of 23S ribosomal RNA (rRNA), 120 nucleotides of 5S rRNA, and 34 large ribosomal proteins, and the small subunit (30S subunit) is composed of 1542 nucleotides of 16S rRNA and 21 small ribosomal proteins [5]. Hereafter, a lowercase letter is used to refer to rRNA domains in the small subunit (*e.g.*, h44 for helix 44 of the 30S subunit) and a capital letter is used for rRNA domains in the large subunit (*e.g.*, H69 for helix 69 of the 50S subunit).

The entire ribosome translation process involves four important steps: mRNA decoding, peptidyl transfer, translocation, and termination (Figure 1.2). Each subunit plays an important and distinct role in ribosome translation. A major function of the small subunit is decoding the mRNA information; whereas, the main function of the large subunit is to catalyze peptide-bond formation between the amino acid on the aminoacyl transfer RNA (aa-tRNA) in the aminoacyl site (A site) and the nascent polypeptide chain in the peptidyl site (P site). In the following section (1.2), the mechanism of bacterial ribosome translation will be discussed in detail.

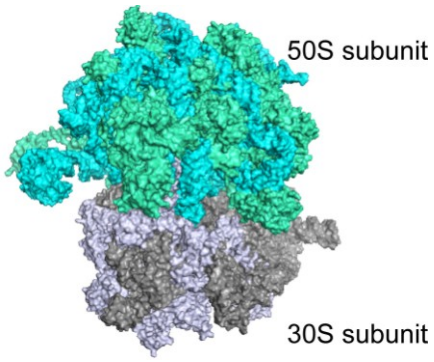

Figure 1.1. A crystal structure of the *E. coli* 70S ribosome is shown (PDB ID: 3R8O+3R8T); the color codes are as follows: cyan, 23S rRNA; green, large ribosomal proteins; gray, 16S rRNA; blue white, small ribosomal proteins.

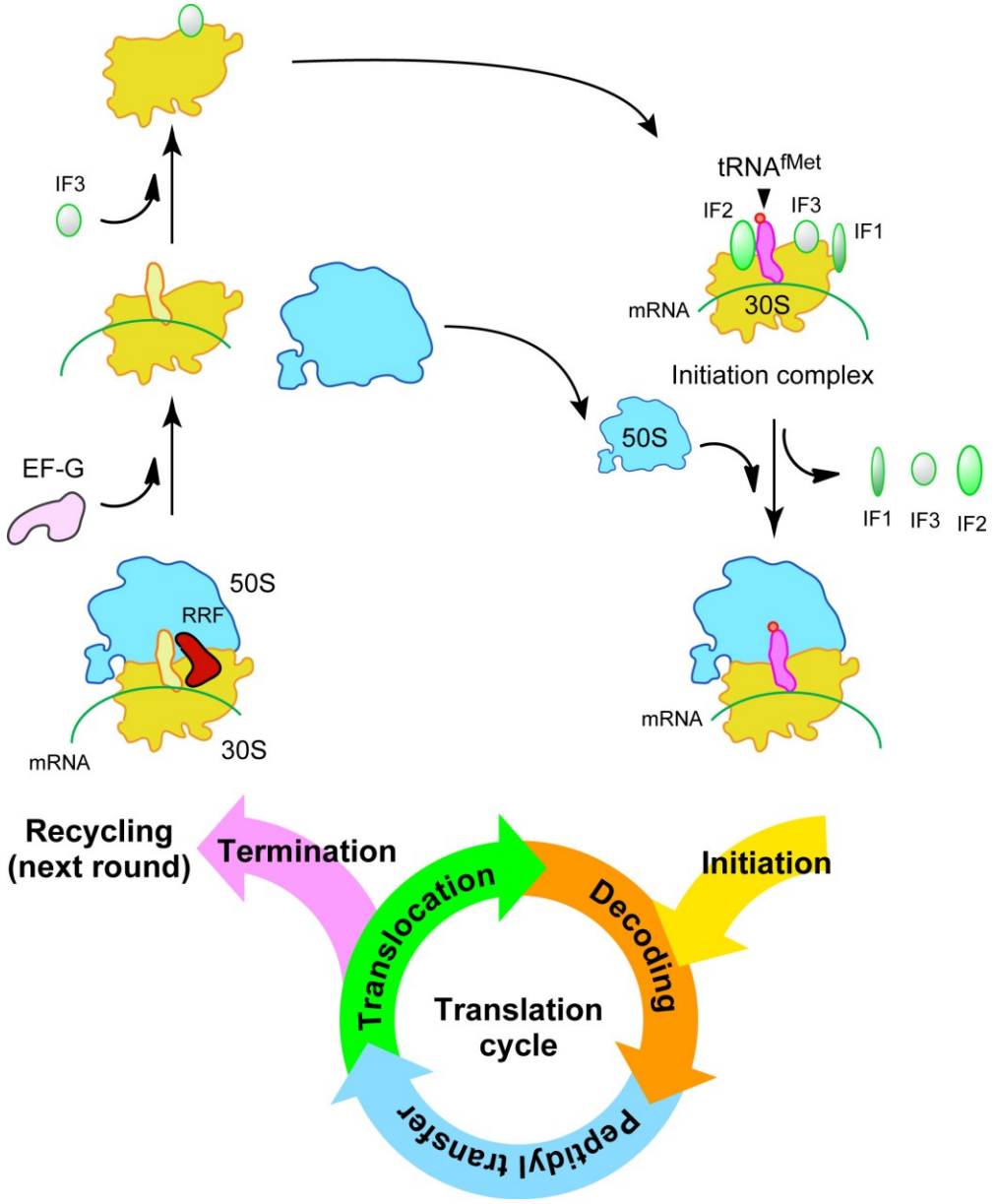

Figure 1.2. A schematic illustrations of the bacterial translation cycle and the initiation and recycling process is shown. In initiation, the 30S subunit forms an initiation complex with mRNA, initiator tRNA ($tRNA^{fMet}$), and initiation factors (IF1, 2, and 3). After the dissociation of IFs and subsequent association of the 50S complex, the ribosome is ready for protein synthesis. In recycling, the ribosome recycling factor (RRF), in combination with the elongation factor (EF-G), facilitates the dissociation of the 70S ribosome into each subunit. See also the following sections for the other processes (decoding, peptidyl transfer, translocation, and termination).

1.2. Cycles of bacterial ribosome translation

1.2.1. Decoding

Once ribosome subunits are loaded onto a target mRNA (ribosome-mRNA complex), translation is initiated by addition of the next aa-tRNA to the A site of the ribosome. The aa-tRNA is delivered in a ternary complex with elongation factor Tu (EF-Tu), which is a G-protein family member, and GTP (Figure 1.3.a) [6, 7]. The initial binding of the aa-tRNA ternary complex to the ribosome (A/T state) involves interactions of the L7/L12 stalk of the 50S subunit with EF-Tu, and Watson-Crick base pairing between the mRNA codon and aa-tRNA anticodon. The mRNA and cognate aa-tRNA interaction induces a conformational change of the universally conserved residues A1492, A1493, and G530 in the 30S subunit in order to stabilize the codon-anticodon complex in the decoding center [8, 9]. When a stable codon-anticodon complex is formed, the 30S subunit undergoes closure of the head and shoulder domains [10] and the aa-tRNA undergoes conformational changes around the anticodon stem region in order to maintain its interactions in the ternary complex with the mRNA codon and EF-Tu (Figure 1.3.b and c) [11-14]. Some mutation results also suggest that the tRNA conformational change upon correct codon recognition transmits signals to EF-Tu and triggers GTP hydrolysis [15-18]. The conversion of GTP into GDP triggers further structural rearrangements of EF-Tu that promote the dissociation of the EF-Tu•GDP complex from the ribosome, as well as movement of the aa-tRNA CCA acceptor end into the A site of the 50S subunit (Figure 1.3.a) [19]. If a near-cognate tRNA is mistakenly incorporated into the ribosome and induces GTP hydrolysis on EF-Tu by escaping the tRNA selection check point, the ribosome can selectively reject the near-cognate tRNA at this proofreading stage. To this, the ribosome is thought to monitor the differing extents of tRNA deformations between cognate and near-cognate tRNAs. Therefore, only cognate tRNA can preferentially move to the A site of the 50S subunit [20, 21].

1.2.2. Peptidyl transfer

After accommodation of the aa-tRNA into the A site of the 50S subunit, the peptidyl-transferase center (PTC) of the 50S subunit undergoes structural rearrangements to organize the

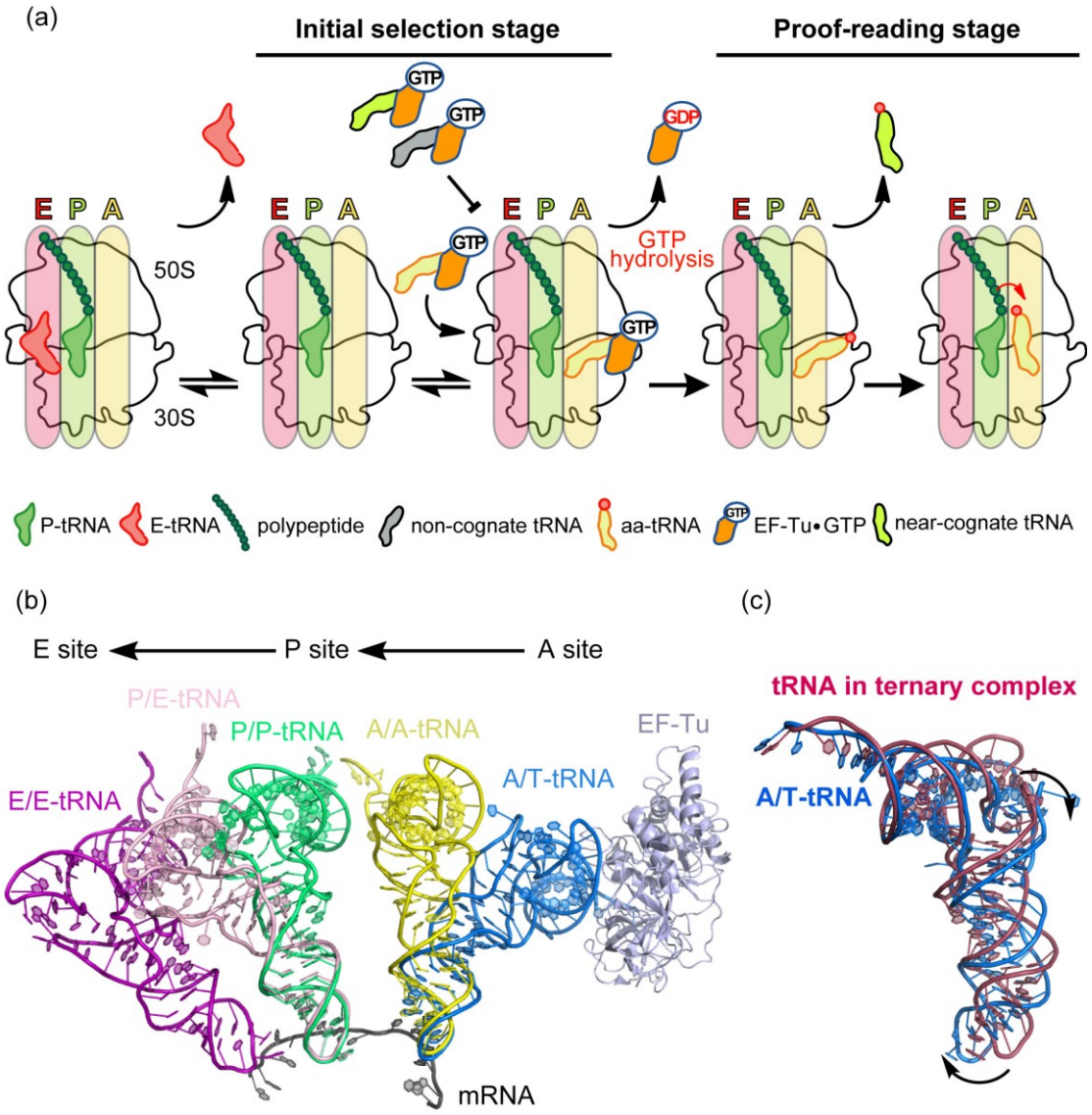

Figure 1.3. (a) A schematic illustration of the tRNA selection stage is shown. In the initial selection stage, the ternary complex entry to the ribosome and the formation of correct codon-anticodon interactions facilitate conformational changes of the ribosome and EF-Tu to trigger an irreversible chemical reaction of GTP hydrolysis (A/T and P/P state). After GTP hydrolysis, EF-Tu dissociates from the ribosome complex and the acceptor end of the aa-tRNA moves into the A site of the 50S subunit (A/A and P/P state). At this step, near-cognate tRNAs will be removed because of different tRNA deformation between the cognate and near-cognate tRNAs even though the ribosome mistakenly recognizes the near-cognate tRNA as a cognate tRNA and allows it to enter the ribosome (proof-reading stage). After the acceptor end of the aa-tRNA projects into the A site, the α-amino group of the aa-tRNA in the A site attacks the carbonyl group of the C-terminal end of the peptidyl-tRNA in the P site, and the polypeptide is transferred to the A-site tRNA. Translational fidelity is not only controlled by the initial tRNA selection and proof-reading stages, but also maintained by recycling factors (RFs) that sense a wrong incorporation of the nascent polypeptide into a near-cognate P-site tRNA and removes tRNAs carrying the wrong polypeptide from the ribosome (see also Section 1.2.4). (b) The tRNA transition pathway is shown (PDB ID: 2XQD+3KNL+3R8N). The color codes are light blue, EF-Tu; blue, A/T-tRNA; yellow, A/A-tRNA; green, P/P-tRNA; light pink, P/E-tRNA; purple, E/E-tRNA. Crystal structures were aligned based on the anticodon stem-loop positions. (c) The tRNA deformation upon entry of the ternary complex into the ribosome is shown (PDB ID: 2XQD+1TTT).

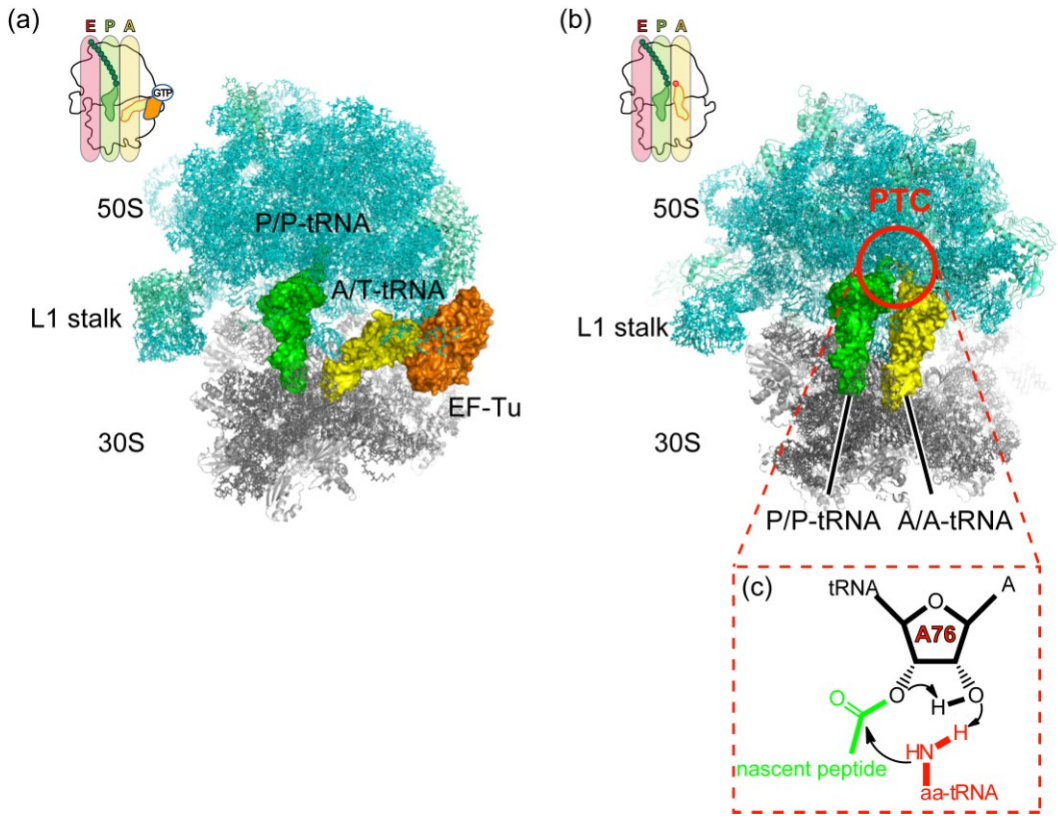

Figure 1.4. Crystal structures of the 70S ribosome with (a) A/T-tRNA and P/P-tRNA (PDB ID: 2XQD+2XQE) and (b) A/A-tRNA and P/P-tRNA (PDB ID: 3KNH+3KNI) shown. Upon dissociation of EF-Tu from the ribosome, the acceptor end of the A-site tRNA moves into the PTC. (c) A proposed model of peptidyl transfer is shown. See main text for further information.

nucleotides for catalyzing peptide-bond formation (Figure 1.4.a and b) [22-24]. The reaction of peptidyl transfer involves the α-amino group of the aa-tRNA in the A site, which attacks the carbonyl group of the C-terminal end of the peptidyl-tRNA in the P site [25]. As a result, the nascent polypeptide chain on the P-site tRNA is transferred to the A-site tRNA (Figure 1.3.a). Although the catalytic mechanism of peptidyl transfer reaction is still under active investigation, the most accepted model involves a substrate-assisted catalysis mechanism (Figure 1.4.c) [23]. In this model, the 2'-OH group of the 3'-terminal adenosine of the P-site tRNA deprotonates the aa-tRNA α-amino group in the A site, which then facilitates nucleophilic attack on the P-site tRNA (Figure 1.4.c). This model is supported by the observation that removal of the 2'-OH group from the P-site tRNA results in remarkable reduction in the rate of peptide-bond formation between a

peptidyl tRNA and puromycin [23]. However, recent studies have shown that the presence of a 2'-OH group does not significantly affect peptide-bond formation if full-length mRNA is used for *in vitro* translation experiments [26, 27]. The nascent elongating polypeptide passes through the exit tunnel of the ribosome after peptide-bond formation.

1.2.3. Translocation of the tRNA and mRNA

After peptidyl transfer, the P site contains deacylated-tRNA and the A site contains peptidyl-tRNA (Figure 1.5.a). The P-site tRNA and A-site peptidyl tRNA have to move forward to the E site and P site, respectively, to empty the A site in advance to sampling of the next ternary complex. This process is called translocation and is catalyzed by elongation factor G (EF-G) [28]. The ribosome state in which the A and P sites are filled with tRNAs is defined as the pre-translocation ribosome complex (PRE), and when the P and E sites are occupied with tRNAs, the post-translocation ribosome complex (POST) is formed. In the transition from PRE to POST, the tRNAs go from the classical P/P and A/A tRNA configurations (*i.e.*, tRNA contacts on both ribosomal subunits in the P and/or A sites) to the hybrid P/E and A/P configurations (tRNAs occupy the P and A sites of 30S and E and P sites of 50S) (Figure 1.5.a) [29]. Biochemical studies revealed that the classical-to-hybrid tRNA transition is a spontaneous event upon peptidyl transfer [29]. Recent single molecule FRET analyses (smFRET) further revealed that the classical-to-hybrid tRNA transition step is reversible and stochastic tRNA fluctuations occur in the PRE complex [30-33].

To form hybrid tRNA configuration, the ribosome must undergo dynamic conformational changes, referred to as ratchet-like intersubunit rotation, in which the 30S subunit rotates counterclockwise with respect to the 50S subunit (Figure 1.5.b) [34]. A smFRET study showed that intersubunit rotation occurs even in the absence of EF-G, and the 30S subunit fluctuates between rotated and unrotated ribosome conformations reversibly, suggesting that the ratchet-like ribosome rotation is a stochastic event [35]. Cryo-EM and smFRET studies showed that tRNA transition from the classical-to-hybrid configuration are coupled with the ratchet-like ribosome rotation [11, 36-38]. In addition to formation of the hybrid tRNA state and the ratchet-like ribosome

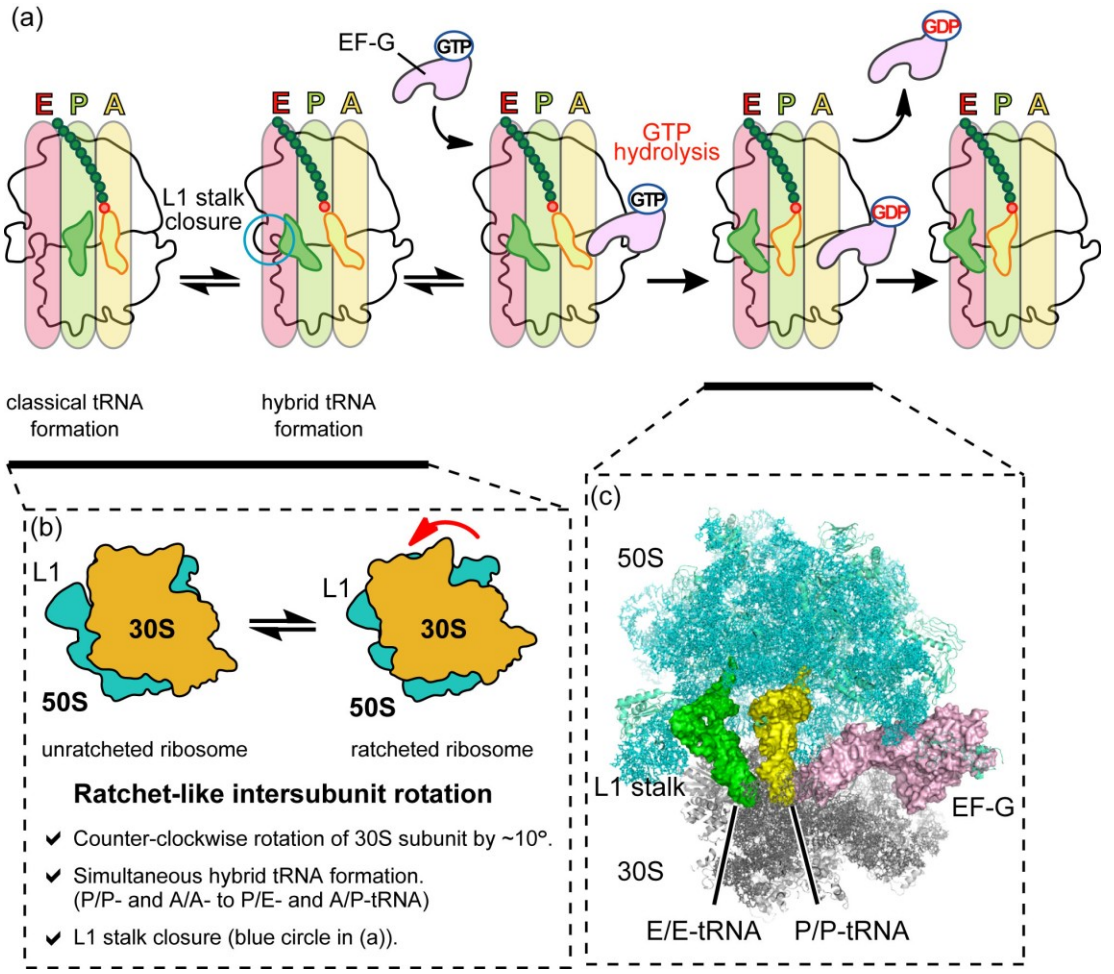

Figure 1.5. A schematic illustration of the translocation step is shown. In the PTC, the nascent polypeptide is transferred to the A-site tRNA and the P-site tRNA becomes uncharged. After peptidyl transfer, the small subunit rotates counter-clockwise with respect to the 50S subunit, the A- and P-site tRNAs on the 50S subunit move to the P and E sites, respectively, and the L1 stalk closes. It is proposed that these motions are stochastic and occur independently to sample the next ribosome conformation. The ratchet-like intersubunit rotation is illustrated in (b). To complete the tRNA translocation from the A and P sites to the P and E sites, EF-G comes into contact with the ribosome in the ratcheted ribosome configuration with the hybrid tRNA formation. GTP hydrolysis induces a conformational change of EF-G that facilitates tRNA movement on the 30S subunit, the back-ratcheting movement in the 30S subunit, and the head swiveling of the 30S subunit. (c) A crystal structure shows the complex of 70S ribosome with the P/P- and E/E -tRNAs and EF-G (PDB ID: 2WRI+2WRJ).

rotation, the translocating ribosome undergoes L1 stalk closure to make direct contact with the hybrid P/E tRNA (Figure 1.5.a, cyan circle) [5, 31, 34, 39-50]. EF-G preferentially recognizes the ribosome in the closed L1 stalk conformation, which suggests an allosteric regulation mechanism between the A and E site [51].

A cryo-EM study suggests a locking-unlocking mechanism, in which tRNA translocation requires unlocking of the PRE complex, as well as formation of the hybrid tRNA configuration, the ratcheted ribosome conformation, and the closed L1 stalk [39]. Unlocking of the ribosome was indicated as a stochastic, multistep process, since formation of the hybrid tRNA configuration and the L1 stalk closure are not highly coupled, even though the closed L1 stalk makes a stable interaction with the hybrid P/E tRNA in the unlocked state [52]. Upon the formation of the unlocked state, EF-G stably interacts with the ribosome and GTP hydrolysis occurs on EF-G, which triggers swiveling of the 30S subunit head domain and the back-ratcheting of the 30S subunit into the unrotated ribosome conformation. This step results in the movement of the hybrid P/E and A/P tRNAs into the classical E/E and P/P tRNA configurations (Figure 1.5.a and c) [51, 53-55]. Upon complete back-ratcheting of the 30S subunit, the entire ribosome moves by three nucleotides (one codon) on the mRNA. The ribosome, with an open A site, is now translocated to the next codon on the mRNA and ready for the next incoming aa-tRNA.

1.2.4. Termination

When the ribosome reaches a stop codon (UAA, UAG, or UGA) on the mRNA, protein synthesis is terminated (Figure 1.6). Stop codons are recognized by a protein called release factor (RF), instead of tRNA molecules [56, 57]. The release factor is classified into two groups, the class-1 release factors, including RF1 and RF2, and a class-2 release factor called RF3. RF1 decodes UAA and UAG stop codons; whereas, RF2 decodes UAA and UGA stop codons. The stop codons are recognized by a specific tripeptide motif of RF; the PxT motif in RF1 and the SPF motif in RF2. These determine stop codon selectivity (Figure 1.6.a and b) [58]. Class-1 release factor binding to the stop codon induces structural rearrangements around a switch loop of the RF by direct interaction with h44 of the 30S subunit and H69 of the 50S subunit, resulting in

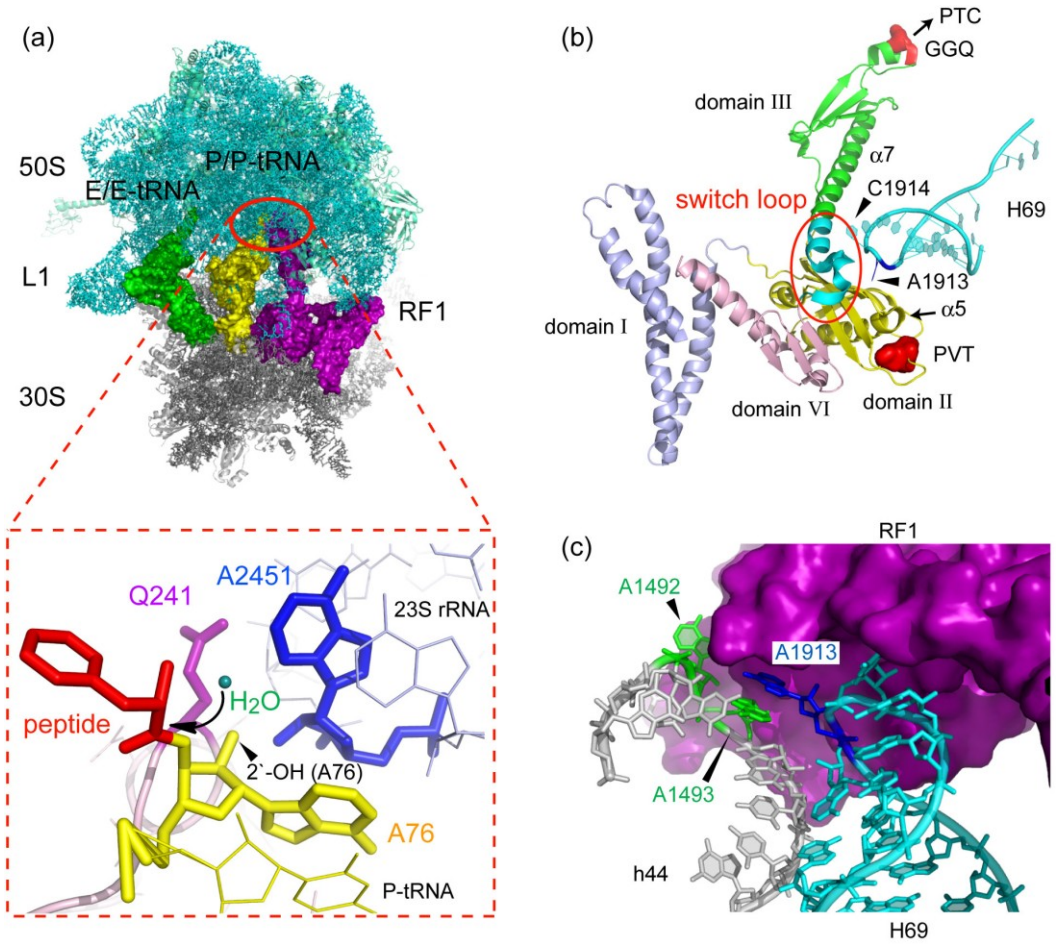

Figure 1.6. (a) Crystal structure of the 70S ribosome with RF1 is shown (PDB ID: 3D5A+3D5B). This crystal structure (and others) indicate a detailed mechanism for the hydrolysis reaction of the elongated peptide from the tRNA catalyzed by RF1. In the proposed mechanism, a water molecule is stabilized by the GGQ loop of RF1, 2'-OH of A76 in P-site tRNA, and 2'-OH of A2451 in 23S rRNA. Then, the water attacks the carboxy group of the C-terminal peptide, releasing the peptide from the ribosome. (b) Crystal structure of RF1 bound to the ribosome in Figure 1.6a showing. The tip of H69 of 23S rRNA and the switch loop of RF1 interact. Comparisons with crystal structures of free RF1 show that the α7 helix of domain III is extended by binding to the ribosome. It is proposed that stable binding of RF1 to the ribosome is necessary for this helix to be extended and reach the PTC [59-61]. Interaction of the switch loop with the ribosome domain may play an important role in inducing conformational changes of both the α7 helix and H69. (c) An enlarged picture of the interface region in the crystal structure of the 70S ribosome with RF1 shows a unique arrangement of bases at A1913 of H69 and A1493 of h44, in which A1913 forms a base-stacking interaction with A1493. It is proposed that this base orientation is important for stable RF1 interactions with the ribosome [59].

the projection of a universally conserved GGQ motif of domain 3 of RF into the PTC (Figure 1.6.b and d) [59-61]. Docking of the GGQ motif in the PTC induces structural rearrangements in the PTC to coordinate a water-mediated catalytic reaction to cleave the nascent popypeptide chain from the peptidyl-tRNA (Figure 1.6.c) [62, 63]. The cleaved polypeptide chain then exits the ribosome through the exit tunnel. Although the class-2 release factor RF3 does not induce peptide release, it enhances efficient recycling by RF1 and RF2 [64, 65].

Interestingly, a secondary function of the release factors was uncovered, in which RF1 and RF2 play an important role in the mechanism of quality control in polypeptide synthesis [66]. The fidelity of protein synthesis is affected by the selection mechanisms of the cognate tRNA over near-cognate tRNA by the ribosome (Figure 1.3). If RF1 and RF2 sense a near-cognate P-site tRNA that incorrectly passes the initial selection and proofreading stage, RFs catalyze the cleavage of polypeptide chain from the near-cognate P-site tRNA and release it from ribosomes, such that ribosomes can maintain the quality of elongating polypeptide even after the initial selection and proofreading stage [66]. RF3 also plays a role in quality control mechanism by enhancing near-cognate tRNA release [66].

1.3. Post-transcriptional modifications and ribosomal RNA

rRNA plays a critically important role in protein biosynthesis and peptide-bond formation. The catalytic activity of rRNA was initially indicated by studies in which ribosomal proteins were removed from ribosomes [67, 68]. Later, the secondary structures of the three rRNAs were determined (Figure 1.7) [69, 70] and three-dimensional structures of the ribosome were solved (Figure 1.8) [46, 71]. These efforts confirmed the idea that rRNA functions as the core catalytic domain in protein synthesis [46, 71]. rRNA is post-transcriptionally modified in several sites by a variety of ribosome-related enzymes (Table 1.1) [72-74]. The importance of rRNA modifications in ribosome activity was implicated by the observation that *in vitro* reconstituted ribosomes composed of *in vitro* transcribed rRNAs showed a severe defect in peptidyl transfer [75]. Lack of post-transcriptional modifications in rRNAs also caused less efficient subunit association *in vitro*. Decreased subunit assembly and defects in peptidyl transfer were partially rescued by

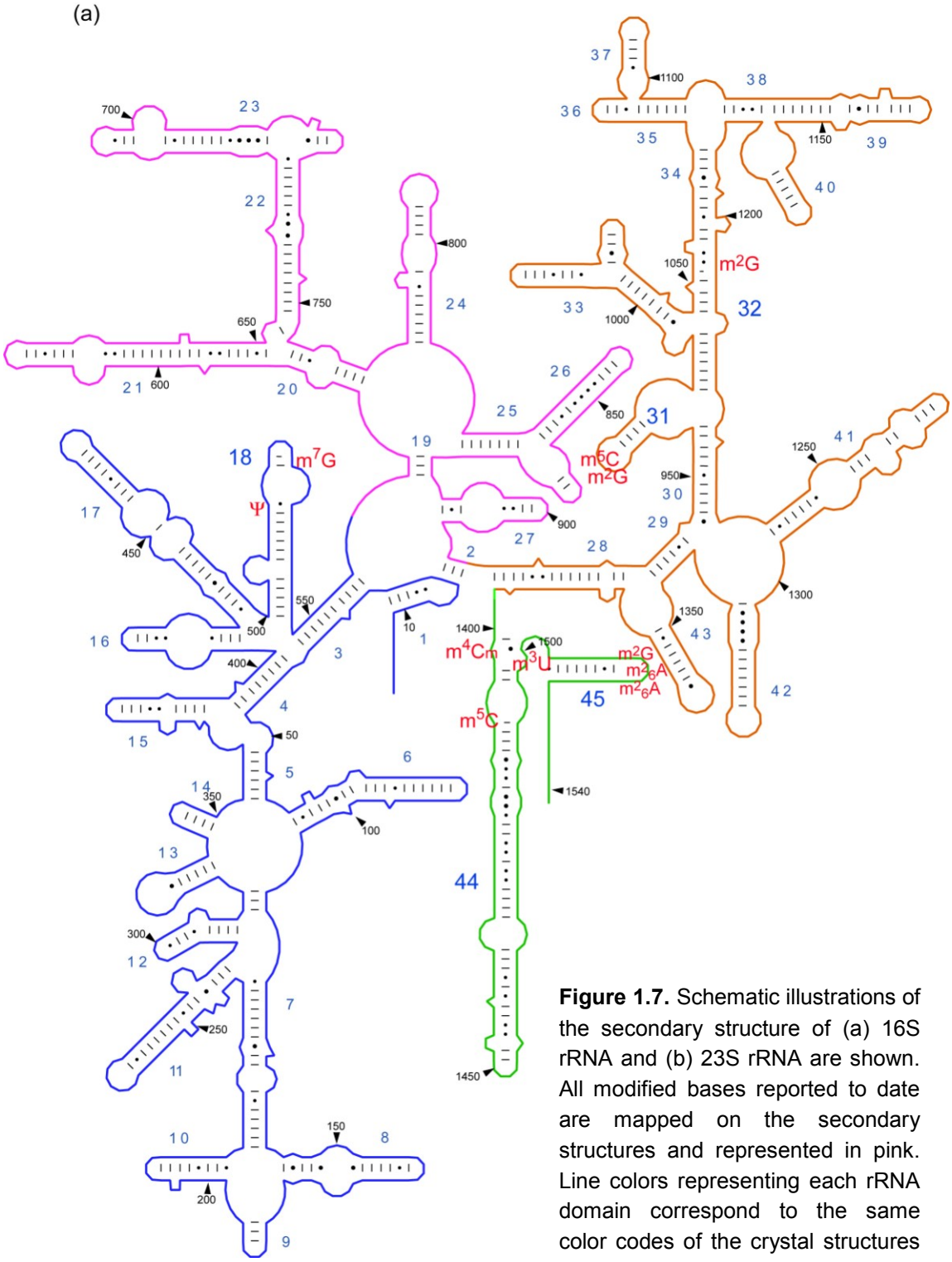

Figure 1.7. Schematic illustrations of the secondary structure of (a) 16S rRNA and (b) 23S rRNA are shown. All modified bases reported to date are mapped on the secondary structures and represented in pink. Line colors representing each rRNA domain correspond to the same color codes of the crystal structures of 30S and 50S subunits in Figure 1.8. These figures are made based on references [46, 69-72].

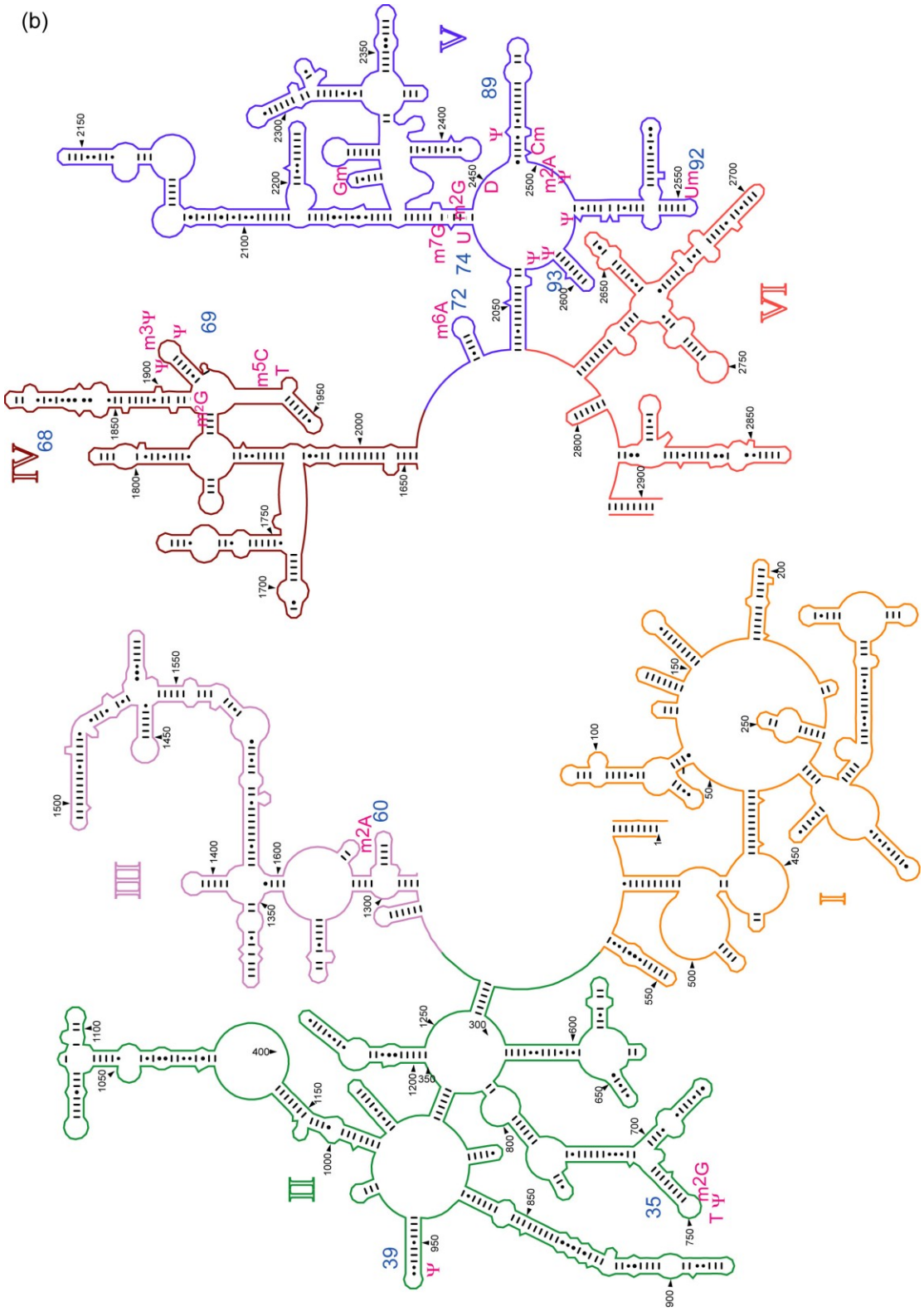

Figure 1.7. (Continued)

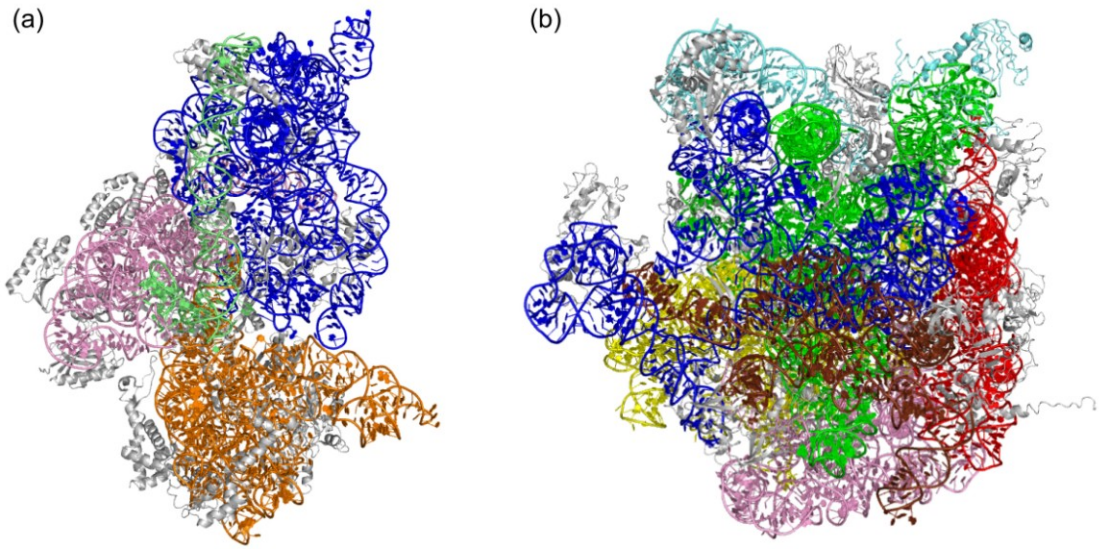

Figure 1.8. Crystal structures of (a) the small subunit (PDB ID: 2XQD) and (b) the large subunit (PDB ID: 2XQE) are shown. Ribosomal proteins are represented in gray, and each rRNA domain is represented by different colors, which correspond to those in the secondary structures in Figure 1.7.

Table 1.1. The list of modified nucleotides found in 16S rRNA and 23S rRNA [74].

rRNA	Base type	Position	Enzymes
16S rRNA	G	m^2G 966	YhhF
		m^7G 527	–
		m^2G 1207	YjjT
		m^2G 1516	–
	C	m^5C 967	YhdB
		m^5C 1407	YebU
		m^4Cm 1402	–
	A	$m^2{}_6A$ 1518	KsgA
		$m^2{}_6A$ 1519	KsgA
	U	m^2U 1498	YggJ
		Ψ 516	YejD
23S rRNA	G	m^1G 745	YebH
		m^2G1835	Ygjo
		m^7G 2069	–
		m^2G 2445	YcbY
		Gm 2251	YjfH
	C	m^5C 1962	YccW
		Cm 2498	–
		s^2C	2501
	A	m^6A 1618	YbiN
		m^6A 2030	–
		m^2A 2503	–
	U	Ψ 746	YabO
		m^5U 747	YbjF
		Ψ 955	YceC
		Ψ 1911	YfiI
		$m^3Ψ$ 1915	YbeA/YfiI
		Ψ 1917	YfiI
		m^5U 1939	YgcA
		D 2446	–
		Ψ 2457	YmfC
		Ψ 2504	YceC
		Um 2552	FtsJ
		Ψ 2580	YceC
		Ψ 2604	YjbC
		Ψ 2605	YciL

substituting the synthetic rRNA around the PTC with a modified RNA from wild-type rRNA [75]. The significance of modified nucleotides in rRNA functionality and stability is also indicated by the fact that *T. thermophilus*, which lives under harsh conditions (*e.g.* high temperature and acidic conditions), contains a larger number of modified nucleotides in its RNAs than mesophilic organisms [76-78].

More than 100 naturally occurring modifications in rRNAs have been reported [74]. The nucleotide modifications can be mainly classified into three types: 1) conversion of uridine to pseudouridine (Ψ); 2) chemical modification(s) of bases (*e.g.*, methylation to generate 3-methyl pseudouridine ($m^3\Psi$ in bacteria); and 3) 2'-hydroxyl methylation (Figure 1.9.a) [72, 73]. Although the complexity of rRNA modifications varies between species, the distribution patterns of modified bases in the tertiary structure of the the different ribosomes are conserved throughout phylogeny [5, 46]. The sites of modified bases, when mapped on the high-resolution x-ray crystal structures, are revealed to cluster within the functionally important regions (Figure 1.9.b and c) [5, 46]. In particular, the modified bases mainly exist in the PTC, the polypeptide exit tunnel, the decoding center, and the intersubunit-bridge regions (Figure 1.9.b and c).

The *E. coli* ribosome contains a total of 36 modifications, 25 in 23S rRNA and the rest in 16S rRNA (Table 1.1) [72, 73]. Pseudouridine (Ψ) is the most frequently observed modified nucleotide. *E. coli* 23 rRNA has ten Ψs and 16S rRNA contains only one. Pseudouridine contains a C-C instead of an N-C glycosidic bond, and an extra imino proton at the N1 position (Figure 1.9.a). The additional imino proton at the Ψ-N1 position serves as a unique hydrogen-bond donor. The isomerization reaction from uridine to Ψ is carried out by site-specific modifying enzymes in bacteria called pseudouridine synthases [79]; whereas, in eukaryotes, an RNA-protein complex is employed to catalyze the uridine to Ψ isomerization. In the eukaryotic system, a small nucleolar RNA (snoRNA) recognizes a target RNA domain selectively and guides the common protein complex that is responsible for catalysis [80-82]. The effect of Ψ modifications on ribosome activity is not fully understood. The only example of a severe defect in a bacterial phenotype as a result of Ψ deletion is in H69 of 23S rRNA; however, recent studies have also cast doubt on the biological function of Ψ modifications in this region (see also Section 1.4.4.) [83]. Besides Ψ

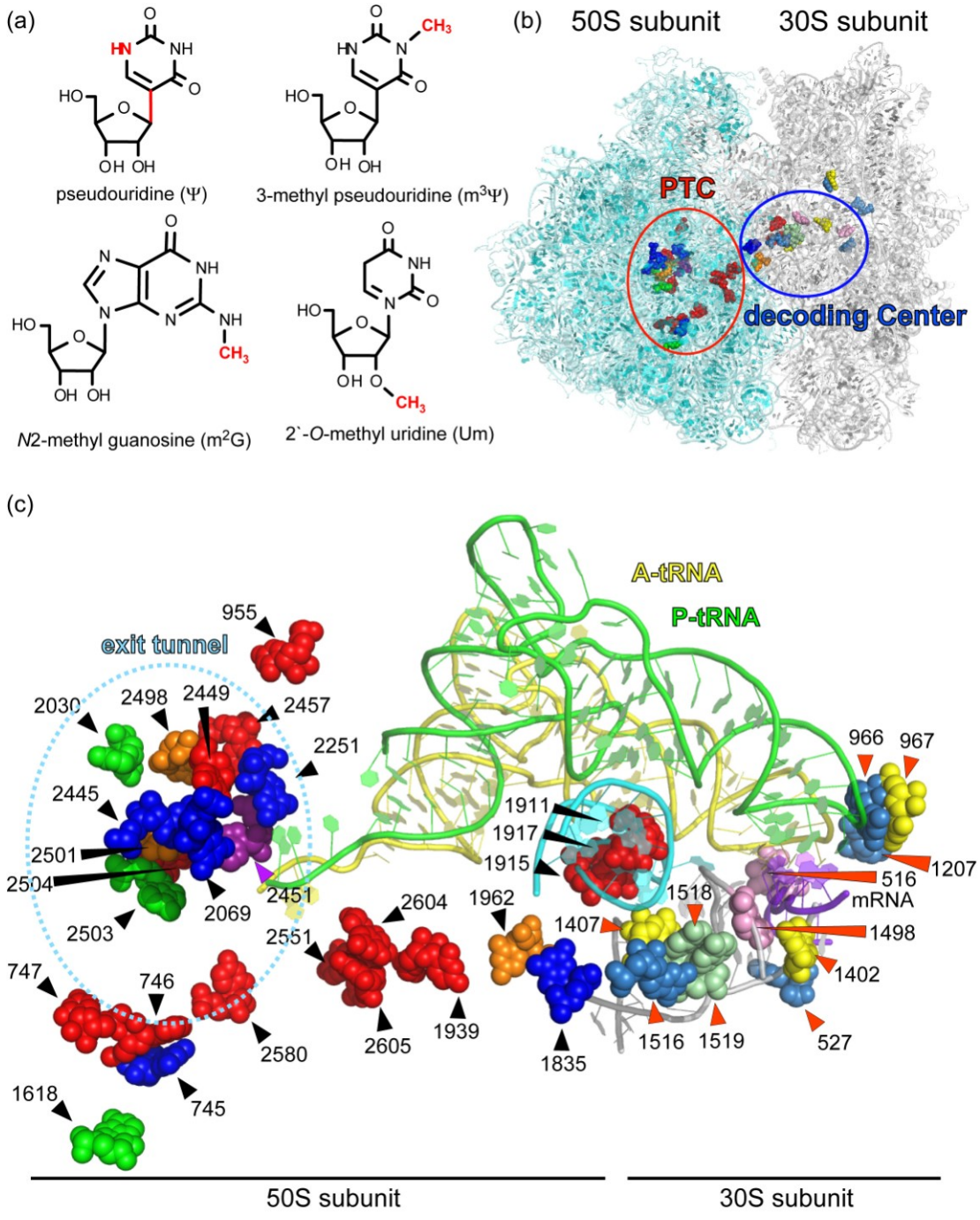

Figure 1.9. (a) Chemical structures of the major classes of modified bases seen in rRNA are shown. (b) A map of modified bases on the *T. thermophilus* 70S ribosome crystal structure is shown (PDB ID: 3KNH+3KNI). The 50S subunit is in cyan and the 30S subunit is in gray. (c) The spatial positioning of bacterial rRNA modifications is shown. The A- and P-site tRNAs are shown in yellow and green, respectively. Color codes for modified bases are as follows: in 23S rRNA, red, U; blue, G; orange, C; green, A; in 16S rRNA, pink, U; light blue, G; yellow, C; light green, A. Nucleotide numbers for 23S rRNA and 16S rRNA are highlighted by black and red triangles, respectively.

modifications, some other rRNA modifications are reported to affect ribosome activity. For example, the absence of 2-methylguanosine (m^2G), the second most abundant modified nucleotide in bacterial ribosomes, affects bacterial growth, although this modification is not always essential. Loss of the methyltransferase enzymes responsible for modification at G1895 of 23S rRNA and G2445 of 23S rRNA leads to cell growth retardation, especially under minimal nutrient conditions [84, 85]. Also, the formation of m^2G1985 in 23S rRNA facilitates 70S ribosome formation *in vitro* [86]. In contrast, however, enzyme deletion experiments for other m^2G modifications have no effect on bacterial cell growth [87]. Thus, it is still unclear how each modified nucleotide influences ribosome function and subsequently bacterial cell phenotypes.

One of the functions of modified nucleotides in rRNA is to prevent the ribosome from unwanted molecular interactions by shifting rRNA conformational states. A prominent example involves antibiotic resistance. The loss of a 2'-OH methyl modification at C1409 of h44 in 16S rRNA and C1920 of H69 in 23S rRNA causes strong antibiotic resistance to the tuberactinomycin-family cyclic peptides viomycin and capreomycin in *M. tuberculosis* [88]. These cyclic peptide antibiotics do not effectively inhibit *E. coli* cell growth. It is proposed that the 2'-OH methylation at C1409 of h44 and C1920 of H69 are important for their antimicrobial effect because these modifications are naturally absent in *E. coli* strains. When a recombinant TlyA methyltransferase, which is responsible for C1409 of h44 and C1920 of H69 methylations, was expressed in *E. coli* cells, 2'-OH methyl modifications at C1409 of h44 and C1920 of H69 were detected and, subsequently, elevated susceptibility to capreomycin and viomycin was observed [88]. However, deletion of the *tlyA* gene and subsequent loss of 2'-OH methylation at these sites in *T. thermophilus* did not affect capromycin and viomycin sensitivity [89]. Thus, the antimicrobial mechanism of the tuberactinomycin-class of cyclic peptide antibiotics is quite complicated. Another well-known example of antibiotic resistance involves kasugamycin. Kasugamycin resistance in bacteria is caused by a loss of the methyltransferase KsgA, which is responsible for methylation at positions A1518 and A1519 of h45 in 16S rRNA [90, 91].

1.4. Helix 69 of the large ribosomal subunit

1.4.1. Structural insight into molecular functions of helix 69

The subunit interactions required for 70S ribosome formation are supported by the highly conserved specific intersubunit bridges (Table 1.2) defined by low-resolution cryo-EM studies [92, 93] and high-resolution crystal structure studies done later (Figure 1.10) [46]. One important bridge is B2a, which lies at the center of the ribosome and forms part of the decoding region [46]. The B2a interaction is composed of H69 of the 50S subunit together with h44 of the 30S subunit. In crystal structures of the ribosome, A1912 of H69 projects into the minor groove of h44 and interacts with C1407 and G1494 (Figure 1.11) [5, 47]. The positioning of A1912 is supported by a reverse-Hoogsteen base pair with Ψ1917 of H69. Nucleotide A1919 also has a minor-groove interaction with non-canonical base pair U1406/U1495 of h44 [5]. This interaction is supported by a non-canonical widened-Hoogsteen base pair with residue A1919 bridged by the 2'-OH of residue A1918 (Figure 1.11).

The significance of the B2a interaction is implicated by mutation studies and highlighted in Table 1.3. Single base substitutions of H69 at residues 1912 or 1919 with any other base causes lower poly(Phe) synthesis, reduced peptidyl transfer processivity, and defects in factor-dependent 70S formation in *in vitro* experimental systems [94]. Moreover, *in vivo* genetic studies revealed that H69 mutations at positions 1914, 1915, 1916, and 1922 lead to internal-codon frameshifting and stop-codon readthrough [95, 96]. Thus, mutation studies at sites involved in the B2a interaction support the idea that this bridge must be stably maintained through the translation cycle.

The B2a interaction plays an important role in stabilizing the 70S ribosome complex during ratchet-like intersubunit rotation [97]. At the same time, subunit ratcheting triggers dynamic reorganization of intersubunit interactions. For instance, H38 of the 50S subunit in the intersubunit bridge B1a is in contact with small ribosomal protein S13 in the unrotated ribosome; whereas, H38 switches its partner to small ribosomal protein S19 upon ratchet-like intersubunit rotation [39]. The 30S subunit rotation with respect to the 50S subunit, thus, produces the twisting torsion between subunits. Since the 70S complex must be maintained in order for processive

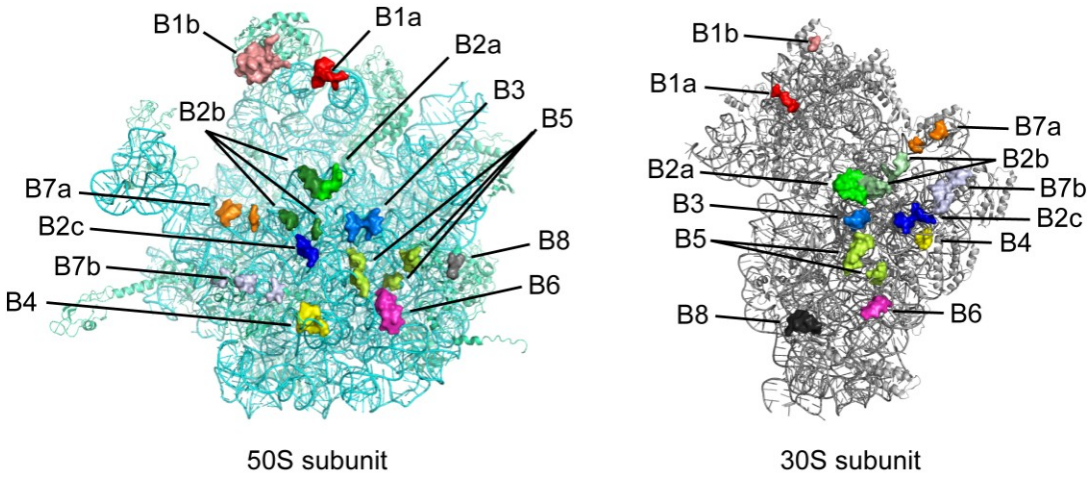

Figure 1.10. Intersubunit bridges are mapped on the *T. thermophilus* 70S ribosome crystal structure (PDB ID: 3KNH+3KNI) and shown in each ribosome subunit.

Table 1.2. A list of intersubunit bridges. This table is adapted from [46].

Bridge	Type	30S subunit	50S subunit
		Region	Region
B1a	Prot-RNA	S13 (92-94)	H38 (886-888)
B1b	Prot-Prot	S13 (N-terminal)	L5 (134-153)
B2a	RNA-RNA	h44 (1408-1410, 1494-1495)	H69 (1913-1914, 1918)
B2b	RNA-RNA	h24 (784-785, 794)	H67 (1836-1837, 1922)
	RNA-RNA	h45 (1516-1519)	H71 (1919-1920, 1932)
B2c	RNA-RNA	h24 (770-771)	H67 (1832-1833)
	RNA-RNA	h27 (900-901)	H67 (1832-1833)
B3	RNA-RNA	h44 (1484-1486)	H71 (1947-1948, 1960-1961)
B4	RNA-RNA	h20 (763-764)	H34 (717-718)
	Prot-RNA	S15 (40-44)	H34 (713, 717)
B5	RNA-RNA	h44 (1418-1419)	H64 (1768-1769)
	RNA-Prot	h44 (1420-1422)	L14 (44-49)
	RNA-RNA	h44 (1474-1476)	H62 (1689-1690)
	RNA-RNA	h44 (1474-1476)	H64 (1989)
B6	RNA-RNA	h44 (1429-1430, 1474-1476)	H62 (1689-1690, 1702-1705)
	RNA-Prot	h44 (1431)	L19 (24, 44)
B7a	RNA-RNA	h23 (698, 702)	H68 (1848-1849, 1896)
B7b	RNA-Prot	h23 (712-713)	L2 (162-164, 172-174,177-178)
	RNA-Prot	h24 (773-776)	L2 (177-178, 198-202)
B8	RNA-Prot	h14 (345-347)	L14 (116-119)

peptidyl transfer reactions to occur, such conformational torsion would be compromised or altered by structural rearrangements. H69 is implicated in having a significant role in this adaptive conformational torsion. Intersubunit rotation and hybrid tRNA formation compress the H69 stem region and induce conformational rearrangements around C1925-G1929; whereas, the main B2a interaction is maintained during intersubunit ratcheting (Figure 1.12) [98].

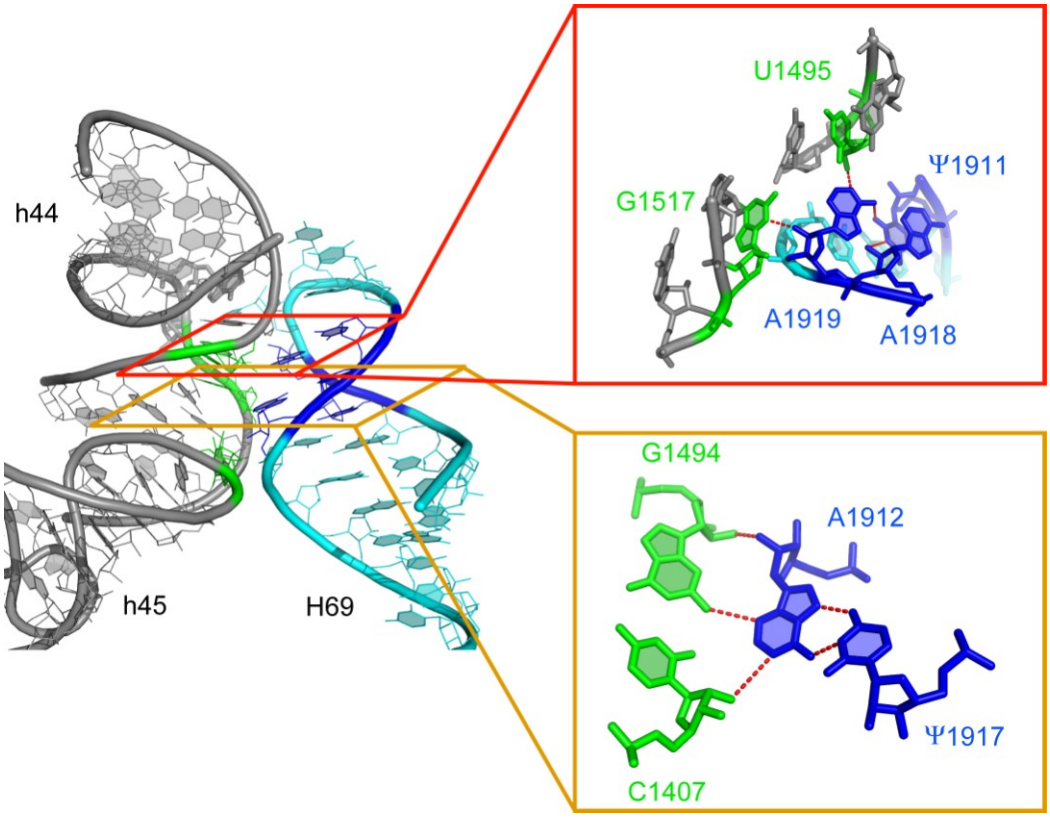

Figure 1.11. Interactions of the intersubunit bridge B2a are shown (PDB ID: 3I1O+3I1P). The red box highlights the A1918-A1919-Ψ1911 network, in which A1919 interacts with U1495 of h44 through its N1 position and G1517 through the 2'-OH. The orange box highlights the formation of the A1912-Ψ1917 Hoogsteen interaction. A1912 participates in a minor groove interaction with h44 through interactions with C1407 and G1494.

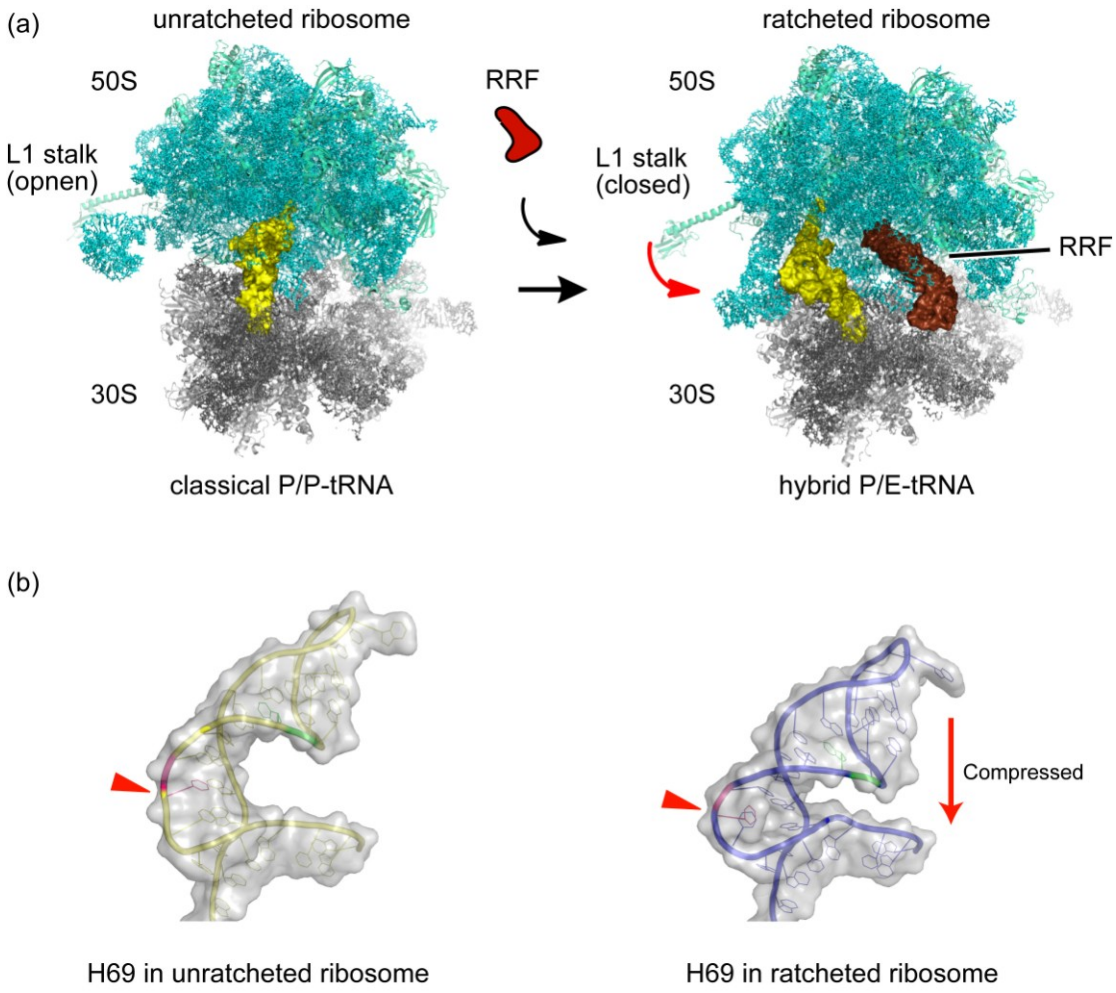

Figure 1.12. (a) The crystal structures of the 70S ribosome with (right) and without (left) ribosome recycling factor (RRF) are shown (PDB ID: 3R8O+3R8T and 3R8N+3R8S, respectively). At the end of bacterial translation, ribosomes are separated into individual subunits and recycled for the next round of translation (see also Figure 1.2). RRF helps the ribosome to dissociate into subunits. After peptide release, the ribosome contains an uncharged P-site tRNA. RRF interacts with the ribosome and induces the hybrid P/E-tRNA configuration. After EF-G binding to the ribosome-RRF complex and GTP hydrolysis, the ribosome complex dissociates two separate subunits. (b) Crystal structures of H69 from *E. coli* 70S ribosomes with or without RRF (corresponding to structures in panel a) are shown. H69 undergoes a dynamic conformational rearrangement around its stem region. In unratcheted ribosomes, H69 goes from an extended conformation to a compressed conformation, which disrupts the terminal base pair (C1925-G1929) and induces a C1925 flipped-out conformation (indicated by the red arrow).

Table 1.3. List of mutations and their effect on ribosome function.

Position	Effect of mutation	Ref.
Ψ1911C	No remarkable defect found (*in vivo*)	96
A1912N	essential residue (*in vivo*)	99
	A1912G causes slow growth rate in competitive assay (*in vivo*)	100
	60% reduced activity and relatively low poly(Phe) synthesis (*in vitro*)	94
	low processivity (*in vitro*)	94
	defect in factor-dependent 70S formation (Ifs+tRNA^{fMet}) (*in vitro*)	94
	no defect in the A-site tRNA stability	94
A1913U	suppress Hirsh tRNA decoding of UGA codon (*in vitro*)	101
	abnormal accommodation process for a subset of tRNA (*in vitro*)	101
	no influence on RF-mediated peptide release (*in vitro*)	101
ΔA1913	non-functional ribosome	99
A1913-(+N)-C1914	non-functional ribosome	99
C1914U	inviable	96
	strong –1/ medium +1 frameshifting (*in vivo*)	95
	UAG readthrough (*in vivo*)	95
	reduced growth rate (*in vivo*)	95
	functional variation	99
C1914A	no remarkable defect *in vivo*	95, 96
C1914G	inviable	96
	no remarkable defect in *lacZ* assay in plasmid experiment	96
	could be functional variation	99
Ψ1915A	long doubling time (*in vivo*)	99
	strong –1/+1 frameshifting (*in vivo*)	99
	strong UAG and UGA readthrough (*in vivo*)	99
	lower A-site tRNA binding (*in vitro*)	99
	defect in 70S formation (*in vitro*)	99
ΔA1916	inviable	95, 96, 99
	long doubling time	95, 96
	strong UGA/UAG/UAA readthrough	95, 96
	strong –1/+1 frameshifting	95, 96
A1916+A	inviable	95, 96
	6-fold longer doubling time	95, 96
	strong UAG/UGA readthrough	95, 96
	strong –1/+1 frameshifting	95, 96

Table 1.3. (continued)

Position	Effect of mutation	Ref.
Ψ1917	essential residue (*in vivo*)	99
A1918G	+1/–1 frameshifting	99
	UAG and UGA readthrough	99
A1919N	low processivity (*in vitro*)	94
	very low poly(Phe) synthesis (*in vitro*)	94
	defect in factor-dependent 70S formation (IFs+tRNA^{fMet}) (*in vitro*)	94
A1919U	faster dissociation of A-site tRNA after peptidyl transfer (*in vitro*)	94
A1919G	functional variation	99
	faster dissociation of A-site tRNA after peptidyl transfer (*in vitro*)	94
G1921C	inviable	96
	very low UAG readthrough	95
G1922A	slow rate of peptide release by RF2 (*in vitro*)	101
	–1 frameshifting	96
	UGA readthrough	96
G1922U	–1 frameshifting	96
	UGA readthrough	96
ΔH69	40% reduced poly(Phe) synthesis (*in vitro*)	59, 102
	loss of RF-mediated peptide release (*in vitro*)	102
	no defect in the A-site tRNA stability	94
	defect in factor-dependent 70S formation (IFs+tRNAini) (*in vitro*)	4
	low factor-independent 70S formation (*in vitro*)	94
C1914A + Ψ1915A + A1916C	defect in 70S formation (*in vitro*) lower A-site tRNA binding	99
Δ(G1910-C1920)	inviable	99

1.4.2. Interaction of helix 69 with tRNAs

In addition to inter-ribosomal subunit interactions, H69 also interacts with some translation-related factors, such as tRNAs [12, 47], release factors (RFs) [59-61], and ribosome recycling factor (RRF) (summarized in Figure 1.13) [99]. Especially, H69 makes direct contacts with the A- and P-site tRNAs. Structure studies revealed that nucleotide A1913 projects into a pocket formed by h44 and the codon-anticodon helix in the A site, and contacts the 2'-OH of ribose 37 of the A-site tRNA [47]; however, positioning of A1913 depends on both ribosome configurations and tRNA occupancies (Figure 1.14). The importance of the A1913 interaction with the A-site tRNA is suggested by pre-steady-state kinetic analyses in which an A1913U mutation alters the A-site tRNA accommodation [100]. The tip of H69, including nucleotides C1914 and $m^3\Psi$1915, interacts with nucleotides 25-26 of the A/T-state tRNA in the ternary complex (aa-tRNA•EF-Tu•GTP) [13, 14]. It has been proposed that the interaction between the H69 loop and the tRNA body is critical to monitor the deformation process of the incoming cognate aa-tRNA in the tRNA selection stage (Figure 1.3.c) [12]. This idea is supported by the observation that a Hirsh suppressor $tRNA^{Trp}$ [101], which has a G24A mutation in the D stem where H69 makes contacts, exhibits a codon-

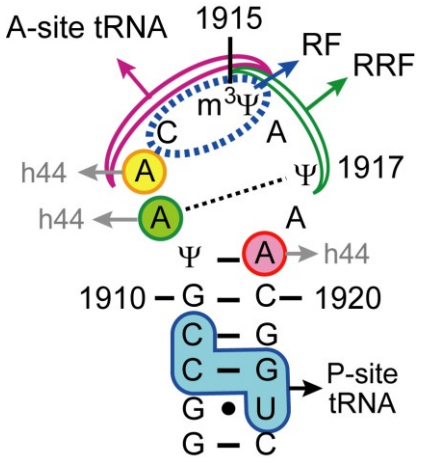

Figure 1.13. The sequence and map of *E. coli* H69 RNA show key interactions with h44, tRNAs, and protein factors (RFs, RRF) (Ψ is pseudouridine and $m^3\Psi$ is 3-methylpseudouridine).

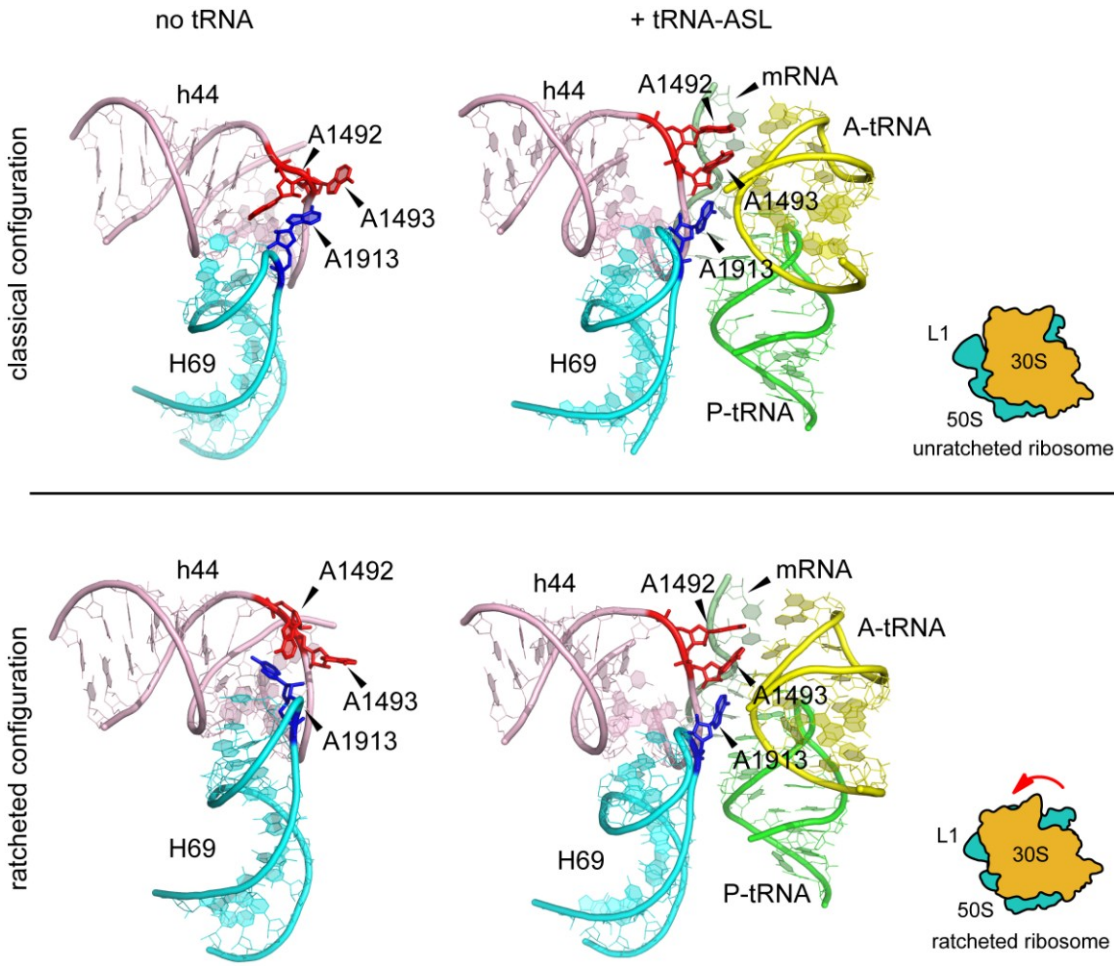

Figure 1.14. The intersubunit bridge B2a region in different ribosome configurations (classical and ratcheted) of the *E. coli* 70S ribosome crystal structures are shown (PDB; 3I1M, 3I1N, 3I1O, 3I1P, 3I1Z, 3I20, 3I21, and 3I22). Color codes are as follows: light cyan, H69 in the 50S subunit; blue, residue A1913; light pink, h44 in the 30S subunit; red, A1492 and A1493 in the decoding site; yellow, A-site tRNA; green, P-site tRNA; light green, mRNA. Crystal structures on the left side are of vacant 70S ribosomes (no tRNA), while ribosomes on the right side were co-crystallized with mRNA and A- and P-site tRNA anticodon stem-loop analogues (+tRNA-ASL). Residue A1913 in the 50S subunit exhibits dynamic conformational changes during the ratchet-like intersubunit rotation between tRNA states.

anticodon interaction-independent miscoding by increasing the forward rate constant of the tRNA selection step [16]. Interestingly, an A1913U mutation suppresses the miscoding event by the Hirsh suppressor $tRNA^{Trp}$ [102], suggesting the importance of a proper interaction between H69 and the A-site tRNA in the initial selection stage. It is also proposed from cryo-EM studies that deformation of the tRNA anticodon-stem region is an important characteristic of the correct codon-anticodon interaction and would affect the H69-tRNA interaction [12]. In the case of the H69 stem (G1921-G1922), this region interacts with the D stem of the P-site tRNA [12, 46]. Since G1922A or G1922U mutations cause a –1 frameshifting or UGA stop-codon readthrough [96], the H69-tRNA interaction would be important for stable P-site tRNA positioning as well. The importance of the interaction between the P-site tRNA and H69 stem is also revealed by crystal structures showing that formation of a compressed H69 structure upon the hybrid P/E tRNA formation causes a loss of this interaction [98]. The tight, but organized, interaction between H69 and A-site and P-site tRNAs would be essential for the processive translocation of tRNA.

1.4.3. Interaction of helix 69 with translation-related protein factors

In addition to tRNA, the tip of H69 (C1914) directly contacts the switch loop of a class I release factor during stop codon recognition, which induces a conformational change in the bound RF in which its α7 helix is extended and causes the GGQ motif in domain 3 to project into the PTC to catalyze the water-mediated, peptide-release reaction (Figure 1.6.b and d) [60]. A ribosome lacking the entire H69 hairpin exhibits a dominant lethal phenotype and strong impairment in the RF-mediated peptide release stage, but affects other translation steps only moderately [59, 103], supporting the significance of a direct interaction between H69 and RFs. The H69 local conformation is also proposed to play a key role in stable RF binding to the ribosome. A crystal structure of the RF1-bound ribosome shows A1913 of H69 projecting towards the minor groove of h44 of the 30S subunit, forming a base-stacking interaction with A1493 of h44 (Figure 1.6.d) [60]. This structure suggests that the H69-h44 conformation provides enough space for RF1 to interact stably with the ribosome. This model is supported by the observation

that A-site binding aminoglycosides, which induce an A1492/A1493 extrahelical conformation in 16S rRNA [8], compete with RF binding to the ribosome [104].

In addition to release factors, cryo-EM also shows direct interactions between RRF and H69 residues 1915-1917, which results in induction of the hybrid P/E tRNA state along with H69/h44 movement toward the E site [99]. Recently, this same movement was observed in a high-resolution X-ray crystal structure in the presence of RRF (Figure 1.12) [98]. Thus, these direct interactions of H69 with translation factors are implicated to serve important functions in active ribosome complex formation (initiation), tRNA translocation (processivity), cognate tRNA selection (fidelity), and translation termination.

1.4.4. Pseudouridine modifications and conformational dynamics of helix 69

A distinct characteristic of H69 is the existence of conserved modified nucleotides in its loop region, including two Ψs at positions 1911 and 1917 and one 3-methylpseudouridine ($m^3\Psi$) at 1915 (Figure 1.13) [105, 106]. Ribosomes lacking Ψ modifications in H69 exhibit slow growth rates *in vivo* and reduced subunit association *in vitro* [83]. A mutant phenotype in a bacterial strain lacking H69 Ψ modifications (RluD(–)) can be rescued by an additional mutation in RF2 at a site adjacent to an H69-interacting residue [107]; however, recent studies revealed that the RluD(–) phenotype was actually a consequence of a mutant RF2 protein that exists in the *E. coli* K-12 strains; whereas, *E. coli* B strains and *Salmonella enterica* containing a fully active RF2 protein do not display this mutant phenotype, even upon deletion of the *rluD* gene encoding for H69 pseudouridine synthase [108]. Although the role of Ψ residues in translation termination process is questionable, the fact is that H69 itself is still indispensable for efficient termination by RFs [59, 103] and its conformational dynamics are likely to be important to facilitate a stable RF interaction with the ribosome [60].

Model studies using small RNAs revealed that Ψ modifications in H69 play an important role in maintaining its loop structure [109, 110]. Pseudouridine modification can contribute to stable single- or double-stranded RNA formation by enhancing base-stacking interactions or through extra imino-proton interactions [77]. Small model RNA oligonucleotides (19-nt) representing H69

and containing all of the nucleotide modifications at positions 1911, 1915, and 1917 exhibited conformational dynamics around the loop region that could be induced by changes in the buffer pH from pH 5.5 to 7.0. Comparative analyses between model solution studies and ribosome crystal structures suggested that under lower pH conditions H69 formed a stacked-in conformation ("closed"), but formed a flipped-out conformation under higher pH condition ("open") [109]. On the other hand, no conformational differences were observed in unmodified H69 model RNAs, regardless of changes in buffer pH. Different conformational dynamics between RNAs with and without Ψs suggest that these modifications elicit unique conformational characteristics in H69. Furthermore, ^{1}H-NMR studies exhibited a rearrangement of base-stacking patterns around the H69 loop by Ψ [110], suggesting a unique function of modifications in the H69 RNA structure.

1.5. Translation inhibition by antibiotics

The discovery of antibiotics to treat bacterial infectious diseases was one of the great breakthroughs in medicine in the 20th century. Unfortunately, the emergence of advanced antibiotic-resistant pathogens has become an urgent issue in the 21st century, which needs to be solved all over the world, especially in developing countries [111, 112]. Thus, understanding the underlying principle of action of antibiotics at the molecular level, and re-evaluating naturally occurring and semi-synthetic antibiotics, are important approaches to combat bacterial infections and to develop unique antibacterial therapeutics.

Targeting functional RNAs with higher-order structures is one promising strategy for antibiotic development. Since the determination of atomic-resolution crystal structures of the ribosome [46] and the discovery that many clinically significant antibiotics elicit their antibacterial effects by preferentially inhibiting bacterial protein synthesis over eukaryotic protein synthesis, bacterial ribosomes are as one of the most promising targets. At the same time, it has also become apparent that the overall structure, the tertiary folding pattern organizing functional regions, and the rRNA sequences in the functionally important domains are very similar between the eukaryotic ribosome (including human) and the bacterial ribosome [113]. How do small molecules

recognize a specific binding site within a large ribonucleoprotein complex, such as the ribosome? Shedding light on antimicrobial activity at the molecular level is essential to answer this question.

Generally, there are two classes of antibiotics, broad spectrum and narrow spectrum [114, 115]. Antimicrobial effects of the broad-spectrum antibiotics range from Gram-positive to Gram-negative bacteria; whereas, effects of the narrow-spectrum antibiotics are limited to the same phylogenetic group [114, 115]. The specificity in the narrow-spectrum antibiotics renders them less susceptible to antibiotic resistance, and they display lower side effects compared to the broad-spectrum antibiotics [114, 115]. There are three types of antibiotics based on their binding sites in the ribosome; 1) the decoding-site antibiotics; 2) PTC and exit tunnel antibiotics; and 3) other types, including those that target translation-related protein factors (Figure 1.15). Antibiotics are further classified into each group based on their chemical structures.

1.5.1. Peptidyl-transferase center- and exit-tunnel-targeting antibiotics

The PTC contains one of the key functional domains for ribosome translation (see Section 1.2.), so it is not surprising that several naturally occurring antibiotics target PTC to inhibit bacterial protein synthesis. These antibiotics include macrolide, lincosamide, and streptogramin (MLS) antibiotics [116, 117]. Among these, the macrolide-class of antibiotics are clinically the most important. The macrolide-class antibiotics are naturally occurring polyketide compounds. The basic structure of the macrolides contains a 14-, 15-, or 16-membered macrolactone ring that has a saccharide substituent at position 5 (Figure 1.15). In crystal structures, the macrolides interact with the exit tunnel adjacent to the PTC [118-122]. In most case, the saccharide substituent at position 5 of the macrolactone ring reaches the PTC to make direct molecular interactions with 23S rRNA. This binding results in steric blocking of the exit tunnel, which in turn inhibits entrance of the growing nascent peptide and causes premature dissociation of the peptidyl-tRNA from the ribosome at a very initial step of translation [123-125]. Dissociation of the premature peptidyl-tRNA from the ribosome causes cells to deplete free tRNAs as a result of accumulation of premature peptidyl-tRNAs in the tRNA pool, resulting in cell toxicity [126-128].

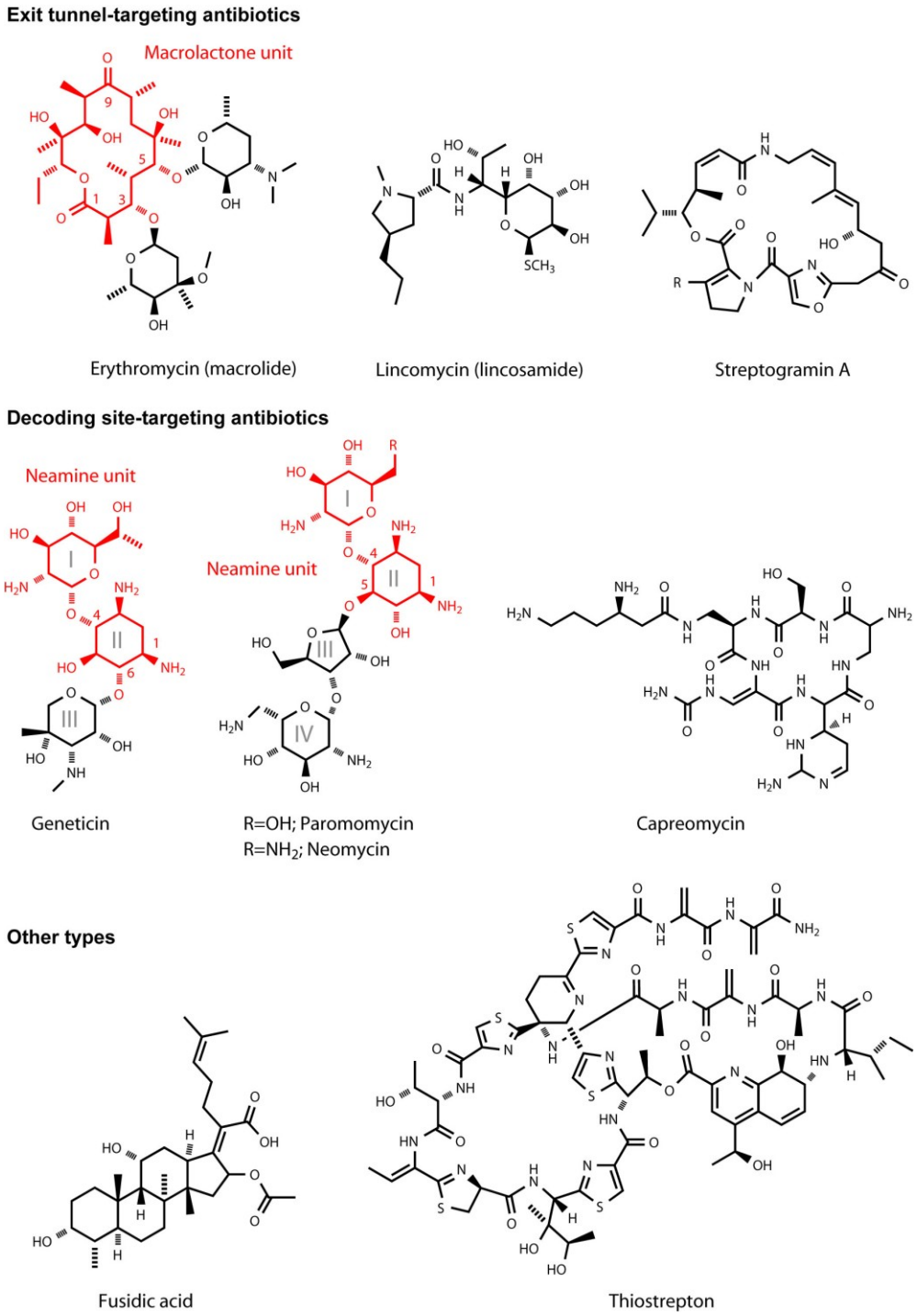

Figure 1.15. Chemical structures of the PTC and exit-tunnel targeting, decoding-site targeting, and other type of antibiotics are shown. For the PTC/exit tunnel and decoding-site-targeting antibiotics, the important common motifs are shown in red.

The binding sites of MLS drugs are overlap with each other; therefore, their mode of action is proposed to be the same.

1.5.2. Decoding-center-targeting antibiotics

The aminoglycoside-class of antibiotics have been clinically important tools for a long period of time; however, the outbreak of antibiotic-resistant pathogens encourages us to understand the underlying principles of their detailed bactericidal mechanisms. Aminoglycosides suppress ribosome protein synthesis by disrupting the tRNA-selection process [129], inhibiting tRNA/mRNA translocation [130], and suppressing ribosome recycling [131]. Aminoglycosides are composed of a highly conserved 2-deoxystreptoamine (2-DOS) subunit, which has 1,3-diamino residues and several hydroxyl groups, and typically connected to several types of aminosugar components (Figure 1.15). The central scaffold of aminoglycosides has been studied extensively in order to design aminoglycoside-based, semi-synthetic and unique antibiotics because of the capability of this class to bind RNA strongly. Furthermore, the mode of aminoglycoside interaction with the ribosome has been explored intensively to target site selectivity and specificity.

The binding site of the aminoglycosides neomycin, paromomycin, gentamicin, and kanamycin on the bacterial ribosome was first determined biochemically; they were shown to interact with h44 of the 30S subunit within the decoding center [132]. Later, geneticin, paromomycin, and apramycin were found to interact with the decoding site of the 30S subunit as analyzed by using NMR spectroscopy [133, 134] and X-ray crystallography [116, 135-137]. In these structure studies, it was revealed that aminoglycosides interact with the conformationally distorted h44 of the 30S subunit through rings I and II (Figure 1.15), and induce or stabilize an extrahelical conformation of residues A1492 and A1493. Both A1492 and A1493 are essential residues for initial tRNA selection and undergo structural changes into flipped-out conformations upon cognate aa-tRNA binding to the decoding center [8, 9]. Similar base orientations of h44 in the cognate tRNA-bound ribosome complex and the aminoglycoside-bound ribosome led to the proposal that aminoglycosides stabilize the h44-mRNA-tRNA complex, which causes decoding errors, stop-codon readthrough, and/or tRNA/mRNA translocation abortion [8, 9].

In addition to the h44-aminoglycoside interaction, a crystallography study revealed that neomycin, paromomycin, and gentamicin also interact with H69 of the 50S subunit [138]. These aminoglycosides contact residues around C1920-C1925 and G1906 of the H69 stem region through rings I and II. In the ribosome recycling step, RRF•EF-G complex formation causes disruption of the intersubunit bridges and accelerates subunit dissociation by pushing H69 away from the subunit interface [138-142]. Since aminoglycoside-H69 interactions are believed to stabilize the H69 conformation in the intersubunit bridge-forming state, it has been suggested that these interactions disrupt the RRF-mediated movement of H69, which results in inhibition of ribosome recycling [138].

Tuberactinomycin-family cyclic-peptide antibiotics, viomycin and capreomycin, were recently found to bind at the interface of the ribosomal subunits and interact with H69 of the 50S subunit and h44 of the 30S subunit simultaneously [143]. Viomycin was the first peptide antibiotic identified in this family; however, the second-generation drug capreomycin is the only member being clinically used for *Mycobacterium tuberculosis* infections [88]. Such peptide antibiotics are proposed to inhibit ribosome translocation by stabilizing the A-site tRNA-binding interaction, while allowing EF-G binding and GTP hydrolysis [144, 145].

1.5.3. Other antibiotics

The GTPase-associated center of 23S rRNA is also reported to be a target site for a thiopeptide antibiotic thiostrepton (Figure 1.15). Although no ribosome crystal structure complex with thiostrepton is available to date, mutagenetic, biochemical, and structural studies indicate that this drug interacts with the ribosomal protein L11 and residues A1067 and A1095 of 23S rRNA [146-148]. Thiostrepton allows GTP hydrolysis on EF-G, but interferes with the subsequent EF-G conformational change by inhibiting the release of inorganic phosphate (Pi), resulting in inhibition of translocation [149, 150]. Thiostrepton also blocks EF-G binding to the ribosome [151]. Thus, thiostrepton targets the EF-G-catalyzed ribosome translocation stage. Fusidic acid is similar to thiostrepton in terms of targeting EF-G function during the ribosome translocation. The binding site of fusidic acid was found in a crystal structure that amino acid residue T84 makes a

direct contact with fusidic acid [152]. In contrast to thiostrepton, which prevents stable binding of EF-G to the ribosome, fusidic acid stabilizes EF-G on the ribosome by trapping the EF-G•GDP•ribosome complex after GTP hydrolysis [153]. As a result, EF-G does not dissociate from the POST ribosome complex, resulting in inhibition of the next aa-tRNA selection step.

1.5.4. Molecular mechanisms of antibiotic resistance

Antibiotics target different cellular components. For instance, MLS and aminoglycoside drugs target bacterial ribosomes to inhibit protein synthesis, β-lactam antibiotics inhibit synthesis of the peptidoglycan layer of the bacterial cell wall, polypeptide antibiotics destabilize the outer membrane of Gram-negative bacteria, and fluoroquinolones interfere with DNA replication [154, 155]. Once antibiotics appeared in medicine, antibiotic resistance began to be reported soon after. The widespread use and inappropriate over-usage of antibiotics are considered the major cause of the outbreak of antibiotic-resistant pathogens [156]. The rapid acquisition and spread of antibiotic-resistant phenotypes is attributed primarily to horizontal gene transfer between different species [157].

Understanding specific mechanisms of antibiotic resistance is essential for the development of new classes of drugs to combat resistant pathogens. There are three types of resistance mechanisms [158]. The first mechanism involves export of toxic compounds to the outside of cells (efflux system) [159, 160]. Since effective antibiotic activity requires a certain intracellular drug concentration, antibiotics need to accumulate inside bacterial cells. If bacteria pump out unwanted antibiotics faster than they accumulate, antibiotic activity will be lowered and bacteria will keep growing. The second strategy involves modification of antibiotics eznymatically into inactive forms. The well-known example is penicillin deactivation by an enzyme, β-lactamase, in penicillin-resistant bacteria [161]. The β-lactamase attacks the β-lactam ring of penicillin, which is responsible for the antibiotic activity, to produce the inactive form β-lactam ring-open penicilloic acid. Aminoglycoside-resistant bacteria also have a modifying mechanism to deactivate drugs [162]. Enzymatic *N*-acetylation, *O*-phosphorylation, or *O*-adenylation of aminoglycoside antibiotics results in their considerably lower binding affinity to rRNA [158, 162, 163]. The last scenario of

antibiotic resistance involves alteration of the antibiotic target site. For instance, MLS drugs target the PTC of 23S rRNA. A base modification of position 2058 of 23S rRNA by methyl transferase Erm confers considerable resistance to members of the MLS group by lowering the drug binding affinity for the modified site; however, such modification does not alter the protein synthesis activity of the ribosome [164]. In the case of aminoglycoside antibiotics, methylation of the N1 position of A1408 or the N7 position of G1405 confers resistance to the neamine-class or geneticin-class aminoglycosides, respectively [165, 166]. Besides the RNA modification-based antibiotic resistance, a site-specific point mutation of rRNA is enough to gain antibiotic resistance [167-170]. The A1408G mutant 16S rRNA is the most relevant mutation clinically [170], which confers considerable resistance to 6'-ammonium-group-substituted aminoglycosides, such as neomycin [167, 169, 171]. Structure and model RNA studies indicate that the A to G mutation at 1408 interferes with docking of ring I of the neomycin-type aminoglycosides (6'-NH_3^+) resulting in the low affinity of the antibiotics for the ribosome [172]. Designing new classes of drugs to combat antibiotic-resistant pathogens requires an even deeper understanding of such drug-resistance mechanisms at the molecular level (see also Section 1.3. for antibiotic drug resistance due to RNA modification).

1.6. Specific aims of the dissertation research

According to the central dogma, protein biosynthesis in the cell is carried out by the ribosome and, importantly, the overall mechanisms of this process are highly conserved throughout all kingdoms of life. The ribosome is composed of two main units, the large ribosomal subunit (50S in bacteria) and the small ribosomal subunit (30S in bacteria), and these units are made up of rRNAs and proteins. Although several high-resolution crystal structures of the ribosome are available, many of the molecular details and roles of rRNAs and ribosomal proteins are still undefined, especially in solution models. The functional relationship of modified nucleotides (*e.g.*, pseudouridine) to ribosome activity is one such enigma.

In my dissertation research, the focus was on helix 69 (H69) of the 50S subunit. The specific aims are outlined next. (1) It is indicated from crystal structures and model studies that H69 is a

structurally dynamic RNA stem-loop component of the ribosome, which forms variable conformational states, but H69 dynamics in the ribosome within the cell are still unclear. Understanding the conformational dynamics of H69 will lead us to further understand the mechanism of ribosome translation. (2) RNA in nature is further modified at specific sites in order to gain extra functions or to expand the genetic code; however, the detailed biological significance of modified bases in rRNA with respect to ribosome activity is still unclear. Helix 69 contains three modified bases in its narrow loop, which makes it a good motif to evaluate the influence of modified bases on RNA conformational dynamics, and subsequently to understand the unknown roles of modified bases in the ribosome. (3) Helix 69 is expected to be a potential drug target site based on its unique higher-order RNA structure and its pivotal role in ribosome protein synthesis at multiple stages. Helix 69 is actually found to have direct interactions with several aminoglycoside-class antibiotics. Efforts to understand the mode of action of drug-H69 interactions are important because the rise of drug resistance in bacteria demands the development of unique antibiotics to combat antibiotic-resistant pathogens.

My goal throughout the dissertation studies was to understand the biological function of H69 dynamics (aim #1) and modified bases (aim #2), followed by gaining insight into the design of unique antibiotics targeting the H69 region (aim #3).

Chapter 2

Probing conformational states of H69 in 50S subunits

(This chapter is adapted from Sakakibara, Y. and Chow, C.S., *J Am Chem Soc* **2011**, *133*, 8396.)

2.1. Abstract

The movement of the small ribosomal subunit (30S) relative to the large ribosomal subunit (50S) during translation is widely known, but many molecular details and roles of ribosomal RNA and proteins in this process are still undefined, especially in solution models. The functional relationship of modified nucleotides to ribosome activity is one such enigma. To better understand ribosome dynamics and the influence of modified nucleotides on such processes, the focus of this work was helix 69 of 23S rRNA, which contains three pseudouridine residues in its loop region. Ribosome probing experiments with dimethylsulfate revealed that specific base accessibilities and individual nucleotide conformations in helix 69 are influenced differently by pH, temperature, magnesium, and the presence of pseudouridine modifications.

2.2. Introduction

In all living organisms, protein biosynthesis is carried out by the ribosome. Interestingly, the protein biosynthesis core domain is mainly composed of ribosomal RNAs (rRNA), which are supported and enhanced by ribosomal proteins (r-protein) [46]. In addition, nucleoside modifications are clustered within functionally important core domains when they are mapped on three-dimensional structures of the ribosome [72]. Although numerous high-resolution crystal structures of the ribosome have been reported, details of ribosome dynamics in solution models are still ambiguous. Furthermore, the biological functions of modified bases that need to be understood for future drug discovery efforts are still unclear.

Helix 69 (H69) in the large ribosomal subunit (50S) is a component of intersubunit bridge B2a (B2a) together with helix 44 (h44) from the small ribosomal subunit (30S) [5, 46, 47]. It contains three modified nucleosides within a narrow region [106, 173] (Figure 2.1a). Tight interactions between H69 and h44 are thought to be important to maintain normal ribosome activity, such as

ribosome association [103, 174], translational fidelity [94, 95, 175], ribosome recycling [99, 176], and possibly accurate ribosome translocation [177]. H69 would be required to obtain conformational flexibility as a central pivot in order to adapt to the twist-like movement of the ribosome, because the B2a interaction is believed to be maintained throughout ribosome translation. Indeed, conformational differences in H69 are observed in the crystal structures from different ribosome preparations [178]. Our previous biophysical model studies using small RNA oligonucleotides representing H69 containing complete base modifications showed conformational dynamics around the loop region that could be induced by changing pH from pH 5.5 to 7.0; under lower pH conditions (pH 5.5), H69 formed a flipped-in conformation ("closed"), whereas it formed a flipped-out conformation under higher pH conditions (pH 7.0) ("open") [109] (Figure 2.1b). On the other hand, no conformational change was observed in unmodified H69 RNAs upon changes in pH. Furthermore, ^{1}H NMR studies showed base-stacking rearrangements in the H69 loop involving pseudouridines [110], suggesting a unique function for these modifications in the ribosome.

Our goal for this study was to determine whether different conformational states of H69 exist on

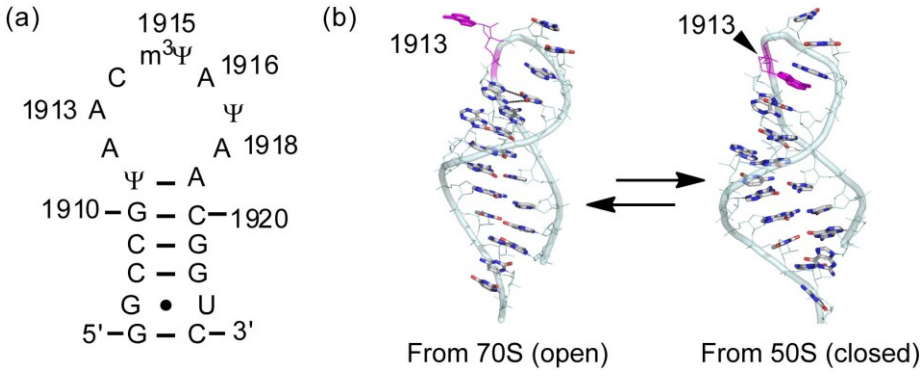

Figure 2.1. (a) *E. coli* H69 RNA sequence (Ψ is pseudouridine and $m^3\Psi$ is 3-methylpseudouridine). (b) H69 "open" conformation from *E. coli* 70S ribosomes (PDB: 3I1P) and "closed" conformation from *D. radiodurans* 50S subunits (PDB: 1NKW). Previous studies on H69 hairpins [111] suggested that the "open" conformation is formed at pH 7.0 and the "closed" conformation is formed at pH 5.5.

full-length 23S rRNA within the context of 50S subunits, and to understand how these states are influenced by solution conditions. Dimethylsulfate (DMS) probing of positional differences (*i.e.*, exposure or protection) of adenine residues (N1 position) in H69 under different pH, magnesium, and temperature conditions was used to provide information about the relative conformations of nucleotides within H69. Details of the experiments are provided in the materials and methods section (2.4).

2.3. Results

2.3.1. Confirmation of uniform dimethylsulfate (DMS) reactivity under different pH conditions

DMS reactivity under various solution conditions was first confirmed to be pH independent by analyzing denatured 23S rRNA (Figure 2.2). To disrupt secondary structures of isolated 23S rRNA, probing was performed in the presence of 4 M urea, 100 mM Na^+, and 1 mM EDTA with different pH buffer conditions. Reverse transcription stop sites generated from DMS reactions were determined by using a primer binding at nucleotides 1929–1948 followed by denaturing gel electrophoresis. DMS probing for both H69 (Figure 2.2a) and the H68 region (Figure 2.2b) under denaturing condition showed no difference in DMS reactivity at pH 5.5 and 7.0, which is consistent with previous results [179, 180].

2.3.2. DMS probing of H69 in isolated wild-type 50S subunits

Probing pH-dependent H69 conformational change in the wild-type 50S subunit ("on ice")

Since DMS reactivity was confirmed to be independent from solution pH conditions, DMS reactivity was then analyzed on structured 23S rRNA in 50S subunits. DMS probing of wild-type *E. coli* 50S subunits under "on ice" and 1 mM Mg^{2+} conditions revealed clear conformational changes in H69 that were induced by pH; reduced reactivity of DMS at residues A1913 and A1916 (relative changes of 42 and 49%, respectively) at pH 5.5 compared to pH 7.0 was observed, suggestive of reduced exposure to solvent (Figure 2.3a and 2.3c (left panels); blue bars). These changes were independent of salt type (K^+ or NH_4^+).

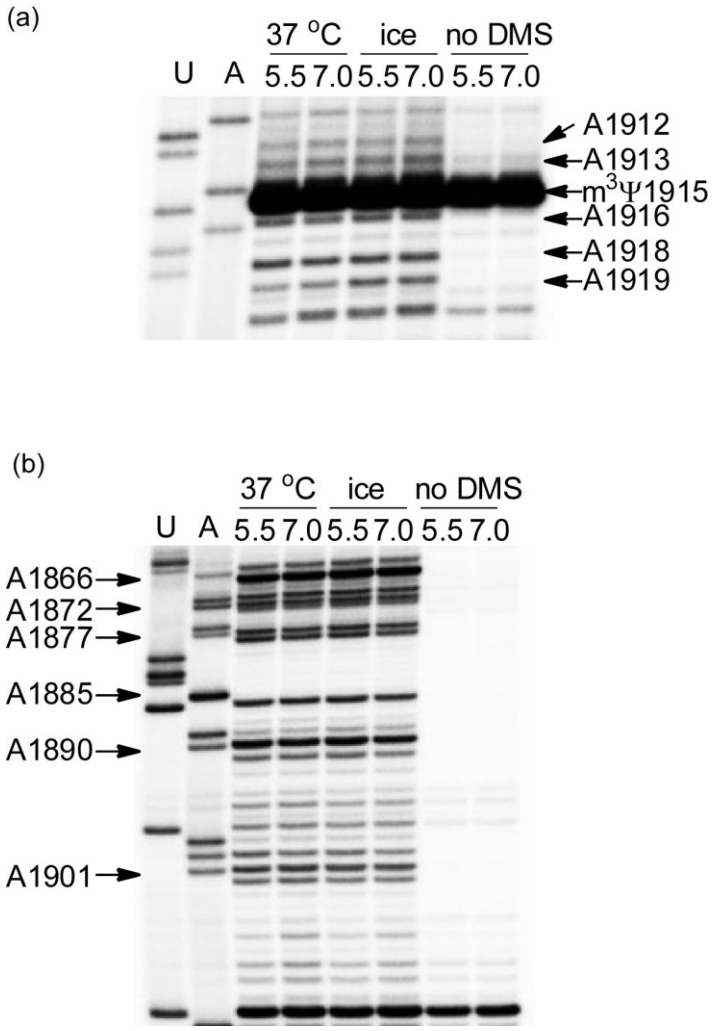

Figure 2.2. Autoradiograms of DMS probing analysis under different pH conditions. (a) H69 region from the denatured wild-type 23S rRNA is shown. Probing performed in 80 mM HEPES (pH 7.0) or MES (pH 5.5), 100 mM NaCl, 1 mM EDTA, 4 M urea, and each DMS condition. RNA was denatured by heating at 95 °C for 3 min followed by quick chilling on ice and immediately carrying out the reaction. (b) The H68 region from the denatured RluD(–) 23S rRNA is shown. Probing conditions were the same as wild-type, but performed with urea. The reason that RluD(–) 23S rRNA was used is that the naturally occurring modification at 1915 ($m^3\Psi$) in wild-type H69 strongly stops reverse transcription and inhibits analysis in the H68 region; however, it should be noted that the same result was obtained when using wild-type 23S rRNA for the denaturing condition DMS probing.

In contrast, little or no reduction in DMS reactivity was observed at A1912 and A1918 (22 and <10%, respectively) upon lowering of pH. The overall reactivity at A1912 was, however, less than that of A1918 at both pH values, indicating less solvent exposure at either condition. Similarly, quantitative analysis of the gel data did not reveal any major changes at A1918 when the Mg^{2+} concentration was increased from 1 to 6 mM, whereas the A1913 conformational change towards the "closed" conformation was suppressed (<20% reduction in reactivity as pH is lowered) (Figure 2.3a and 2.3c (right panels); blue bars). This result is consistent with previous biophysical model studies [109], and this was further confirmed (see Chapter 4).

The effects of Mg^{2+} on the A1913 conformational change may be due to competitive metal-ion binding to a site in the H69 loop, which could reduce flipping of residue A1913 to the "closed" conformation at lower pH. Residue A1912 is even less exposed at higher Mg^{2+} concentrations, and pH-dependent conformational changes at this position are minimal at 6 mM Mg^{2+} (Figure 2.3a and 2.3c (right panels); blue bars), which is consistent with the formation of a reverse-Hoogsteen base pair with Ψ1917, as observed in some crystal structures [5, 45-47, 99, 176-178]. In contrast, A1918 in the loop remains exposed at both sets of "on ice" conditions.

Probing pH-dependent H69 conformational change in the wild-type 50S subunit (37 °C)

DMS probing of 50S subunits was also carried out at physiological temperature (37 °C) (Figure 2.3b and 2.3c; red bars). DMS reacts faster at 37 °C than at 0 °C, which affects the solution pH due to byproduct formation; therefore, the DMS concentration was lowered to 10 mM and a shorter reaction time (20 min) was employed. As with the "on ice" conditions, reactions at 37 °C in 1 mM Mg^{2+} revealed A1913 protection at pH 5.5 and exposure at pH 7.0. In contrast, A1916 showed much different behavior than it did in the "on ice" experiments; specifically, it showed high reactivity at pH 7.0 as observed at low temperature, but the reactivity was not reduced at pH 5.5 (Figure 2.3c (left panel); red bar). This result is consistent with NMR experiments on hairpin RNAs in which raising the temperature reduced base-stacking interactions in the loop region at high pH, but had diminished effects at low pH, as well as different effects on A1916 and A1913 [109, 110, 181].

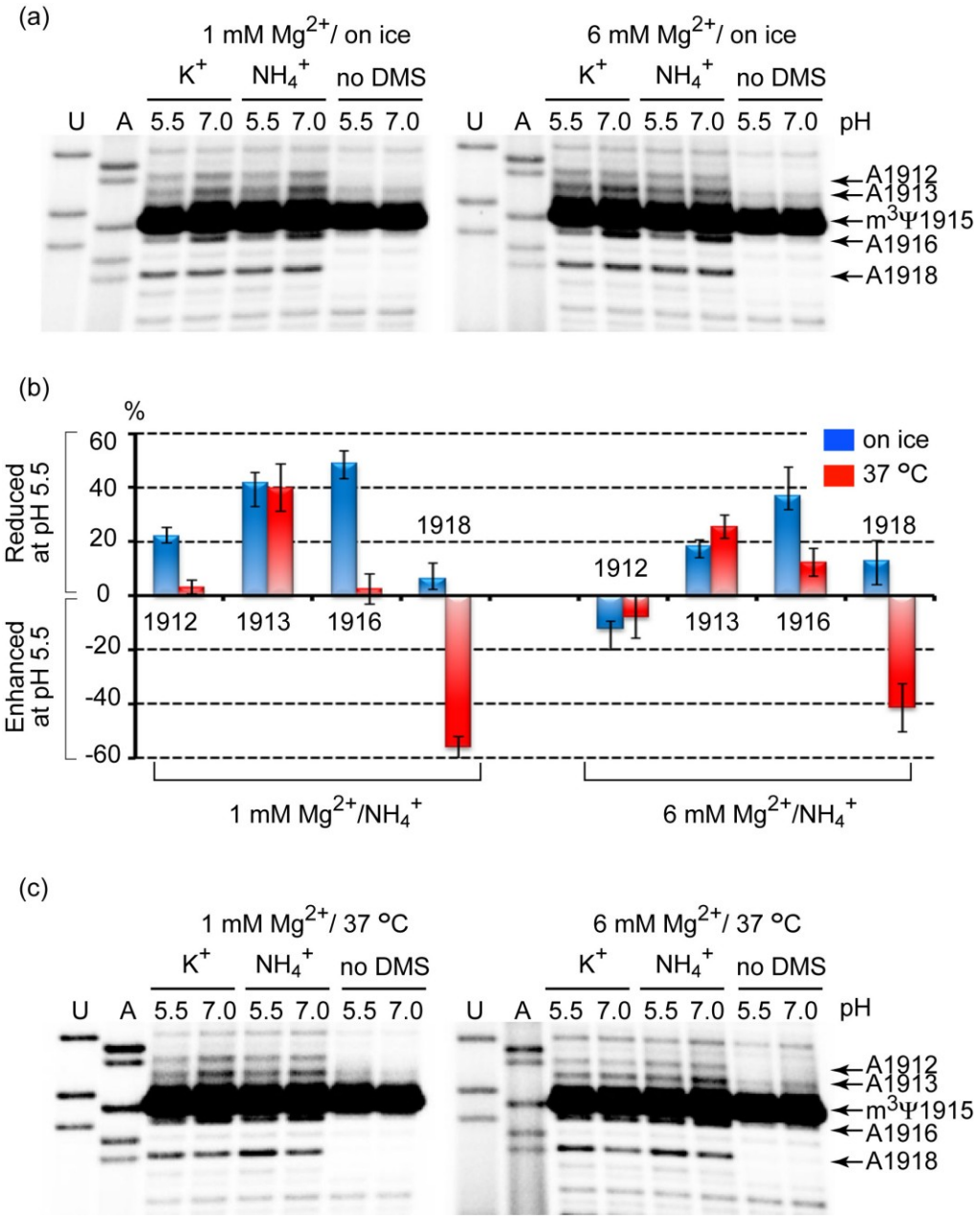

Figure 2.3. DMS probing on wild-type *E. coli* 50S subunits. (a) Autoradiograms for "on ice" conditions (50 mM DMS/2 h). DMS sites were determined by reverse transcriptase stop sites. (b) Percent change of reactivity at pH 5.5 relative to pH 7.0. Data were normalized to a non-specific stop site (1920). The strong stop site at position 1915 occurred due to N3 methylation. Positive values indicate reduced reactivity and negative values reveal enhanced reactivity at pH 5.5 relative to pH 7.0. (c) Autoradiograms for 37 °C reactions (10 mM DMS/20 min). Positions corresponding to modified sites are indicated on the right side of the gels.

Possible existence of an energetic barrier for A1918 positioning

At 37 °C, the behavior of residue A1918 was clearly different than at lower temperature. Unlike the other adenosine residues in H69, A1918 was more reactive (increased exposure to DMS) at low pH and less reactive (protection from DMS) at high pH (55% and 40% enhanced reactivity at pH 5.5 relative to pH 7.0 in 1 mM and 6 mM Mg^{2+}, respectively) (Figure 2.3c; red bar). To rule out the possibility that lower DMS concentrations or shorter reaction times at 37 °C could result in different reaction profiles at A1918 from that of "on ice" conditions, two additional probing conditions were employed (10 mM DMS, 2 h, "on ice" and 50 mM DMS, 1 h, "on ice"). Neither condition led to any changes in the reaction profile at A1918. These results lead us to propose temperature-induced conformational changes of H69 that differ from the pH-induced changes (Figure 2.4).

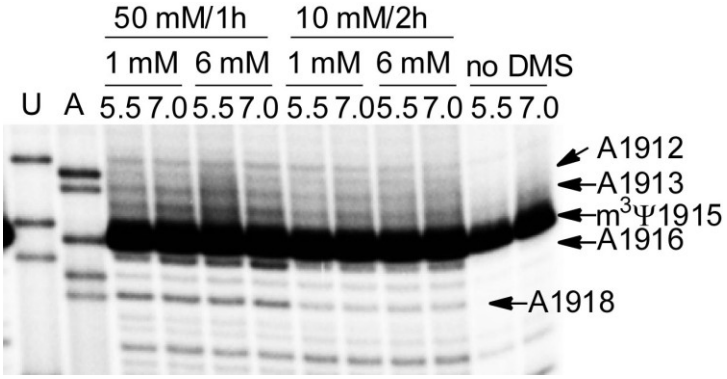

FIgure 2.4. Autoradiogram of pH-independent DMS probing analysis with short reaction times and lower DMS concentrations under "on ice" conditions in order to confirm the A1918 conformational change observed at 37 °C. Positions corresponding to chemically probed sites are indicated on the right side of the gel. In short reaction times, data show different reactivity at A1916 between different pH conditions; whereas, A1918 shows no difference in its reactivity. At lower DMS concentrations, it is not so clear that H69 undergoes conformational changes; however, it can be said that A1918 does not change its reactivity.

Our previous thermal melting analyses using synthetic oligonucleotides showed that H69 forms a slightly more stable stem-loop structure at pH 5.5 (T_m: 66.3 °C, ΔG^o_{37}: –5.2 kcal/mol) compared to pH 7.0 (T_m: 65.1 °C, ΔG^o_{37}: –4.7 kcal/mol) [109]. Taking into account the model studies, temperature-induced H69 fluctuations in the 50S subunit could be explained as follows; at low temperatures, A1918 cannot overcome the small energetic barrier to stack inside the loop; whereas at higher temperatures the barrier can be overcome in order for A1918 to move inside of the H69 loop. It is quite possible that within the ribosome, association or interactions with other ribosome components could shift the equilibrium and relative nucleotide positions of H69. This dynamic behavior and range of nucleotide conformational states is not surprising given the number of biological roles proposed for H69 [94, 95, 103, 174, 182].

To further investigate the energetic barrier around A1918, temperature-dependent DMS probing was performed as well (Figure 2.5a and b). In this assay, cacodylate buffer was employed because both HEPES and MES buffers show temperature-dependent pH changes. To unify the probing conditions, 100 mM NH_4Cl, 6 mM Mg^{2+}, 10 mM DMS, and 20 min reaction times were used for all reaction temperatures. Quantified data show that the same DMS reactivity of A1918 was observed around 15 °C at different pH conditions, but a 34% difference in reactivity (reduced at pH 7.0 compared to pH 5.5) when the temperature increased to 37 °C (Figure 2.5b), suggesting a different energetic barrier for base flipping at different pH conditions. Thus, although the relative position of A1918 in H69 is still unknown, these data reveal that A1918 positioning would require thermal energy to overcome this energetic barrier.

DMS probing was also performed on isolated 23S rRNA to gain insight into the influence of ribosomal proteins on H69 conformation (Figure 2.5c). Isolated rRNAs contain 23S and 5S rRNA but not any ribosomal proteins. To fold into the proper secondary structure, the isolated rRNA was denatured and renatured. Because 23S rRNA was very sensitive to divalent metal ion-catalyzed non-specific degradation when it was heated for denaturation, the isolated 23S rRNA was first denatured without Mg^{2+}, then after that, refolded into structured 23S rRNA in the presence of Mg^{2+} at 37 ^oC. By using the refolded 23S rRNA, DMS probing was performed under both on ice and 37 ^oC conditions. Unexpectedly, the A1918 conformational differences under

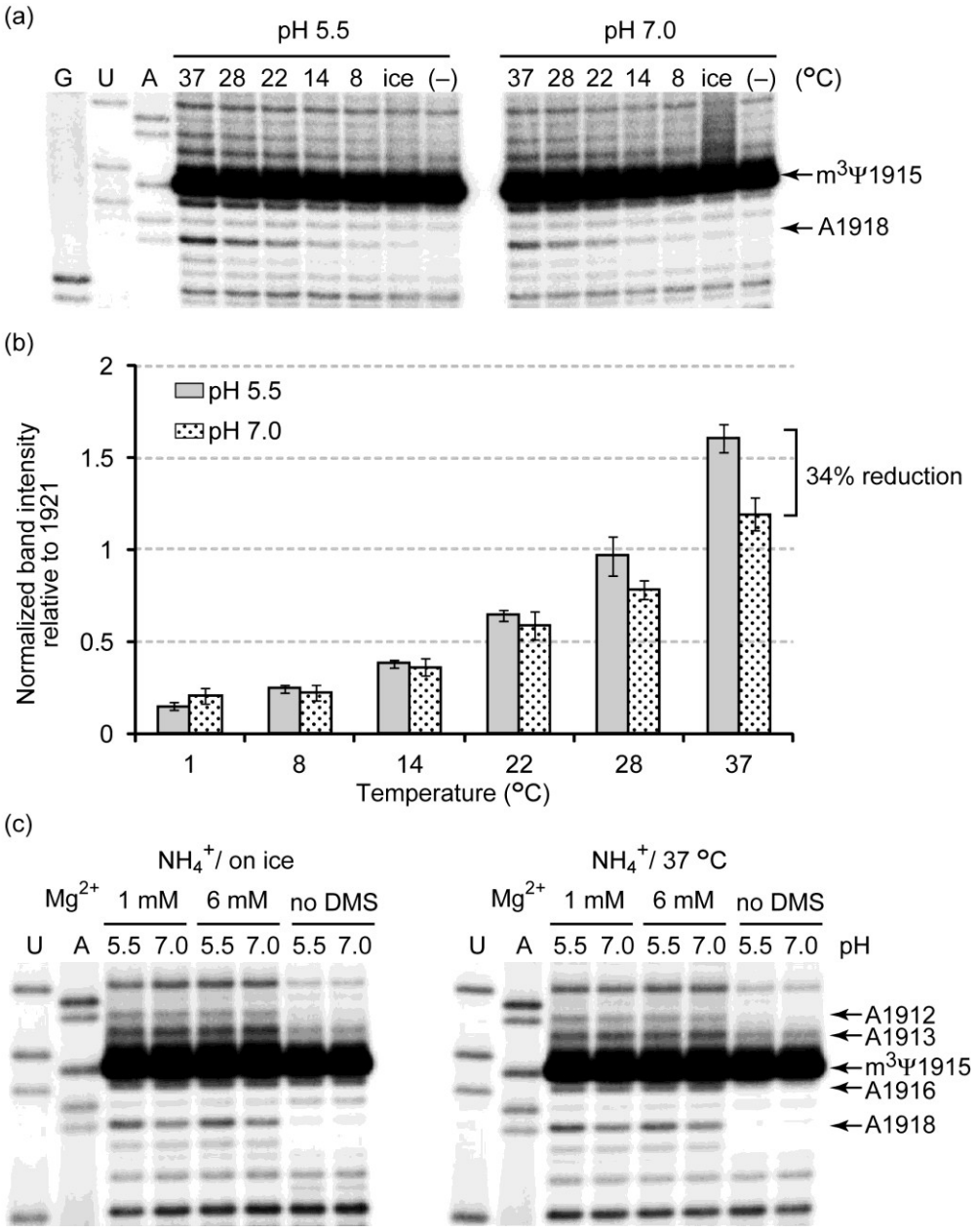

Figure 2.5. (a) Autoradiograms for temperature-dependent DMS probing analysis specific for position A1918. In this experiment, potassium cacodylate buffer (instead of MES or HEPES buffers) was used to examine all conditional probing analyses simultaneously since cacodylate buffer is temperature-insensitive. (b) Normalized band intensities of pH 5.5 and pH 7.0 are shown. Data were normalized as mentioned in Figure 3. (c) Autoradiograms for DMS probing analysis of isolated 23S rRNA under on ice (left) and 37 °C (right) conditions. Probing conditions were the same in the 50S subunit probing experiments. Probing conditions were 80 mM cacodylate buffer, 100 mM NH_4Cl, 6 mM Mg^{2+}, 10 mM DMS, and 20 min reaction time.

different pHs were observed in both "on ice" and 37 °C conditions in probing assays of isolated 23S rRNA (Figure 2.5c). The A1913 conformational change was diminished in isolated 23S rRNA compared to 50S subunits. These results could indicate that ribosomal protein-associated rRNA folding affects H69 structure and dynamics, although no H69-ribosomal protein interaction can be observed in crystal structures. However, it is difficult to exclude the possibility that isolated 23S rRNA does not contain completely folded structural motifs even after the refolding process *in vitro*. Thus, it will be interesting to investigate a possible function of ribosomal protein-associated rRNA folding in H69 structure and dynamics. Our attention was turned, however, to the 50S subunits, which contain r-proteins.

A1919 which is predicted to be an accessible residue in the crystal structure is less reactive toward DMS

In the case of A1919, the base was unreactive towards DMS under all conditions tested, even though it appears from x-ray crystal structures to have its N1 position exposed (Figure 3d). Since DMS reactivity is not sensitive to base-stacking formations unlike DEPC probing, it can be excluded that A1919 is involved in a specific base-stacking interaction with neighboring bases. Imino proton NMR analysis of the model H69 stem-loop RNA indicated that A1919 forms a base

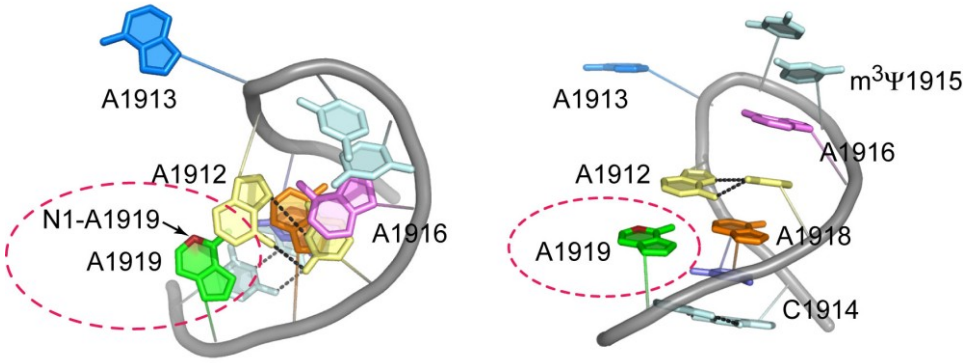

Figure 2.6. The crystal structure of H69 from the 70S ribosome is shown (PDB: 3I1P). The structures of H69 indicate exposure of the position N1 at A1919 (red atom) from the loop and stem region of H69. It is proposed that this A1919 orientation projects this base toward h44 of the 30S subunit to form the bridge B2a. The potential formation of a reverse-Hoogsteen interaction between A1912 and Ψ1917 is shown by the black dotted lines.

pair with Ψ1911 [5, 109, 110, 181], which is consistent with the lack of DMS reactivity in 50S ribosomes. Genetic studies with mutations at A1919 show lower translation activity and abnormal 70S formation [94], suggesting that A1919 positioning is important for these ribosome functions [5, 45-47, 99, 176-178].

2.3.3. DMS probing for H69 of isolated H69 pseudouridine-deficient 50S subunit

Ψ modifications in H69 influence on the conformational dynamics

To understand the influence of modified bases (Ψ1911, m^3Ψ1915, Ψ1917) on H69 conformational states, 50S subunits from Ψ synthase-deficient *E. coli* strains (RluD(–) 50S) [83] were employed in DMS-probing experiments. RluD(–) 50S subunits contain U1911, U1915 or m^3U1915, and U1917 in place of Ψ at the corresponding positions in wild-type ribosomes. At position 1915, a strong nonspecific primer extension stop was still observed (Figure 2.7a) due to partial methylation at U1915 [183]. The DMS-probing analysis of RluD(–) 50S subunits showed little pH-induced change (<10%) at A1913 at 37 °C (Figure 2.7a and 2.7b; yellow bars). Although there was still a small pH-induced conformational change at A1913 under "on ice" conditions (21% reduction of exposure at pH 5.5) (Figure 2.7b; green bars), the influence of the Ψ residues on A1913 exposure was clearly observed, especially under 37 °C conditions. At low Mg^{2+}, the same temperature-dependent change in exposure at A1918 was observed in RluD(–) 50S subunits as with wild-type ribosomes, but the effect was diminished by 30% (Figures 2.3b and 2.7b; red and yellow bars). At high Mg^{2+}, the same level of enhancement in DMS reactivity at A1918 was observed at pH 5.5 as with wild-type 50S subunits, suggesting that some effects due to Ψ deficiency in 23S rRNA may be overcome by Mg^{2+} binding.

The most noticeable difference between the Ψ-deficient and wild-type 50S ribosomes occurs at position 1916. The conformational change identified in wild-type 50S subunits under "on ice" conditions is almost completely diminished in RluD(–) 50S subunits. These results are also consistent with NMR and circular dichroism spectroscopic analyses that showed the influences of Ψs on base-stacking interactions in H69 around positions 1915-1917 [110]. In the model systems,

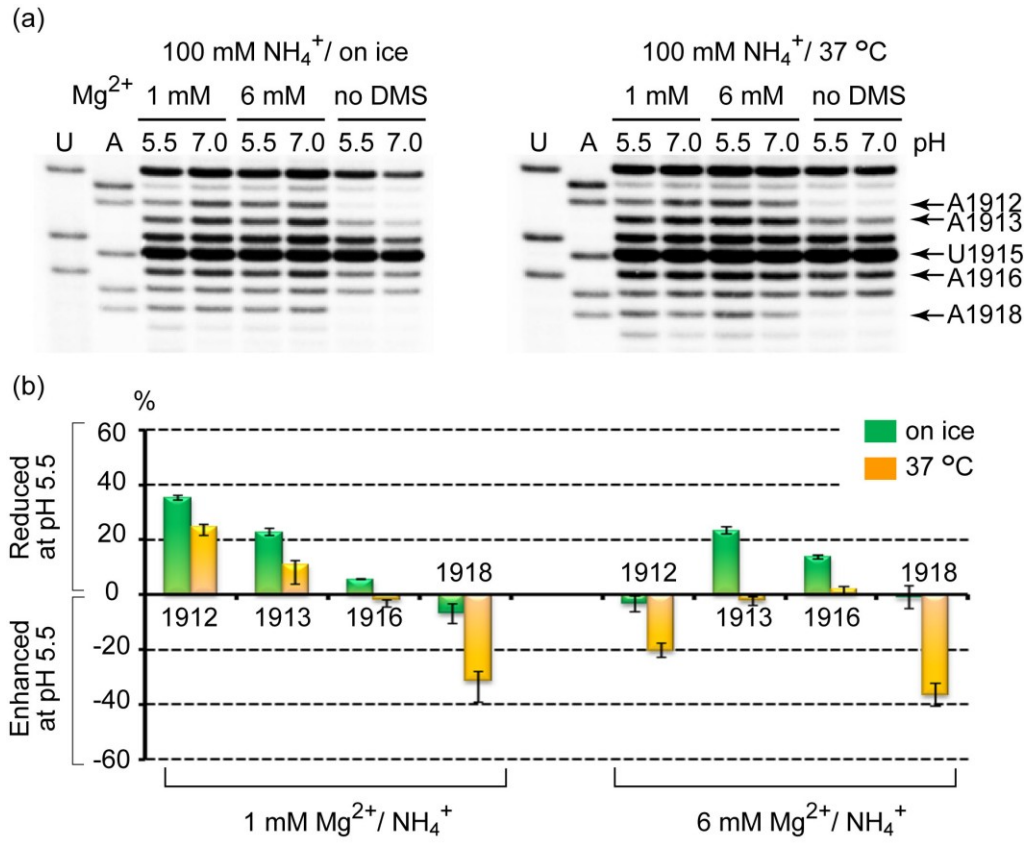

Figure 2.7. (a) DMS probing of RluD(–) 50S subunits under "on ice" (left) and 37 °C (right) conditions. Positions corresponding to DMS-modified sites are indicated on the right side of the gels. (b) Percent change of probing efficiency on RluD(–) 50S subunits at pH 5.5 relative to pH 7.0.

base-stacking interactions in the H69 loop are less favored at high pH when Ψs are present. Similarly, the pH-dependent conformation changes at A1916 are diminished by as much as 40% in RluD(–) 50S subunits at low Mg^{2+} and 20% at high Mg^{2+} concentrations (compare Figure 2.3 and Figure 2.7).

Position A1912 appears to be more exposed in Ψ-deficient 50S subunits compared to wild-type ribosomes, which is also consistent with the model studies. In unmodified H69 hairpins, the loop-closing base pair (U1911-A1919) was not observed, which could influence the exposure of A1912 to solvent (and therefore DMS), although the exposure of A1919 in RluD(–) 50S subunits did not change.

2.3.4. Conclusions for probing conformational states of H69 in 50S subunits

DMS probing [184] and previous studies [109, 110] on model RNAs reveal that H69 is structurally dynamic and can exist in multiple conformational states in which the individual nucleotide positions vary. Pseudouridine modifications play a role in organizing the H69 structure. The probing results are supported by the fact that mutations (*e.g.*, A1916G) and Ψ-deficient ribosomes are both defective in ribosome assembly [94, 182]. The fact that some nucleotide positions remain constant is also likely important for ribosome function. For example, little or no variability is observed at residues A1912 and A1919, which have important functional roles. Mutations A1912G and A1919G both have strong growth phenotypes and inhibit translation [182]. The relative position of A1919 is still unclear because crystal structures do not show base-pair formation with this nucleotide (Figure 2.6), but an A1919-Ψ1911 pair is observed in solution NMR studies with model RNAs [109]. It is possible that 70S ribosome formation causes rearrangement of the H69 conformation, such that the position of A1919 is altered in crystal structures. Probing studies on 70S ribosomes have helped to clarify this discrepancy between the solution data and x-ray structures (see also Chapter 3).

In summary, DMS probing under different solutions conditions revealed that H69 within 50S subunits can exist in multiple conformational states and Ψ modifications play a role in regulation

of these states. A variety of H69 conformation states are expected to exist during translation and, at the same time, local nucleoside conformations of H69 are maintained during conformational changes at other positions, suggesting that point mutations, loss of modification, or ligand binding at this site could influence H69 conformation and result in disruption of this process. Such information will be useful for future antibiotic drug development, with specific targeting of these conformational states.

2.4. Materials and methods

The following materials were used: dimethyl sulfate (DMS) (Sigma-Aldrich), 2-(4-morpholino)-ethane sulfonic acid (MES) (Fisher Bioreagents), 4-(2-hydroxyethyl)-1-piperazine ethan sulfonic acid (HEPES) (Fisher Scientific), 2-mercaptoethanol (2-ME) (Sigma-Aldrich), ammonium chloride (NH_4Cl) (Sigma-Aldrich), magnesium chloride ($MgCl_2$) (Fisher Chemicals), potassium chloride (KCl) (Fisher Chemicals), sodium chloride (NaCl) (Fisher Chemicals), 2-amino-2-hydroxymethyl-propane-1,3-diol (Tris) (Fisher Bioreagents), lysogeny broth (LB) (Becton, Dickinson and Company), phenol-chloroform-isoamyl alcohol (25:24:1) (PCI) (Fisher Bioreagents), ImProm^{II} Reverse Transcriptase (RT) (Promega), adenosine 5'-triphosphate γ-^{32}P (^{32}P-ATP) (Perkin Elmer), polyacrylamide gel electrophoresis (PAGE), nuclease and proteinase free sucrose (MP Biomedicals), and urea +98% pure (Sigma-Aldrich), DNA primer for primer extension (5'-CGACAAGGAATTTCGCTACC-3', 20mer) (Sigma-Genosys).

The following buffers were used: cell lysate buffer: 20 mM HEPES-KOH (pH 7.5 on ice), 10 mM $MgCl_2$, 100 mM NH_4Cl, 4.6 mM 2-mercaptoethanol, 0.5 mM EDTA; ribosome buffer: 20 mM HEPES-KOH (pH 7.5 on ice), 6 mM $MgCl_2$, 30 mM NH_4Cl, 4.6 mM 2-mercaptoethanol; dissociation buffer: 20 mM HEPES-KOH (pH 7.5 on ice), 1 mM $MgCl_2$, 200 mM NH_4Cl, 4.6 mM 2-mercaptoethanol; ribosome subunit stock buffer: 20 mM HEPES-KOH (pH 7.5 on ice), 10 mM $MgCl_2$, 30 mM KCl; ribosome stock buffer: 20 mM HEPES-KOH (pH 7.5 on ice), 6 mM $MgCl_2$, 30 mM NH_4Cl; activation buffer: 20 mM HEPES-KOH (pH 7.5 at 37 °C), 6 mM $MgCl_2$, 100 mM NH_4Cl or 150 mM KCl; probing buffer (pH 5.5): 80 mM MES-KOH (pH 5.5 on ice or at 37 °C), 1 or 6 mM

$MgCl_2$, 100 mM NH_4Cl or 150 mM KCl; probing buffer (pH 7.0): 80 mM HEPES-KOH (pH 7.0 on ice or at 37 °C), 1 or 6 mM $MgCl_2$, 100 mM NH_4Cl or 150 mM KCl; DMS stop buffer: 3 M 2-mercaptoethanol, 1 M Tris-HCl (pH 7.5), 10 mM $MgCl_2$; refolding buffer: 10 mM HEPES-KOH (pH 7.5 at 37 °C), 100 mM KCl or 100 mM NH_4Cl; denaturing loading dye: 80% formaldehyde, 20% glycerol, 0.1% bromophenol blue, 0.1% xylene cyanol; and 0.5x gel running buffer: 45 mM Tris-HCl pH 8.3, 45 mM boric acid, 1.25 mM EDTA.

2.4.1. Isolation of 70S ribosomes and ribosomal subunits

Bacterial ribosomes were isolated and purified by performing a sucrose density gradient (Figure 2.8) [185]. In the sucrose density gradient, 30S, 50S, and 70S ribosomes loaded on the top of a sucrose layer migrate at different rates during ultracentrifugation. The migration rate of a molecule is proportional to its molecular mass and the sucrose density level used in the system. For example, 30S subunits migrate slower than 50S subunits, and 50S subunits migrate slower than 70S ribosomes. For ribosome isolation, usually a 10-30% sucrose gradient is used to separate 70S ribosomes and each subunit in different buffer components. To separate 30S and 50S subunits, all buffer components used for the sucrose density gradient should have low magnesium concentrations (1 mM) and relatively high salt concentrations (200 mM NH_4Cl) to facilitate subunit dissociation (ribosome dissociation buffer); whereas, they should have high magnesium concentrations (>6 mM) and low salt concentrations (30 mM NH_4Cl) to isolate the tightly coupled functional 70S ribosome (ribosome buffer). Regarding 70S ribosome isolation conditions, it was found that the tightly coupled 70S ribosome tolerates such conditions; however, the loosely coupled 70S ribosome dissociates rapidly under this condition. Because the tightly coupled 70S ribosome has a competent activity but the loosely coupled 70S ribosome does not, such optimized isolation conditions provide only with the tightly coupled 70S ribosomes when using the ribosome buffer [185]. Also, salt concentration is the other important factor to isolate functional ribosomes [186]. Inappropriate magnesium concentrations, as well as high salt concentrations (such as greater than 500 mM) in the salt wash step can facilitate efficient subunit dissociation; however, it should be noted that too much salt and/or too many salt washes lead to

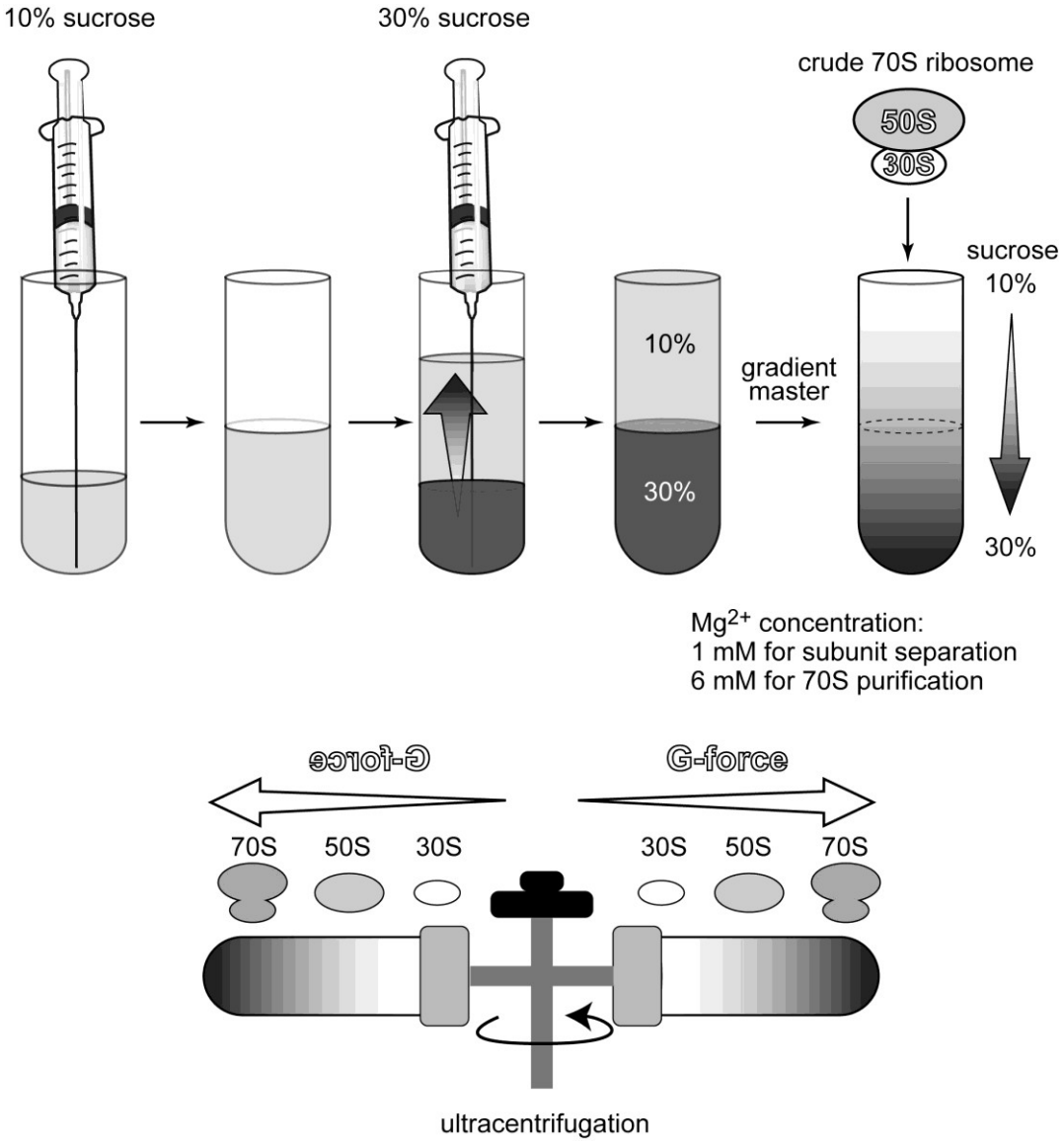

Figure 2.8. A schematic illustration of the sucrose density gradient used for ribosome isolations is shown. First, 10% sucrose was layered on the bottom of tube, then 30% sucrose was layered from the bottom of tube, carefully. By using the master gradient program, the sucrose gradient density from 10% to 30% was set. The crude 70S ribosome was layered on the sucrose cushion very carefully so as not to disturb the sucrose surface. Ribosomes were then separated by ultracentrifugation.

loss of ribosome components, such as large ribosomal proteins L7/L12 [185, 186]. It was found that the dissociation of ribosome components depends on salt type, ribosome concentration, and $MgCl_2$ concentration. For instance, high NaCl concentrations remove large amounts of ribosomal proteins even in the presence of $MgCl_2$, but NH_4Cl does not. In the absence of $MgCl_2$, both NaCl and NH_4Cl facilitate dissociation of ribosomal proteins [186]. Therefore, to avoid unwanted removal of ribosome components, salt washes and salt concentrations during the preparation and loading of crude 70S samples should be optimized. For such reasons, these experiments were not performed with the salt wash under 0.5 M NH_4Cl for ribosome isolation, and instead employed 0.2 M NH_4Cl for both 50S and 70S ribosome isolation. Besides the importance of salt for ribosome isolation, the salt type and ribosome preparation are also significant for the activity of isolated ribosomes, since isolated ribosomes at least slightly lose their activity under some conditions [187]. In particular, it was shown that NH_4Cl is the most effective salt type to activate 50S subunits. In contrast, NaCl does not activate 50S subunits at all, even in the presence of sufficient Mg^{2+} [187]. Therefore, the conditions used in ribosome isolation must be taken into consideration and optimized for further experiments. Furthermore, as mentioned in the following section, the method to prepare ribosome samples was also important in order to obtain pure 50S subunits.

One liter culture of *E. coli* MRE600 cells (obtained from G. Garcia, University of Michigan) was grown to mid log-phase (OD_{600} of 0.5) and the cell culture was cooled down on ice for 10 min and collected by centrifugation at 5,000 rpm for 10 min at 4 °C. The timing when the cells are harvested affects considerably the activity of isolated ribosomes [185]. Cell pellets were resuspended in 30 mL of the cell lysate buffer at 4 °C. The cells were lysed by passing through a cold French press two times at 12,000 psi. DNase I was added to the cell lysate at 0.01 unit/µl final concentration, which was incubated on ice for 15 min and centrifuged twice for 30 min at 11,000 rpm at 4 °C. The supernatant was collected and the NH_4^+ concentration was adjusted to 0.2 M, then centrifuged at 42,000 rpm for 4 h at 4 °C to pellet crude 70S ribosomes. The crude 70S ribosome pellets were washed and resuspended in the dissociation buffer for subunit

isolation and the ribosome buffer for 70S ribosome isolation. Subsequent procedures are different between subunit isolation and 70S ribosome isolation.

Ribosome subunit isolation

The crude 70S ribosome was washed once with the dissociation buffer. The crude 70S ribosome pellet was then resuspended in the dissociation buffer with continuous gentle shaking for 1 h on an ice bath (this step was critical to obtain pure 50S subunits without 30S subunit contamination (see also "results for optimization of ribosome isolation" and Figure 2.9). The resuspended crude 70S ribosome was cleared by centrifugation at 10,000 rpm for 5 min at 4 °C, and the ribosome concentration of supernatant was then determined by NanoDrop (Thermo Scientific). The ribosome concentration can be calculated based on the extinction coefficient for 70S ribosomes in which 1 OD_{260} unit is equal to 23 pmol of 70S ribosomes in bacteria [185]. Fifty OD_{260} of the crude 70S ribosome were layered on 40 ml of a 10-30% sucrose cushion made with the dissociation buffer and centrifuged for 17 h at 19,000 rpm (Figure 2.8). As mentioned in the section "results for optimization of ribosome isolation", the amount of loading crude 70S ribosome affects the purity of 50S subunits. Peaks corresponding to 30S and 50S subunit were monitored at 260 nm and pooled individually (Figure 2.9a). The Mg^{2+} concentration of pooled ribosome subunits was adjusted to 10 mM and the subunits were pelleted by centrifugation for 20 h at 48,000 rpm. The 50S subunit pellet was resuspended in the ribosomal subunit stock buffer by gentle shaking for 1 h on ice bath. The purity of isolated 50S and 30S subunits was checked by extracting 23S and 16S rRNA by standard phenol-chloroform extraction followed by 0.8% agarose gel analysis, respectively (Figure 2.9c-2.9f). The isolated ribosome subunits was distributed into small aliquots, and stored at –80 °C. The ribosome subunit concentration was determined by using the extinction coefficient such that 1 OD_{260} unit is equal to 34.5 pmol of 50S subunit and 69.0 pmol of 30S subunit in bacteria [185].

Phenol-chloroform (PCI) extraction was performed as follows: an equal volume of PCI was added to the ribosome solution and mixed rigorously by voltexing for 20 sec. The mixed solution was centrifuged at 13,000 rpm for 10 min, then the supernatant nwas transferred to a new tube.

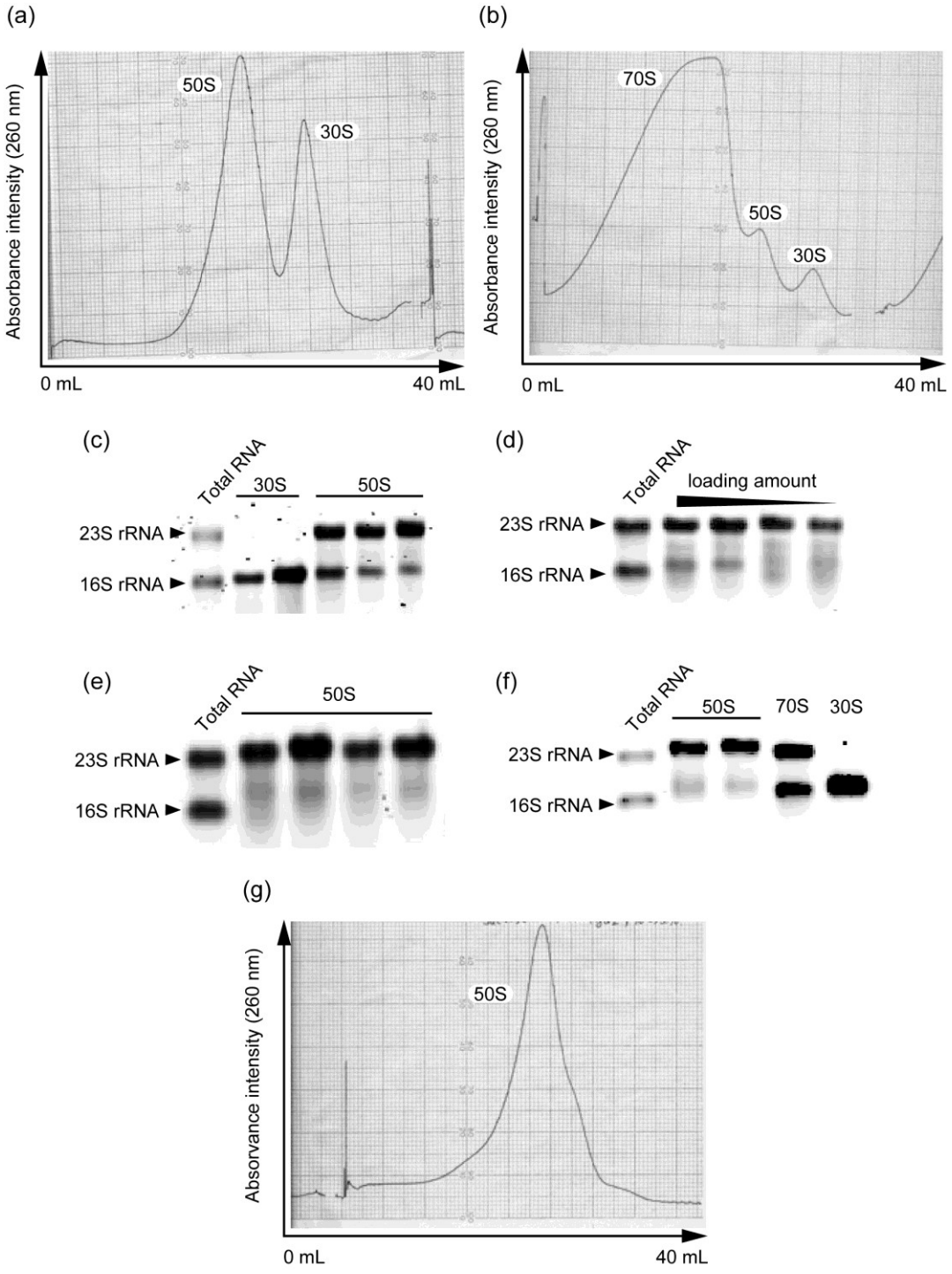

Figure 2.9. Ribosome profiles after (a) subunit isolation under a 1 mM Mg^{2+} concentration and (b) 70S ribosome isolation under a 6 mM Mg^{2+} concentration are shown. (c–f) Agarose gel analyses of isolated subunit purity after sucrose density gradients followed by phenol-chloroform extraction of rRNAs. (g) Sucrose density gradient check of the isolated 50S subunit.

This procedure was repeated once, then chloroform extraction was performed once to remove phenol completely from the aqueous layer. One-tenth volume of 3 M NaOAc (pH 5.3) was added, then 3~3.5 equal volume of cold ethanol was added. The solution was placed at –20 °C for 20 min, then RNA was pelleted by centrifugation at 13,000 rpm for 30 min at 4 °C. The RNA pellet was washed by 70% ethanol, and dissolved in ddH_2O or the denaturing loading dye.

70S ribosome isolation

The crude 70S ribosome was washed once with the ribosome buffer. The crude 70S pellet was then resuspended in the ribosome buffer with continuous gentle shaking for 1 h at 0~2 °C. The resuspended crude 70S ribosome was cleared by centrifugation at 10,000 rpm for 5 min. The concentration of ribosomes in the supernatant was then determined using the Nano-Drop spectrometer. Fifty to one hundred OD_{260} (depends on volume need to be layered on the sucrose cushion) of the crude 70S ribosome was layered on 40 mL of 10-30% sucrose cushion made of the ribosome buffer and centrifuged for 17 h at 19,000 rpm. The peak corresponding to 70S ribosome was detected at 260 nm and pooled (Figure 2.9b). The pooled 70S ribosome was pelleted by centrifugation for 24 h at 24,000 rpm. It should be noted that ultracentrifugation at 48,000 rpm to pellet the 70S ribosome as for subunit isolation should be avoided because of G-force-induced subunit separation [185]. The 70S pellet was resuspended in the ribosome stock buffer by gentle shaking for 1 h on an ice bath. The isolated 70S ribosome was distributed into small aliquots and stored at –80 °C.

Results for optimization of ribosome isolation

Ribosome profiles after sucrose density gradient showed that each subunit and 70S ribosome were isolated properly (Figure 2.9a and 2.9b). The purity of isolated ribosome subunits was double checked simply by running a 0.8% agarose gel following the standard phenol-chloroform extraction of rRNAs. Agarose gel analysis showed that the 30S subunits from the peak in Figure 2.9a were pure; however, the 50S subunits from the peak in Figure 2.9a were apparently contaminated with 30S subunits even after sucrose density gradient purification

(Figure 2.9c). To reduce 30S subunit contamination, the amount of crude 70S ribosome that was loaded onto the sucrose density cushion was reduced, and ribosome subunits were purified under the same conditions. Lowering the loading amount of the crude 70S ribosome (less than 25 OD_{260}) gave pure isolated 50S subunits (Figure 2.9d). Although pure 50S subunits could be prepared by reducing the loading amount on sucrose cushion and reducing the concentration of crude 70S when dissolving the crude 70S pellet in the dissociation buffer, the total amount of isolated 50S subunits after the sucrose density gradient purification was too low to be used for further experiments, such that further optimization was performed. The crude 70S ribosome was prepared by simple overnight incubation at 4 °C to dissolve the ribosome pellet; however, subunit dissociation was also enhanced by dissolving 70S crude ribosome pellet with continuous shaking under low magnesium concentration (Figure 2.9e). To check purities of ribosome subunits, agarose gel analysis was performed with isolated subunits and 70S ribosomes (Figure 2.9f). Agarose gel analysis showed a clear band corresponding to 23S rRNA for isolated 50S subunits. Also, the 50S purity was checked by sucrose density gradient (Figure 2.9g). These data clearly show pure 50S subunits isolated from the crude 70S ribosome without 30S subunit contaminations. The purified 50S subunits were used for all experiments in this dissertation work.

2.4.2. Chemical probing

One of the fascinating characteristics of functional RNA biomolecules is their higher-order structures and molecular dynamics, such that it is important to detect specific RNA structure and analyze the relationship between RNA structure and function. There are many ways to investigate RNA structures, including crystal structure and cryo-EM studies. Chemical probing has been considered as one of the powerful techniques to study nucleic acid structures, including nucleotide sequence, secondary structure of RNA and DNA, tertiary structure of RNA, and nucleic acid-protein interactions under solution conditions.

Many chemical reagents have been developed for the purpose of studying nucleic acid structures (Figure 2.10) [188]. For instance, dimethylsulfate (DMS), diethylpyrocarbonate (DEPC), and hydrazine were used to analyze RNA sequences and tertiary structures [189, 190]. DMS

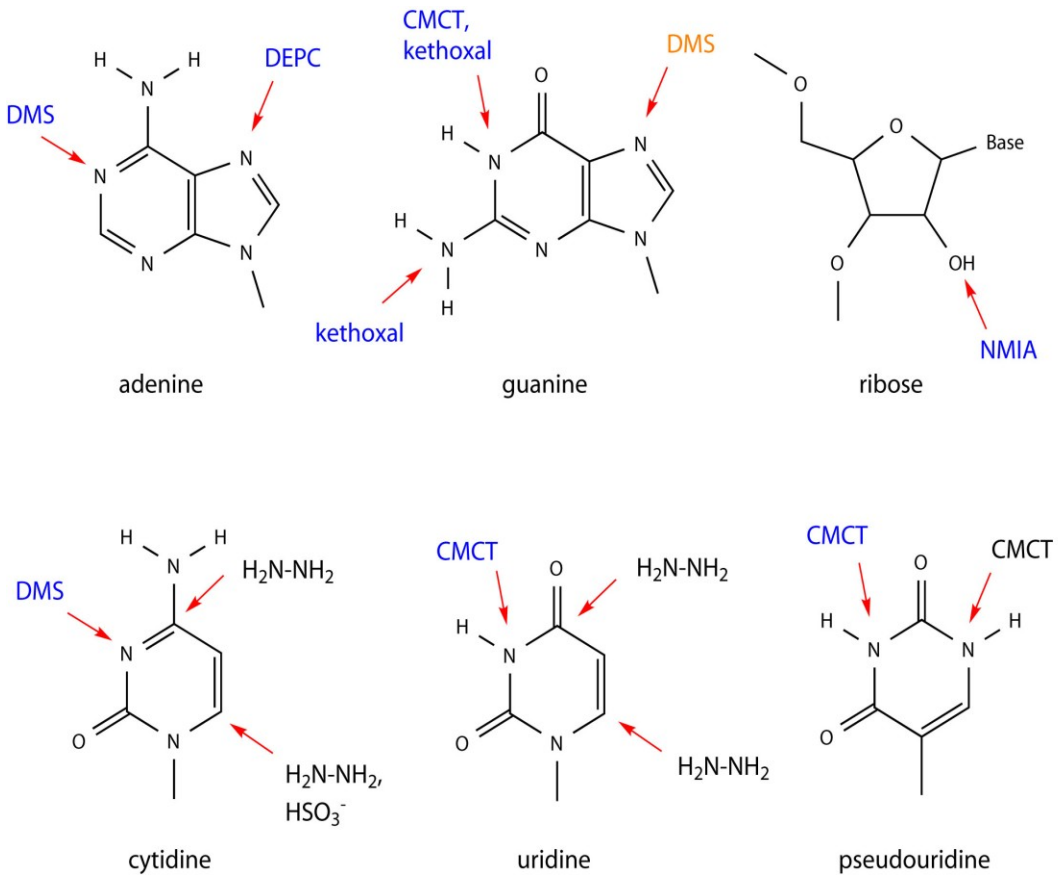

FIgure 2.10. Types of chemical probing and target site are shown. DMS; dimethylsulfate, DEPC; diethylpyrocarbonate, NMIA; *N*-methylisatonic anhydride, CMCT; 1-cyclohexyl-(2-morpholinoethyl) carbodiimide metho-p-toluene sulfonate. Blue color shows chemical probing detected by direct reverse transcription analysis, orange color shows chemical probing detected after RNA strand scission by aniline treatment, and black color shows chemical probing used for only sequencing reaction but not for structural analysis.

attacks the N7 position of guanine and N1 position of adenine, DEPC reacts with the N7 position of adenine, and hydrazine reacts with cytidine and uridine (Figure 2.10). If the RNA molecules are labeled at the 5' or 3' ends with ^{32}P, subsequent RNA strand scission will reveal the RNA sequences. If one performs these reactions under mild conditions, such as near physiological conditions, it is possible to study base-pairing formation and non-canonical base-base interactions in RNA molecules [189]. Hydrazine cannot be used for this purpose because it requires relatively harsh reaction conditions. Even if one uses large RNA molecules or wild-type ribonucleoprotein particles such as the ribosomes, which cannot be analyzed by ^{32}P RNA labeling methodologies, some chemical probing reagents still allow us to study RNA dynamics through the use of primer extension assays with reverse transcriptase (Figure 2.11) [29, 132, 191, 192]. In the following paragraph, reverse transcription-based RNA structural analysis will be discussed.

In the late 1980's, Moazed and Noller reported a clever application of chemical probing for analyzing ribosome-tRNA interactions [191]. By using a series of chemical probing reactions followed by reverse transcriptions, they found reactivity changes (protection or deprotection) in the presence or absence of tRNAs under various conditions, and they proposed the hybrid tRNA formation during translocation (see also Chapter 1) [29]. Furthermore, they found that some clinically important antibiotics interact with ribosomal RNAs at specific sites [132]. Thus, they demonstrated the power of chemical probing analysis and its broad potential to study RNA biomolecules.

Currently, one can look at Watson-Crick base pairing (N1 of A by DMS, N1 and N2 of G by kethoxal, N3 of C by DMS, N3 of U by 1-cyclohexyl-(2-morpholinoethyl) carbodiimide metho-p-toluene sulfonate (CMCT)), base-stacking interactions (N7 of A by DEPC), Hoogsteen surface accessibility (N7 of G by DMS, N7 of A by DEPC), and local conformational flexibility (2'-OH of any nucleotide by ; *N*-methylisatonic anhydride (NMIA) and its derivatives, in-line probing) by using chemical probing-based, RNA-structure analysis (Figure 2.10). DMS attacks the N1 position of A and produces 1-methyladenosine (m^1A) which inhibits Watson-Crick base-pair formation with the complementary base, such that reverse transcription is stopped at one nucleotide before m^1A (Figure 2.11). A unique characteristic of DMS probings that its chemical

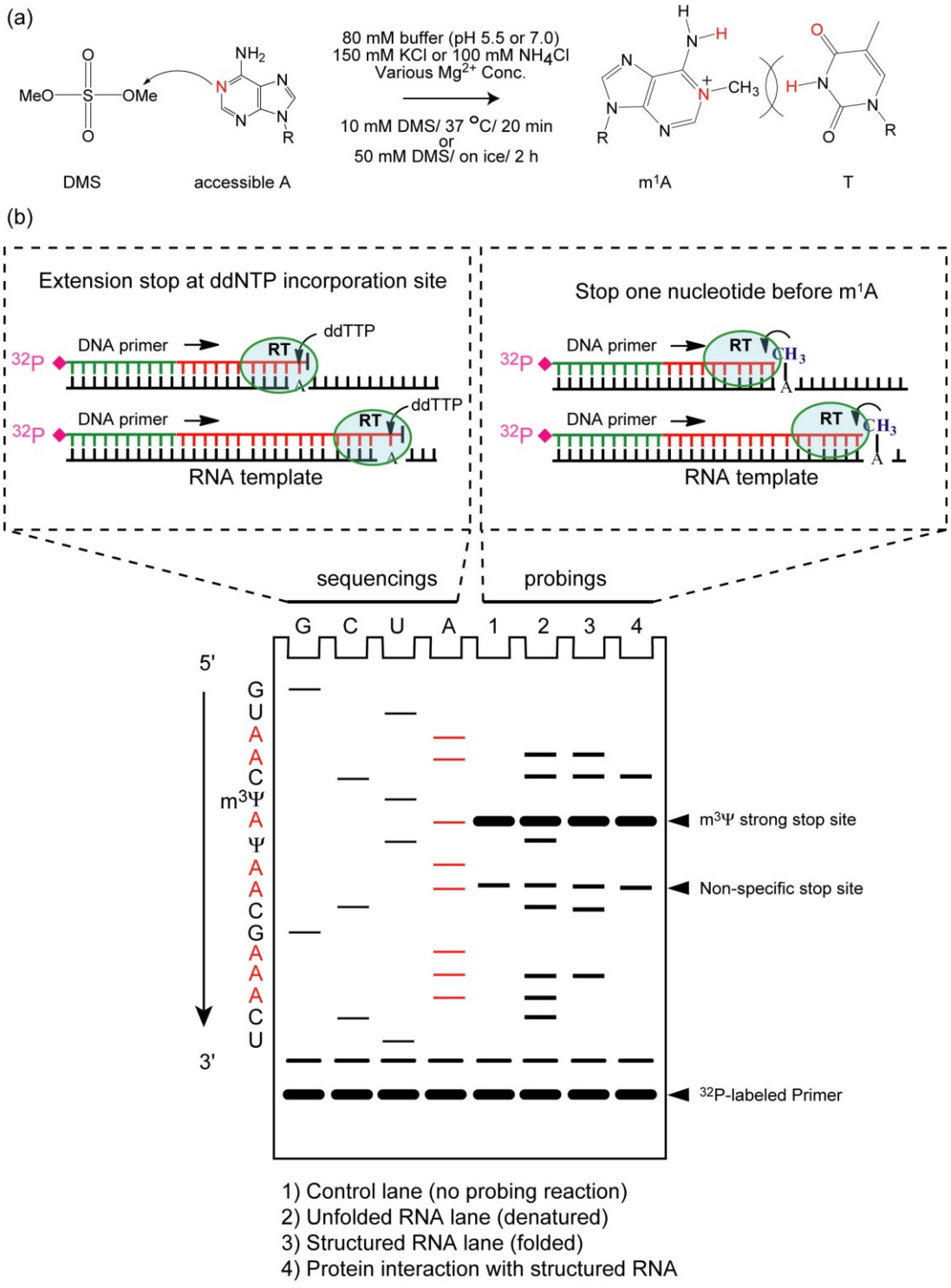

Figure 2.11. (a) One example for the chemical probing reaction is shown. (b) A schematic illustration of reverse transcription-based primer extension assay of RNA after chemical probing. The modified site on the gel is one nucleotide prior to the actual modified site because the dideoxy sequencing stops reverse transcription after incorporating a complementary base; whereas, the probing site modification stops reverse transcription without incorporation of the complementary base.

reactivity toward N1 of A does not change under a broad pH range from 5.0 to 8.0 (see results in this Chapter) [179]. In the case of DEPC, it attacks the N7 of A and facilitates a ring-opening reaction, which blocks reverse transcription (Figure 2.12b). DMS also attacks the N7 of G to produce 7-methylguanosine (m^7G) (Figure 2.12c). The N7 position of G does not participate in Watson-Crick base-pair formation during reverse transcription; therefore, it does not inhibit reverse transcription directly. Instead, treatment of m^7G with sodium borohydride followed by aniline-induced strand scission removes m^7G and cleaves the RNA strand at the m^7G position (Figure 2.12k). Subsequent reverse transcription detects the site of m^7G modification created by DMS. Although hydrazine cannot be used for structural analysis, it is still important because hydrazine reacts with uridine, whereas the isomerized base pseudouridine is resistant to modification (Figure 2.12d and 2.12e). Discrimination of pseudouridine over uridine is also possible by using 1-cyclohexyl-(2-morpholinoethyl) carbodiimide metho-p-toluene sulfonate (CMCT). CMCT reacts with the N3 of U and the N3 and N1 of Ψ (Figure 2.12f-h). Although the reactivity of CMCT is different between U and Ψ and N3 and N1 of Ψ, subsequent incubation under alkaline conditions (pH 10.3) for sufficient time (>3 hours) removes the CMCT adducts only from N3 of U and N1 of Ψ, but not from the N3 of Ψ [193, 194]. Very harsh alkaline conditions (ammonia + high temperature) are required for removal of the N3-Ψ adduct of CMCT [194].

Besides base-targeting strategies, local nucleoside flexibility is also a target for RNA structure studies. Nucleosides free from any specific interaction, such as those around internal bulge or loop regions, conformationally fluctuate in solution. Such molecular motion allows the 2'-OH of these sites to sample multiple states, which increases nucleophilicity of the 2'-OH to attack the phosphate backbone and then cleave the RNA strand (in-line probing) (FIgure 2.12i). It is proposed that nucleophilicity of the 2'-OH is influenced by local nucleoside flexibility and the ability to sample multiple conformations [195]. While in-line probing requires labeled RNA, NMIA (*N*-methylisatonic anhydride) attacks such 2'-OHs in flexible positions in a non-base-specific manner and leaves a bulky group at the 2'-OH, which inhibits reverse transcription (Figure 2.12j) [196]. This method is called selective 2'-hydroxyl acylation and primer extension (SHAPE). Since both methodologies are non-base-specific, they have extensive potential for studying RNA

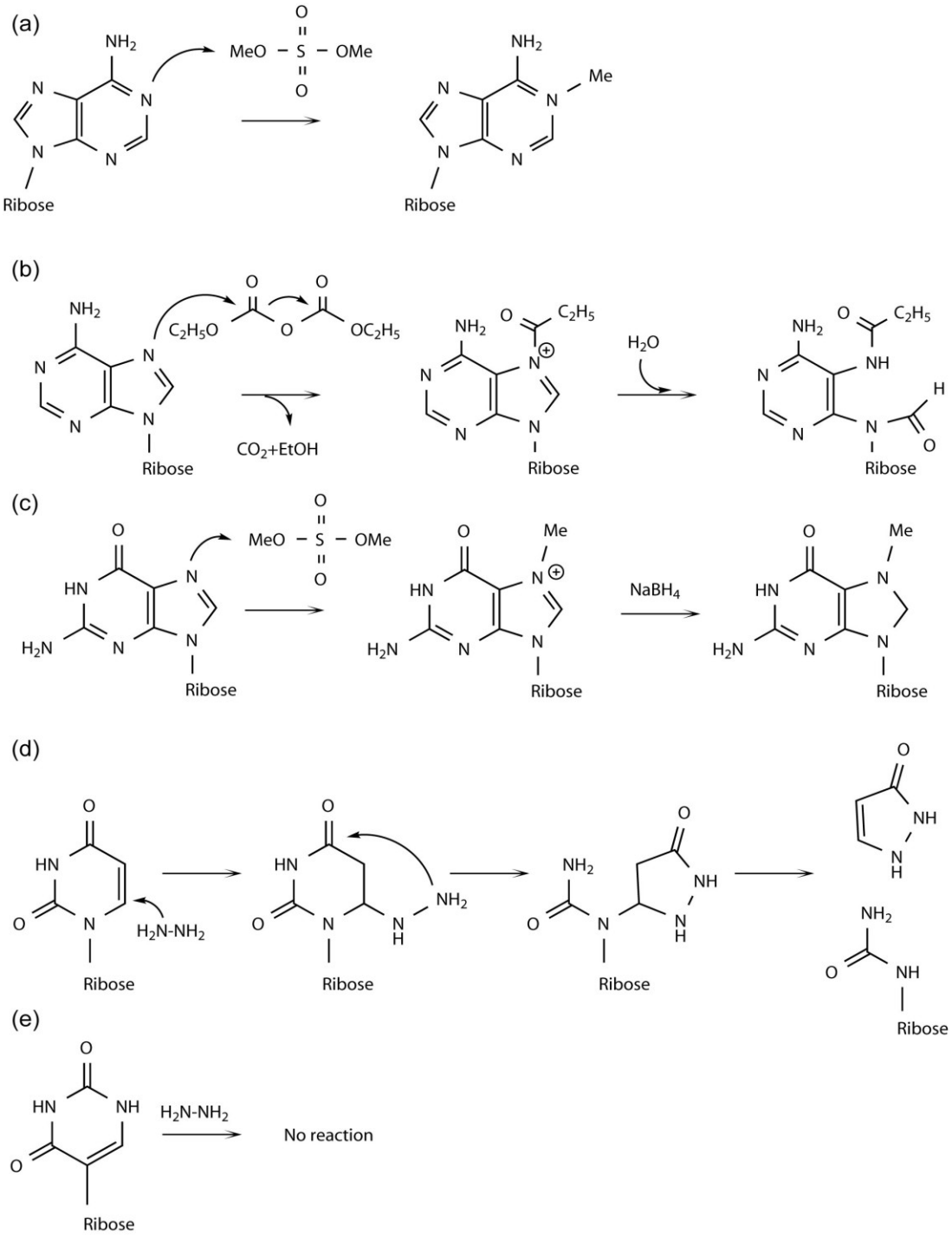

Figure 2.12. (a) DMS reaction with A. (b) DEPC reaction with A. (c) DMS reaction with G. (d) Hydrazine reaction with U. (e) Hydrazine reaction with pseudouridine.

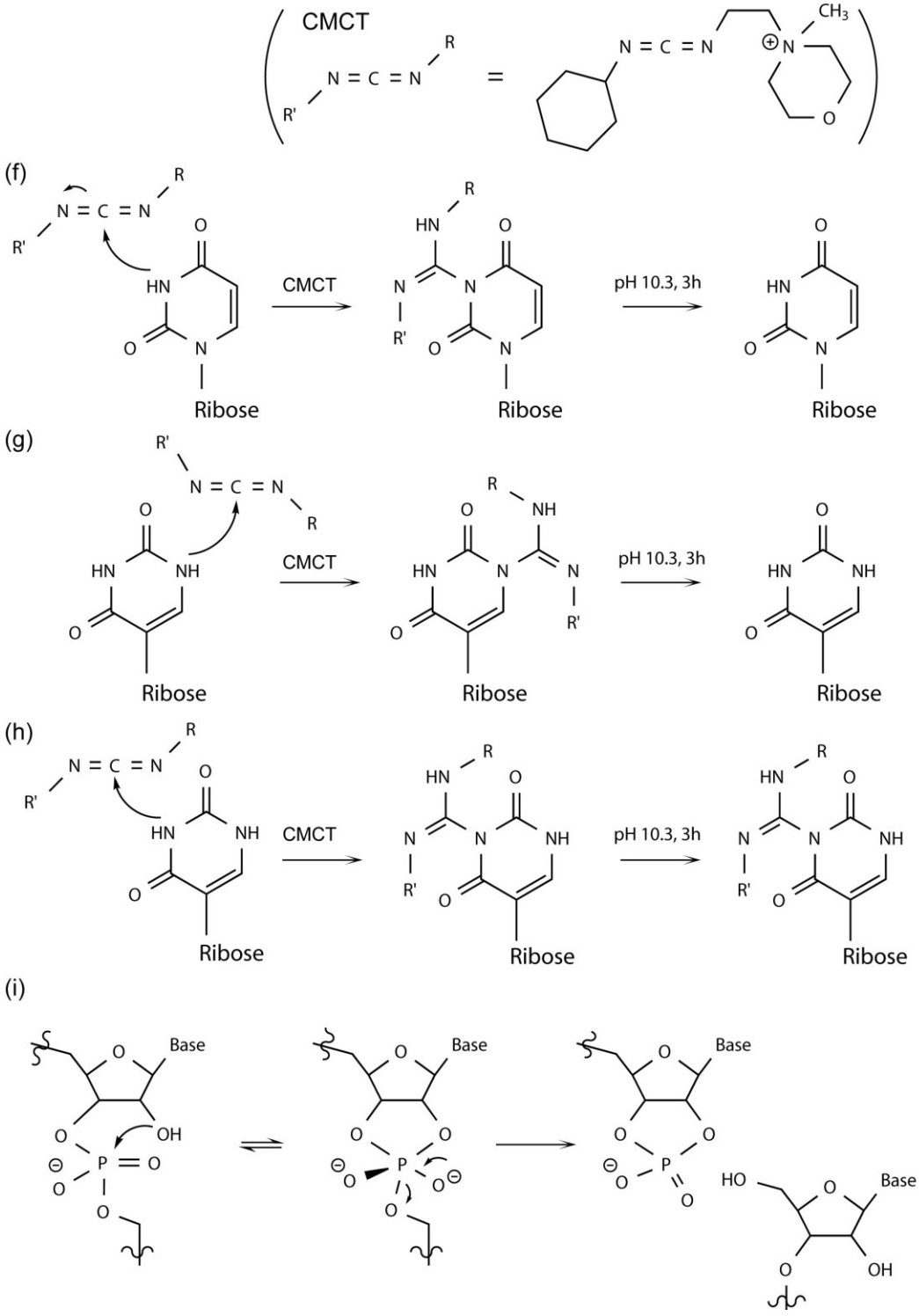

Figure 2.12. (continued) (f) CMCT reaction with U followed by alkaline treatment. (g) CMCT reaction with N1 of Ψ followed by alkaline treatment. (h) CMCT reaction with N3 of Ψ followed by alkaline treatment. (i) In-line probing.

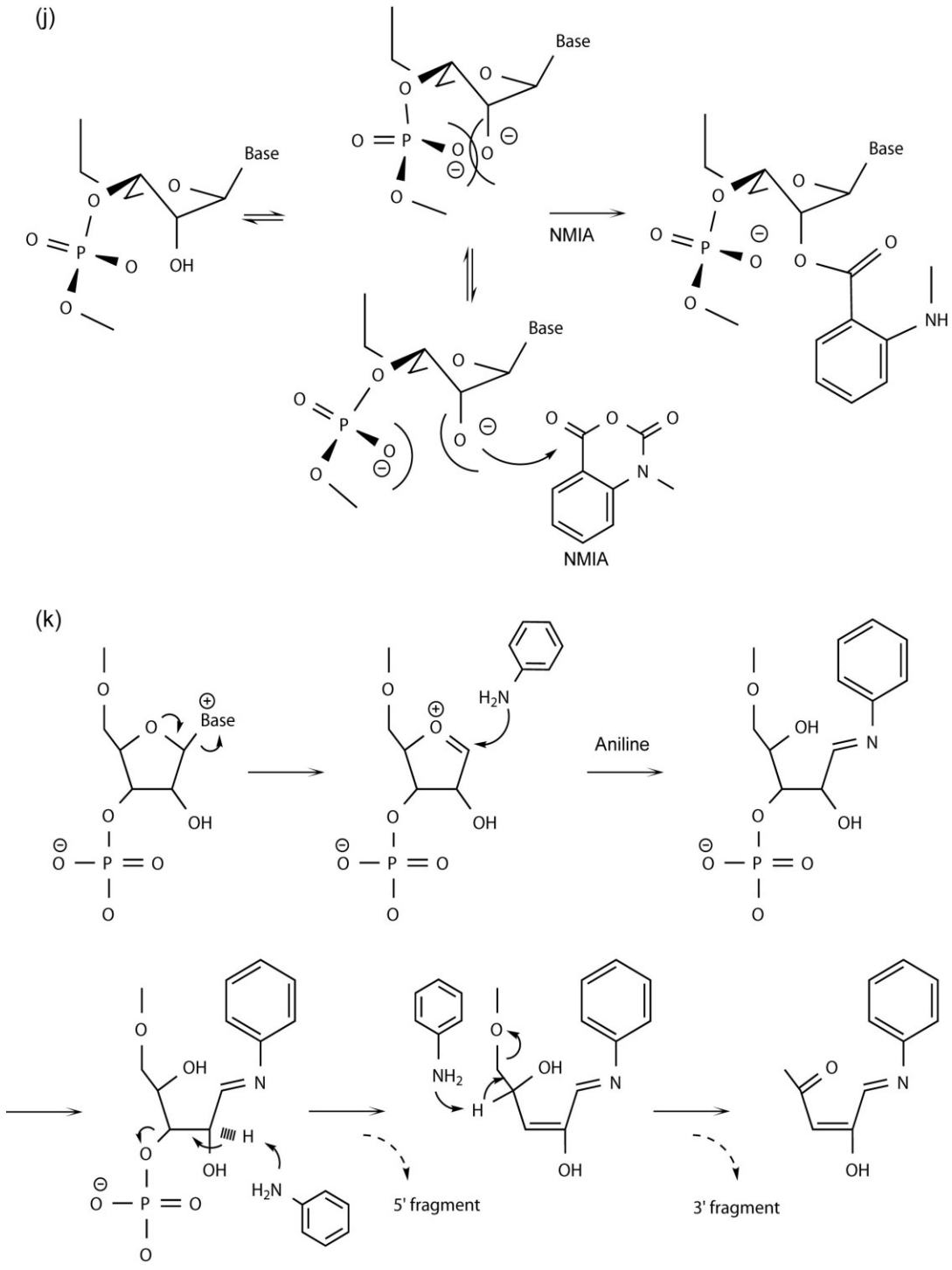

Figure 2.12. (continued) (j) SHAPE reaction. (k) Reaction mechanism of RNA strand scission by aniline acetate is shown.

structures in solution. The only limitation for SHAPE and in-line probing is that slightly high pH probing conditions (pH 8.0~8.3) are necessary to obtain sufficient nucleophilicity of the 2'-OH.

2.4.3. Experimental procedure for dimethylsulfate (DMS) probing

DMS probing of the 50S subunit

The 50S subunit was reactivated in the activation buffer for 10 min at 37 °C. Ten µl (the final 50S subunit concentration was adjusted to become 0.2 µM in 50 µl) of the reactivated 50S subunit was resuspended in 38 µl of each probing buffer and pre-incubated for 10 min at 37 °C, which was then set on ice for a minimum of 5 min. The probing reaction was initiated under 2 different conditions in 50 µl volumes; 1 mM DMS for 20 min at 37 °C or 5 mM DMS for 2 h on ice. DMS was quenched by the addition of DMS stop buffer followed by ethanol precipitation. The precipitated 50S was treated with the general phenol-chloroform isolation method to isolate 23S rRNA which was then resuspened in ddH_2O. Degradation of the DMS-modified 23S rRNA was checked on a 0.8% agarose gel, and no degradation was observed for any probing conditions. It should be noted that all buffer pHs were adjusted for exactly the same buffer concentration, temperature, and salt concentration.

DMS probing of the structured 23S rRNA

The 23S rRNA was prepared by general phenol-chloroform extraction from the isolated 50S subunit. For probing structured 23S rRNA, the isolated 23S rRNA was dissolved in refolding buffer and denatured at 90 °C for 3 min and then renatured slowly. Since rRNA degradation was observed during the denaturing-renaturing step if Mg^{2+} was present, Mg^{2+} was not added during this step to avoid such any unwanted non-specific degradation. After the incubation of the renatured 23S rRNA in the presence of 6 mM Mg^{2+} for 15 min at 37 °C. DMS probing was initiated. Five µl (5 pmol) of the 23S rRNA was resuspended in 18 µl of each probing buffer and incubated for 10 min at 37 °C. After placing the pre-incubation mixture on ice for at least 5 min, probing was performed as mentioned above in 25 µl volumes. Subsequent treatments were identical to the procedure described above.

DMS probing of the denatured 23S rRNA

To confirm that DMS probing of the 50S subunit reflects the RNA structure and conformation but not different DMS reactivities under various pH conditions, we performed DMS probing analysis with denatured 23S rRNA. Denatured 23S rRNA was prepared as following. First, 23S rRNA was isolated from the 50S subunit by the standard phenol-chloroform extraction method followed by ethanol precipitation. The isolated 23S rRNA was resuspended in a 7 M urea water solution and denatured in boiling water for 3 min, then put on ice directly. DMS probing was initiated as described in DMS probing analysis of the structured 23S rRNA, except Na^+ and EDTA were used instead of K^+ and Mg^{2+} and 4 M urea was included.

2.4.4. Experimental procedure for reverse transcription followed by polyacrylamide gel electrophoresis

Fifty pmol of 20-mer DNA primer (5'-CGACAAGGAATTTCGCTACC-3') (Sigma-Genosys), 5 µl of 10x T4 polynucleotide kinase (PNK) buffer (New England Biolab), and 1 µl of fresh [γ-^{32}P]-ATP (Perkin elmer) were mixed and the total volume was adjusted to 49 µl with ddH_2O. One µl of 10 units/µl of T4 PNK (New England Biolab) were added and gently mixed. The mixture was incubated at 37 °C for 50 min, then incubated at 70 °C for 10 min to inactivate T4 PNK. A 5' end labeled DNA with ^{32}P was passed through Sephadex G-25 (Sigma-Aldrich) to remove unreacted [γ-^{32}P]-ATP. The total volume was adjusted to 50 µl (1 µM DNA concentration) if there was significant volume change after passing through G-25. Radioactivity of the 5' ^{32}P-labled DNA was checked simply with a Geiger or scintillation counter. Reverse transcription-based primer extension analysis of H69 after chemical probing was performed by using 0.8 pmol of 5' ^{32}P-labeled DNA (see detailed instruction below), such that adjusting the volume to 50 µl at this step is important to obtain approximately 1 µM labeled DNA concentration. The reason that primer extension was not performed based on ^{32}P intensity is because an extra amount of DNA primer present in the reaction may disturb gel analysis by forming a dirty smearing band after position 1915 of H69. Therefore, a long exposure time was taken to obtain quantifiable band intensity instead of increasing the amount of DNA.

Five hundred ng of the DMS-modified 23S rRNA were resuspended with 0.8 µl of 1 µM 5' P^{32} end-labeled DNA solution (0.8 pmol used in one primer extension reaction). The mixture was incubated for 3 min at 80 °C and slowly cooled down to the room temperature for 5 min then put on ice. Reverse transcription was initiated by adding the master mixture prepared with RT, dNTPs, and 5x RT buffer at a total volume of 5 µl on ice. The mixture was incubated at 43 °C for 1 hour. Two µl of the denaturing loading buffer was added, and the mixture was incubated in a boiling water bath for 3 min followed by quick placement on ice. The denatured sample solution (7 µl) was loaded on one lane, and the extension products were analyzed by 10% 7 M urea-containing sequencing polyacrylamide gel electrophoresis (PAGE). The PAGE condition was 1:50 cross-linking ratio of bis-acrylamide and acrylamide concentration, and the sequencing gel apparatus (size, 42 cm x 33 cm; thickness, 0.4 mm) was used. The running buffer was 0.5x TBE (45 mM Tris-HCl pH 8.3, 45 mM boric acid, 1.25 mM EDTA), and the running condition was 1,300 V, room temperature, and usually 2.5~3.0 hours running time. The gel was carefully transferred onto a film (Kodac Biomax) and wrapped with plastic wrap, and the gel was exposed to a phosphorimager screen (Amersham) at –20 °C for usually 12 h and overnight. It should be noted that the exposure time may considerably affect data resolution. For instance, if newly purchased [γ-^{32}P]-ATP was used to label the primer DNA and the ^{32}P-labeled DNA primer was used soon, over 12 h exposure of gels onto phosphorimager screen may result in a strong smearing after 1915 but good for before 1913. On the other hand, if old ^{32}P-labled DNA primer was used, an overnight exposure may not be enough to obtain good resolution both before and after the 1915 region, particularly at position 1913. Therefore, optimizing the exposure time or repeating multiple times was necessary to improve data resolution or obtain good quality gel data. Because of such reasons, gels were used to take at least 2 gel images with different exposure time (*e.g.*, 9 hours and 24 hours) to obtain data for before and after the 1915 region in this thesis work. The gel pictures were obtained on a Typhoon (9200) and analyzed with ImageQuant software (GE Healthcare), respectively.

Fluorescein-labeled DNA can also be used for H69 primer extension experiments in place of ^{32}P. All instructions for RT reaction are the same as above, except using 1 pmol of fluorescein-

labeled DNA primer for one RT reaction. For PAGE, a thicker gel (1 mm or 1.5 mm) and small gel apparatus (20 x 16 cm) may be better because the gel can be transferred onto the Typhoon phosphorimager plate directly. If a gel is wrapped in plastic wrap, it will give low resolution data. Also, if a gel is washed with ddH_2O, it also has low resolution data, probably because the absorbance of fluorescein is sensitive to pH changes, in which the absorbance is decreased in pH conditions lower than neutral pH (see Sigma Genosys product information). Thus, gels should be directly placed on the Typhoon for analysis. Regarding gel thickness, using a sequencing gel (0.4 mm thickness) did not improve the gel resolution. The running condition was 350 V, 3 to 3.5 hours at room temperature in the dark. It also should be noted that loading the samples as thin a layer as possible also gives better gel resolution.

2.4.5. Experimental procedure for quantification of autoradiogram

Each band intensity was measured by using ImageQuant software version 5.1 (GE Healthcare). For normalization, two different types of bands were chosen as the standard bands; one is the constitutive base-modification-dependent specific primer extension stop band ($m^3\Psi$1915), and the other is an RNA secondary structure-dependent nonspecific primer extension stop band (position 1921). Background deduction was manually performed by using control lanes. Normalized values were calculated by dividing each target band by one of standard bands, and then comparing normalized relative intensities of each band across different experimental conditions (pH 5.5, 7.0, salt type, and temperature). The percent change of DMS reactivity at pH 5.5 was calculated simply by dividing the normalized value at pH 5.5 by the normalized value at pH 7.0 as shown in the following formulas. To determine standard deviation, at least three sets of experiment were compared.

For instance, the normalized value of A1913 was calculated as;

$$\text{Normalization} = \frac{I_{obs}(\text{A1913}_{pH7.0})}{I_{obs}(\text{C1920}_{pH7.0})}$$

(I_{obs}; Observed band intensity taken by Image Quant software)

To obtain the percent change of DMS reactivity under the condition pH 5.5;I_{obs}

$$\%\ \text{change at pH 5.5} = \left(1 - \frac{\text{Normalized A1913}_{pH\,5.5}}{\text{Normalized A1913}_{pH\,7.0}}\right) \times 100$$

Chapter 3
Dynamic conformational rearrangements of H69 upon ribosome subunit association

(This chapter is adapted from Sakakibara, Y. and Chow, C.S., *ACS Chem Biol* **2012**.)

3.1. Abstract

As part of the central core domain of the ribosome, helix 69 of 23S rRNA participates in an important intersubunit bridge and contacts several protein translation factors. Helix 69 is believed to play key roles in protein synthesis. Even though high-resolution crystal structures of the ribosome exist, the solution dynamics and roles of individual nucleotides in H69 are still not well defined. To better understand the influence of modified nucleotides, specifically pseudouridine, on the multiple conformational states of helix 69 in the context of 50S subunits and 70S ribosomes, chemical probing analyses were performed on wild-type and pseudouridine-deficient bacterial ribosomes. Local structural rearrangements of helix 69 upon ribosomal subunit association and interactions with its partner, helix 44 of 16S rRNA, are observed. The helix 69 conformational states are also magnesium dependent. The probing data presented in this study provide insight into the functional role of helix 69 dynamics and regulation of these conformational states by post-transcriptional pseudouridine modification.

3.2. Introduction

As stated in Chapters 1 and 2, protein biosynthesis is carried out by the ribosome in all living organisms, and the overall mechanisms in this process are highly conserved throughout phylogeny. The previous chapter focused on the 50S subunit of the ribosome to understand the multiple conformational states of H69 in solution. However, it was not clear whether such multiple conformational states of H69 exist in the 70S ribosome and how the formation of the B2a intersubunit bridge influences the conformational state of H69. Therefore, the research focus in this chapter is mainly the conformation of H69 in the 70S ribosome.

Bacterial ribosomes are composed of small (30S) and large (50S) subunits that associate into 70S ribosomes, with the catalytic core domain being composed of rRNA [5, 46, 47, 177]. As stated in above capters, the rRNA plays a key role in decoding cognate tRNA-mRNA interactions [47, 197]. catalyzing peptide-bond formation [68, 198, 199] and contributing to tRNA translocation [192, 200]. Post-transcriptional nucleotide modifications, including pseudouridine (Ψ), are clustered within this functionally important domain of the ribosome [72, 73, 173].

The subunit interactions required for 70S ribosome formation are supported by highly conserved intersubunit bridges [46, 92, 93]. A key bridge, B2a, forms part of the decoding center and is composed of helix 69 (H69) of the 50S subunit and helix 44 (h44) of the 30S subunit [46]. In ribosome crystal structures, residue A1912 of H69 projects into the minor groove of h44 and interacts with C1407 and G1494 of h44 [5, 47]. The positioning of A1912 seems to be supported by a reverse-Hoogsteen base pair with Ψ1917 (Figure 3.1a). Nucleotide A1919 has a minor groove interaction with U1406/U1495 of h44 [5]. This interaction is supported by another non-canonical Hoogsteen base pair between Ψ1911 and A1919 and a bridging 2'-OH of A1918

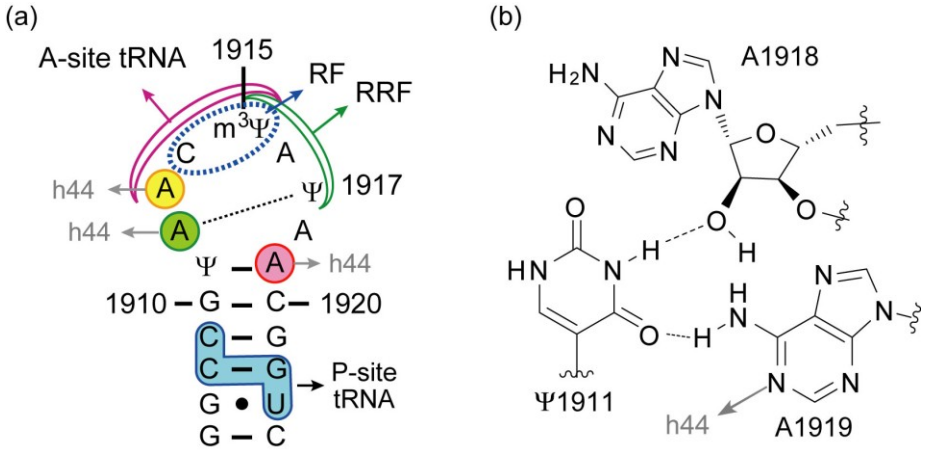

Figure 3.1. (a) The sequence and map of *E. coli* H69 RNA show key interactions with h44, tRNAs, and protein factors (RFs, RRF) (Ψ is pseudouridine and $m^3\Psi$ is 3-methylpseudouridine). (b) The Ψ1911-A1918-A1919 hydrogen-bonding network is observed in *E. coli* 70S ribosome structures .

(Figure 3.1b). The B2a interaction plays an important role in maintaining subunit association as the 30S subunit rotates relative to the 50S subunit during translocation [97, 98]. Results from mutation studies also reveal the biological significance of bridge B2a [94-96]. Single-base substitutions of residues A1912 or A1919 reduce protein synthesis and peptidyl-transfer processivity, and lead to defects in 70S formation [94]. Mutations at C1914, $m^3\Psi$1915, A1916, and G1922 result in frameshifting and stop-codon readthrough [95, 96].

As described in detail in Chapter 1, H69 interacts with tRNAs [21, 47], release factors (RFs) [59-61], and ribosome recycling factor (RRF) (summarized in Figure 3.1a) [99]. Contacts with A1913 are believed to play a role in A-site tRNA accommodation [100]. The importance of proper H69-A-site-tRNA interactions is supported by the observation that an A1913U substitution suppresses mutant tRNA accommodation compared to the wild-type H69 [102]. The H69 stem (G1921–G1922) interacts with the D stem of the P-site tRNA [46], and G1922 mutants cause frameshifting and stop-codon readthrough [96]. The tip of H69 (C1914) contacts the switch loop of RF1 during stop-codon recognition [60]. Ribosomes lacking H69 also exhibit strong impairment in peptide release by RFs, although other translation steps are only moderately affected [59, 103]. Direct interactions between RRF and H69 ($m^3\Psi$1915–Ψ1917) are also observed [99]. Overall, these interactions of H69 with protein factors and tRNAs appear to play key biological roles, which emphasizes the importance of structural dynamics and the ability of the RNA component to adopt multiple conformational states.

Dimethylsulfate (DMS) probing studies discussed in Chapter 2 revealed that H69 within 50S subunits can exist in multiple conformational states that can be induced by changes in pH, Mg^{2+} concentration, and temperature, as well as being influenced by Ψ modifications [184]. Several different conformational states of H69 are observed in crystal structures, in which the A1913 position forms a stacked (closed) conformation in 50S subunits and a flipped-out (open) conformation in 70S ribosomes [5, 177]. The available biological and structural data suggest that these multiple conformational states of H69 play important roles in translation. Therefore, H69 has been proposed to be a suitable candidate for unique antibiotic targeting [138, 184, 201]. A better understanding of the conformational states of H69 in the context of both 50S subunits and

70S ribosomes under solution conditions will help guide the design of new targeting agents. In this study, the H69 conformational states were analyzed by selective 2'-hydroxyl acylation and primer extension (SHAPE) [196], and chemical probing with diethylpyrocarbonate (DEPC) [189] and DMS [191]. By comparing H69 conformational states in 70S ribosomes with those in 50S subunits, specific regions undergoing dynamic structural rearrangements upon subunit association were identified. In addition, similar studies on pseudouridine-deficient ribosomes have allowed the contributions of non-standard nucleotides to these rearrangements to be determined.

3.3. Results

3.3.1. Probing H69 structural rearrangements upon subunit association

Probing H69 structural rearrangements

Subunit association of the ribosome was expected to alter the accessibility of certain nucleotides towards chemical reagents. For example, the exposure of adenine residues of H69 under different conformational states in 70S ribosomes or 50S subunits can be revealed through DMS reactivity at the N1 position. To probe H69 conformational dynamics in 70S ribosomes, SHAPE analysis was employed. SHAPE reactivity is based on local nucleotide conformation-dependent 2'-hydroxyl nucleophilicity [196]. If a base is involved in interactions such as Watson-Crick pairing or stacking, the corresponding nucleotide is constrained, which in turn reduces the 2'-OH nucleophilicity. On the other hand, if a base can move freely and is not involved in such interactions, the 2'-OH of this nucleotide is highly reactive towards the SHAPE reagent (*N*-methylisatonic anhydride, or NMIA) [196]. SHAPE analysis was therefore expected to provide useful information about the conformational states of H69 in 50S subunits and 70S ribosomes.

Changes in conformational flexibility of A1918 and A1913

At 37 °C under physiological buffer conditions, SHAPE analysis reveals that the 2'-OH of A1918 is reactive (unconstrained) in 50S subunits, but much less reactive (seven-fold reduction; constrained) in 70S ribosomes (Figure 3.2a, b, c; these data were normalized to a non-specific stop site 1921, which is located in the stem region of H69). This probing pattern is consistent with

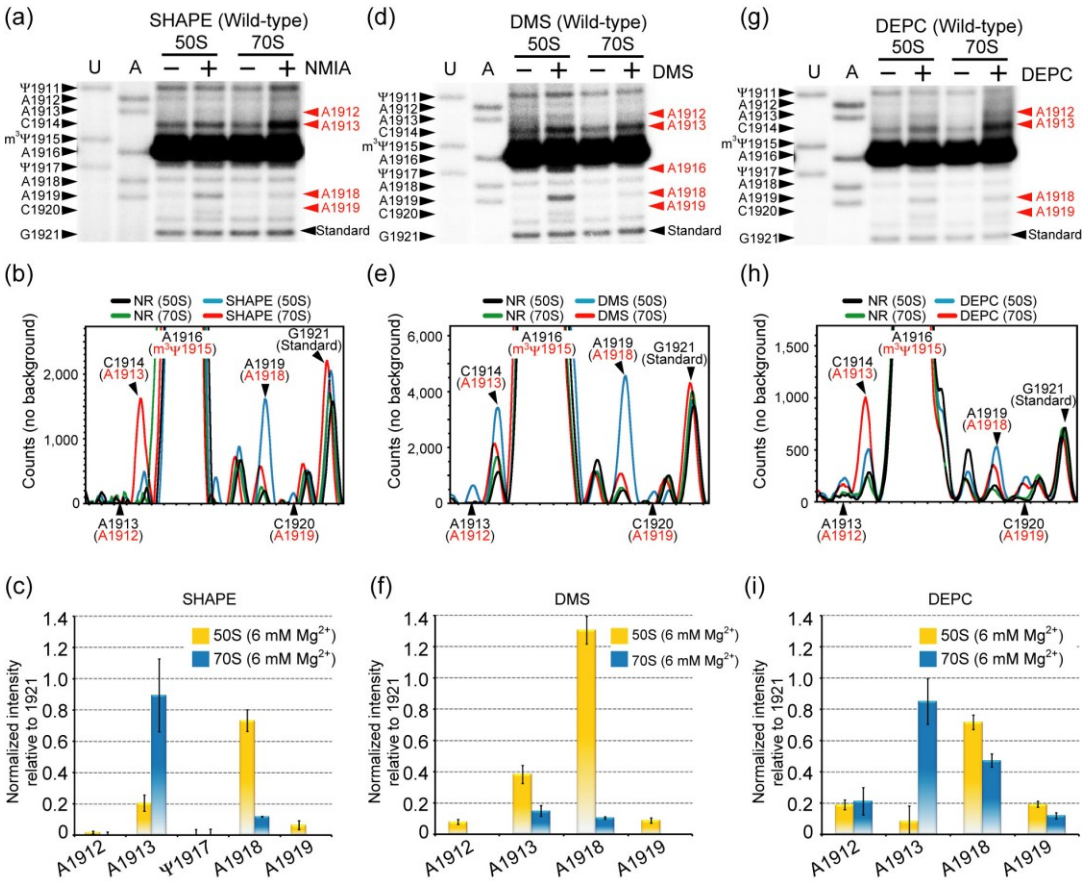

Figure 3.2. Autoradiograms (top) and quantification (center, bottom) of SHAPE (a, b, c), DMS (d, e, f), and DEPC (g, h, i) probing analyses on wild-type 50S subunits and 70S ribosomes are shown. In panels a, d, and g, the *E. coli* H69 sequence corresponding to the dideoxy nucleotide stop sites (U and A reactions) is on the left side, and chemical modification sites, which cause a primer extension stop at the 3' nucleotide, are in red on the right side. The normalized intensities for modified sites were calculated by subtracting non-specific primer extension stops (black and green traces, panels b, e, and h) from total intensity (blue and red, panels b, e, and h), and then normalizing to a uniform band (position 1921) (panels c, f, and i). The actual stop sites are indicated in black and the chemical modification sites are shown in red (panels b, e, and h).

X-ray crystal structures of 70S ribosomes, which show that the 2'-OH of A1918 is involved in a widened-Hoogsteen interaction with Ψ1911 and A1919 (Figure 3.1b). Reactivity of the A1918 2'-OH indicates that this site is flexible and accessible to NMIA in 50S subunits, but that ribosome assembly and bridge B2a formation confine its orientation. In contrast, the A1913 2'-OH shows greater than four-fold higher reactivity in 70S ribosomes relative to 50S subunits, indicating that A1913 becomes less constrained upon subunit association (Figure 3.2c). Alternatively, A1913 might have a unique local conformation within the 70S ribosome that is ideal for increased SHAPE reactivity [196]. The remaining H69 loop nucleotides (Ψ1911, A1912, C1914, m^3Ψ1915, A1916, Ψ1917, A1919) are found to be constrained in both 50S and 70S ribosomes. These results suggest that H69 forms a well-ordered loop structure in 50S subunits and 70S ribosomes, but A1913 has increased flexibility while A1918 becomes more constrained upon subunit association. SHAPE analysis on isolated 70S ribosomes was also compared with reassociated 70S ribosomes (generated from 50S and 30S subunits) under the same reaction conditions, and no difference was observed (Figure 3.3).

Changes in exposure of A1913 and A1918 in 70S ribosomes

SHAPE analysis shows that A1913 gains flexibility upon subunit association. Nucleotide A1913 also has different conformations in crystal structures of 50S subunits and 70S ribosomes [5, 177]. Therefore, DMS probing was employed to examine the N1 accessibility of A1913 (Figure 3.2d, e). In this case, A1913 shows a two-fold difference in reactivity between 50S subunits and 70S ribosomes, with lower accessibility in 70S ribosomes (Figure 3.2f). Residue A1912 is weakly reactive in 50S subunits and unreactive in 70S ribosomes. In contrast, A1918 is strongly protected from DMS with a greater than ten-fold decrease in reactivity as a result of subunit association, consistent with previous probing data [202]. This difference could result from a change in H69 structure or protection due to 30S subunit interactions.

To further explore base accessibility in H69, DEPC was employed (Figure 3.2g, h). This reagent reacts with adenosine N7 and is also sensitive to variations in base-pairing or base-stacking interactions [189]. In contrast to the DMS results, DEPC probing reveals that A1913 is a

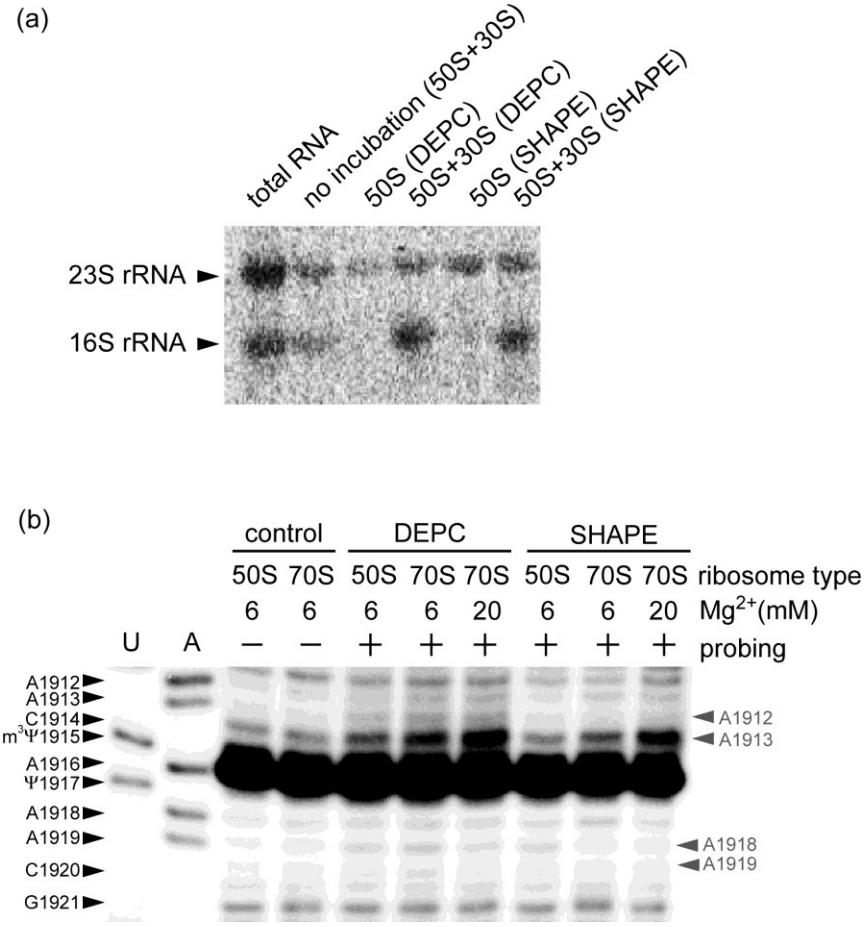

Figure 3.3. Chemical probing analysis of 50S and 70S ribosomes after reassociation process. (a) Agarose gel result shows the integrity of the rRNAs after the reassociation process (0.8% agarose in 0.5x TBE buffer). The isolated 50S and 30S subunits were reactivated independently, and then mixed together at 1:1.5 ratio under high Mg^{2+} concentration (20 mM) and incubated at 37 °C for 30 min for reassociation. The reassociated ribosomes were distributed for each probing condition (DEPC or SHAPE) and the Mg^{2+} concentration was adjusted 6 or 20 mM. After pre-incubation at 37 °C for 20 min, probing was initiated by adding DEPC or NMIA. Subsequent treatment was identical as described in Section 3.5. The no incubation sample contains rRNAs that were extracted before reassociation. (b) An autoradiogram of the probing analysis for the reassociated ribosomes.

weakly reactive site in 50S subunits and eight-fold more reactive in 70S ribosomes (Figure 3.2i). This result suggests the release of A1913 from base-stacking interactions, most likely with A1912, upon subunit association. The results of DEPC probing at position 1918 also differ from those with DMS. Although the relative trend is similar, this residue shows less than a two-fold difference in reactivity between 50S subunits and 70S ribosomes. These differences are likely attributed to varying accessibilities of the N1 and N7 positions of A1913 and A1918. Indeed, in 70S ribosome high-resolution crystal structures, the N1 position of A1918 projects into the H69 loop; whereas, the N7 of A1918 faces the solvent-accessible surface [5].

The role of A1913 in H69

DEPC probing shows liberation of A1913 from a protected to an accessible state and SHAPE analysis shows its increased conformational flexibility in 70S ribosomes. In contrast, reduced DMS, DEPC, and NMIA reactivity of A1918 in 70S ribosomes compared to 50S subunits indicates protection of its N1, N7, and 2'-OH, respectively. These data suggest that formation of intersubunit bridge B2a results in confinement and/or protection of A1918, while in turn leading to conformational flexibility of A1913 on the opposite side of the H69 loop. Residue A1913 has been proposed to be important for cognate and near-cognate tRNA selection through direct contact with ribose 37 of the A-site tRNA anticodon stem loop [47, 203]. A crystal structure of 70S ribosomes also shows that the A1913 base rotates around its C-N glycosidic bond upon A-site tRNA binding [203]. Interestingly, the N7 of A1913 interacts with position 38 of cognate tRNAs through a Mg^{2+} ion; whereas, the Mg^{2+} ion bridges an interaction between A1913 of H69 and G1494 of h44 with near-cognate tRNA (Figure 3.4) [203]. Thus, it is possible that A1913 liberation from base-stacking interactions in the H69 loop and acquisition of local conformational elasticity upon 70S ribosome formation are necessary in order for the ribosome to have translational fidelity and to monitor incoming tRNAs.

The positioning of A1913 has also been proposed to be important for RF-mediated peptide release during translation termination [60]. A crystal structure of the 70S ribosome-RF1 complex shows A1913 projecting into the minor groove of the A site of 16S rRNA [60]. This interaction is

believed to prevent extrusion of A1493 of h44 and promote RF binding to the ribosome [60]. This model is supported by the observation that aminoglycosides, which induce A1492/A1493 base flipping in 16S rRNA [8], compete with RF binding [104]. Interestingly, the RF- and A-site tRNA-binding regions of H69 are quite similar, although the A1913 positioning is quite different. Thus, the local nucleotide flexibility of residue A1913 and H69 structural rearrangements likely play an important role in sensing or regulating local interactions, in a manner similar to that of A1492/A1493 in 16S rRNA.

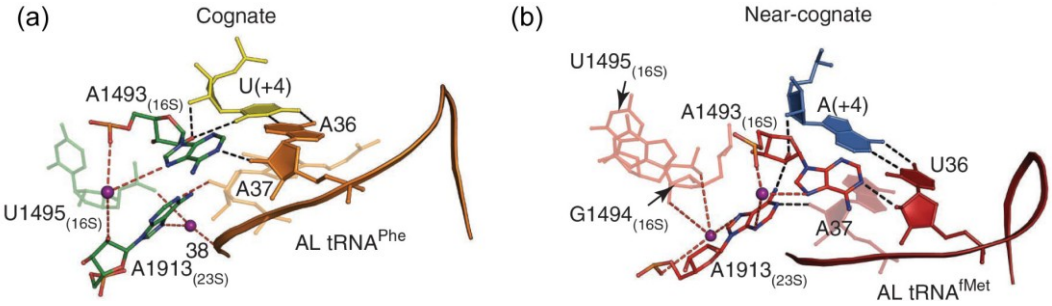

Figure 3.4. Molecular interactions during decoding (a) the cognate or (b) near-cognate tRNA are shown. This figure is adapted from Yusupov M, 2010 [220]. In these crystal structures, A1913 rotates and switches its interactions with h44 of the 30S subunit and the cognate or near-cognate tRNA.

3.3.2. The Ψ1911-A1918-A1919 network

DEPC probing shows slightly reduced reactivity at A1919 in 70S ribosomes when compared with 50S subunits (Figure 3.2g). Even though the band intensity is quite low (Figure 3.2i), this change is reproducible. In crystal structures of bacterial 70S ribosomes, a non-canonical Hoogsteen interaction between Ψ1911 and A1919 bridged by the 2'-OH of A1918 is observed (Figure 3.1b) [5]. However, SHAPE analysis reveals that the 2'-OH of A1918 is reactive in 50S subunits but unreactive in 70S ribosomes, and DMS probing shows that the N1 of A1918 is

accessible in 50S subunits but protected in 70S ribosomes. These data suggest that A1918 does not participate in a Ψ1911-A1918-A1919 network in 50S subunits.

These probing results lead to the hypothesis that A1918 moves into the H69 loop upon subunit association and interacts with Ψ1911-A1919, leading to further protection of A1919 N7 from DEPC. Therefore, DEPC probing was carried out under higher Mg^{2+} concentration (20 mM) in order to stabilize the Ψ1911-A1918-A1919 interaction (Figure 3.5a-c). Further protection of A1919 N7 in 70S ribosomes is observed (Figure 3.5a, c). Sites in the neighboring helix 68 (H68) were used to confirm that DEPC reactivity is the same under these conditions (Figure 3.6). In the case of A1918, its reactivity is further reduced (two-fold) in 70S ribosomes under the higher Mg^{2+} conditions, although not completely eliminated (Figure 3.5c).

3.3.3. Influence of Mg^{2+} ion on H69 structure: increased exposure of A1913 at high Mg^{2+}

In contrast to other residues in H69, A1913 exhibits elevated DEPC reactivity in 20 mM Mg^{2+} (Figure 3.5b, c). This result suggests that the Mg^{2+}-stabilized ribosome conformation favors the flipped-out structure of A1913 (Figure 3.5d). SHAPE analysis (Figure 3.5e) supports this result, and increased reactivity of A1913 is observed under the higher Mg^{2+} conditions. In contract, the DMS-probing pattern for A1913 is not affected by changing the Mg^{2+} concentration (Figure 3.5f), suggesting solvent exposure of only one side of the base. The link between altered conformational dynamics with increased Mg^{2+} concentration and A1913 base flipping may play a role in factor-binding events. For example, binding of cognate tRNA or stop-codon recognition by RFs may cause reduced H69 conformational flexibility around A1918, but increased exposure of A1913. Moreover, it is known that elevated Mg^{2+} concentrations cause lower translational fidelity *in vitro* [6]. This result would suggest that A1913 is able to interact with both cognate and near-cognate tRNAs in high Mg^{2+}, perhaps due to improper positioning.

3.3.4. Importance of Ψ modifications in regulating H69 conformational states

A distinct characteristic of H69 is the conserved modified nucleotides in its loop region, including Ψ at positions 1911 and 1917 and 3-methylpseudouridine ($m^3\Psi$) at 1915 [105, 106].

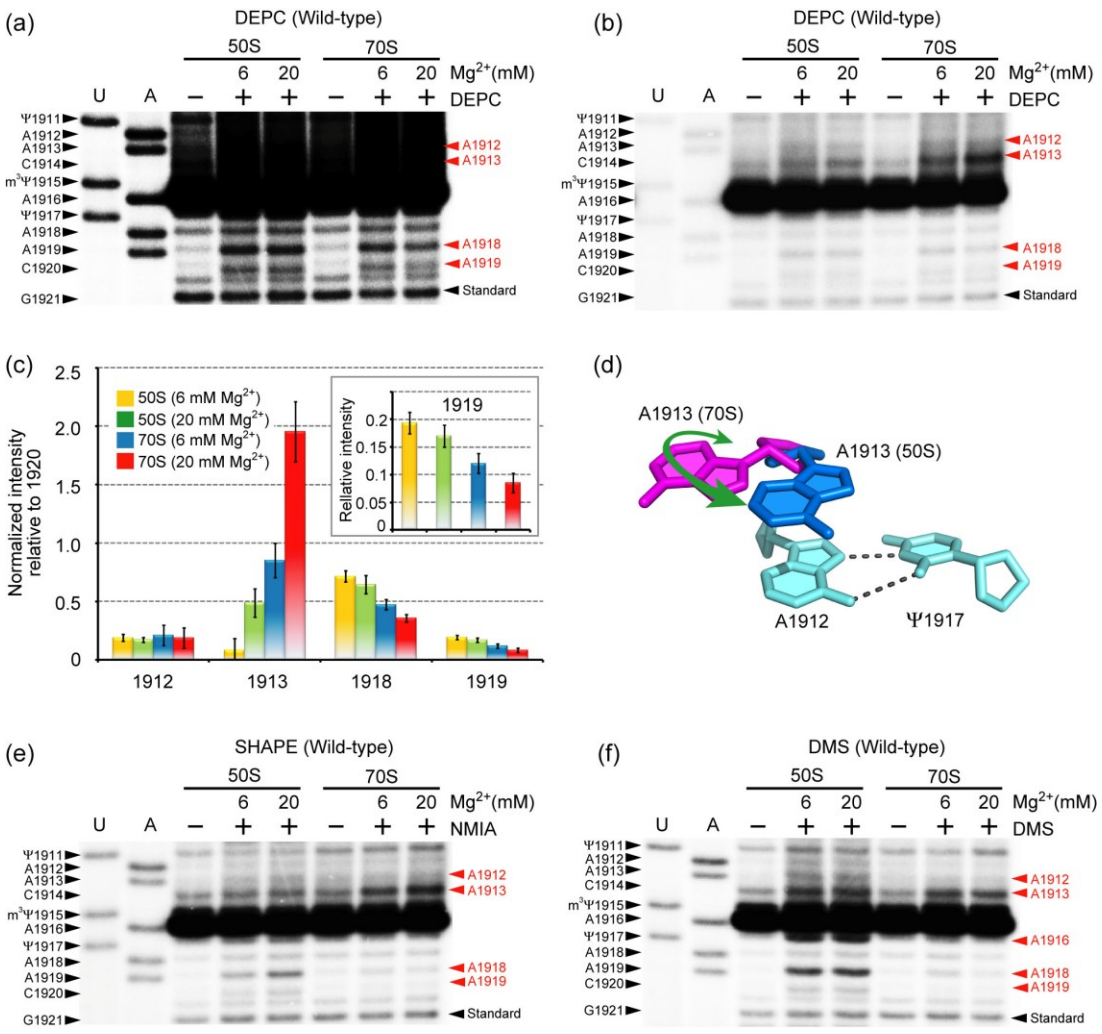

Figure 3.5. Autoradiograms show DEPC probing of H69 in wild-type 50S subunits and 70S ribosomes under low and high Mg^{2+} conditions with longer (a) and shorter (b) gel exposure times. Chemical modification sites are shown in red on the right side of the gel. (c) Quantification analysis for the DEPC probing is shown (inset: normalized band intensity at position 1919). (d) The proposed A1913 conformational change is illustrated. Autoradiograms for SHAPE (e) and DMS (f) analyses under 6 and 20 mM Mg^{2+} concentrations are shown.

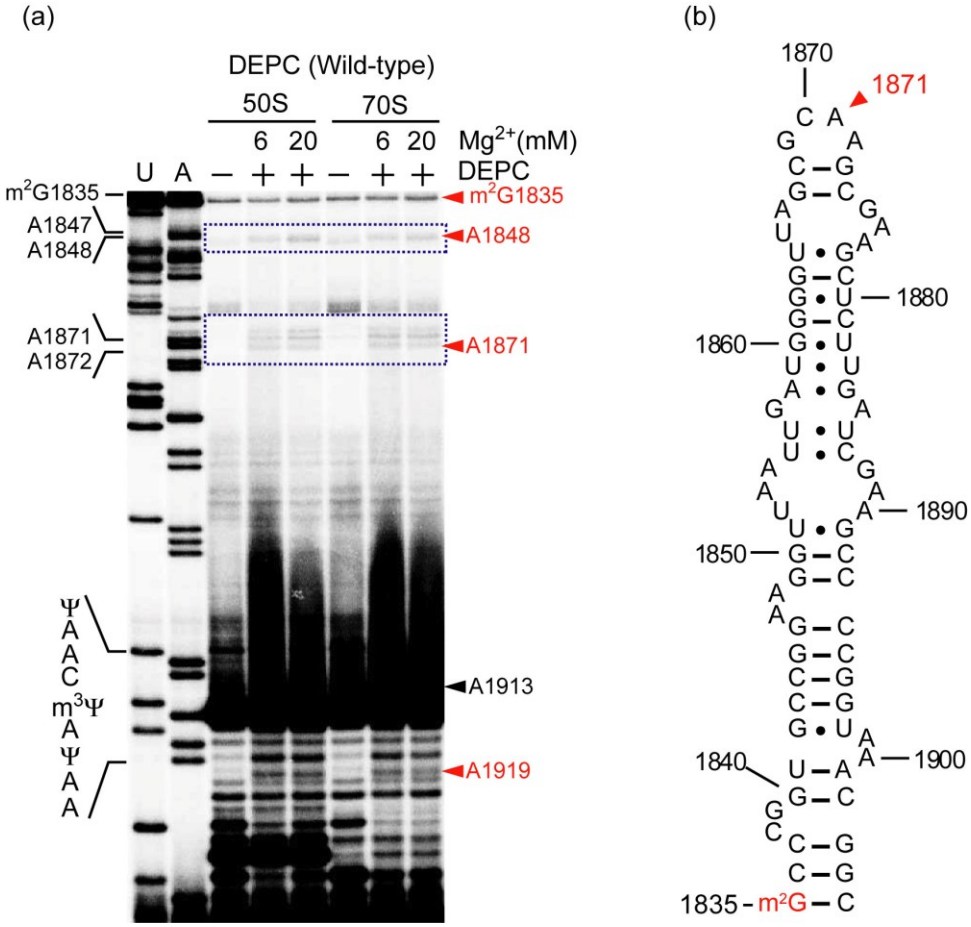

Figure 3.6. The autoradiogram for DEPC probing under low and high Mg^{2+} conditions and the secondary structure of H68 of 23S rRNA are shown. Analysis of the H68 region shows that changing the Mg^{2+} concentration does not alter DEPC reactivity at N7 of A1871 and A1848, and the increased A1913 reactivity is predominantly attributed to H69 conformational changes. Because of the strong reverse transcription stop at $m^3\Psi$1915, it is challenging to show the H69 and H68 regions on the same image. Position 1835 is naturally modified at the N2 position of G in *E. coli* 23S rRNA, such that modified base-dependent reverse transcription stops can be used for band normalizations as described in the main text.

Ribosomes lacking Ψ modifications in H69 exhibit slow growth rates *in vivo* and reduced subunit association *in vitro* [83]. A mutant phenotype in a bacterial strain lacking H69 Ψ modifications (RluD(–)) can be rescued by mutations in RF2 protein at a site adjacent to H69-interacting residues [107]. However, recent studies revealed that the RluD(–) phenotype is actually the consequence of mutant RF2 in the *E. coli* K-12 strains; whereas, *E. coli* B strains and *Salmonella enterica* containing fully active RF2 do not display the mutant phenotype, even upon deletion of the *rluD* gene encoding for H69 pseudouridine synthase [108]. Although the role of Ψ residues in translation termination is questionable, H69 itself is still indispensable for efficient termination by RFs [59, 103] and its conformation is likely to be important [60]. Previous model studies using small RNAs revealed that Ψs in H69 play an important role in maintaining the loop structure [109, 110]. To better understand the role of Ψ modifications in H69 structure during subunit association, SHAPE analysis was also carried out on Ψ-deficient ribosomes (RluD(–) [83]) and compared with data on wild-type *E. coli* ribosomes (Figure 3.7a, unmodified H69).

Changes in H69 loop flexibility

SHAPE analysis shows less than two-fold increased NMIA reactivity at A1913 in 70S RluD(–) ribosomes relative to 50S subunits and two-fold reduced reactivity of A1918 in 70S ribosomes relative to 50S subunits (compared to a four-fold increase at 1913 and seven-fold reduction at 1918 in wild-type ribosomes) (Figure 3.7b; in this case the data was normalized to m^2G1835, a non-specific reverse transcriptase stop site (Figure 3.6b)). Furthermore, A1913 displays four-fold higher NMIA reactivity than A1918 in wild-type 50S subunits, but displays similar levels of reactivity in RluD(–) 50S subunits. The diminished reactivity at A1918 in RluD(–)compared to wild-type ribosomes implies a difference in helix 69 conformation. Substitution of U for Ψ at position 1911 could affect the 1911-1918-1919 network, resulting in reduced protection or increased flexibility of the A1918 2'-OH. This effect would, however, be indirect because the hydrogen-bonding capability of U on the Watson-Crick face is the same as Ψ (N3-H). A weakened 1911-1918-1919 interaction could in turn affect subunit association of RluD(–) ribosomes. Nucleotides A1912, C1914, A1916, and U1917 are also found to be less constrained

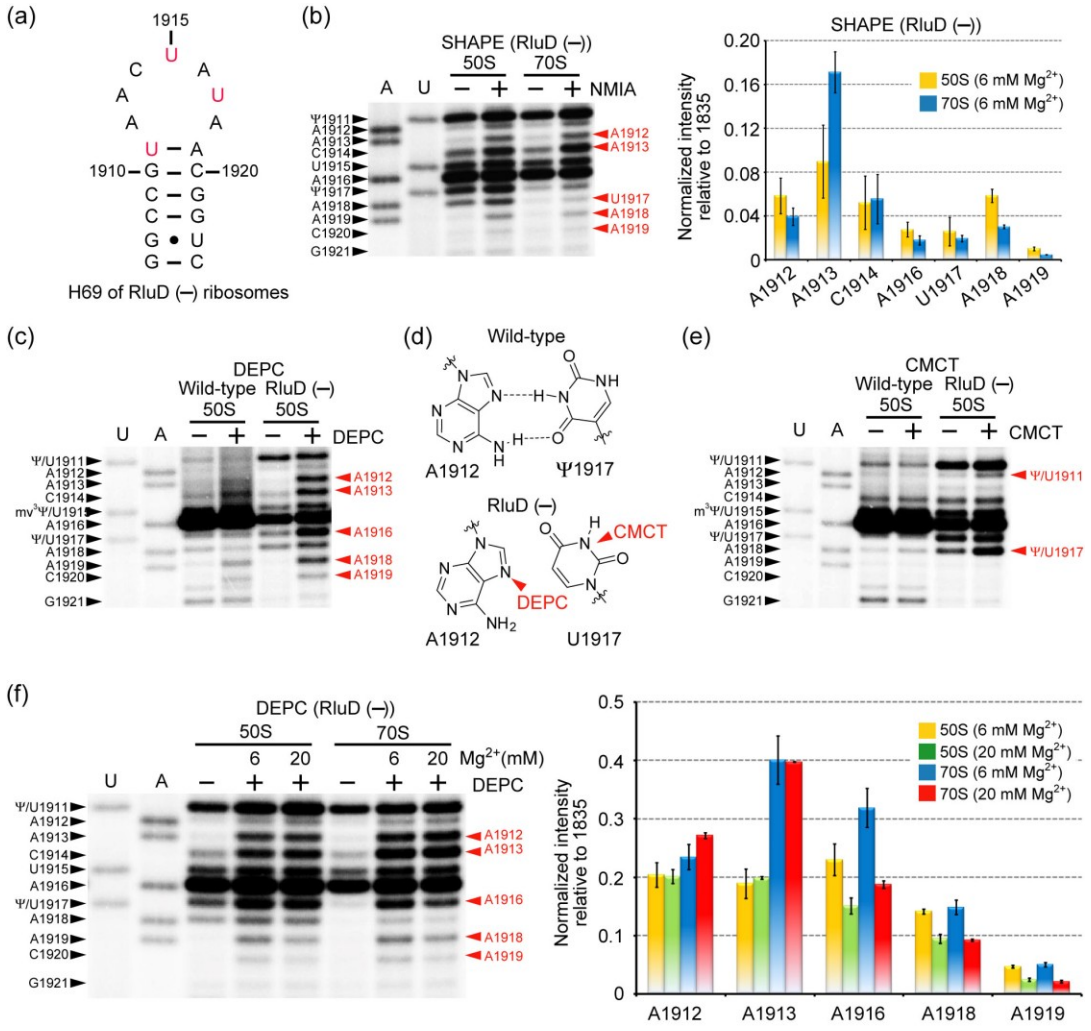

Figure 3.7. (a) The RluD(–) H69 RNA sequence is shown. (b) Autoradiogram (left) and quantification (right) of SHAPE reactivity on RluD(–) ribosomes are shown. Chemical modification sites are in red on the right side of the gel (m^2G1835 was used for normalization). Comparisons of DEPC- (c) and CMCT-probing (e) patterns between wild-type and RluD(–) 50S subunits are shown. (d) DEPC and CMCT reactive sites in RluD(–) ribosomes are indicated. (f) Autoradiogram (left) and quantification (right) of DEPC reactivity of RluD(–) 50S and 70S ribosomes under low and high Mg^{2+} conditions are shown.

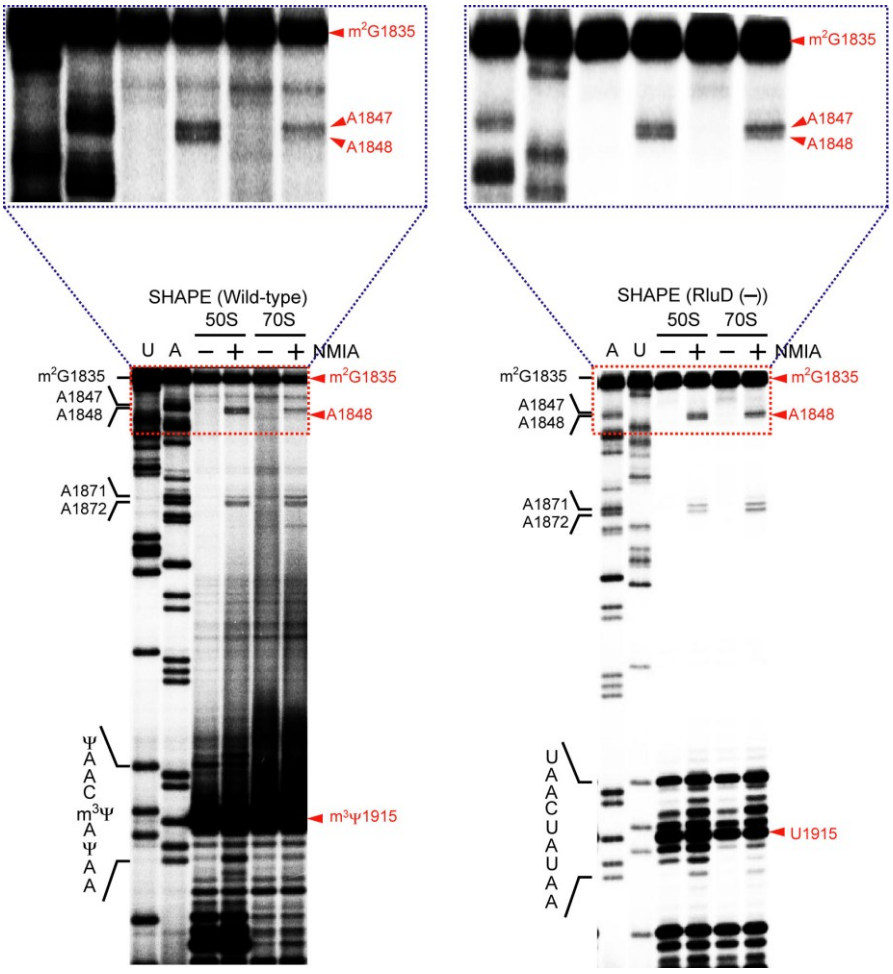

Figure 3.8. Autoradiograms for SHAPE analysis on wild-type (left) and RluD(–) ribosomes are shown. Position A1848 shows protection from the SHAPE reaction in 70S ribosomes.

in RluD(–) compared to wild-type 50S subunits (Figure 3.7b). The level of reactivity at C1914 on wild-type ribosomes is unclear, however, because this position is completely masked by a strong reverse transcription stop at $m^3\Psi$1915. Nonetheless, the observation that many loop components are less constrained in RluD(–) ribosomes indicates a less organized H69 structure in comparison to wild-type H69, consistent with previous model studies [109, 110]. Despite these differences, SHAPE analysis shows clear evidence for intersubunit bridge B7a [5] formation in both wild-type and RluD(–) ribosomes, as indicated by decreased flexibility at position A1848 of the neighboring H68 upon subunit association (Figure 3.8).

Changes in H69 nucleotide accessibility

In support of the SHAPE data, DEPC probing on RluD(–) 50S subunits shows increased exposure of A1912 and A1916, as well as A1913 and A1918, relative to wild-type 50S subunits (Figure 3.7c). If A1912 interacts with U1917, either the N1 or N7 of A1912 are expected to be protected from DMS or DEPC, respectively; however, both sites in RluD(–) 50S subunits are highly reactive, suggesting a lack of such interaction in the unmodified RNA (Figure 3.7d) [184]. To further confirm the lack of an A1912-U1917 interaction, CMCT (1-cyclohexyl-(2-morpholinoethyl) carbodiimide metho-*p*-toluene sulfonate) was used to probe the pseudouridine/uridine residue. Although Ψ is known to react with CMCT to a lesser extent than U [193], a control experiment under denaturing conditions with the same CMCT concentration and reaction time revealed strong reactivity at Ψ1917 (Figure 3.9). Under native RNA folding conditions, the N3 of Ψ1917 was protected from CMCT in wild-type ribosomes; whereas, the N3 of U1917 in RluD(–) 50S subunits showed high reactivity, suggesting greater accessibility than the modified RNA (Figure 3.7e). These results indicate the importance of Ψ1917 for reverse-Hoogsteen formation with A1912 (Figure 3.7d). These observations suggest that unmodified H69 forms a less structured loop conformation due to a lack of the 1912-1917 Hoogsteen interaction and base-stacking interactions, consistent with model studies [109, 110].

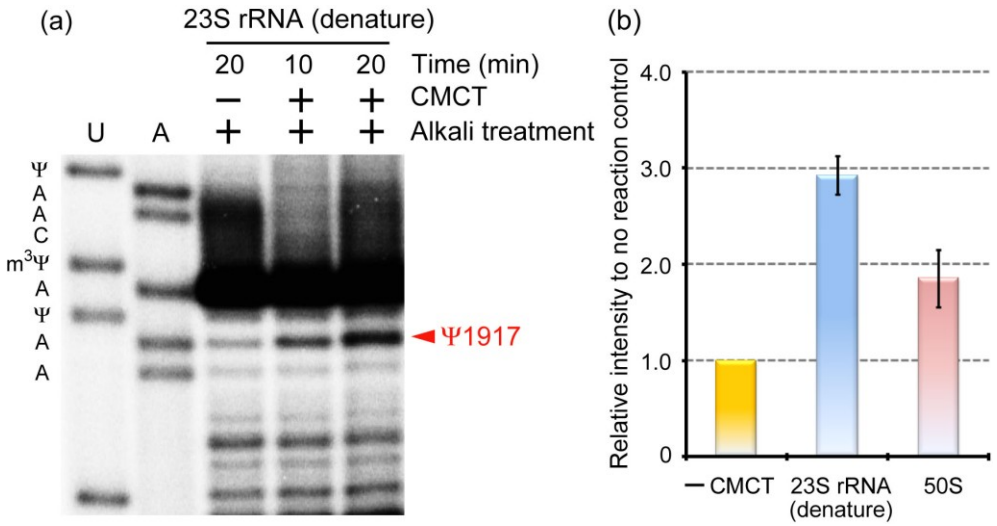

Figure 3.9. (a) Autoradiogram for CMCT reactivity under denaturing conditions and (b) relative band intensities compared to the no reaction (– CMCT) band are shown. CMCT probing conditions (10 min) used to probe 50S subunits as described in the main text are sufficient to label the N3 of Ψ1917, and comparison between the denaturing conditions and 50S subunit probing conditions exhibits 40 to 50% protection of the N3 of Ψ1917 from CMCT in the structured H69 of 50S subunit.

Changes in Mg^{2+} dependence

DEPC probing was also performed on RluD(–) ribosomes under varying Mg^{2+} conditions (Figure 3.7f). DEPC reactivity is increased 2-fold and 1.5-fold at A1913 and A1916, respectively, in 70S ribosomes relative to 50S subunits in 6 mM Mg^{2+}. In contrast, the level of A1916 reactivity is similar in 50S subunits and 70S ribosomes under 20 mM Mg^{2+} conditions. The reactivity of A1912 is increased slightly (less than 1.5-fold) in 70S ribosomes compared to 50S subunits. Residues A1918 and A1919 exhibit similar trends in relative reactivities in wild-type and Ψ-deficient ribosomes. The most noticeable difference between RluD(–) and wild-type ribosomes occurs at A1913. The elevated DEPC reactivity in 70S ribosomes with increased Mg^{2+} does not occur with Ψ-deficient ribosomes. These results suggest that, in the absence of Ψs, H69 has an altered Mg^{2+}-dependent conformation, which could alter the B2a interaction during subunit association. Furthermore, increased DEPC reactivity at A1916 in RluD(–) ribosomes could be interpreted as a loss in base-stacking interactions [110]. Mutagenesis studies showed that

deletions or additions at position 1916 (ΔA1916 and +AA1916) lead to diminished viability, and point or multiple mutations around positions 1914 to 1918 are lethal to bacteria [175]. Combined with probing results, these data suggest that nucleotide positioning in H69, particularly at A1913 and A1916, is one of the key factors in regulating ribosome function. Mutations or Ψ deletions in H69 disrupt well-defined conformational states, and therefore could affect ribosome function, although the *in vivo* effects may be subtle [108].

3.4. Discussion

In this chapter, a detailed conformational analysis of the H69 region of 23S rRNA in 50S subunits and 70S ribosomes was carried out through a series of chemical-probing reactions. The data reveal conformational rearrangements of H69 upon subunit association. In this process, residue A1913 is more exposed with greater flexibility in 70S ribosomes compared to 50S subunits (summarized in Figure 3.10). The movement of A1913 in 70S ribosomes might play a role in tRNA selection and peptide release by RFs. Residue A1913 has been proposed to monitor the incoming aminoacyl tRNA through direct interactions with the anticodon stem loop [47]. On the other hand, A1913 has also been proposed to project into the minor groove of h44 and base stack with A1493, which would provide a structure that favors interactions with RF1 [60]. Many studies reveal that H69 has interactions through both its stem and loop [21, 46, 47, 59-61, 99]. Residue A1913 seems to play a key role in the mechanism of stabilizing subunit association, and thus, the fact that this nucleotide can accommodate multiple conformations in solution as observed in crystal structures is perhaps not surprising. The adaptability of A1913 is therefore likely to play an important role in translation. Disruption or enhancement of such activity (*e.g.*, high Mg^{2+} or loss of Ψs in H69) could cause abnormal ribosome activities, such as low translational fidelity [6] or aberrant translation termination [107].

Conformational adaptability at residues A1918 and A1919 may play a role in forming the conformational states of H69 necessary for tRNA translocation and ratchet-like motions of the ribosome [98]. Indeed, crystal structures having a hybrid tRNA state (P/E state) induced by RRF or RF3 show conformational compression of H69 and large movement of H69 toward the E site

without disrupting the intersubunit bridge B2a [98, 204]. An interchangeable network at the stem-loop junction of H69 involving A1918 and A1919, and also causing disruption of the terminal base pair (C1925-G1929) as observed in crystal structures, might play a role in ribosome energetics during translation [98]. In conclusion, we show that multiple positionings of specific nucleotides in H69 is possible, and that pseudouridine modifications do play a role in H69 dynamic behavior. These results show a previously unseen view of conformational complexity of H69 during ribosome translation cycles, or ribosome motions. Developing a deeper understanding of H69 structural changes and determination of its conformational states at each step of translation will be useful for future antibiotic drug development with specific targeting of the individual conformational states.

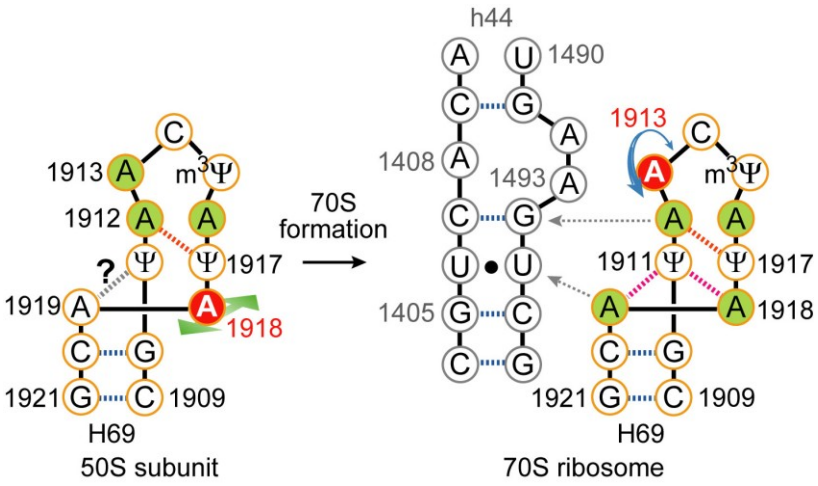

Figure 3.10. A schematic illustration shows the proposed H69 structural rearrangement at A1913 and A1918 upon subunit association and interactions with h44 of 16S rRNA (red circles = flexible nucleotides; green circles = protected nucleotides, as determined by SHAPE and DEPC; red dashed lines = non-canonical base-pair interactions). The probing data cannot confirm a hydrogen-bonding interaction between A1919 and Ψ1911.

3.5. Materials and methods

Ribosomes were prepared as discussed in Chapter 2.

3.5.1. 2'-hydroxyl acylation analyzed by primer extension (SHAPE)

SHAPE (2'-hydroxyl acylation analyzed by primer extension) was performed as described in the literature [196]. Simply, ribosomes were reactivated in the presence of 150 mM KCl at 37 °C for 15 min, buffer was exchanged with SHAPE buffer (50 mM HEPES, 150 mM KCl, 6 mM $MgCl_2$, pH 8.0 at 37 °C), and the ribosome concentration was adjusted to 0.3 μM. Ribosomes in SHAPE buffer were incubated for over 15 min at 37 °C and the reaction was initiated by addition of 100 mM *N*-methylisatonic anhydride (NMIA) (Invitrogen) at a final concentration of 5 or 10 mM. The SHAPE reaction was done for 20 min at 37 °C and stopped by adding cold ethanol. Ribosomes were recovered by centrifugation and extracted with phenol-chloroform. The extracted rRNA was analyzed by standard primer extension assay with a 5'-^{32}P-labeled DNA primer targeting positions 1929 to 1948 of 23S rRNA (5'-CGACAAGGAATTTCGCTACC-3'; 20mer DNA from Sigma-Genosys). Gel images were taken on a Typhoon 9200 (GE Healthcare). All probing experiments were performed three independent times and data analyses were completed with three experimental data sets to obtain standard errors. Band intensities were measured by using ImageQuant TL software (GE Healthcare). The background volume of a non-reacted control band was subtracted from the net band volume. Then, the relative intensity was calculated by dividing the corrected target band intensity by the standard band intensity.

3.5.2. Diethylpyrocarbonate (DEPC) and dimethylsulfate (DMS) probing

DEPC and DMS probing reactions were carried out using a modified literature procedure [189, 191]. The isolated ribosome was reactivated in the presence of 100 mM NH_4Cl at 37 °C for 15 min. Two μl of DEPC (Sigma-Aldrich, St. Louis, MO) or 2 μl of 1:50 diluted DMS (Sigma-Aldrich) in cold ethanol was added to reactivated ribosomes in 40 μl of reaction buffer (80 mM HEPES, 100 mM NH_4Cl, 6 mM $MgCl_2$, pH 7.3 at 37 °C) in the presence of 0.3 μM ribosomes. Samples were then incubated at 37 °C for 20 min with gentle agitation in the case of DEPC probing. The

reaction was terminated by adding 20 µl stop buffer (3 M 2-mercaptoethanol, 1 M Tris-HCl, pH 7.5, 10 mM $MgCl_2$) followed quickly by ethanol precipitation. The subsequent treatment was identical to the procedure described above for the SHAPE experiments.

3.5.3. CMCT modification

Reactions with 1-cyclohexyl-(2-morpholinoethyl) carbodiimide metho-p-toluene sulfonate (CMCT) modification were performed as follows. The isolated ribosome was reactivated in the presence of 100 mM NH_4Cl at 37 °C for 15 min. The reaction was initiated by addition of an equal volume of CMCT solution (42 mg/ml; Sigma-Aldrich) to reactivated ribosomes in 15 µl CMCT reaction buffer (50 mM HEPES, 100 mM NH_4Cl, 6 mM $MgCl_2$, pH 8.1 at 37 °C). The modification was performed at 37 °C for 10 min and terminated by adding cold ethanol followed quickly by precipitation. The subsequent treatment was identical to the procedure described above for the SHAPE experiments.

3.5.4. Probing studies for reassociated ribosomes

The isolated 50S and 30S subunits were independently reactivated in the presence of 100 mM NH_4Cl at 37 °C for 15 min. The reactivated 50S and 30S subunits were mixed together at 1:1.5 mole ratio and then incubated at 37 °C for 30 min under high Mg^{2+} concentration (20 mM HEPES, 60 mM KCl, 20 mM $MgCl_2$, pH 7.3 at 37 °C). Excess 30S subunit was used to facilitate subunit association. The reassociated 70S ribosome was distributed into each probing buffer condition (80 mM HEPES, 70 mM NH_4Cl, 30 mM KCl, 6 mM or 20 mM $MgCl_2$, pH 7.3 at 37 °C for DEPC, and 50 mM HEPES, 150 mM KCl, 6 mM or 20 mM $MgCl_2$, pH 8.0 at 37 °C for SHAPE) and the ribosome concentration was adjusted to 0.3 µM. This solution was pre-incubated at 37 °C for 15 min, and probing reactions were initiated by adding DEPC or NMIA as mentioned above. The subsequent treatment was identical to the procedure described above for the SHAPE experiments.

3.5.5. Data analysis

Gel data were analyzed by ImageQuant TL (GE Healthcare). Band intensity was measured and background intensity was subtracted manually. The nonspecific band intensity was also measured in the no-reaction lane and subtracted. This band intensity was normalized with respect to a standard band; position 1921 or 1835 were used for wild-type or RluD(–) ribosomes, respectively. In the case of wild-type ribosome experiments, 1921 showed very consistent band intensities throughout any probing experiment; however, in the case of RluD(–) ribosome experiments, 1921 was less consistent throughout all conditions. Furthermore, because SHAPE is a base-nonspecific probing method, any position that could show a local nucleoside flexibility in the H69 loop cannot be employed due to potential reactivity to SHAPE. Thus, the position 1835 was employed for RluD(–) experiments. Position 1835 has a naturally occurring base modification (m^2G), such that m^2G1835 should stop reverse transcription in a nonspecific manner. It should be noted that m^2G1835 is buried deep inside of the 50S and 70S ribosome in crystal structures; therefore, this position should be a non-reactive to chemical probing, including SHAPE. All experiments, except for reassociated 70S ribosome probing, were performed at least three times independently and standard errors were calculated.

Chapter 4
A tool for monitoring small molecule binding to helix 69 RNA

4.1. Abstract

Helix 69 (H69) of 23S ribosomal RNA is a unique model system, not only for shedding light on the impact of modified bases on ribosome translation, but also as a suitable candidate for exploring antibiotic targeting. H69 lies at the functionally important core domain of the ribosome, participates in a key intersubunit bridge (B2a) interaction, and plays an important role in translation [5]. H69 takes on multiple conformational states [5] and participates in key molecular interactions with translation factors [12, 60, 99, 205] at different steps of translation. In previous chapters, I have shown that H69 undergoes dynamic conformational rearrangements upon ribosome association, particularly at positions A1913 and A1918. To better understand the conformational changes of H69 in solution, a tool that allows us to monitor ongoing H69 conformational states in solution would be significant. For this purpose, we introduced an adenine analogue, 2-aminopurine, as a fluorescent probe at position 1913 of a short model hairpin representing H69 RNA (2AP-H69). Here, we demonstrate that H69 loop conformational changes can be monitored by fluorescence changes upon altering the solution pH, Mg^{2+} concentration, temperature, and level of pseudouridine modification. The 2AP-H69 conformational variations observed in this study correlate well with previous biophysical and biochemical analyses. By using this convenient fluorescence monitoring system, we found that aminoglycoside antibiotics have different impacts on H69 loop conformational states.

4.2. Introduction

As stated in previous chapters, H69 of the large ribosomal subunit (50S) is one of the key components in ribosome function, and plays roles in subunit association [103, 174], transfer RNA (tRNA) selection [100, 102], translation termination [59, 60, 103], and ribosome recycling [99, 176]. H69 is located at a region adjacent to the decoding center in the 70S ribosome and forms an intersubunit bridge called B2a together with helix 44 (h44) of the small subunit (30S) [5, 46].

B2a is maintained during the ratchet-like intersubunit rotation and plays a role in keeping the ribosomal subunits associated (see details in Chapter 1).

As discussed earlier in the thesis, H69 contains three post-transcriptional modifications; pseudouridine (Ψ) at positions 1911 and 1917, and 3-methylpseudouridine ($m^3\Psi$) at position 1915 (Figure 4.1a) [105, 106]. The RNA sequence of H69, particularly around the loop region (1911-1918), is highly conserved throughout phylogeny. Thus, Ψ modifications are thought to play important functions as part of this key domain. Indeed, mutagenesis studies in *E. coli* K-12 strains revealed that removal of the three Ψs in H69 by deleting the *rluD* gene (encoding for the pseudouridine synthase that converts Us to Ψs in H69) causes a very slow growth rate *in vivo* and abnormal ribosome association *in vitro* [83]. This Ψ-deficient phenotype can be rescued by a point mutation in release factor 2 (RF2) [107]. Other genetic studies revealed that some point mutations on the H69 loop cause a lethal growth phenotype and others result in error-prone ribosomes (Table 1.3) [94-96, 175].

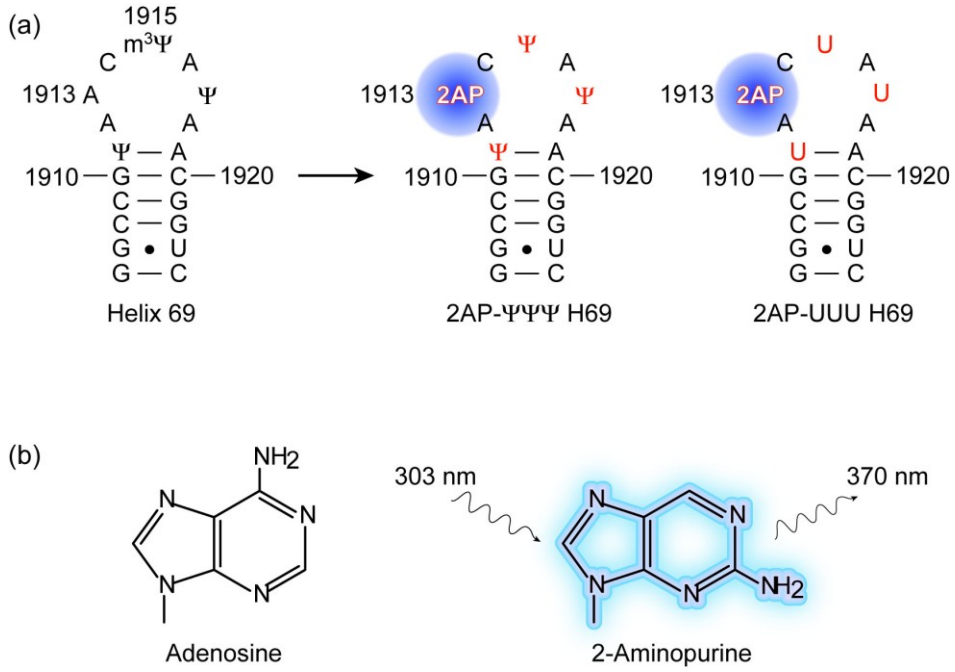

Figure 4.1. (a) A schematic illustration of 2AP-incorporated H69 RNA is shown. (b) The chemical structures of adenosine and 2-aminopurine (2AP) are shown. 2AP is excited at 303 nm and emission is monitored at 370 nm.

One of the important characteristics of H69 is its ability to exist in multiple conformations as observed in high-resolution ribosome crystal structures under different environments [5, 177, 178]. As mentioned in Chapters 2 and 3, the wild-type H69 forms different conformations upon changing solution pH, Mg^{2+} concentration, and solution temperature; whereas, those unique structural properties are diminished by removing Ψ modifications [109, 110, 184, 206]. Such conformational dynamics would contribute to conformational elasticity. Elasticity of the double-stranded stem region of H69 releases a twisting energy generated from the ratchet-like subunit rotation by inducing conformational rearrangements of its stem [98]. Thus, H69 is a dynamic RNA domain, and regulating these H69 conformational dynamics with a small-molecule ligand could be a promising way to disturb bacterial ribosome translation. Developing a monitoring system is therefore important for both studying H69 dynamics in solution and discovering H69-binding small molecules.

Besides characterization of the function of H69 conformational variations, we are also interested in developing tools to monitor these different H69 conformational states in solution, as well as in a rapid and convenient manner. Current experimental techniques to monitor conformational changes of nucleic acids and molecular interactions between small molecules and nucleic acids include circular dichroism (CD) spectroscopy, isothermal titration calorimetry (ITC), and nuclear magnetic resonance (NMR) spectroscopy, among others. One of the critical issues in these methods is the requirement for large amounts of RNA sample, as well as time-consuming data analysis in some cases. The development of a unique tool that can report conformational changes of H69 in solution as a consequence of environmental changes or small-molecule binding on a small scale as well as simple sample preparation and analysis would allow us not only to understand the role of H69 conformational states, but also to carry out novel drug discovery screening.

In this study, 2-aminopurine (2AP), an adenine analogue, was introduced into position 1913 of the small hairpin H69 RNA (2AP-H69; Figure 4.1a and b), which was proposed to undergo local conformational changes under different solution environments (see Chapter 3) [206]. Comparisons of 2AP-H69 RNA fluorescence of the fully modified and unmodified H69 models

revealed a remarkable influence of the Ψ modifications on H69 loop conformational states. Results are consistent with the previously observed conformational changes. Furthermore, we tested aminoglycoside antibiotic binding to 2AP-H69. These results indicate the potential application of 2AP-incorporated model H69 RNAs to both structural and small-molecule binding studies.

4.3. Results

4.3.1. Design of a tool in order to monitor different conformational states of H69

To develop a unique tool that enables us to monitor different H69 loop states in solution, H69 model RNAs containing a fluorescent adenine analogue, 2-aminopurine (2AP), at position 1913 in the presence or absence of Ψs at neighboring positions 1911, 1915, and 1917 (2AP-ΨΨΨ or 2AP-UUU, respectively) were designed (Figure 4.1a and b). The 2AP nucleotide is sensitive to changes in environment, particularly base-stacking interactions, resulting in decreases in its fluorescence as a result of stacking and/or protection from solvent [207, 208]. Based on probing studies discussed in Chapter 3, A1913 was proposed to be base stacked with a neighboring nucleotide in the 50S subunits, but exposed and pulled away from the H69 loop within the context of 70S ribosomes [206]. Therefore, it was proposed that it would be possible to sense the 1913 position and local conformational changes by introducing 2AP at this site. If 2AP1913 forms a similar local conformation in the model system as within the 50S subunit, then its relative fluorescence would be decreased due to base stacking; whereas, if 2AP1913 is exposed and/or flipped out from the H69 loop as observed in 70S ribosomes, then a higher level of fluorescence would be observed. Comparison of the fluorescence intensities between 2AP-H69 RNA completely digested with RNase A (to obtain fragmented RNA) and structured 2AP-H69 RNA revealed a 35–40% decrease in 2AP fluorescence for structured 2AP-H69 RNA in both the modified (2AP-ΨΨΨ) and unmodified (2AP-UUU) cases, indicating formation of base-stacking interactions at position 1913 for these RNAs (Figure 4.2a-c). These results also indicated that the 2AP-ΨΨΨ and 2AP-UUU RNA concentrations were the same, even though the RNA concentrations were determined based on the extinction coefficient of unmodified H69 RNA

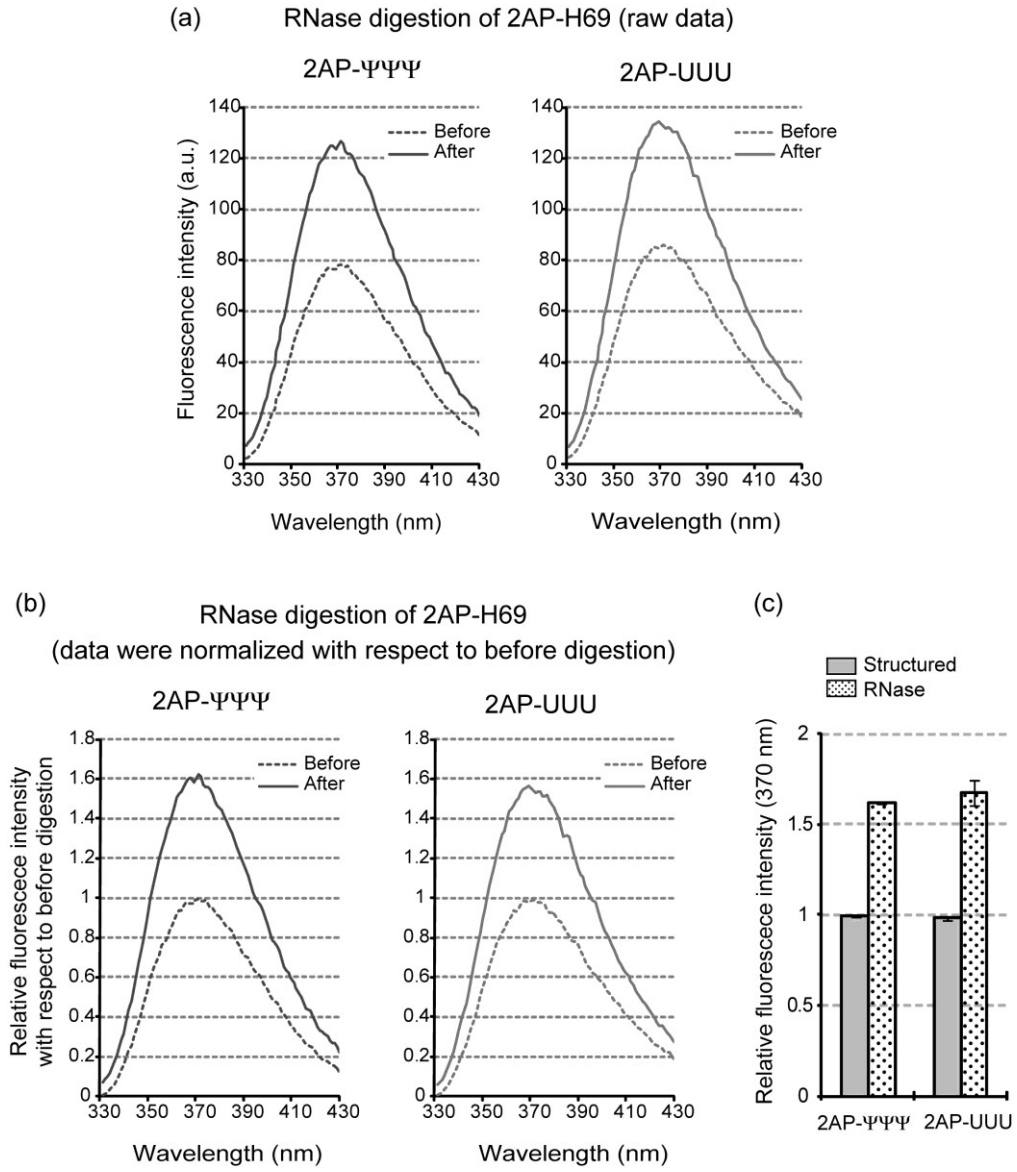

Figure 4.2. (a) Fluorescence measurements for 2AP-ΨΨΨ and 2AP-UUU before (dashed) and after (solid) RNase A treatment are shown. (b) Relative fluorescence curves (values were normalized to data before the RNase digestion) and (c) relative fluorescence intensities at the emission maximum (370 nm) are shown. Data were collected in buffer containing 20 mM K^+-cacodylate, pH 7.3, 70 mM NH_4Cl, and 30 mM KCl. FI is fluorescence intensity (arbitrary units), and Fr is relative fluorescence intensity.

sequence (no 2AP or Ψ modification), due to the inavailability of nearest-neighbor extinction coefficients for either 2AP or Ψ.

4.3.2. Monitoring fluorescence changes of 2AP-H69 under different buffer pHs

Previous model studies indicated a unique conformational transition of the H69 loop upon changes in the solution pH, which was modulated by Ψ modifications [109]. Since the original fluorescence intensity of the 2AP base itself is not influenced by changes in buffer pH from 5.0 to 10.0 (Figure 4.3 and reference [208]), the conformational changes of 2AP-H69 RNA were examined by monitoring 2AP fluorescence upon changes in buffer pH. The 2AP-UUU RNA showed only a 10% reduction in fluorescence at pH 5.5 relative to pH 7.0, whereas the 2AP-ΨΨΨ RNA exhibited a 35% reduction in fluorescence intensity under the same conditions (Figure 4.3). H69 is proposed to be in conformational exchange between the open and closed loop conformations with respect to position 1913, with the closed conformation being preferred under low pH conditions and the open conformation forming under high pH conditions [109]. Thus, reduced fluorescence upon decreasing the solution pH is attributed to enhanced base-stacking interactions of 2AP1913 in the 2AP-ΨΨΨ RNA and formation of a closed loop conformation.

4.3.3. Pseudouridine modifications are essential for Mg^{2+} sensitivity

To further test the characteristics of the 2AP-H69 RNA, Mg^{2+}-titration experiments were performed, since H69 within the ribosome shows different sensitivity to Mg^{2+} concentrations in the presence or absence of the natural Ψ modifications. More specifically, high Mg^{2+} concentrations facilitate exposure of A1913 in H69 [206]. In 2AP-ΨΨΨ, the fluorescence intensity was increased by 60% in 3 mM Mg^{2+} relative to no Mg^{2+}; whereas, 2AP-UUU exhibited less than a 20% increase in fluorescence as the Mg^{2+} concentration was raised (Figure 4.4). These results indicate the importance of Ψ modifications for Mg^{2+} ion binding to H69, or for H69 loop conformation dynamics as a result of Mg^{2+} ion binding. Further increases in fluorescence by adding up to 20 mM Mg^{2+} were also observed with 2AP-ΨΨΨ; however, no additional changes were observed with the 2AP-UUU RNA (Figure 4.4c). Notably, the change in fluorescence of 2AP-ΨΨΨ induced by Mg^{2+}

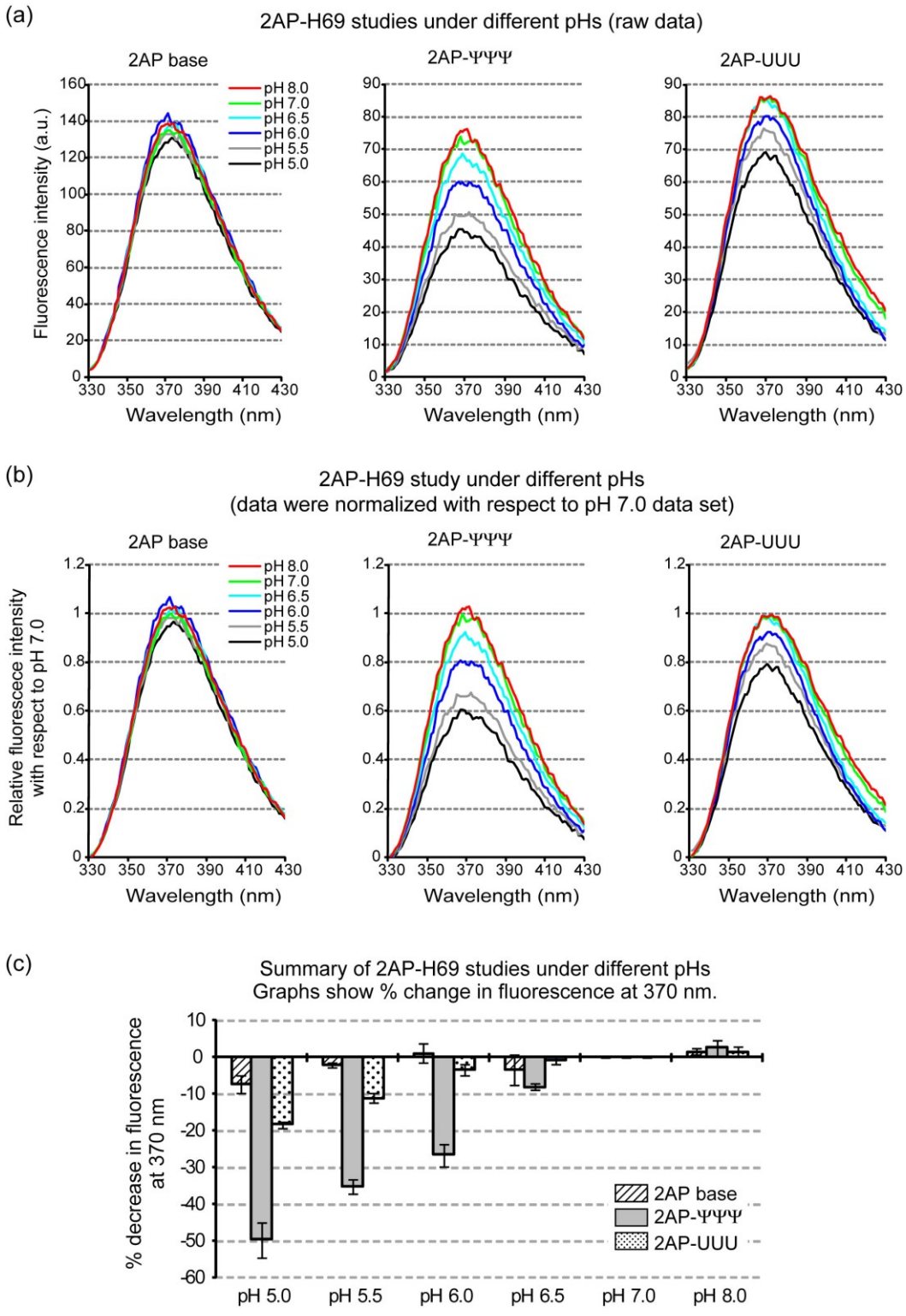

Figure 4.3. (a) Raw data and (b) normalized data for fluorescence intensity changes with buffer pH are shown. (c) Relative fluorescence intensities at the emission maximum (370 nm) upon changing buffer pH are shown.

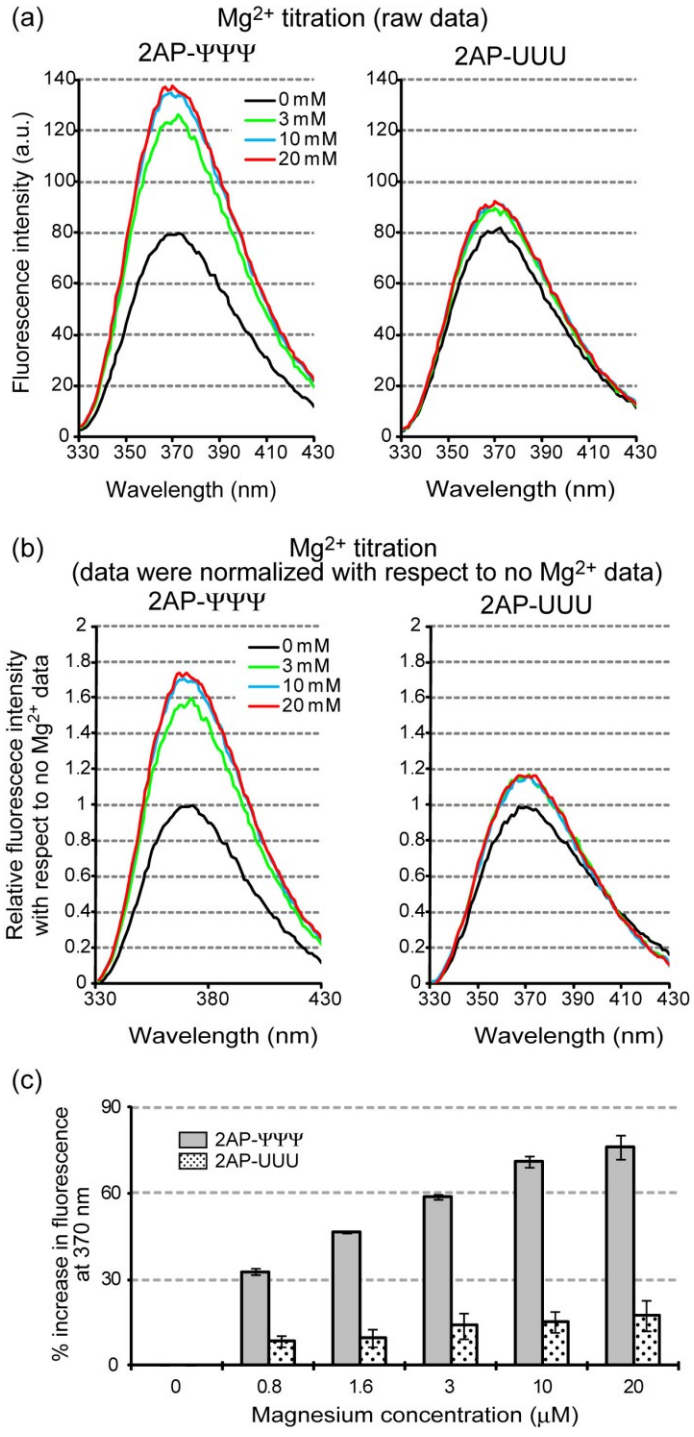

Figure 4.4. (a) Raw data and (b) relative fluorescence curves for Mg^{2+}-binding experiments are shown. (c) Relative fluorescence intensities at the emission maximum (370 nm) are shown.

was saturated (~75%) to a similar extent to that of complete RNase A digestion (~60%), suggesting a high level of exposure of 2AP1913 in the presence of Mg^{2+}. RNase A digestion experiments confirmed that the concentration of the 2AP base at 1913 in 2AP-UUU was the same as for modified RNA; therefore, the Mg^{2+} titration data indicate that the loop conformation of 2AP-UUU does not favor Mg^{2+} binding and/or Ψ modifications of H69 play an important role in organizing the loop structure that favors metal binding.

4.3.4. H69 conformational fluctuations studied upon changing system temperature

One remarkable characteristic of Ψ modifications in H69 is their different positional effects on H69 stability [209]. For instance, a single Ψ modification at position 1911 stabilizes H69 structure (Ψ1911-U1915-U1917; ΔG°_{37} –5.9 kcal/mol) compared to unmodified H69 RNA (ΔG°_{37} –4.8 kcal/mol); whereas, additional Ψ modifications at 1915 and 1917 (Ψ1911-Ψ1915-Ψ1917; ΔG°_{37} –4.8 kcal/mol) destabilize the overall H69 structure relative to the single Ψ1911 modification. Single Ψ modifications at 1915 or 1917 slightly destabilize the H69 structure (ΔG°_{37} –4.2 kcal/mol and –4.6 kcal/mol, respectively). Furthermore, wild-type H69 exhibits increased structural stability under low pH conditions (ΔG°_{37} –4.7 kcal/mol at pH 7.0 versus –5.2 kcal/mol at pH 5.5); whereas, the stability of unmodified H69 did not change (ΔG°_{37} –4.8 kcal/mol at pH 7.0 versus –4.7 kcal/mol at pH 5.5) [109]. Therefore, we examined the influence of Ψ modifications on loop conformational states, as well as stability. At pH 7.0, the 2AP-ΨΨΨ RNA and free 2AP base showed the same temperature-dependent trend, and the 2AP-UUU RNA showed a similar, but 10% reduced fluorescence response (Figure 4.5). At pH 6.0, the 2AP-UUU and 2AP base exhibited the same trend as a pH 7.0; however, an opposite effect of ~25% increased fluorescence was observed for 2AP-ΨΨΨ upon increasing the temperature from 10 to 37 °C (Figure 4.6). Since H69-ΨΨΨ is more stable than H69-UUU under lower pH conditions, it is unlikely that these unusual observations are due to unfolding of H69-ΨΨΨ, but more likely, they are the result of local conformational fluctuations around the H69 loop region that occur upon raising the temperature.

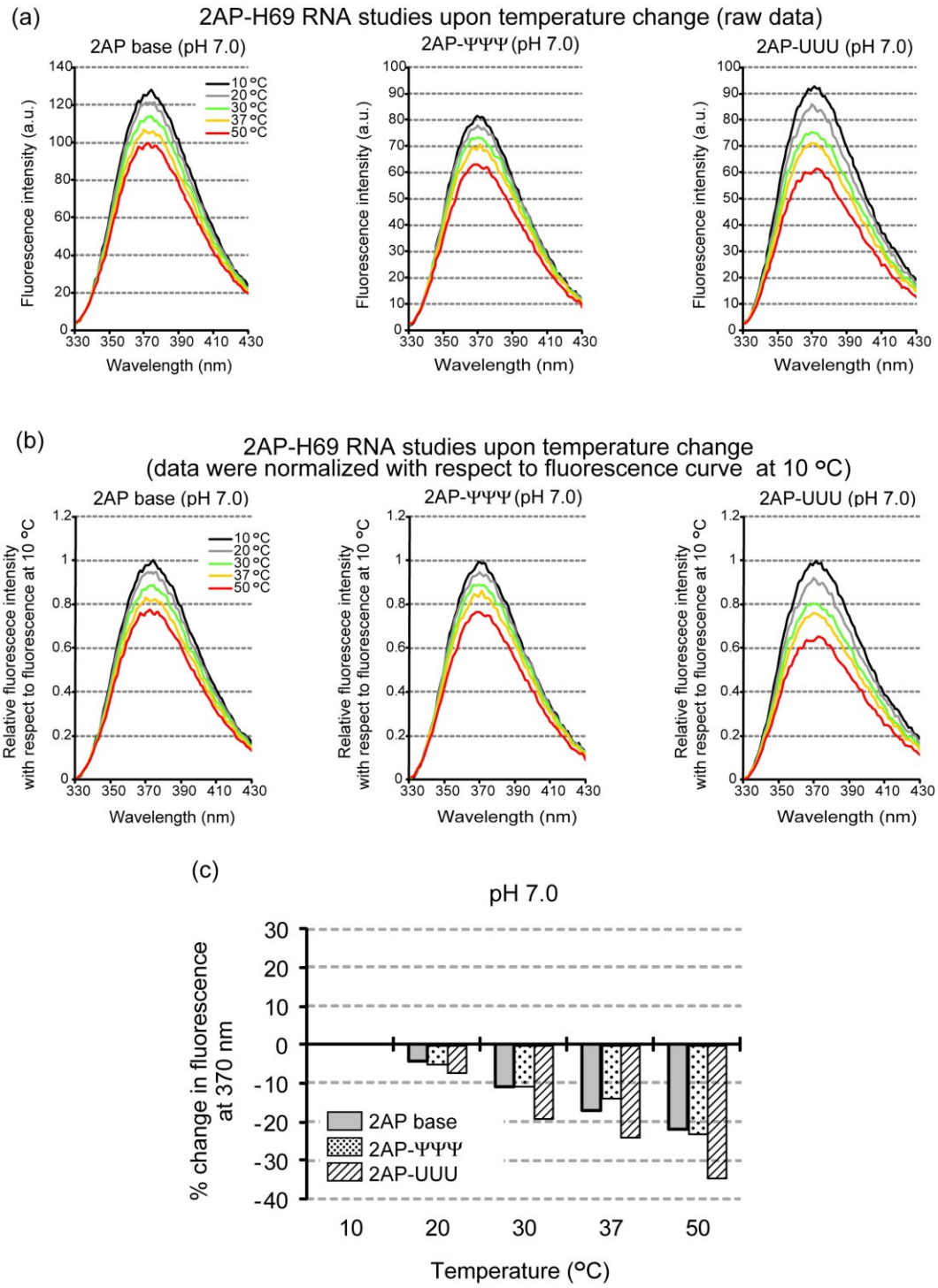

Figure 4.5. (a) Raw data and (b) normalized fluorescence intensity upon changing temperature at pH 7.0 are shown. (c) Relative fluorescence intensities at the emission maximum (370 nm) upon changing temperature at pH 7.0 are shown.

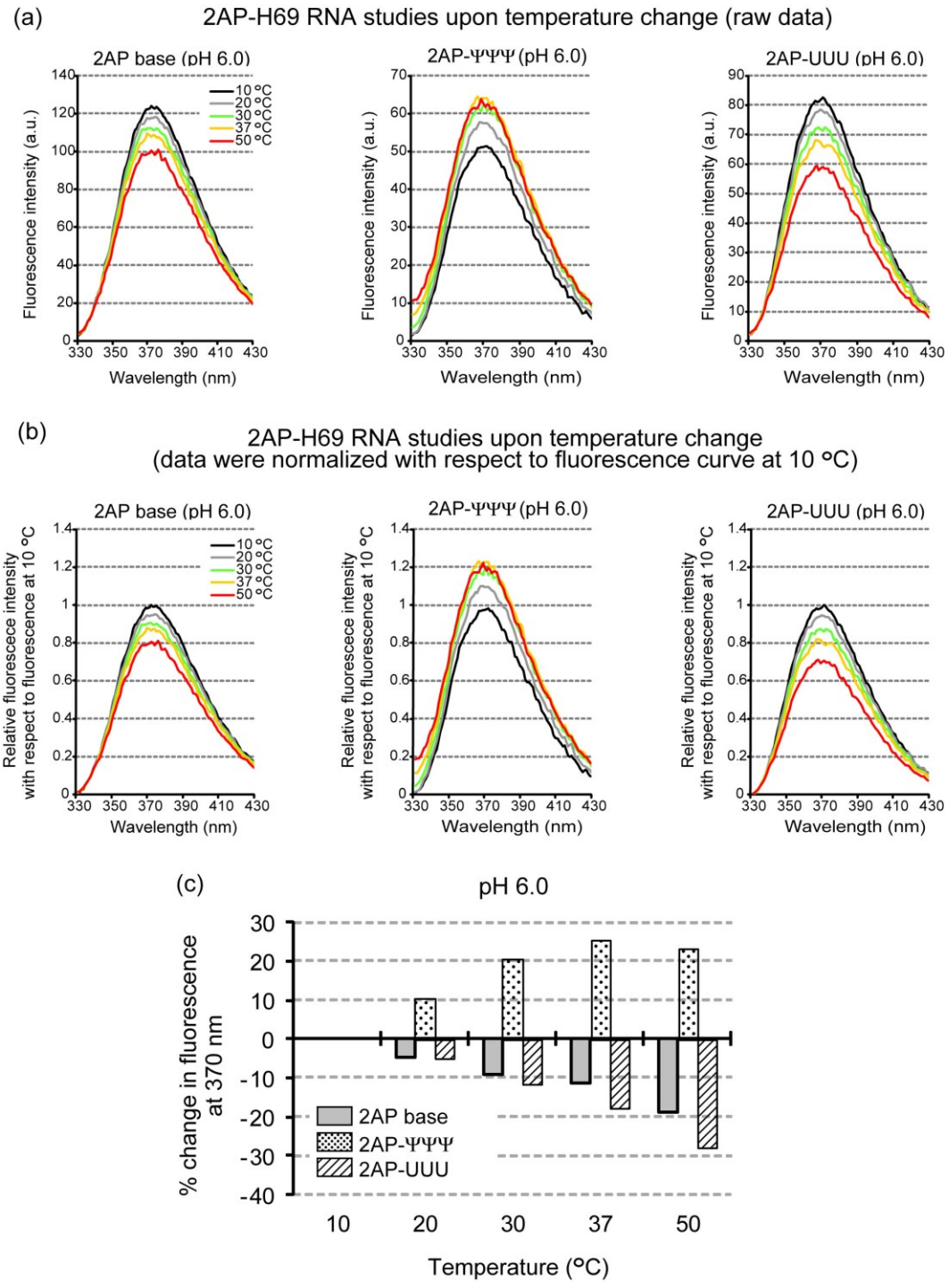

Figure 4.6. (a) Raw data and (b) normalized fluorescence intensity upon changing temperature at pH 6.0 are shown. (c) Relative fluorescence intensities at the emission maximum (370 nm) upon changing temperature at pH 6.0 are shown.

4.3.5. Application of 2AP-H69 to small-molecule binding studies

Crystallography and *in vitro* model studies showed that the aminoglycoside antibiotics interact directly with the H69 stem region with relatively strong binding affinity [138, 201]. It has been proposed that the H69-aminoglycoside interaction stabilizes bridge B2a, and favors a H69 conformation that inhibits ribosome recycling factor (RRF)-mediated subunit dissociation [138]. Because RRF is predicted to induce conformational changes that cause H69 to move away from the subunit surface, it appears that aminoglycosides impact these key H69 conformational states and inhibit important motions. To test this hypothesis, binding studies with the aminoglycosides neomycin, paromomycin, and gentamicin were carried out with 2AP-ΨΨΨ and 2AP-UUU RNAs in the absence of Mg^{2+}. Interestingly, the addition of 8 μM neomycin induced a 45% fluorescence increase in 2AP-ΨΨΨ; whereas, the same concentrations of paromomycin and gentamicin changed the fluorescent signal by just 20% and 10%, respectively (Figure 4.7a). 2AP-UUU exhibited 10-20% fluorescence increases upon the addition of 8 μM aminoglycosides (Figure 4.7b). Further increases in 2AP-ΨΨΨ fluorescence were observed by increasing the neomycin concentration up to 25 μM; however, no further fluorescence changes were observed in the case of 2AP-UUU.

To estimate the binding affinity of neomycin to 2AP-H69, dissociation constants (K_d) for neomycin were determined from the fluorescence titration curves. Apparent K_d values are 2.5 μM for 2AP-ΨΨΨ and 2.2 μM for 2AP-UUU (Figure 4.8). Those results, particularly the K_d for 2AP-ΨΨΨ, are in good agreement with electrospray ionization mass spectrometry (ESI MS) binding studies that gave apparent K_d values of 3.0 μM for $\Psi m^3\Psi\Psi$-H69 and 9.0 μM for UUU-H69 (Duc A.C., Ph.D. Thesis, 2009). The reason why 2AP-UUU exhibits a lower K_d value compared to ESI MS data is probably due to the very small changes in 2AP fluorescence (<10%), which makes it difficult to determine the dissociate constant accurately. Nonetheless, these results indeed show binding interaction between aminoglycosides and 2AP-H69 and indicate that structurally similar aminoglycosides, neomycin, paromomycin, and gentamicin, have different effects on the H69 loop conformation, which are clearly influenced by Ψ modifications. In contrast, the binding affinities of aminoglycosides are not impacted significantly by the presence of modifications.

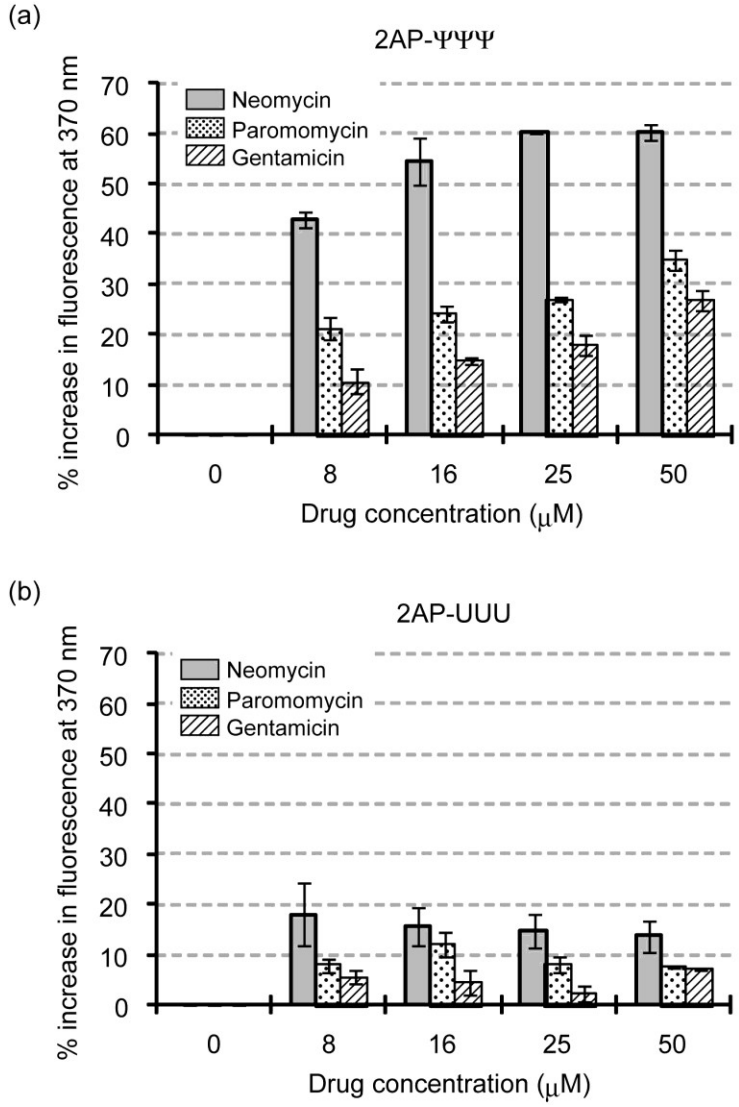

Figure 4.7. Fluorescence intensity changes of (a) 2AP-ΨΨΨ and (c) 2AP-UUU upon the addition of aminoglycoside antibiotics are shown. Data were normalized relative to spectra in the absence of antibiotic.

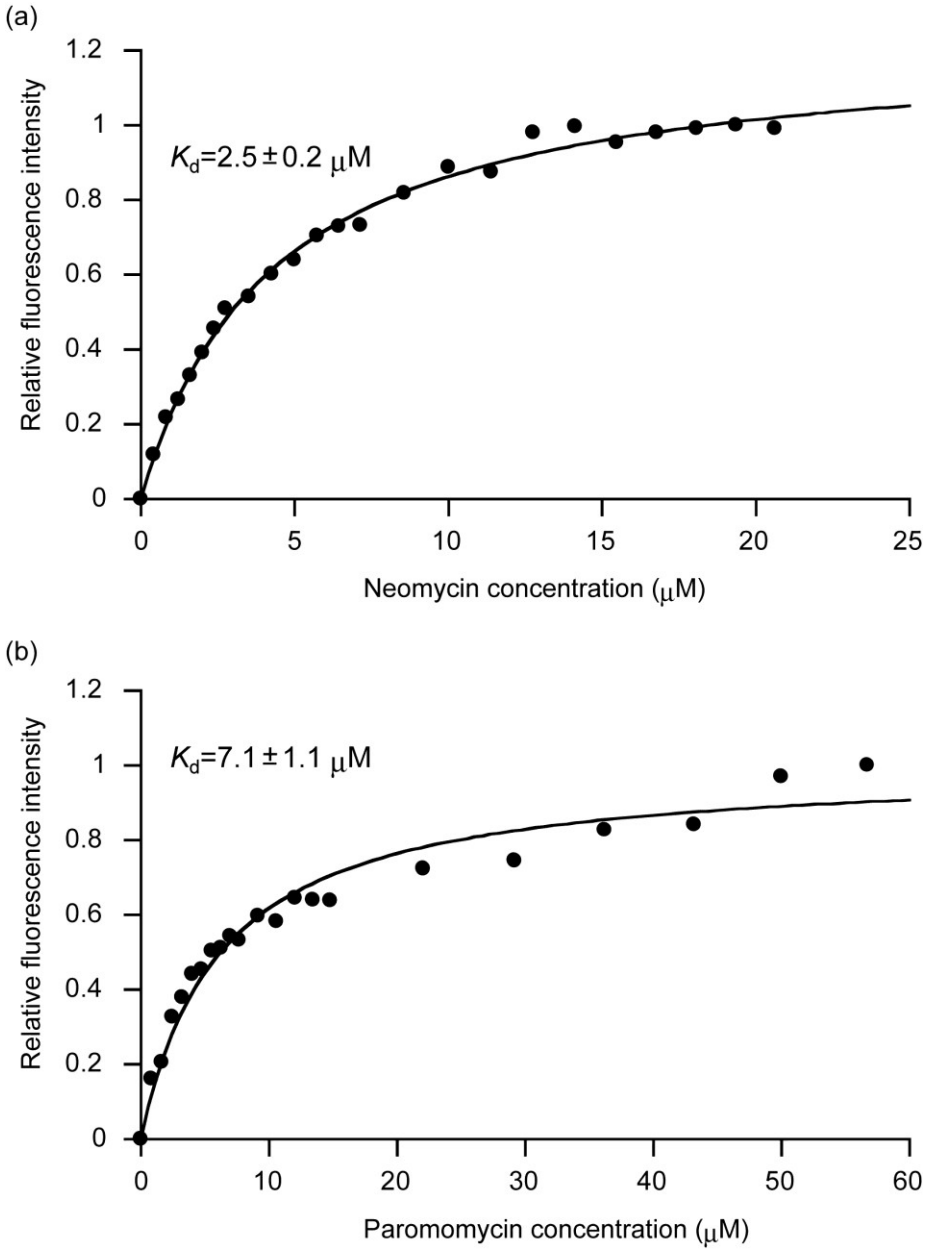

Figure 4.8. Fluorescence titration curves of 2AP-ΨΨΨ with (a) neomycin and (b) paromomycin are shown. Relative fluorescence was calculated by using the maximum and minimum fluorescence intensities. The minimum corresponded to the intensity without aminoglycoside, and the maximum was the intensity at saturation (20 μM for neomycin and 60 μM for paromomycin). Data were fit to the quadratic equation to obtain dissociation constant K_d.

Based on the 70S ribosome crystal structures with aminoglycosides, their binding site is the H69 stem region (G1921-U1923). Also, ESI MS binding analysis of the H69-neomycin interaction revealed a 1:1 binding stoichiometry (Duc A.C., Ph.D. thesis, 2009). These results, in combination with ESI MS data, suggest that neomycin binding to the H69 stem region induces or stabilizes different conformational states of the adjacent H69 loop. Thus, we propose that there is communication between the loop and stem of H69, which is influenced by the presence of Ψ modifications.

4.3.6. Dual monitoring of small molecule binding to helix 69 RNA

Although the 2AP-H69 monitoring system provides clues about different conformational states induced by small-molecule ligands, information about their binding affinity is lacking if a given antibiotic does not cause significant changes in fluorescence. Therefore, we were interested in developing a unique method to observe both ligand binding and induced-conformational states of H69. In previous studies using the TOPRO (3-methyl-2-((1-(3-(trimethylammonio)propyl)-4-quinolinylidene)methyl) benzothiazolium) dye, it was demonstrated that small-molecule binding to RNA can be monitored by a displacement of the dye molecule from RNA (Figure 4.9a) [210]. TOPRO interacts with moderate affinity (low μM range) to RNA bulges and loops and exhibits strong fluorescence; however, once it is released from the RNA, TOPRO loses fluorescence intensity (this process is referred to as FID, or fluorescence intercalator displacement). Importantly, TOPRO dissociation is enhanced by small-molecule interactions with RNA (see also Chapter 6) [210]. By using TOPRO, we hypothesized that small-molecule binding and H69 loop conformational changes could be monitored simultaneously by FID and 2AP-H69 fluorescence (Figure 4.9b).

4.3.7. Background test for possible interactions between TOPRO and 2AP

First, TOPRO and free 2AP were tested for possible interactions that might lead to energy transfer or quenching. When combined, TOPRO and free 2AP did not reveal any direct interactions; 2AP fluorescence was not affected and TOPRO fluorescence was not observed

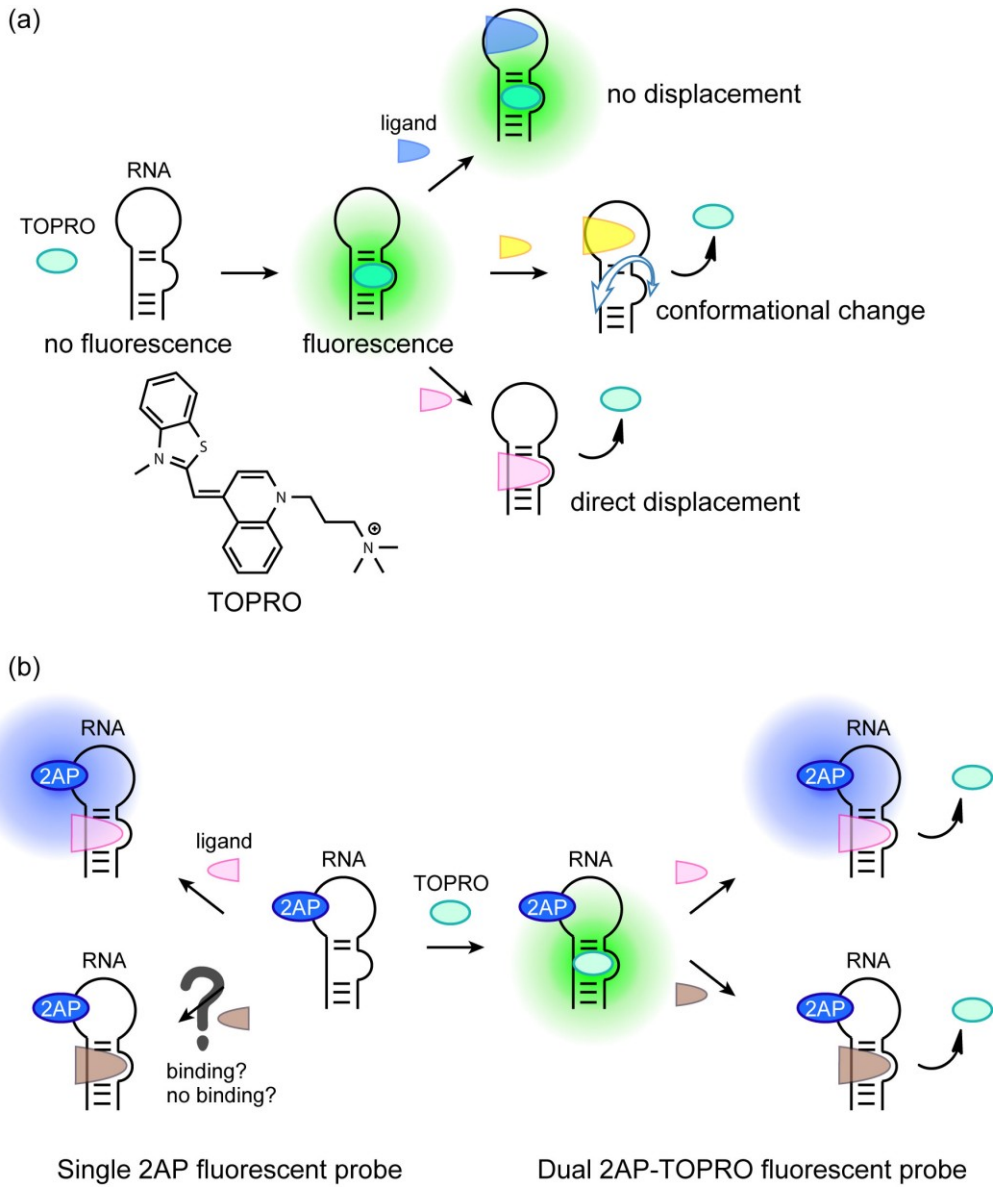

Figure 4.9. (a) A schematic illustration of fluorescence intercalator displacement (FID) is shown. TOPRO fluorescence is increased as a result of TOPRO-RNA interactions. If there is an RNA conformational change that induces TOPRO release or competitive binding of a ligand with TOPRO, the dye fluorescence will decrease. (b) A schematic illustration of 2AP fluorescence monitoring and dual 2AP-TOPRO fluorescence probing methods are shown. Because 2AP fluorescence increases require exposure of 2AP to solvent, it is not possible to detect a simple binding event that does not induce a nucleotide conformational change at the 2AP position; however, dual 2AP-TOPRO fluorescence probing would allow monitoring of both small-molecule binding events and RNA conformational changes simultaneously.

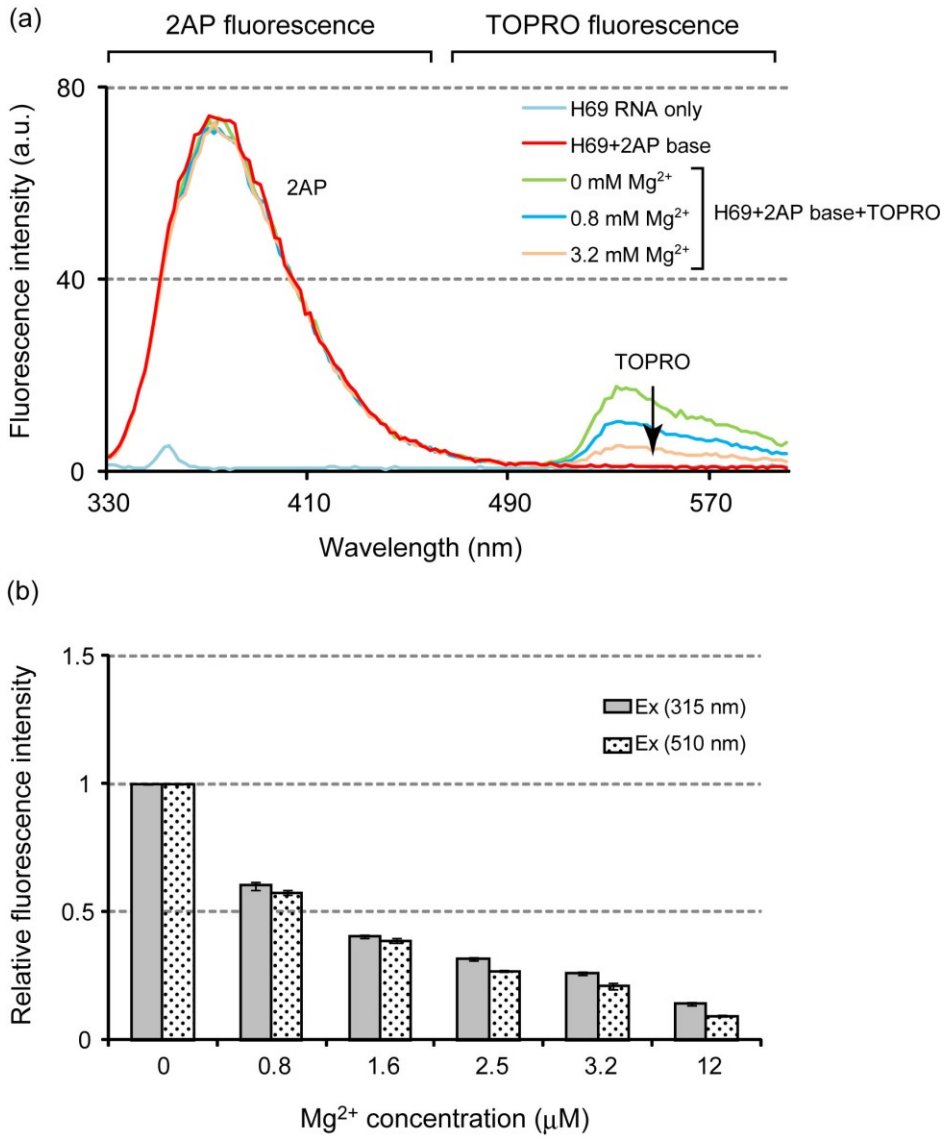

Figure 4.10. (a) The control data to check molecular interactions between 2AP and TOPRO are shown. Both free 2AP and TOPRO were excited at 315 nm. In this experiment, 2AP nucleoside was mixed with H69-UUU RNA (unmodified RNA without 2AP at position 1913), then TOPRO was added to the solution before titrating with Mg^{2+}. (b) Normalized TOPRO fluorescence at the emission maxima (540 nm) relative to intensities in the absence of Mg^{2+} is shown. Data were collected by exciting TOPRO at both 315 and 510 nm, and TOPRO fluorescence was measured at 540 nm. These data show that the two excitation wavelengths produce the same results.

(data not shown). To further test for possible side effects, FID was performed in the presence of free 2AP (Figure 4.10). In this test, the 2AP nucleoside was added to a solution containing 1 μM UUU H69 RNA, then TOPRO was added at 1 μM final concentration (1:1 ratio of RNA:TOPRO). Although 2AP fluorescence did not change at all after adding the dye, TOPRO fluorescence was induced by the presence of H69 RNA (Figure 4.10a). Interestingly, TOPRO can also be excited by 315 nm light and exhibits enough fluorescence intensity for analysis; given that its fluorescence characteristics did not change between 315 and 510 nm excitation, 315 nm excitation was used for further experiments (Figure 4.10b). Displacement of TOPRO from H69 RNA was observed upon addition of Mg^{2+}; whereas, no fluorescence change was observed for 2AP fluorescence, indicating that there is no reciprocal influence of TOPRO on 2AP fluorescence, and *vice versa*.

4.3.8. Dual monitoring of Mg^{2+} binding and H69 loop conformational change

To test for dual monitoring capability, 2AP-ΨΨΨ H69 RNA was first employed in a Mg^{2+} titration experiment. The addition of TOPRO to 2AP-ΨΨΨ decreased 2AP fluorescence by ~35% (Figure 4.11). Because no interaction was observed between TOPRO and the free 2AP (Figure 4.10), this decline in 2AP fluorescence is attributed to a change in stacking interactions between 2AP1913 and TOPRO, indicating binding of TOPRO in the H69 loop region. With increasing Mg^{2+} concentrations, TOPRO fluorescence at 540 nm was decreased, but 2AP fluorescence at 370 nm was increased (Figure 4.11). 2AP fluorescence increased by 20 and 40% in the presence of 3.2 and 10 mM Mg^{2+}, respectively. These values are not equal to those in the absence of TOPRO dye (60 and 70%, respectively; Figure 4.4), possibly due to TOPRO interactions with H69 that change the binding affinity of Mg^{2+} for H69 or simply inhibition of the Mg^{2+} interactions with H69.

2AP-UUU H69 RNA was also tested in this dual monitoring system. As observed in 2AP-ΨΨΨ, 2AP fluorescence also decreased (by 50%) after adding TOPRO to 2AP-UUU. With increasing Mg^{2+} concentrations, TOPRO fluorescence decreased and 2AP fluorescence increased (Figure 4.12). Comparison of the data between 2AP-UUU and 2AP-ΨΨΨ revealed that 2AP fluorescence of 2AP-UUU was recovered to the same extent as that without TOPRO, but

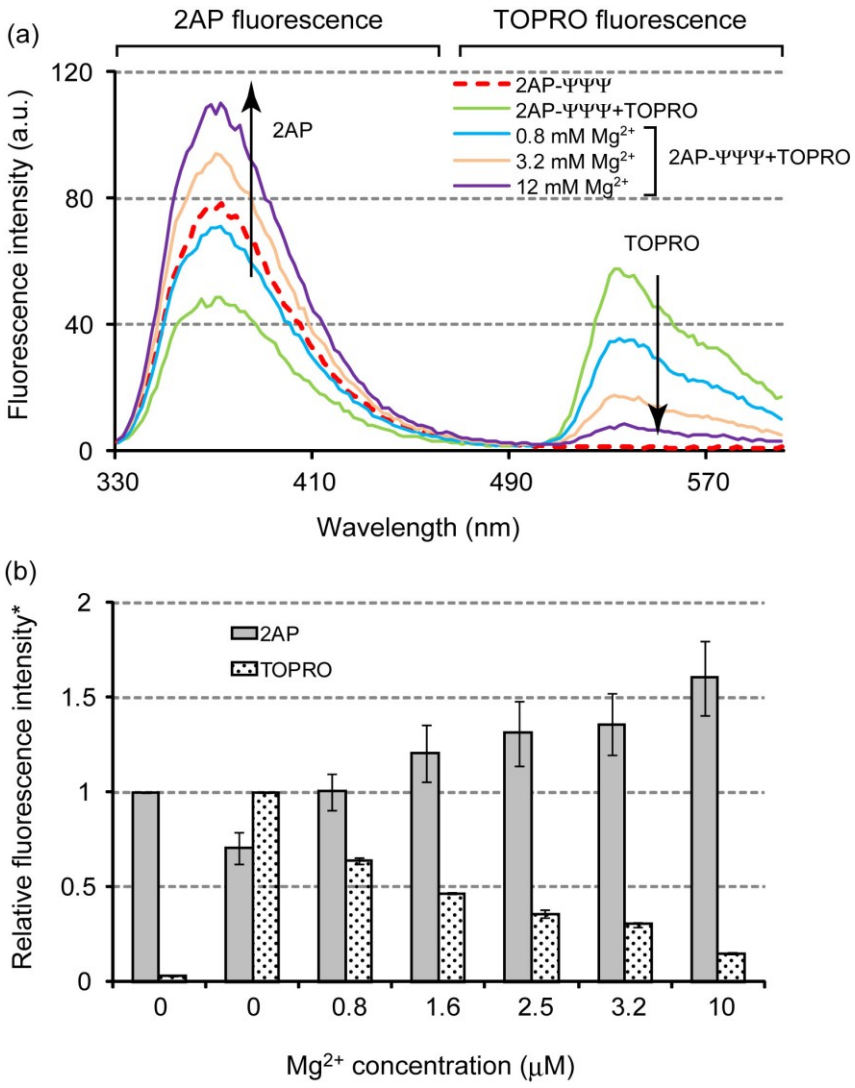

Figure 4.11. (a) Mg^{2+} titration curves for the dual monitoring system with 2AP-ΨΨΨ are shown. Both 2AP-ΨΨΨ and TOPRO were excited by 315 nm. (b) Relative fluorescence intensities of 2AP-ΨΨΨ and TOPRO in the dual monitoring system are shown. The 2AP fluorescence was measured at 370 nm and normalized relative to the intensities in the absence of TOPRO. TOPRO fluorescence was measured at 540 nm and normalized relative to intensities in the absence of Mg^{2+}.

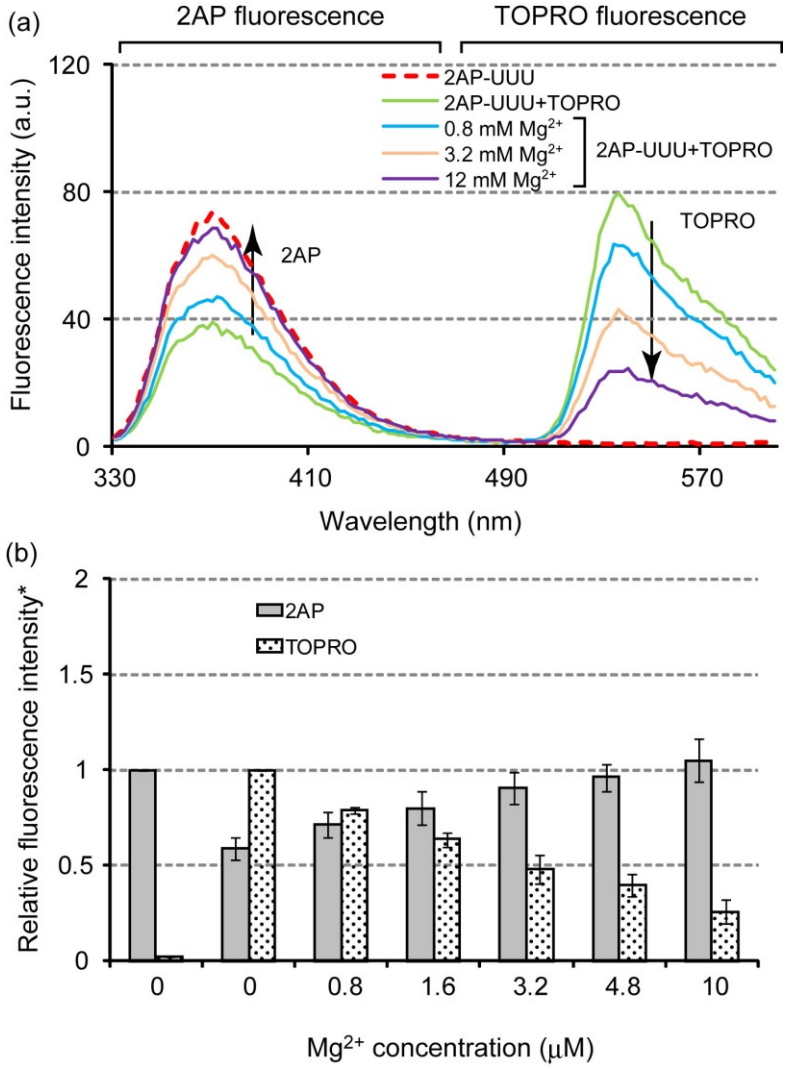

Figure 4.12. (a) Mg^{2+} titration curves for the dual monitoring system with 2AP-UUU are shown. Both 2AP-UUU and TOPRO were excited at 315 nm. (b) Relative fluorescence intensities of 2AP-UUU and TOPRO in the dual monitoring system are shown. The 2AP fluorescence was measured at 370 nm and normalized relative to the intensities in the absence of TOPRO. TOPRO fluorescence was measured at 540 nm and normalized relative to intensities in the absence of Mg^{2+}.

did not exhibit more fluorescence intensity, which is in good agreement with the experiments without TOPRO. Since TOPRO displacement was observed, these data indicate that Mg^{2+} interacts with 2AP-H69, both modified and unmodified, but only modified H69 undergoes a loop conformational change.

4.3.9. Dual monitoring of neomycin binding to 2AP-H69

Neomycin was shown to induce different H69 loop conformational states relative to other structurally related aminoglycosides. Therefore, neomycin was also used in dual monitoring experiments. TOPRO fluorescence decreased and 2AP fluorescence was elevated with increasing neomycin concentration in both 2AP-ΨΨΨ and 2AP-UUU (Figure 4.13a and b). The behavior of 2AP fluorescence was consistent with previously discussed 2AP-H69 experiments, in which 2AP-ΨΨΨ showed greater fluorescent changes than 2AP-UUU upon neomycin binding. In contrast, the TOPRO fluorescence changes were similar for neomycin binding to 2AP-ΨΨΨ versus 2AP-UUU. To test for possible differences with excitation wavelength, TOPRO fluorescence was monitored following excitation at 510 nm (Figure 4.13c and d). No difference was observed between 315 and 510 nm excitation wavelengths, indicating that neomycin has unique effects on the modified H69 loop conformation.

Further FID analyses were performed with H69 RNA with or without Ψ modifications (H69-ΨΨΨ or H69-UUU; no 2AP) and compared to 2AP-H69 (2AP-ΨΨΨ or 2AP-UUU) (Figure 4.14). In the case of modified H69, no difference was observed in the displacement of TOPRO regardless of whether 2AP was present or not; whereas, with unmodified H69 RNA, TOPRO was displaced more easily from H69-UUU than 2AP-UUU. These results are consistent with the observations that Ψ modifications modulate H69 loop conformations differently than uridine (see Chapters 2 and 3). The differences in 2AP1913 and A1913 that were observed in the unmodified UUU RNA may reflect differences in binding by neomycin or TOPRO to the loop region of H69.

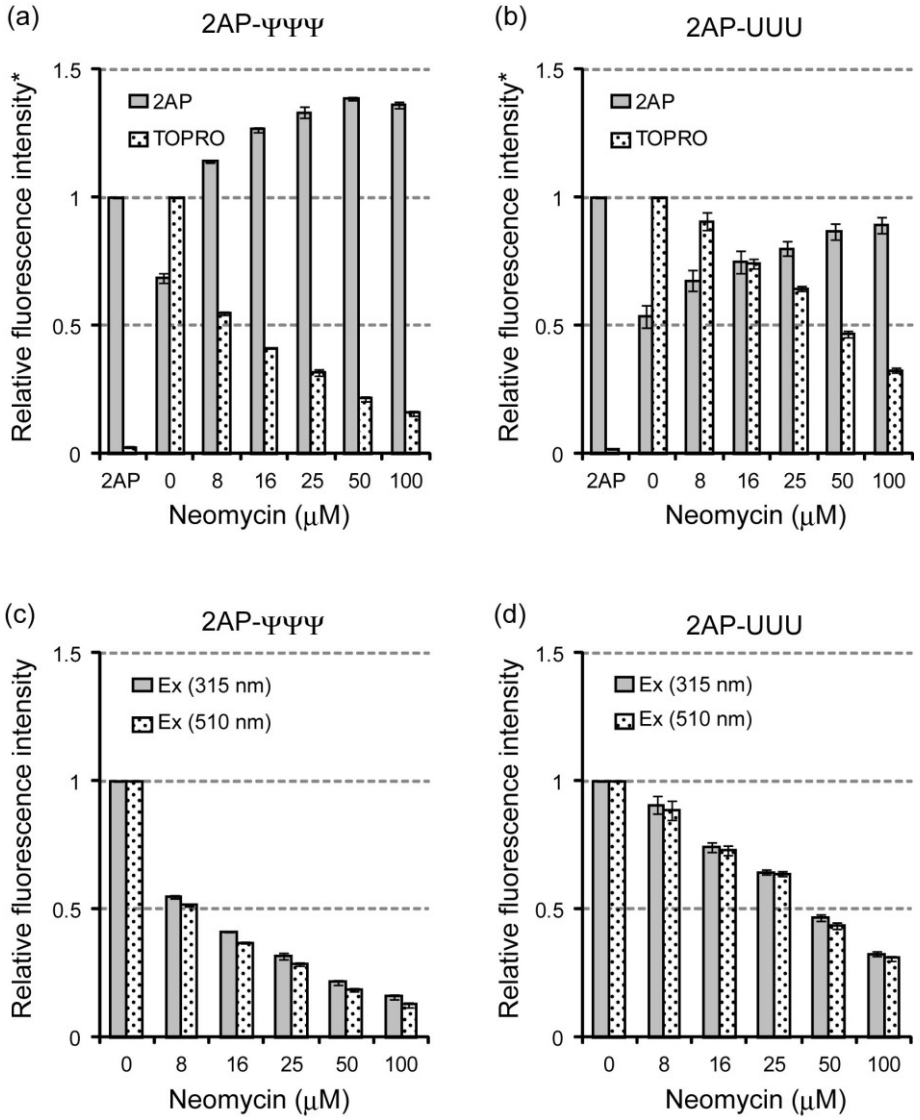

Figure 4.13. Relative fluorescence intensities in a dual monitoring system of (a) 2AP-ΨΨΨ and (b) 2AP-UUU titrations with neomycin are shown. Data processing was identical as described in Figure 4.11 and 4.12. Comparison of TOPRO fluorescence of (c) 2AP-ΨΨΨ and (d) 2AP-UUU excited at 315 nm and 510 nm is shown.

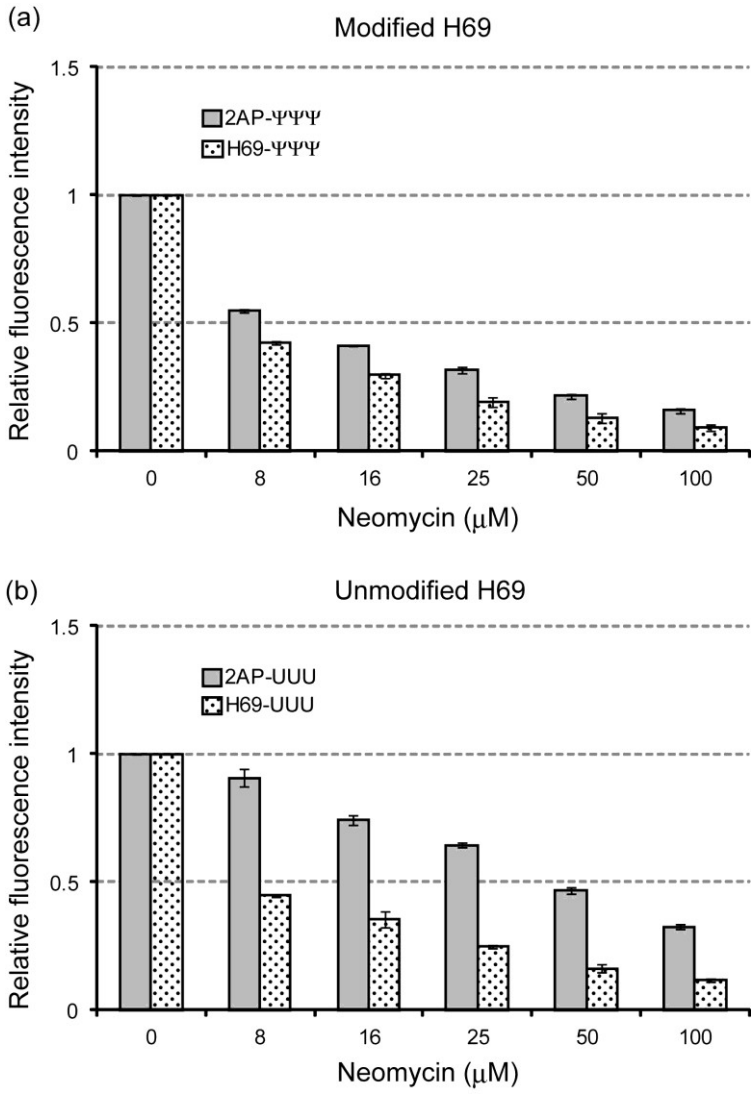

Figure 4.14. Comparisons of TOPRO displacement by neomycin between 2AP-H69 and H69 RNAs are shown. (a) 2AP-ΨΨΨ and H69-ΨΨΨ or (b) 2AP-UUU and H69-UUU are compared. TOPRO was excited at 510 nm, and TOPRO fluorescence was measured at 540 nm.

4.4. Discussion

Nucleotide 1913 of H69 in the 50S subunit is proposed to undergo local conformational changes over the cycle of ribosome translation. Indeed, the relative positioning of A1913 is influenced by factor binding and tRNA occupancies in the 70S ribosome crystal structures [5, 60, 177, 178]. Therefore, conformational changes at 1913 are thought to serve an important function in ribosome translation. In this study, we demonstrated that H69 conformational states can be monitored by substituting the A1913 residue with an adenine analogue, 2-aminopurine, as a fluorescent probe. Fluorescence results correlate well with previous studies, suggesting that the observed 2AP-H69 fluorescence changes are likely the consequence of different H69 loop conformational states. By using 2AP-H69 RNA, we found that environmental pH, Mg^{2+} concentration, temperature, and Ψ modifications, but not salt type, are important factors to determine H69 loop conformational states, consistent with previous studies (summarized in Figure 4.15).

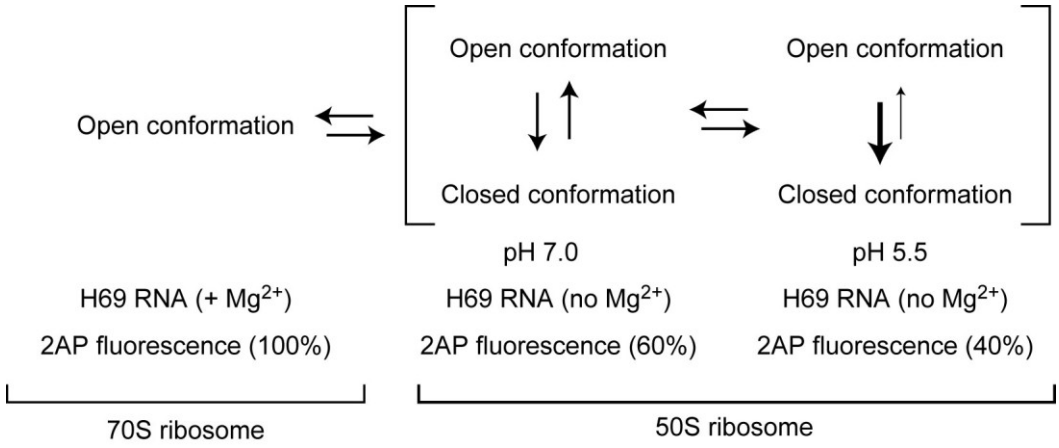

Figure 4.15. The proposed conformational relationship between 2AP fluorescence and H69 conformation is illustrated. In this hypothesis, the open and closed loop conformations of H69 are in conformational equilibrium, and this equilibrium can be shifted by addition of Mg^{2+}, or by changing the environmental pH. In the case of H69 in the context of the full ribosome, such conformational dynamics could be regulated by ribosome association and/or factor binding events (see also the discussion in Chapters 2 and 3).

In Mg^{2+}-titration experiments, we showed that the presence of sufficient amounts of Mg^{2+} (> 5 mM) leads to a high-fluorescence state, and post-transcriptional Ψ modifications are essential for acquiring this state (Figure 4.15). In some high-resolution ribosome crystal structures, Mg^{2+} ions bound to the H69 loop were observed and the binding patterns in various structures were similar in which the metal ion interacted with the H69 loop through a phosphate backbone pocket [60]. Therefore, it is possible that Mg^{2+} ions interact with the H69 loop region in solution as well; however, it is still unclear whether such Mg^{2+} ion binding facilitates loop conformational changes and results in solvent exposure of residue 1913 to contribute to the increased fluorescence intensity. We cannot exclude the possibility that the amino group at position 2 of 2AP1913 influences H69 conformation. Nonetheless, the important fact shown in this study is that Ψ modifications are the key factor for eliciting a Mg^{2+} ion-dependent H69 loop conformational state, and these results are in good agreement with our previous studies [109, 110, 184]. It seems highly likely, based on our results, that the lack of Ψ modifications alters the specific H69 loop conformations, such as loss of efficient base stacking interactions around residues 1915-1917, which could, in turn, lead to a loss in Mg^{2+} ion interactions in this region. To understand the influence of Mg^{2+} ions on H69 conformational dynamics, further studies will need to be performed to determine the relative positioning of A1913 (and 2AP1913) in solution under various conditions.

Temperature-dependent 2AP-H69 studies showed increases in 2AP-ΨΨΨ RNA fluorescence under low pH conditions with increasing temperature; whereas, the 2AP-UUU RNA and free 2AP showed a decrease in fluorescence under similar conditions. In previous thermal melting studies, modified H69 was stabilized in low pH conditions; whereas, pH changes did not alter unmodified H69 stability. Thus, the observed changes in 2AP-ΨΨΨ fluorescence could be attributed to different stability of the loop region. The 2AP-ΨΨΨ RNA may form a more closed conformation at pH 6.0 (*i.e.*, more stable), and raising the temperature may disrupt these stable base-stacking interactions. This idea is supported by the observation that the addition of Mg^{2+} diminished the effects of increased 2AP-ΨΨΨ fluorescence with increased temperatures, because Mg^{2+} facilitates exposure of residue 1913. Although the relative positioning of 1913 and other loop components need to be determined for a deeper understanding of this system, these results

suggest that the function of Ψ modification is to organize H69 structure in order to create a small energy barrier to the different loop conformational states.

Besides conformational studies, we also demonstrated the potential application of 2AP-H69 RNA to monitor the influence of small-molecule binding on H69 loop conformation. The 2AP-H69 RNA revealed that among a series of aminoglycoside antibiotics, only neomycin strongly impacts the H69 loop conformation (Figure 4.16). Regarding paromomycin and gentamicin, it appears that they interact with H69 with modest affinity, but they have less ability to alter the H69 loop conformation upon binding to the adjacent stem region. These observations strongly suggest a conformational communication between the loop and stem region of H69. We postulate that neomycin has a different binding interaction and/or different effect on the H69 loop conformation than paromomycin or gentamicin, even though its chemical structure is very similar. At this point, it is not known how this effect on H69 loop conformation influences antibiotic activity, but single-molecule ribosome studies also suggested that neomycin has a different impact on structural

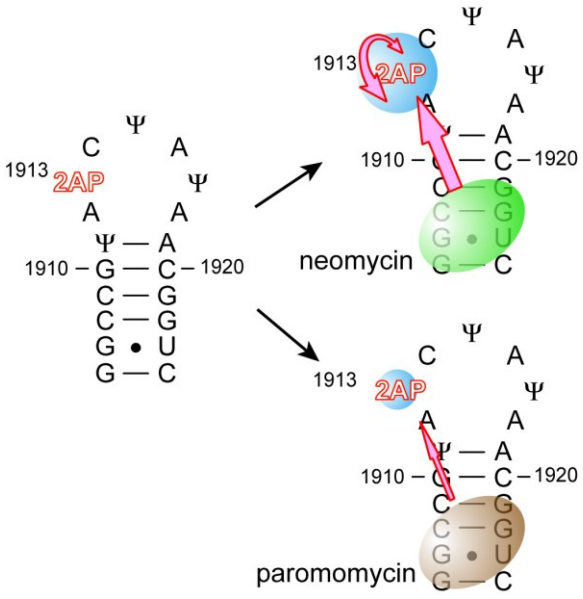

Figure 4.16. A schematic illustration of the 2AP-H69 experiments. The most notable finding in this chapter is the different binding activities of aminoglycoside antibiotics towards H69 loop conformational states. These observations indicate conformational communication between the loop and stem regions of H69.

dynamics of ribosome-tRNA complexes compared with other aminoglycosides [211]. Therefore, further investigation will be necessary in order to better understand the molecular basis of antibiotic activity of aminoglycoside antibiotics. The 2AP-H69 RNA could be a helpful tool for screening large pools of small molecules, and to study the impact of small-molecule binding on H69 loop conformation in combination with other methods, such as CD spectroscopy, ITC, and SPR.

In summary, we demonstrated a 2AP fluorescence-based method to monitor different H69 loop conformational states. These studies revealed that H69 conformational states are modulated by Ψ modifications and other environmental factors, such as pH, Mg^{2+}, and temperature. We also demonstrated neomycin binding-dependent loop conformational states by using the 2AP-H69 system. These results will help us to understand the intricate higher-order H69 structure and the function of Ψ modifications and to develop unique antibiotics targeting specific H69 conformational states.

4.5. Materials and methods

4.5.1. RNA oligonucleotides preparation

All 19-nt RNA oligonucleotides were ordered from and synthesized by Dharmacon (Lafayette, CO). RNAs were purified on 20% denaturing polyacrylamide gels (1:19 cross-linking ratio of bisacrylamide:acrylamide, 0.5x TBE buffer); corresponding bands were visualized by the UV shadowing method, and RNAs were extracted with the crush-and-soak method (soaking buffer: 20 mM Tris-HCl, pH 7.5, 250 mM NaCl, and 1 mM EDTA) at 16 °C with shaking. After 4~5 hours, the buffer was collected and additional buffer was added and incubated at 4 °C overnight with shaking. Eluted RNAs were concentrated and desalted by ultrafiltration on YM-3 columns (Microcon), and dissolved in double-deionized water (ddH_2O). The purified RNAs were checked by MALDI mass spectrometry. RNA concentrations were determined based on the extinction coefficient of 19-nt unmodified H69 RNA, because the nearest-neighbor extinction coefficients for 2-aminopurine and pseudouridine have not been measured or reported.

4.5.2. 2-Aminopurine fluorescence experiments

General information on the 2AP fluorescence studies under different pHs and temperatures is in follows. The 2AP-RNA was dissolved in 15 µl of renaturing buffer (5 mM K^+-cacodylate, pH 7.0, 70 mM NH_4Cl, and 30 mM K^+) and denatured at 80 °C for 3 min followed by slowly cooling down to room temperature over 30 min in the dark. Annealed 2AP-RNA was transferred into 45 µl assay buffer (20 mM K^+-cacodylate, varying pH, 70 mM NH_4Cl, and 30 mM K^+) and incubated for 5 min at room temperature before starting data collection. In the case of aminoglycoside binding experiments, 2AP-RNA was dissolved into 60 µl assay buffer (20 mM K^+-HEPES, pH 7.3 at 22 °C, 70 mM NH_4Cl, and 30 mM KCl). Aminoglycoside solutions for titration experiments were prepared in the same buffer, and fluorescence changes were measured by adding 0.5 µl aminolgycosides per titration point. The 2AP-RNA was excited at 315 nm and fluorescence emission spectra were collected on a Cary Eclipse fluorescence spectrophotometer (Agilent Technology, Santa Clara, CA). All fluorescence spectra data were measured at 22 °C at 1.5 µM RNA concentrations unless stated otherwise. A buffer background at each pH condition was subtracted from the fluorescence data. In the case of titration experiments, although volume change due to titration was very small, it was considered and fluorescence intensity was corrected based on RNA concentration change. Normalized fluorescence data were obtained by using the following formula: $F_r = (F_{min} - F_x)/(F_{min} - F_{max})$, in which F_r is the relative fluorescence intensity, F_{min} is minimum fluorescence intensity, F_{max} is the maximum fluorescence intensity, and F_x is fluorescence intensity at each titration point. It should be mentioned that use of assay buffer conditions at each pH with or without 3 mM Mg^{2+} during annealing exhibited the same results and conclusions.

RNase A digestion experiments were performed as follows. RNA samples were prepared as mentioned above and fluorescence curves in the absence of RNase A were collected. One µl of RNase A (1 µg/ml; Ambion, Austin, TX) was then added and the sample was incubated in the dark at 60 °C for 30 min followed by further incubation at 37 °C overnight in the dark to complete the RNA digestion. Collection of fluorescence changes at different time points and gel analysis revealed that overnight incubation is sufficient for complete digestion of both ΨΨΨ- and UUU-H69 RNAs.

4.5.3. Data fitting for dissociation constant calculation

Dissociation constant (K_d) was obtained by titrating a small amount of each aminoglycoside into 2AP-H69 RNA. Usually 0.5 µl was added each time and the mixture was incubated for 2 min, then data were collected with five consecutive collection modes. The averaged fluorescence curves were used to obtain a fluorescence intensity at 370 nm. The intensity at 370 nm was plotted over the aminoglycoside concentration, and the plotted data were fit to a quadratic equation [163].

$$\frac{\sum RL}{\sum R + \sum RL} = \frac{([R]_0 + [L]_t + K_d) - \sqrt{([R]_0 + [L]_t + K_d)^2 - 4[R]_0[L]_t}}{2c}$$

In this equation, $\sum RP$ is the sum of the RNA-aminolgycoside complex, $\sum R$ is the free RNA, $[R]_0$ is the initial concentration of RNA, $[L]_t$ is the total ligand concentration in the system, K_d is the dissociation constant of measured aminoglycoside, and c is a constant that relates fluorescence intensity to concentration. After fitting the data plots to the quadratic equation, a formula was obtained that can be best fit to the data plots. By performing goal seek analysis on Excel software, an aminoglycoside concentration that gives the value of 0.5 was obtained and defined it as the dissociation constant K_d.

4.5.3. Dual fluorescence probing

The dual fluorescence monitoring experiments were performed as follows. The 2AP-H69 RNA (1.5 µM) was denatured and refolded as mentioned above. Initial fluorescence was measured with both 315 nm (for 2AP) and 510 nm (for TOPRO) excitation wavelengths, then 200 µM of TOPRO dye solution in the assay buffer, which was prepared from 1 mM TOPRO in DMSO (Invitrogen), was added to 2AP-H69 at a 1.5 µM final concentration. 2AP and TOPRO fluorescence were measured. The emission maxima at 370 nm for 2AP and 540 nm for TOPRO were used for all analyses.

For the control experiments to check for possible interactions between 2AP and TOPRO, three different experiments were performed. First, 2AP nucleoside was mixed with TOPRO and fluorescence was measured with 315 and 510 nm excitation. Second, 2AP nucleoside was mixed

with 1 μM H69-UUU RNA. After measuring 2AP fluorescence, TOPRO was added to this solution and 2AP and TOPRO fluorescence spectra were obtained. Lastly, TOPRO was mixed with 1 μM H69-UUU RNA, then mixed with 2AP nucleoside. These three different control experiments revealed no direct molecular interactions or fluorescence energy transfer between the free 2AP nucleoside and TOPRO, because no change in fluorescence by the addition of 2AP to TOPRO, or TOPRO to 2AP, respectively, was observed. Therefore, it was concluded that a change in fluorescence of 2AP-H69 RNA or TOPRO could be attributed directly to molecular binding events.

Chapter 5
Footprinting analysis of antibiotic-H69 interactions in the ribosome

5.1. Abstract

Understanding the underlying mechanism of action of antibiotics at the molecular level is a significant process ultimately to combat bacterial infections due to the emergence of advanced antibiotic-resistant strains. Development of a unique antibiotic targeting a higher order functional RNA is one promising way to overcome this issue. Here we investigate the interaction of antibiotics with H69 in the 70S ribosome by using DMS footprinting and DEPC probing. We show that the aminoglycoside antibiotics neomycin and paromomycin interact efficiently with the H69 stem. These interactions are not observed with isolated 50S subunits. Lack of pseudouridine modifications in the H69 loop reduced the aminoglycoside-H69 affinity; whereas, the interaction of aminoglycoside with h44 of the 30S subunit remained strong under these conditions. Taken together, these results indicate a requirement of a well-ordered functional helix 69 conformation for efficient drug bindings. Our data suggest that helix 69 is a suitable target for the development of novel therapeutics.

5.2. Introduction

As stated in Chapter 1, the aminoglycoside-class antibiotics are clinically important; however, the outbreak of antibiotic-resistant bacteria prompts us to understand their detailed bactericidal mechanism more deeply. Aminoglycoside antibiotics inhibit bacterial ribosome function by binding to ribosomal RNA (rRNA). Their interactions with specific rRNA regions disrupt ribosomal proofreading [129], inhibit tRNA/mRNA translocation [130], and impact on ribosome recycling [138]. Clinically important aminoglycosides are composed of the highly conserved 2-deoxystreptoamine (2-DOS) subunit, which has a 1,3-diamino functionality and several hydroxyl groups, and is typically connected to several types of aminosugar components (see also Chapter 1) (Figure 5.1). Because of the extensive ability of aminoglycosides to bind RNA, the central

scaffolds are considered as promising models in the design of semi-synthetic and unique antibiotics having improved and different molecular characteristics; *e.g.,* guanidinoglycoside and neomycin dimers [212-214]. Furthermore, elucidating the structural aspects of aminoglycoside binding is important in order to gain insight into target site selectivity and specificity, because the underlying principle of action of aminoglycoside antibiotics is not fully known.

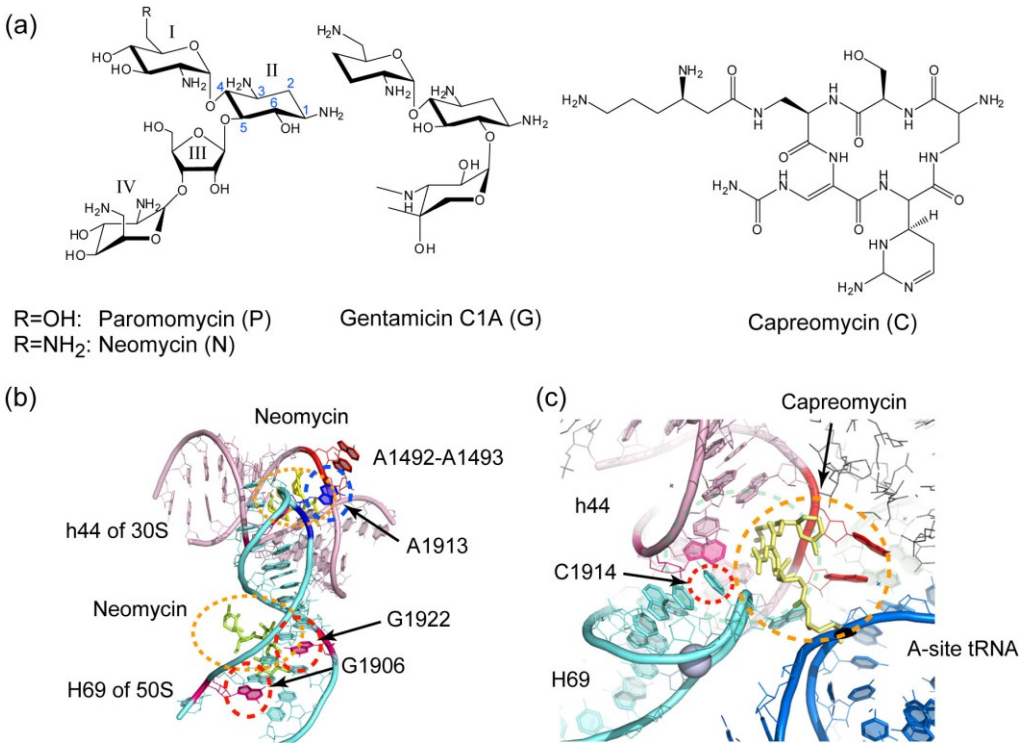

Figure 5.1. (a) Chemical structures of aminoglycoside and peptide antibiotics, paromomycin, neomycin, gentamicin C1A, and capreomycin are shown. Crystal structures of 70S ribosomes with (b) neomycin (PDB ID: 2QAL+2QAM) and (c) capreomycin (PDB ID: 3KNH+3KNL) are shown .

A primary binding site for aminoglycosides on the bacterial ribosome is h44 of the 30S subunit adjacent to the decoding center [8, 10, 135], namely the intersubunit bridge B2a region, which is composed of h44 and H69 in the 50S subunit (see also Chapter 1). Bridge B2a comprises part of the A site, which plays an important role in the tRNA-selection step by monitoring codon-anticodon interactions. A series of studies using model A-site RNAs revealed that aminoglycosides interact with h44 and induce an extrahelical A-site conformation in which A1492 and A1493 are flipped-out [8, 10, 133]. Similar base orientations can be found in crystal structures of the ribosome complexed with cognate tRNA and mRNA [8, 10], leading to the proposal that aminoglycosides stabilize the h44-mRNA-tRNA complex, causing decoding errors, stop codon readthrough and tRNA/mRNA translocation stops. In addition to the h44-aminoglycoside interaction, crystallography studies revealed that neomycin, paromomycin, and gentamicin are able to interact with H69, offering a possible mechanism for how aminoglycosides can inhibit the ribosome recycling process [138]. Furthermore, in crystal structures, H69 makes direct contacts with cyclic peptide antibiotics of the tuberactinomycin family, viomycin and capreomycin [143].

As stated and pursued in previous chapters, H69 plays important roles in normal ribosome function, including subunit association [103, 174], translational fidelity [94, 95, 182], tRNA translocation [177], translation termination [59-61, 103], and ribosome recycling [99, 176]. H69 lies at the heart of the ribosome and participates in bridge B2a with h44 through water-mediated and direct hydrogen-bonding interactions [5, 46]; for instance, A1912 interacts with C1407 and G1494 of 16S rRNA, A1913 projects into the shallow groove around positions A1492 and A1493, and A1919 hydrogen bonds with U1495 and G1517 of 16S rRNA. Since the B2a interaction is maintained during the ratchet-like motion of ribosome translocation [178], the conformation of H69 should be dynamic in order to adapt to ongoing structural reorganizations between ribosomal subunits and to keep them anchored. Indeed, the importance of the H69 orientation is predicted from structure studies with the ribosome recycling factor (RRF) [98]. In this study, it was suggested that H69-bound aminoglycosides stabilize the RNA structure in the B2a-forming state and inhibit RRF-mediated H69 displacement. Thus, H69 could be a unique target to inhibit

ribosome activity in several ways; however, the molecular details of aminoglycoside-H69 interactions on the full ribosome are still unclear, especially in solution, even though crystal structures of the ribosome complexed with aminoglycosides are available. Understanding how current antibiotics act on H69 is significant for the development of novel therapeutics. Here, we investigate the interaction of aminolgycoside antibiotics neomycin, paromomycin, and gentamicin and the peptide antibiotic capreomycin to elucidate the relationship between binding activity and antibacterial activity.

5.3. Results

5.3.1. Antibiotic footprinting analysis of vacant 70S ribosomes and 50S subunits

Footprinting analysis reveals binding of aminoglycoside antibiotics to the H69 stem region

Although crystal structures of 70S ribosomes with aminoglycoside and peptide antibiotics revealed their interaction with H69 [138, 143], it was still unclear whether they bound to H69 in solution. To further investigate binding of aminoglycoside and peptide antibiotics, we performed a footprinting analysis in the presence of these molecules followed by aniline-induced strand scission (see Chapter 1 for further details about strand scission). Notable protection of N7 of G at a specific position, G1922, was readily found after strand cleavage. At 5 μM drug concentration, structurally similar aminoglycosides neomycin, paromomycin, and gentamicin protected N7 of G1922 from DMS by 68, 58 and 54%, respectively; on the other hand, only weak protection by the peptide antibiotic capreomycin was observed, even at 50 μM drug concentrations (28% at 50 μM) (Figure 5.2). When each drug concentration was increased to 50 μM, neomycin and paromomycin protected N7 of G1922 as with 5 μM; whereas, protection by gentamicin decreased to 20%. In a gentamicin titration experiment, the protection level increased between 5 and 10 μM, but decreased above 25 μM concentrations. Gentamicin has a 4,6-substituted 2-DOS moiety instead of the 4,5-substituted 2-DOS found in neomycin and paromomycin (Figure 5.2). Thus, it is possible that the different chemical structures alter the binding mode of gentamicin, which has a secondary or tertiary binding site that, at higher concentrations, diminishes binding to H69 but not to h44.

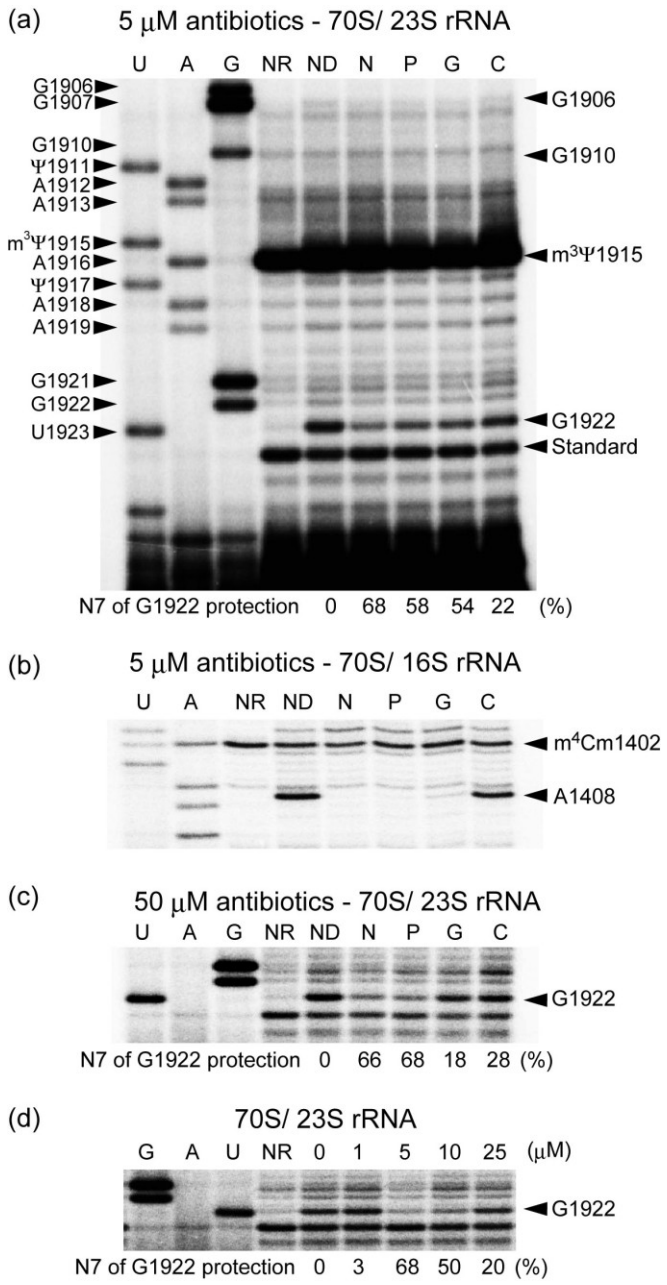

Figure 5.2. Autoradiograms for DMS footprinting analyses of antibiotic binding to H69 in 70S ribosomes are shown. (a) Data with 5 μM antibiotic are shown (U, A, and G are sequencing lanes; NR, no reaction control; ND, no drug control; N, neomycin; P, paromomycin; G, gentamicin; C, capreomycin). Band intensities were normalized to a non-specific position indicated as standard on the right side of the gel and % protection of G1922 was calculated relative to no drug control. (b) Footprinting analysis of h44 of the 30S subunit is shown. The same rRNA sample as in panel a was used. In this case, position 1402 was used to normalize band intensities. (c) Footprinting analysis of H69 in the presence of 50 μM antibiotic is shown. (d) Footprinting analysis of H69 with different gentamicin concentrations is shown.

In addition to protection of residue G1922, protection at the N7 position of G1906 by aminoglycoside antibiotics was also found in spite of low resolution due to the strong stop at $m^3\Psi$1915 (Figure 5.2). Protection of G1906 and G1922 at their N7s indicates that the aminoglycoside-class antibiotics bind to H69 from the major groove side of the H69 stem, as was observed in crystal structures and NMR analyses (Figure 5.2) [138, 201]. The binding mode for peptide antibiotic capreomycin to H69 is different than that of the aminoglycoside antibiotics [143]. Capreomycin interacts with H69 and h44 simultaneously in a crystal structure (Figure 5.2). The lack of protection in the H69 stem by footprinting analysis is in good agreement with the crystal structure data; however, we cannot exclude the possibility that capreomycin may require mRNA and tRNAs for its simultaneous interaction with H69 and h44.

Besides interactions of aminoglycoside antibiotics with H69 in 70S ribosomes, the known binding site on 16S rRNA was also examined using the same rRNA samples under identical conditions. Neomycin, paromomycin, and gentamicin are known to protect a specific nucleotide, A1408 at N1, in the A site of the 30S subunit from DMS probing which can be readily detected as a reverse transcription stop site without strand scission [132]. Protection of the N1 of A1408 in the presence of all three aminoglycosides was observed, indicating that aminoglycoside antibiotics interact with both h44 and H69 as observed in X-ray crystal structures (Figure 5.2). In contrast, capreomycin did not protect A1408 of h44. Considering the crystal structure of the ribosome complexed with capreomycin, it appears that the peptide drug contacts h44 from the opposite side of the aminoglycoside-binding region [143]; therefore, lack of protection from chemical reactivity at residue A1408 by capreomycin is consistent.

H69 as a secondary binding site

To compare binding affinities of neomycin for the A site of the 30S subunit and H69 of the 50S subunit, a neomycin titration was performed on 70S ribosomes. Neomycin strongly protected A1408 of h44 even at 0.5 μM (Figure 5.3); whereas, at least 5 μM neomycin was required for detectable protection in H69 (Figure 5.3). The stronger binding of neomycin on h44, relative to H69, is in good agreement with reported dissociation constants (K_d) obtained by performing

biophysical experiments on model A-site RNAs. The reported K_d of neomycin for the A-site RNA ranges from 60 nM to 0.2 μM, depending on the method and conditions [133, 163, 215, 216], and our experimental K_d value using a small hairpin A-site RNA determined by isothermal calorimetry (ITC) was 0.44 μM (unpublished data, measured under near physiological condition of 20 mM HEPES, 70 mM NH_4Cl, 30 mM KCl, pH 7.3 at 25 °C by Adhnan Mohamed). As stated in Chapter 4, the K_d values of aminoglycosides for the small hairpin H69 RNA with modified bases (Ψ1911-m^3Ψ1915-Ψ1917) are 1.1 μM for neomycin and 6.5 μM for paromomycin (unpublished data

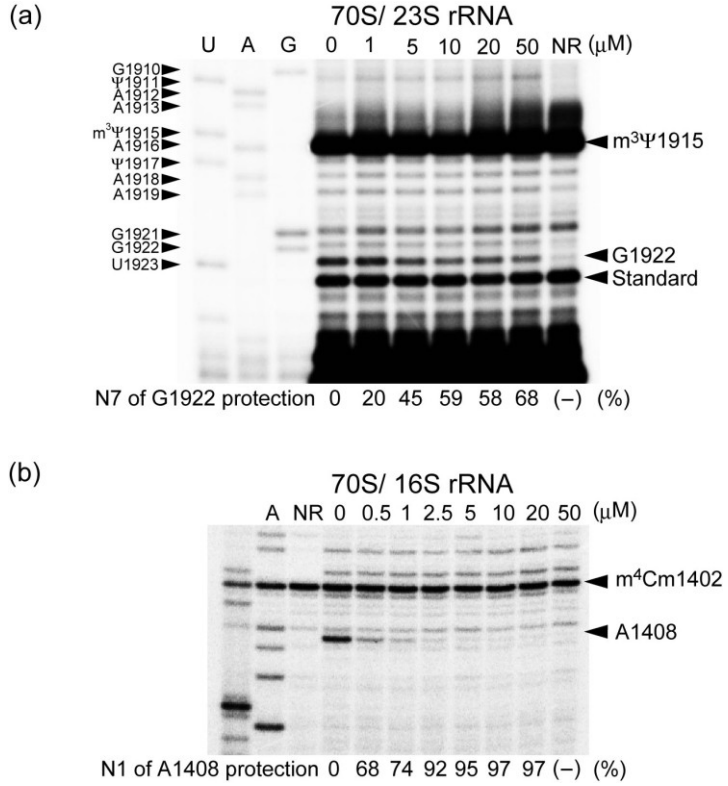

Figure 5.3. Autoradiograms for footprinting analysis of (a) H69 region and (b) h44 region under various neomycin concentrations are shown. The same rRNA samples were used for analyses of H69 and h44 to compare the extent of neomycin binding to H69 and h44.

obtained by surface plasmon resonance (SPR)). As such, in combination with footprinting analyses, it is suggested that H69 is a secondary binding site for aminoglycoside antibiotics.

Lack of drug binding to H69 in isolated 50S subunits

We also evaluated the binding capability of antibiotics with isolated 50S subunits. Although weak binding was observed only in the presence of 50 μM neomycin (data not shown), the antibiotics examined did not alter the footprinting patterns in isolated 50S subunits at 5 μM concentrations compared to the control (Figure 5.4). Comparison of the footprinting data at 5 μM

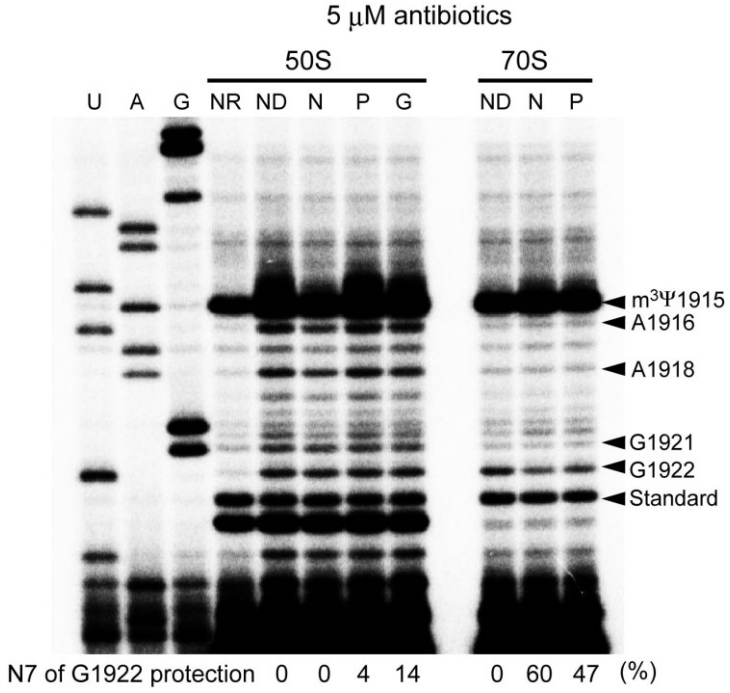

Figure 5.4. Footprinting analysis of 50S subunits under various drug concentrations. Data were compared with 70S ribosome analyses. Samples from 50S and 70S ribosomes were simultaneously treated with sodium borohydride reduction followed by aniline-induced strand scission. U, A, and G are sequencing lanes; NR, no reaction control; ND, no drug control; N, neomycin; P, paromomycin; G, gentamicin.

antibiotic with 70S ribosomes versus isolated 50S subunits revealed a remarkable difference between them, in which the environment of N7 of G1921 is more accessible (exposed) in isolated 50S subunits than in 70S ribosomes (Figure 5.4). Subunit association and intersubunit B2a formation between H69 of 50S and h44 of 30S subunits cause protection of A1912, A1916, and A1918 from DMS reaction at N1 position; however, according to crystal structures, neither G1921 nor G1922 are involved in this intersubunit-related interaction. When tRNAs are present, G1921 and G1922 interact with the D-stem of the P-site tRNA, through its minor groove. Therefore, the different accessibility of the N7 of G1921 can be interpreted as a local conformational rearrangement in the H69 stem region that is coupled with ribosomal subunit association. As stated in Chapter 3, the H69 loop undergoes a dynamic conformational rearrangement upon subunit association (see Chapter 3), such that it is not surprising that the H69 stem region also undergoes conformational changes upon subunit association. It is likely that such conformational rearrangements supply a suitable binding scaffold for aminoglycoside antibiotics.

5.3.2. Binding of aminoglycoside neomycin alters DMS and DEPC probing patterns of H69

To investigate antibiotic binding effects on H69, direct DMS and DEPC probing was performed in the presence of aminoglycoside and cyclic peptide antibiotics. Primer extension assays after DMS probing exhibited no change in reactivity at any residue in the presence of 5 μM aminoglycoside antibiotics; however, DEPC probing revealed protection of A1913 in the presence of 5 μM neomycin (Figure 5.5). A1918 and A1919 were also protected in DEPC reactions, and the observed trend of protections at these sites is similar to previously mentioned results at 20 mM Mg^{2+} concentration (Figure 5.5). These results indicate that neomycin induces a conformational change of the H69 loop or throughout the entire ribosome, which alters DEPC reactivity toward the H69 loop region. A detailed mechanism for this behavior is not known, but this binding activity is consistent with the observation in Chapter 4, in which only neomycin induce a different H69 loop conformation and caused an increase in 2AP1913 fluorescence. Therefore, it can be suggested that the H69 conformational change can be induced by the interaction of neomycin with the H69 stem in 70S ribosomes.

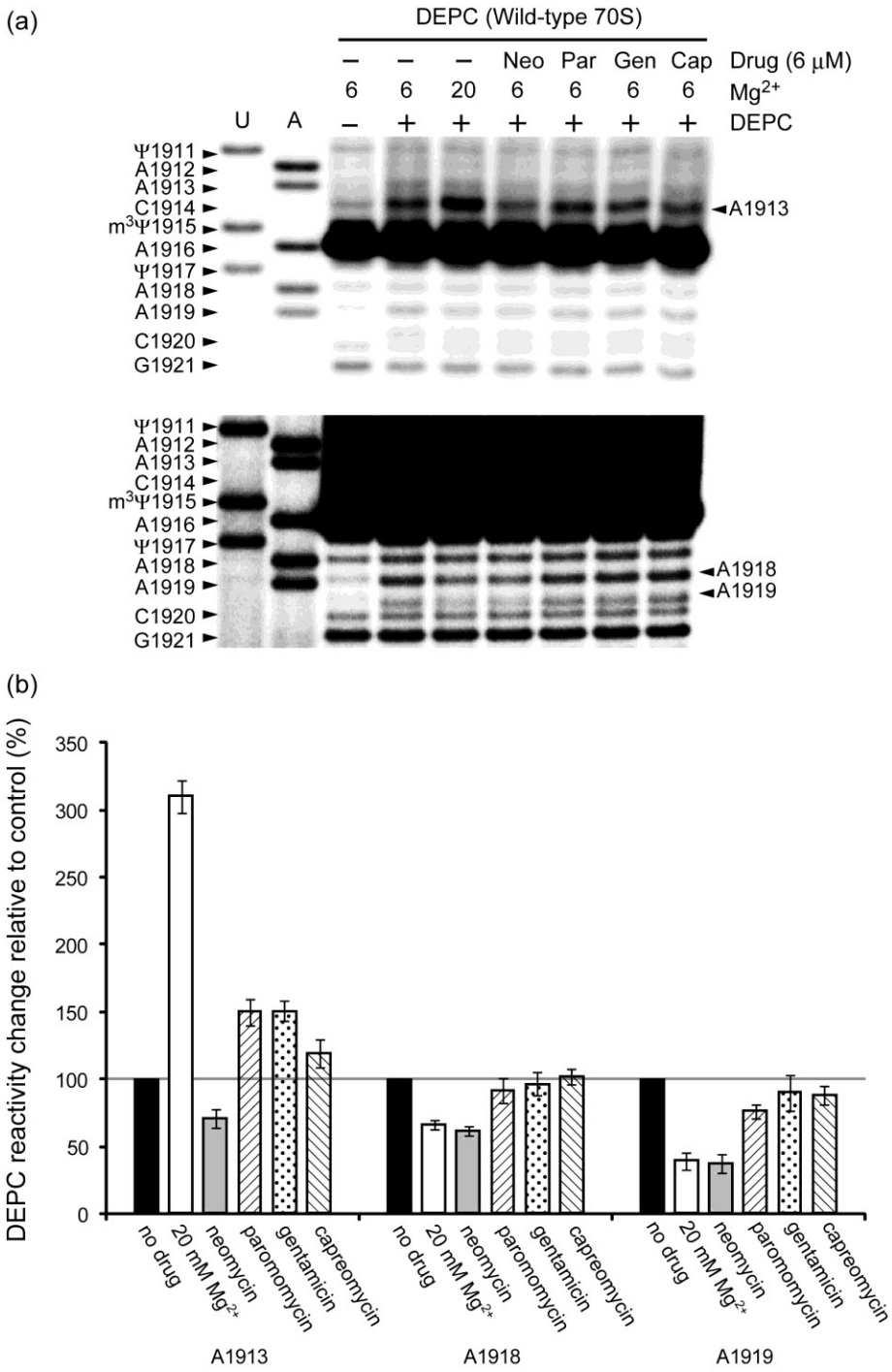

Figure 5.5. (a) Autoradiograms from DEPC probing of 70S ribosomes in the presence of 5 μM drugs and 20 mM Mg^{2+}. (b) Quantification data of DEPC reactivity change relative to control conditions (no drug, 6 mM Mg^{2+}) are shown. Band intensities were normalized to the non-specific band at 1921 (see Chapter 3), and percent change was calculated.

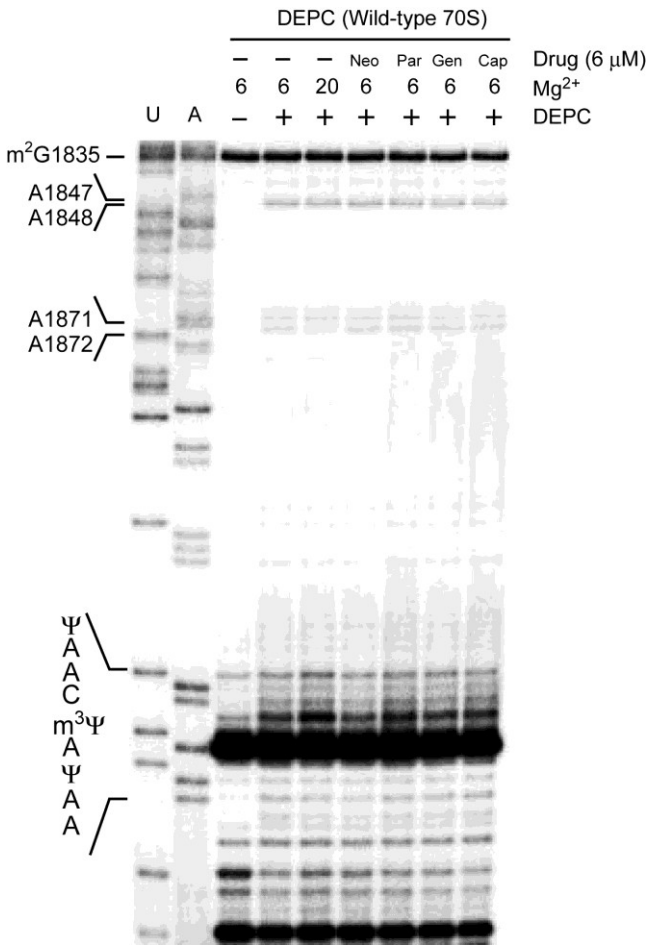

Figure 5.6. The entire gel picture for Figure 5.5 is shown to demonstrate that there is no change in DEPC reactivity in H69 probing experiments. As shown in the A1871 and A1847 regions, DEPC reactivity is the same in the presence of drugs or high Mg^{2+} concentrations; therefore, different reactivities of H69 are attributed to the different nucleoside conformational states induced by neomycin.

The biological function of the neomycin-induced H69 conformational change is likely to be important. Toeprinting analyses with aminoglycoside antibiotics also showed that neomycin has a stronger influence than paromomycin on POST-to-PRE ribosome back translocation [217]. Furthermore, single molecule FRET experiments showed that neomycin-bound ribosomes had an increased population of the hybrid-tRNA configuration over the classical-tRNA configuration with increasing concentrations of the drug. Other aminoglycosides did not show such a transition of ribosome configurations [211]. Thus, this result provides further evidence that neomycin has a secondary binding activity. Probing studies in this chapter showed H69 loop conformational changes upon neomycin binding to the H69 stem. Since this differential binding activity of aminoglycosides is not observed in h44 of the 30S subunit, it can be suggested that the H69 loop conformational state influences the ribosome conformation or tRNA configuration, such that a different tRNA configuration or back-translocation are observed in the presence of neomycin at relatively high concentration. In support of this hypothesis, we observed A1913 protection in DMS probing under higher neomycin concentrations (50 μM), indicating the influence of the H69-neomycin interaction on ribosome conformation.

5.3.3. Antibiotic footprinting analysis of H69 pseudouridine-deficient 70S ribosomes: pseudouridine modifications are necessary for efficient binding of aminoglycosides to H69

In nature, RNA is modified at many specific sites in order to gain extra function or to expand the genetic code. As mentioned previously, H69 contains three pseudouridines (Ψ) in its loop (Figure 5.1). SHAPE experiments show a disordered H69 conformation in RluD(–) 70S ribosomes, and in previous studies we demonstrated that Ψ modifications in H69 are associated with the modulation of H69 conformational dynamics (see Chapters 2 and 3). As such, we hypothesized that a lack of Ψ modifications in H69 would affect the binding affinity of aminoglycsodie antibiotics. Although no protection was observed at 5 μM drug concentrations, weak protection at residue G1922 of RluD(–) 70S ribosomes was found at 50 μM neomycin and paromomycin (Figure 5.7). Protection by gentamicin and capreomycin was not found in H69 of RluD(–) 70S ribosomes. In contrast to reduced binding to unmodified H69, aminoglycoside antibiotics were found to bind h44

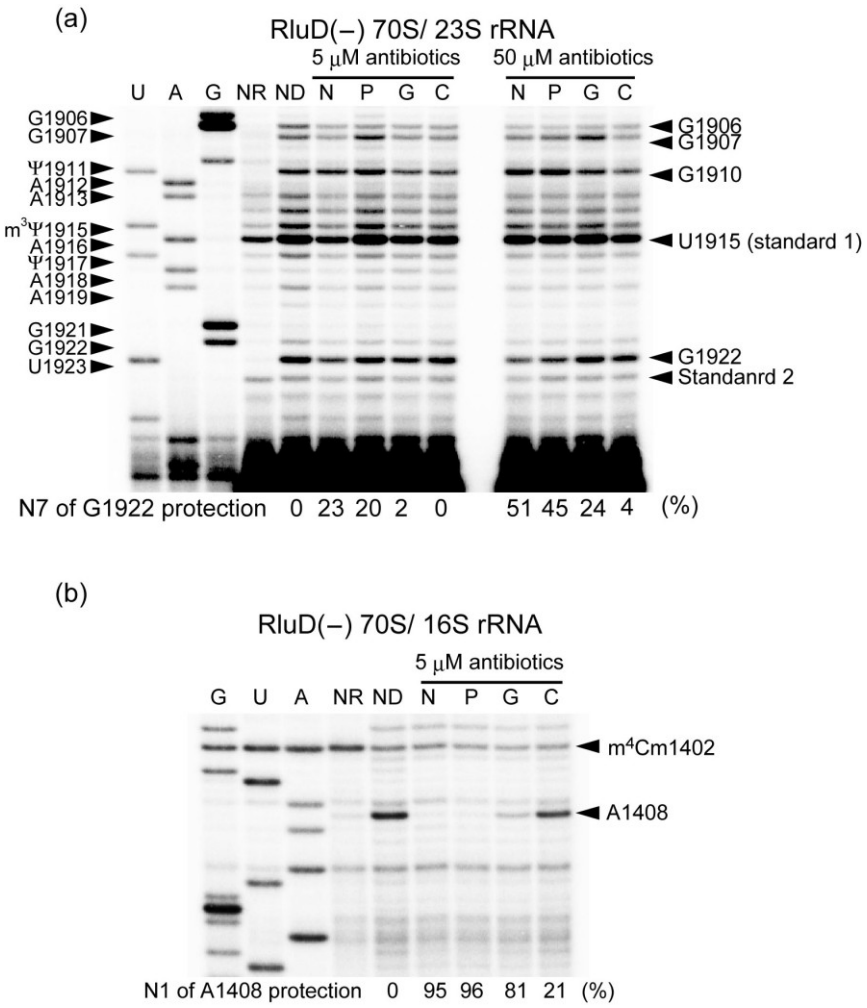

Figure 5.7. Autoradiograms for DMS footprinting of (a) H69 and (b) h44 in RluD(–) 70S ribosomes are shown. In this case, two independent standard bands (standard 1 and 2 indicated on the right side of the gel picture) were used to compare data. Percent protection at G1922 are shown at the bottom of gel pictures. The same rRNA samples were used to analyze drug binding to both H69 and h44.

of 30S subunit as well as to the wild-type 70S ribosomes and protect A1408 from DMS probing (Figure 5.7), indicating that mutations on H69 of the 50S subunit do not influence the A-site interaction with aminoglycosides. Since clear indications of bridge B2a formation are observed through protection of residues A1918 and A1912, it appears that the conditions used in this study were sufficient to favor 70S ribosome formation (see Chapter 3), and the possibility of RluD(–) 70S ribosome dissociation can be excluded. Thus, it can be suggested that lack of Ψ modifications causes a change in the overall H69 conformation in 70S ribosomes. Indeed, a different accessibility of the H69 stem region was found at G1910 (Figure 5.7). The N7 of G1910 exhibited strong reactivity in RluD(–) 70S ribosomes. This reactivity was not observed in wild-type 70S ribosomes or 50S subunits, and it indicates that a change in loop conformation caused by the loss of Ψ modifications could also influence the H69 stem conformation.

5.4. Discussion

In this chapter, we employed DMS footprinting to evaluate antibiotic binding to H69 in 70S ribosomes. Our data clearly show that neomycin, paromomycin, and gentamicin bind to the H69 stem region and protect positions G1922 and G1906 at low drug concentrations, in good agreement with crystal structure data. The interaction of H69 and aminoglycosides is believed to be a secondary interaction when the A site is taken into consideration because of the stronger protection pattern at residue A1408 and lower K_d values for the A site. However, it is not excluded that a synergistic mechanism of aminoglycosides binding to H69 and h44 simultaneously could be present, since they are located in such close proximity within the 70S ribosome.

Furthermore, we propose that the H69 stem region undergoes conformational rearrangements coupled with ribosomal subunit association as observed in the loop region (see Chapter 3). Like induced-fit models of general protein-ligand interactions, the formation of intersubunit bridge B2a induces a conformational change that is cooperatively recognized by aminoglycosides. This reorganization will cause translocation stops, miscoding of mRNA and RRF-mediated ribosome dissociation, partly due to changes in the conformational dynamics of H69. These results also suggest that aminoglycosides would recognize not only a preferred RNA

sequence of *E. coli* H69 over eukaryotic H69, but also a specific H69 structure. Furthermore, we found that neomycin alters the H69 loop conformation, but paromomycin and gentamicin do not, even though they have very similar chemical structures as neomycin. Ribosome toeprinting analysis revealed that neomycin has stronger effects on the Post-to-Pre back-transition than paromomycin [217]. The binding mode of these aminoglycosides to h44 of the 30S subunit is likely to be the same, in which they induce the extra-helical A1492/1493 conformation of h44 of the 30S subunit [8, 133, 138, 218, 219]. Therefore, it is possible that the different impact on H69 conformation can facilitate the back-transition from Post-to-Pre ribosome conformation. Our results suggest the significance of further understanding the underlying principles of H69 structure and function in entire ribosome structures.

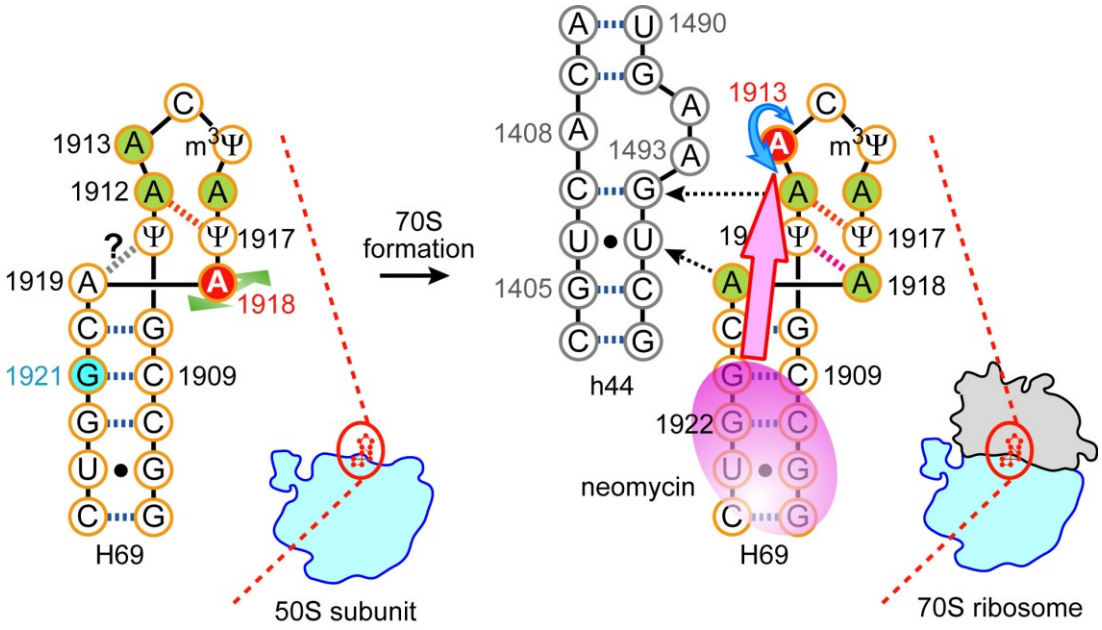

Figure 5.8. Summary of DMS footprinting and DEPC probing analyses is shown. Red circles, flexible nucleotides; green circles, protected nucleotides as determined by SHAPE and DEPC in Chapter 3; red dashed lines, non-canonical base-pair interactions; light blue circle, more accessible in the major groove surface.

We also evaluated the binding affinity of aminoglycosides for Ψ-deficient H69 within ribosomes. The ability of aminoglycosides to protect specific bases was reduced in 70S ribosomes lacking Ψ on H69. We also found that the Ψ-deficient H69 shows different accessibility at the N7 of G1910 in the stem region, suggesting a more open major-groove conformation of the H69 stem in Ψ-deficient ribosomes. Thus, it could be suggested that lack of Ψ causes indirect alterations of the H69 stem conformation, resulting in loss of recognition of H69 by aminoglycosides.

The K_d values measured by fluorescence, ESI-MS, and SPR are 2.0, 9.0, and 1.3 μM for unmodified H69, respectively (see Chapter 4). Although the K_d values depend on the methods and conditions selected for binding studies, aminoglycosides bind to unmodified H69 in the low micromolar level, which is inconsistent with these footprinting results. It is unclear why such a disagreement arises with no binding activity of aminoglycosides on RluD(–) ribosomes, but other ribosome components, other than H69, might play a role in regulating key conformational changes. We cannot exclude the possibility that a different H69 stem conformations, due to a absence of Ψs in H69, interfered with aminoglycoside-H69 interactions. Therefore, further studies to understand the relationship between H69 conformation and H69-binding ligands would be necessary.

5.5. Materials and methods

The procedures for ribosome isolation and DMS and DEPC probing reactions are identical to those in Chapters 2 and 3.

5.5.1. Chemical footprinting analysis

DMS footprinting in the presence of aminoglycoside and peptide antibitocs

The isolated 70S ribosome was incubated for reactivation at 37 °C for 15 min under the following conditions; 20 mM HEPES, 6 mM Mg^{2+}, 100 mM NH_4Cl, pH 7.3 at 37 °C. Buffer conditions were adjusted for DMS footprinting (80 mM HEPES, 6 mM Mg^{2+}, 100 mM NH_4Cl, pH 7.3 at 37 °C) and ribosome concentration was adjusted to 0.3 μM by dilution. The 70S ribosomes

were again incubated at 37 °C for 10 min in footprinting buffer. Each antibiotic tested (neomycin, paromomycin, gentamicin, and capreomycin stocks in footprinting buffer at 100 or 1,000 μM) was added at a 5 or 50 μM final concentration, and incubated at 37 °C for an additional 10 min. DMS footprinting was initiated by the addition of 1 μl DMS in cold ethanol (20 mM DMS final reaction concentration), and incubation proceeded at 37 °C for 10 min. The reaction mixture was quickly terminated by adding 10 μl stop buffer (3 M 2-mercaptoethanol, 1 M Tris-HCl pH 7.5 at r.t., 10 mM $MgCl_2$) followed by ethanol precipitation. The pelleted ribosome was dissolved in buffer (50 mM Tris-HCl, 2 mM EDTA, pH 7.5 at r.t.). The rRNAs were prepared by general phenol-chloroform extraction (see Chapter 1). All footprinting assays were performed at least three times independently.

Aniline-induced strand scission at N7 of G

Aniline-induced strand scission was performed as follows. The chemically probed rRNAs were dissolved in 10 μl 1 M Tris-HCl (pH 8.3) with 2.5 μg of carrier tRNA, and incubated on ice in the dark for 30 min in the presence of freshly prepared 10 μl 0.2 M sodium borohydride. The reaction was quenched by adding 10 μl 3 M sodium acetate (pH 5.3) and cold ethanol, then quickly precipitated by centrifugation. The RNA pellet was rinsed with 70% ethanol and dried briefly. The RNA pellet was dissolved in 10 μl freshly prepared 1 M aniline-acetate (pH 4.5), and incubated at 60 °C for 20 min. The reaction was terminated by putting the tube on ice for 1 min followed by addition of 100 μl 0.2 M sodium acetate (pH not adjusted). The quenched solution was treated by phenol-chloroform and chloroform extraction followed by ethanol precipitation. The pelleted rRNA was used for reverse transcription as stated in Chapters 2 and 3.

Chapter 6
Exploring a unique drug target site in the 50S subunit

6.1. Abstract

The emergence of advanced antibiotic-resistant pathogens has prompted researchers to discover unique drug target site to combat bacterial infectious diseases. One such candidate is H69, as discussed in the previous chapters, which has multiple conformational states, each of which would be able to be targeted selectively by small ligands. To explore another possible target on the ribosome, an RNA domain called helix 68 of 23S rRNA (H68) was tested. Helix 68 is present at the exit site of the ribosome and its sequence and secondary structures are partially conserved (Figure 6.1). H68 is proposed to play a role in regulating tRNA translocation from the P to E site (Figures 6.1 and 6.2); however, its overall importance is still an enigma. According to chemical probing results on the ribosome, we showed that subunit association alters local nucleotide flexibility of H68, which comprises intersubunit bridge B7a. Further probing studies in the presence of aminoglycoside antibiotics revealed that neomycin changes the DMS probing pattern on H68. In addition, fluorescence intercalator displacement analysis, in-line probing, and isothermal calorimetry reveal a moderate binding affinity of aminoglycosde antibiotics to H68, and such interactions are influenced by Mg^{2+}. In combination with the potential function of H68 in translation, these results suggest that H68 could also serve as a unique drug target site in the ribosome.

6.2. Introduction

Transfer RNA translocation from the A to E site of the ribosome is one of the main molecular events in protein synthesis (see Chapter 1). The interactions between ribosome and tRNAs change upon tRNA movements to the next site, and these interactions are tRNA position and type specific [29, 191, 192]. Disruption of specific interactions between a tRNA and the ribosome causes deleterious effects on ribosome translation. For instance, introduction of a 2'-OMe in ribose 70 or 71 of the P-site tRNA strongly blocks EF-G-mediated tRNA translocation [220].

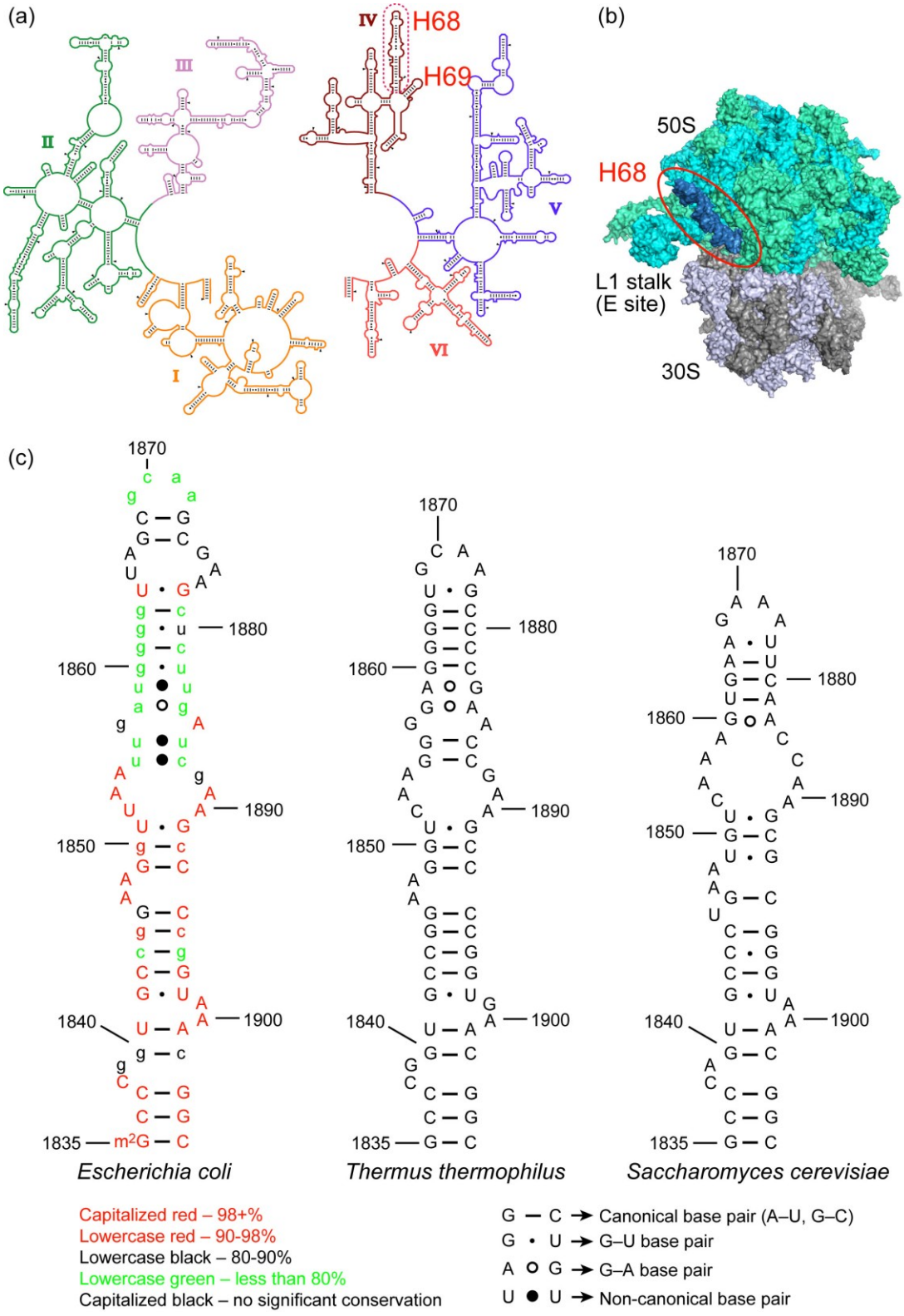

Figure 6.1. The location of H68 is shown on (a) the secondary structure map of 23S rRNA [69] and (b) the crystal structure of the ribosome (PDB ID: 3R8O+3R8T). (c) RNA sequence conservation and secondary structures of H68 in three organisms are shown [69].

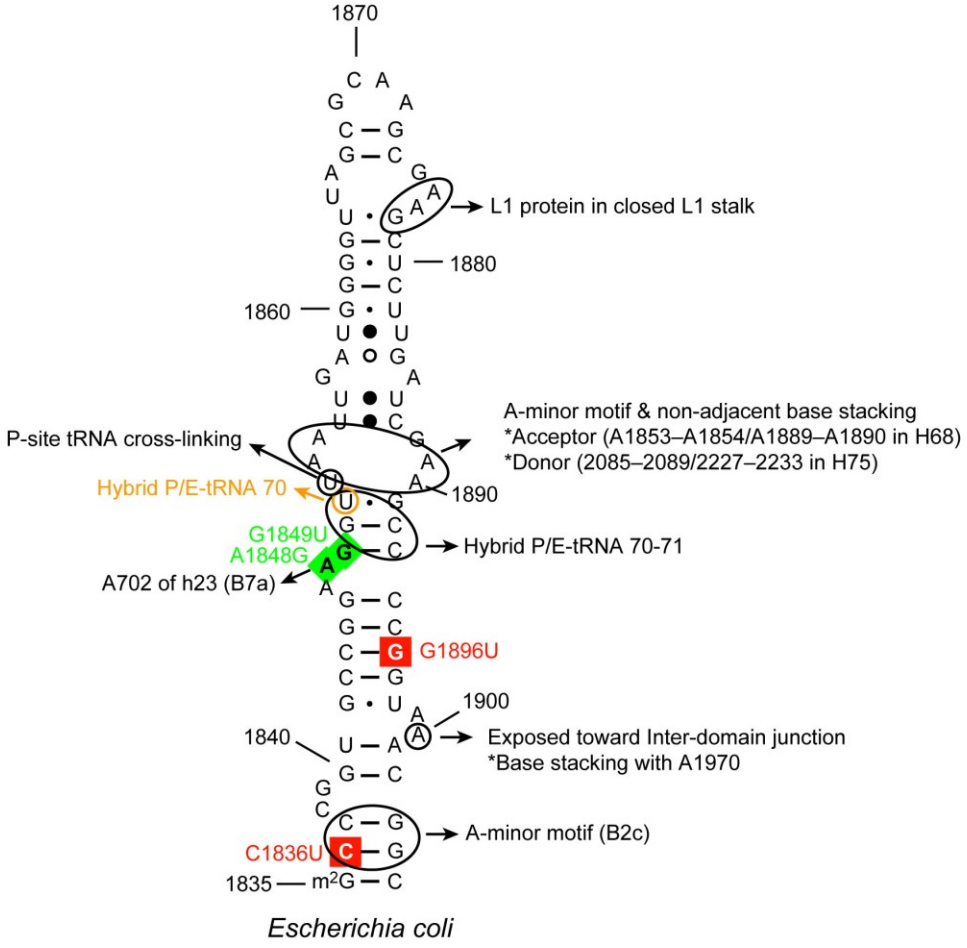

Figure 6.2. The important interactions and residues of H68 are shown on the secondary structure of H68. Deleterious point mutations that cause considerably reduced growth rates, inefficient subunit associations, and stop codon readthrough are shown by red boxes, and point mutations that cause a slight change in growth rate and less efficient subunit association are shown by green boxes. Nucleotide U1851, circled in orange, represents the position that is predicted to undergo a dynamic conformational rearrangement based on MD simulations [240].

Position 71 of the E-site tRNA makes direct contact with H68 of 23S rRNA through a ribose-zipper interaction, in which U1851 and its corresponding ribose interact with the 2'-OH of the P-site tRNA 71 (Figures 6.2 and 6.3) [48]. Since crystal structures show no other specific interactions between the acceptor end of the P-site tRNA and the ribosome, it was suggested that the 2'-OMe of nucleotide 71 blocks tRNA translocation from the P/P to P/E hybrid state by disrupting stable interactions between the E-site tRNA and H68 (Figure 6.3a and b).

H68 forms part of the E site (Figures 6.1, 6.2, and 6.3). A well-known function of the E site is ejecting deacylated tRNA from the ribosome, which is mediated by the large ribosomal protein L1 [221]. Cross-linking experiments showed direct contacts between L1 and H68 through nucleotides 1864-67 and 1876-78 of H68 (Figures 6.2 and 6.3c) [221, 222]. In addition, nucleotides 1852 and 1878 of H68 were found to interact with the P-site tRNA by cross-linking analysis (Figure 6.2) [223]. However, further understanding of how these molecular interactions affect ribosome activity, such as tRNA translocation and tRNA release from the ribosome, is necessary.

A cryo-EM map of the ribosome reveals different conformational states of H68 than those observed in crystal structures, in which H68 undergoes conformational changes upon entry of the P-site tRNA into the E site [224]. Furthermore, detachment of the P-site tRNA from H69 and destabilization of the major H69 conformation suggest an inter-helix communication between H68 and H69 for smooth movement of the tRNA from the P to E site [224]. Moreover, a recent crystal structure of translocating ribosomes shows that H68 moves by 2 to 3 Å toward the acceptor stem of P/E tRNA to support a stable hybrid P/E-tRNA configuration (Figure 6.3a) [98].

Molecular dynamics (MD) simulations also predicted the importance of H68-tRNA interactions for tRNA translocation [225]. In this simulation, $tRNA^{Phe}$ makes direct interactions with U1851 of H68 upon formation of the hybrid P/E-tRNA state. The universally conserved U1851 residue forms a base-pair with G1891 in the empty E site; whereas, upon forming the hybrid P/E-tRNA configuration during this simulation, this base pair is disrupted and U1851 is projected toward G70 of $tRNA^{Phe}$ (Figure 6.3d) [225]. A parallel MD simulation using $tRNA^{fMet}$, an initiator tRNA containing a rigid anticodon stem-loop (ASL) conformation, did not induce this conformational

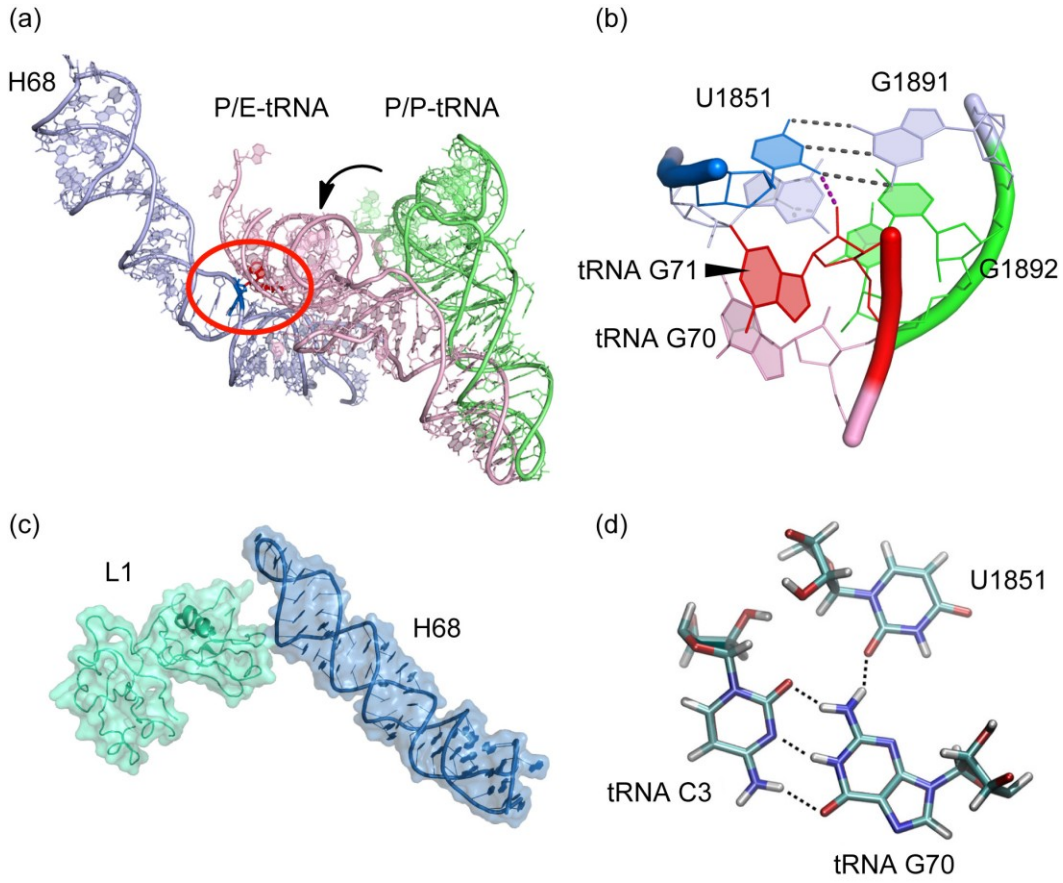

Figure 6.3. (a) Crystal structures show the molecular interactions of H68 with the hybrid P/E-tRNA but not the classical P/P-tRNA (PDB ID: 3R9N, 3R8O, 3R8S, 3R8T). During tRNA translocation after peptidyl transfer, the acceptor stem of P/P-tRNA moves into the E site and forms the P/E-tRNA configuration, which is stabilized by interactions between the tRNA elbow region, L1, and H68. The detailed interaction represented by a red circle is shown in Figure (b). (b) The 2'-OH of tRNA G71 makes a direct contact with U1851/G1891 (PDB ID: 3R8N+3R8S). The importance of this interaction was observed by the strong translocation inhibition by tRNA with a 2'-OMe at position 70 or 71 [220]. (c) Crystal structure containing E-site tRNA show L1 and H68 interaction as a result of L1 stalk closure (PDB ID: 3KNI). (d) The proposed molecular interaction occurs as a result of a flipped-out conformational change at U1851 upon the tRNA transition from the P/P to P/E configuration. This figure is adapted from [225].

rearrangement of U1851 [225]. This result is supported by the observations that $tRNA^{fMet}$ has a weaker interaction with the L1 stalk and occupies the classical P/P-tRNA state as a result of rapid disruption of the $tRNA^{fMet}$-L1 stalk interaction. In contrast, elongator tRNAs, such as $tRNA^{Phe}$, have a strong interaction with the L1 stalk and occupy the hybrid P/E-tRNA state; however, the population of the hybrid P/E state over the classical P/P state is dependent on the type of elongator tRNA [226-228]. These results suggest the significance of the H68-tRNA interaction as well as L1-tRNA interaction to cooperatively stabilize the hybrid tRNA configuration.

Genetic studies support the idea of importance of H68 in ribosome activity (summarized in Figure 6.2). H68 is involved in intersubunit bridges B2b and B7a (see also Figure 1.10 in Chapter 1) [46]. Mutation studies revealed the significance of these intersubunit bridges in normal cell growth and ribosome activity [229]. Base mutations C1836A or C1836G in bridge B2b are inviable. Co-expression of these mutant subunits with wild-type ribosomes revealed deleterious loss of incorporation of mutant subunits into 70S ribosomes. A viable C1836U mutation exhibits growth retardation compared to wild-type and causes a decline in 70S ribosome formation. In the case of bridge B7a, A1848N (N, any base type) mutations affect stable ribosome formation *in vitro* and *in vivo*, consistent with the importance of bridge formation between A702 in the 30S subunit and A1848 in the 50S subunit (B7a). A mutation of B7a neighboring base A1896 to U causes considerable defects in subunit association and substantial UAG stop-codon readthrough. The viable C1836U mutation also results in substantial UAG stop-codon readthrough. At the terminal stem of H68, there is a naturally occurring m^2G at 1835. Deletion of the enzyme responsible for m^2G1835 modification revealed that this modification enhances subunit association *in vitro* (see Chapter 1) [86]. Furthermore, a deletion of H68 caused a considerable reduction in growth rate *in vivo* and substantially lower subunit association *in vitro* [230], indicating the importance of H68 for proper ribosome activity. These results strongly suggest the importance of H68 in normal ribosome activities; however, little is known about the underlying mechanism of the E site and H68 function.

Since H68 has been revealed as a functionally important segment in the ribosome, this domain could be a possible target site for drug discovery. Indeed, the work reported in this

chapter shows that the aminoglycoside antibiotic neomycin changes the conformation of H68. Because the molecular basis of aminoglycoside antibiotic activity is still not fully understood and recent smFRET analyses found different impacts of aminoglycosides on ribosome conformation (see Chapters 4 and 5) [211], it could be worth pursuing the possibility of using H68 as a new drug target for disruption of the molecular interactions between H68 and hybrid P/E-tRNA or physically blocking the intersubunit bridges B2b or B7a.

6.3. Results

6.3.1. DMS probing analysis of H68 of 23S rRNA

While carrying out footprinting assays with aminoglycosides on 50S subunits, H68 was observed to undergo conformational changes in the presence of neomycin (Figure 6.4). This conformational change was dependent on Mg^{2+} concentration and temperature. When Mg^{2+} was increased to 6 mM and chemical probing was performed under "on ice" conditions, the reactivity at A1900 and A1901 was reduced (Figure 6.4). Little or no conformational change was observed when probing was performed at 37 °C under 3 or 6 mM Mg^{2+} concentrations (data not shown). These results suggest that neomycin binding to H68 is dependent on H68 conformational dynamics, because a lower temperature would reduce molecular motions. Regarding the Mg^{2+}-dependent DMS reactivity, it is possible that Mg^{2+} competes with neomycin or induces an H68 conformation change that does not favor an H68-neomycin interaction. However, since the intracellular free magnesium concentration is estimated to be around 1 to 2 mM in bacteria [231], which is much less than the *in vitro* conditions in this work, neomycin may bind to the ribosome at H68 *in vivo*. Indeed, it is proposed that neomycin has another secondary or more binding site that modulates the tRNA configuration relative to the ribosome; whereas, other aminoglycoside antibiotics do not display this activity [211]. In smFRET experiments, under higher neomycin concentrations, ribosomes prefer the P/E-hybrid tRNA configuration instead of the classical configuration [211]. A detailed mechanism exploring how aminoglycosides from the same class have such different impacts on the ribosome is not clear. Thus, understanding the function of antibiotics in more detail is necessary, and footprinting data suggest the possibility that H68 may

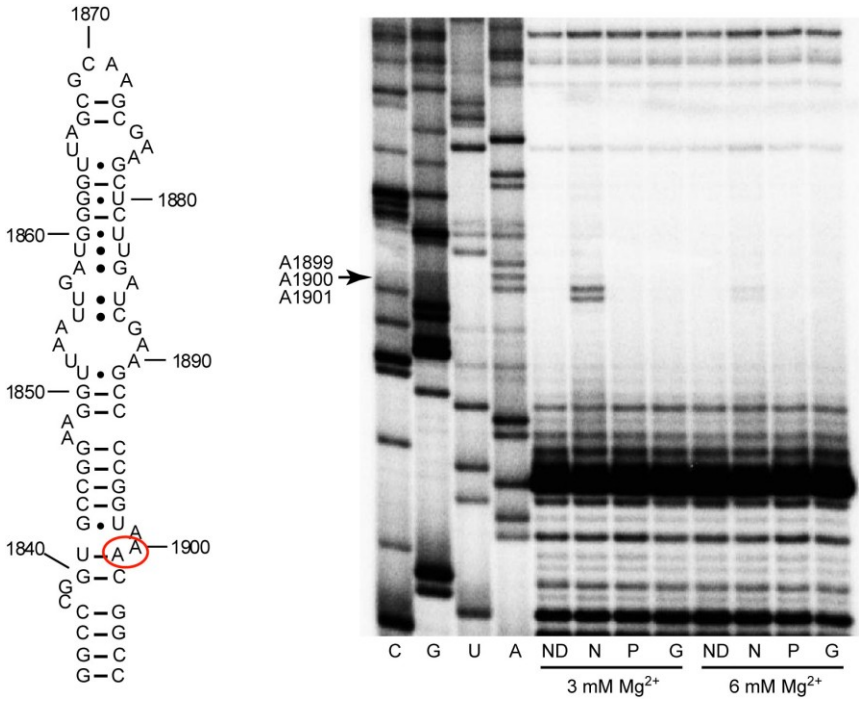

Figure 6.4. An autoradiogram of DMS probing data in the presence of 50 μM aminoglycoside antibiotics and the secondary structure of H68 are shown. The circle shows the site where DMS reactivity change was observed in the presence of neomycin (N, neomycin; P, paromomycin; G, gentamicin; ND, no drug control). Probing was performed under on ice conditions in the presence of 3 or 6 mM Mg^{2+}. The probing conditions were identical to those described in Chapter 2.

be another secondary binding sites for aminoglycoside antibiotics. As such, the characteristics of H68 in terms of drug binding were further tested in this work.

6.3.2. Structural analysis for the possible importance of the domain IV junction

The DMS reactive residue A1900 lies at the center of the domain IV junction (Figure 6.5) [5, 69]. A1900 is a universally conserved residue, and a remarkable characteristic of A1900 might be its conformation as observed in crystal structures (Figure 6.5a and b) [69]. A1900 is flipped out of H68 and exposed to the junction composed of H66, 67, 68, and 71. It base stacks with A1970. Based on crystal structures, the DMS probing result is interpreted such that neomycin alters the conformation of the domain IV junction and causes an exposure of A1900 to the environment where it becomes reactive towards DMS.

Further studies revealed that mutations of residues surrounding A1900 cause abnormal phenotypes (Figure 6.5a and b) [229]. Mutations at A1832/A1833, C1836, A1932, or G1972/G1973 cause cell death or severe growth retardation, reduced 70S ribosome formation *in vivo*, and higher UAG stop codon readthrough. Compensatory mutations for A1832/A1833 and G1972/G1973, in which they can form stable base pairs, did not completely rescue the abnormal phenotypes [229], suggesting that proper conformation at the domain IV junction, rather than base-pair formation, is an important factor for normal ribosome function. Indeed, A1900 base stacks with A1970, whose conformation is likely supported by stable interactions between C1832-G1973 and C1833-G1972 (Figure 6.5b). If such a stable scaffold is disrupted, then the domain IV junction may not function properly. C1836 lies adjacent to A1900, and disruption of the stable C1836-G1904 base pair may alter projection of A1900 at the junction. In the case of A1932, it is difficult to know how this residue influences the domain IV junction; however, a crystal structure of 70S ribosomes with ribosome recycling factor (RRF) shows a direct contact between RRF and the 70-71 region (Figure 6.5c) [98]. It is possible that a dynamic conformational change around the domain IV junction is induced by RRF and facilitates subunit dissociation, consistent with mutation studies in which junction mutants disable 70S ribosome formation [229].

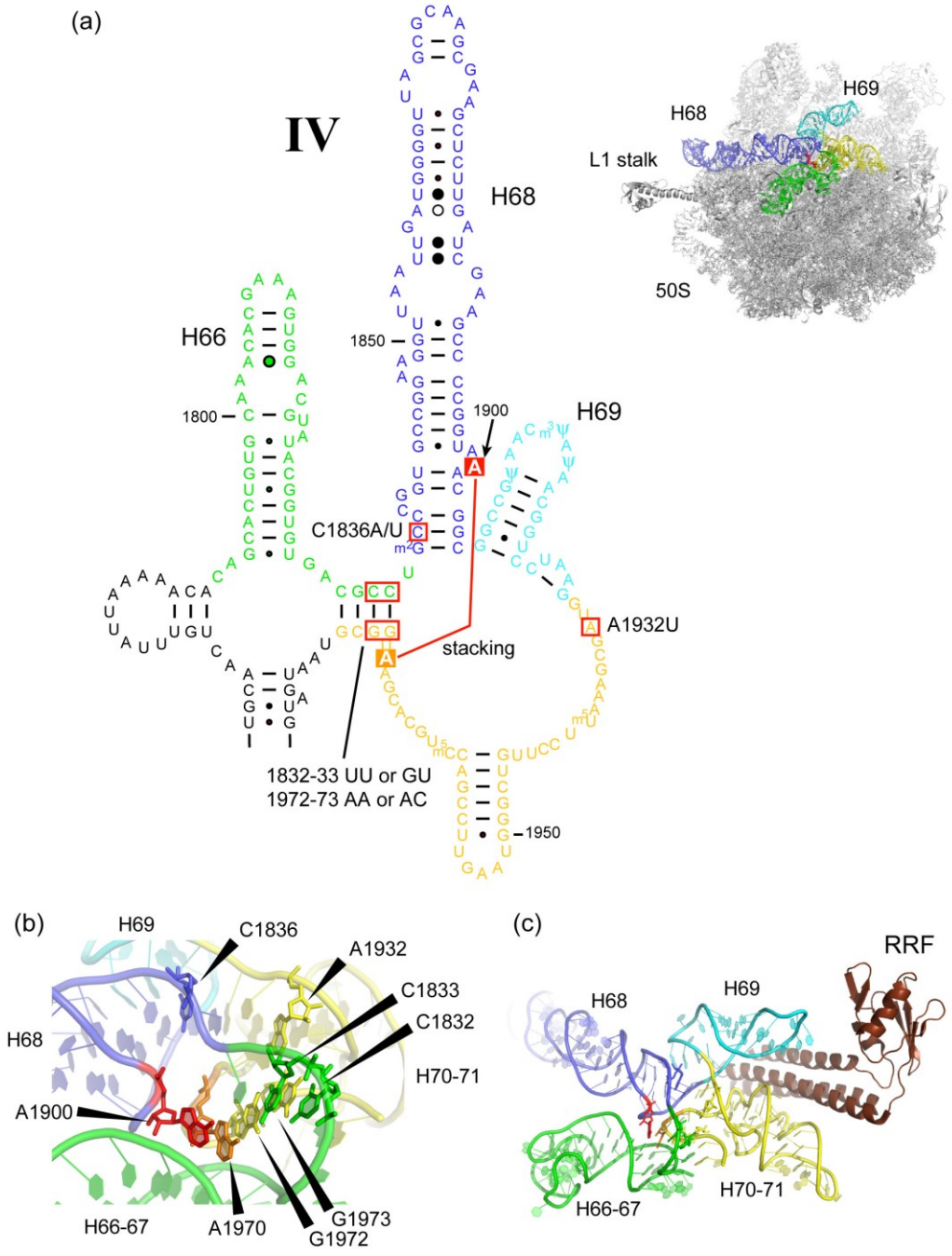

Figure 6.5. The secondary structure of domain IV (from H66 to H71) is shown. Color codes are green, H66-67; blue, H68; cyan, H69; yellow, H70-71. These color codes are identical to those of the inset crystal structure (PDB ID: 3R8N+3R8S). Sites that exhibited severe loss of ribosome function when mutated are marked by red boxes. Residues A1900 and A1970, which form a base-stacking interaction, are shown by filled boxes. (b) Crystal structure of the domain IV junction is shown (PDB ID: 3R8N+3R8S). (c) Crystal structure of the domain IV junction with RRF is shown (PDB ID: 3R8N+3R8S).

6.3.3. In-line probing study of H68

To examine the relationship between H68 conformation and antibiotic interactions, a small model H68 RNA was prepared by *in vitro* transcription and in-line probing analyses were performed [195]. In-line probing is based on the flexibility of a nucleotide (Figure 6.6a). As shown in Figure 6.6b, in–line probing results show that H68 nucleotide flexibilities are altered in the presence of neomycin. The sites altered by neomycin are positions 1900 (site 1) and 1852/1890 (site 2) (Figure 6.6b). At site 1, neomycin altered the local conformational flexibility at both 3 and 10 mM Mg^{2+}. Paromomycin, gentamicin, and capreomycin had no effect at 3 mM Mg^{2+}; and, paromomycin and gentamicin altered site 1 flexibility to a lesser extent at 10 mM Mg^{2+}. In the case of site 2, neomycin, paromomycin, and gentamicin decreased conformational flexibility (Figure 6.6b, region 1889-1891 and 1852). Neomycin increased local nucleotide flexibility at U1883 at 3 mM Mg^{2+}. This site shows strong hydrolysis at 10 mM Mg^{2+} without aminoglycosides (more flexible), which indicates that neomycin has a different impact on H68 conformational flexibility than other aminoglycosides and the changes are similar to Mg^{2+}-dependent conformational flexibility changes.

X-ray crystal structures show that the flexible sites of H68 (sites 1 and 2) comprise functionally important sites. Site 1 (region 1900) shows projection of A1900 into the domain IV junction, which likely stabilizes the overall structure of domain IV (Figure 6.5b). Site 2 is adjacent to the tRNA-binding region (Figure 6.3a and b). Thus, altered conformational flexibility of H68 as a result of aminoglycoside binding, could change the functionality of H68. For instance, decreased conformational flexibility at 1852 could destabilize or stabilize the interaction between the hybrid P/E-tRNA and H68. In addition, a different H68 conformation, induced by neomycin, could expose A1900, as observed in DMS probing (Figure 6.4).

6.3.4. Fluorescent intercalator displacement (FID) assay

To measure the relative binding affinity of aminoglycoside antibiotics for H68, a fluorescence intercalator displacement (FID) analysis was employed (Figure 6.7) [210]. FID is based on the

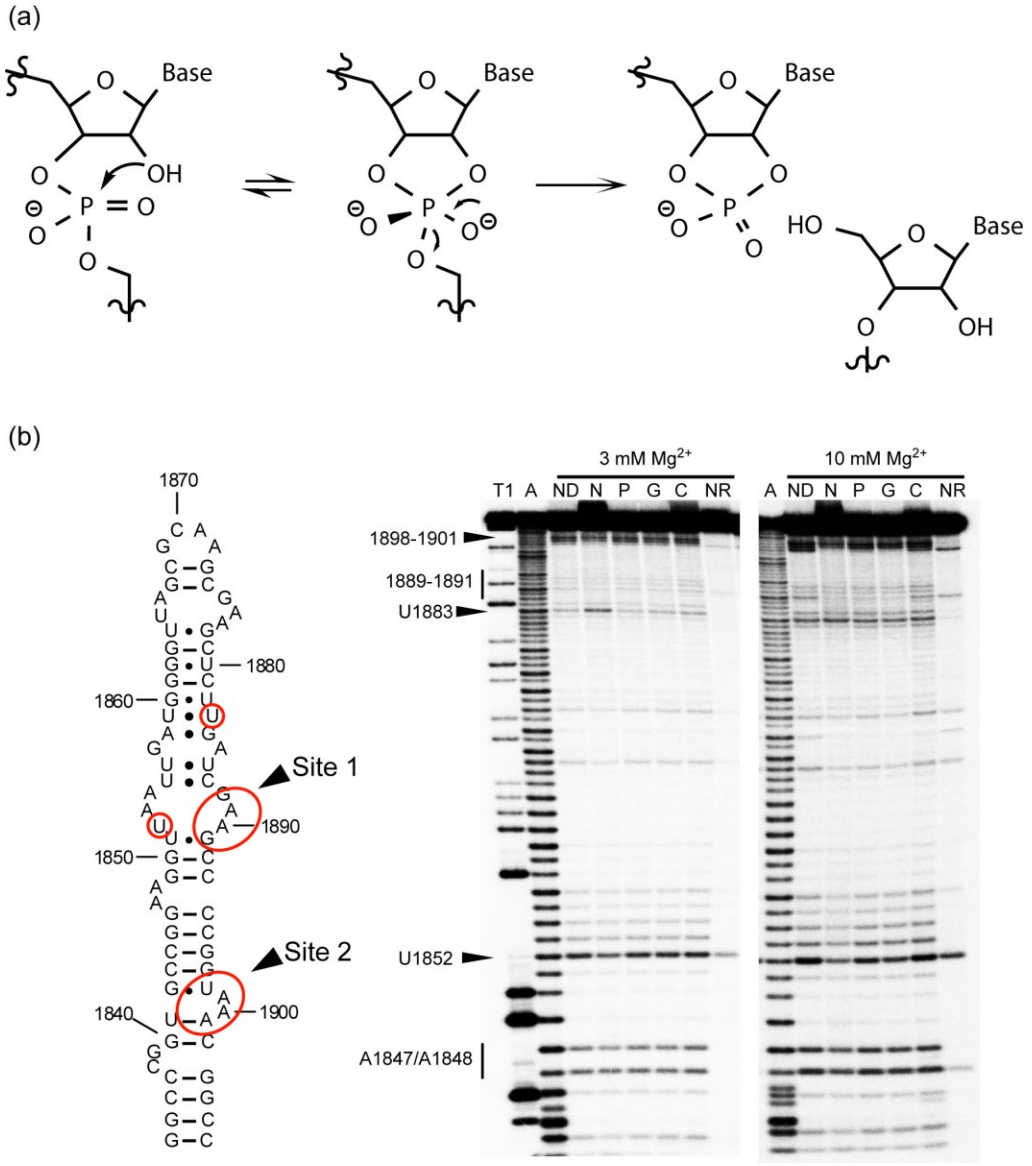

Figure 6.6. (a) The proposed reaction mechanism of in-line probing is shown. (b) The observed conformational flexibility sites mapped on the secondary structure of H68 and the autoradiograms of in-line probing data are shown (T1, G sequence generated by RNase T1 digestion; A, partial alkaline treatment; ND, no drug control; N, neomycin; P, paromomycin; G, gentamicin; C, capreomycin; NR, no reaction control). The aminoglycoside concentration was 250 μM in all cases. In-line probing was performed by incubating at room temperature for 2 days in the dark.

competitive binding of a small molecule with a reporter dye molecule, TOPRO (Figure 6.7a). The TOPRO fluorescence is increased upon its interactions with RNA; whereas, free TOPRO does not fluoresce. Because the TOPRO interaction with RNA is weak, if another ligand molecule binds to the same RNA more strongly, then it will displace TOPRO from the RNA and the fluorescence will be diminished. Even if a ligand molecule does not bind to the same site as TOPRO, but does induce a conformational change in the RNA, TOPRO could be displaced from the RNA causing a decrease in TOPRO fluorescence (Figure 6.7a). Thus, by observing changes in the fluorescence from TOPRO, one can trace a binding event between a ligand and RNA molecule.

FID experiments done in collaboration with Adhnan Mohamed showed that aminoglycoside antibiotics neomycin, paromomycin, and gentamicin all bind to H68 in the absence of Mg^{2+}; whereas, a control molecule, chloramphenicol, does not bind to H68 (Figure 6.7b). Paromomycin and gentamicin interactions with H68 were markedly diminished by the addition of 3 mM Mg^{2+}; in contrast, neomycin binding was not affected by Mg^{2+}. These results indicate two possibilities: (1) neomycin has a different binding site compared to paromomycin and gentamicin, and it is not affected by magnesium; or (2) the addition of magnesium alters the H68 conformation and influences the paromomycin and gentamicin binding modes but not that of neomycin. Since further addition of magnesium also displaced TOPRO from H68, we could not analyze the relationship between magnesium ions and aminoglycoside antibiotics binding interactions by FID. Nonetheless, FID data are consistent with the conclusions from DMS and in-line probing.

6.4. Discussion

H68 has been proposed to play an important role in ejecting the tRNA from the E site of the ribosome; however, its biological function is still undefined. From probing data and model studies in this thesis work, it was demonstrated that neomycin has moderate affinity (approximately 1.0 μM based on FID) for H68, whereas paromomycin and gentamicin have weak affinity (>8.0 μM) for H68 under physiological conditions (70 mM NH_4Cl, 30 mM KCl, 3 mM $MgCl_2$). Interestingly, only the interaction of neomycin induces a conformational change in H68 within the context of

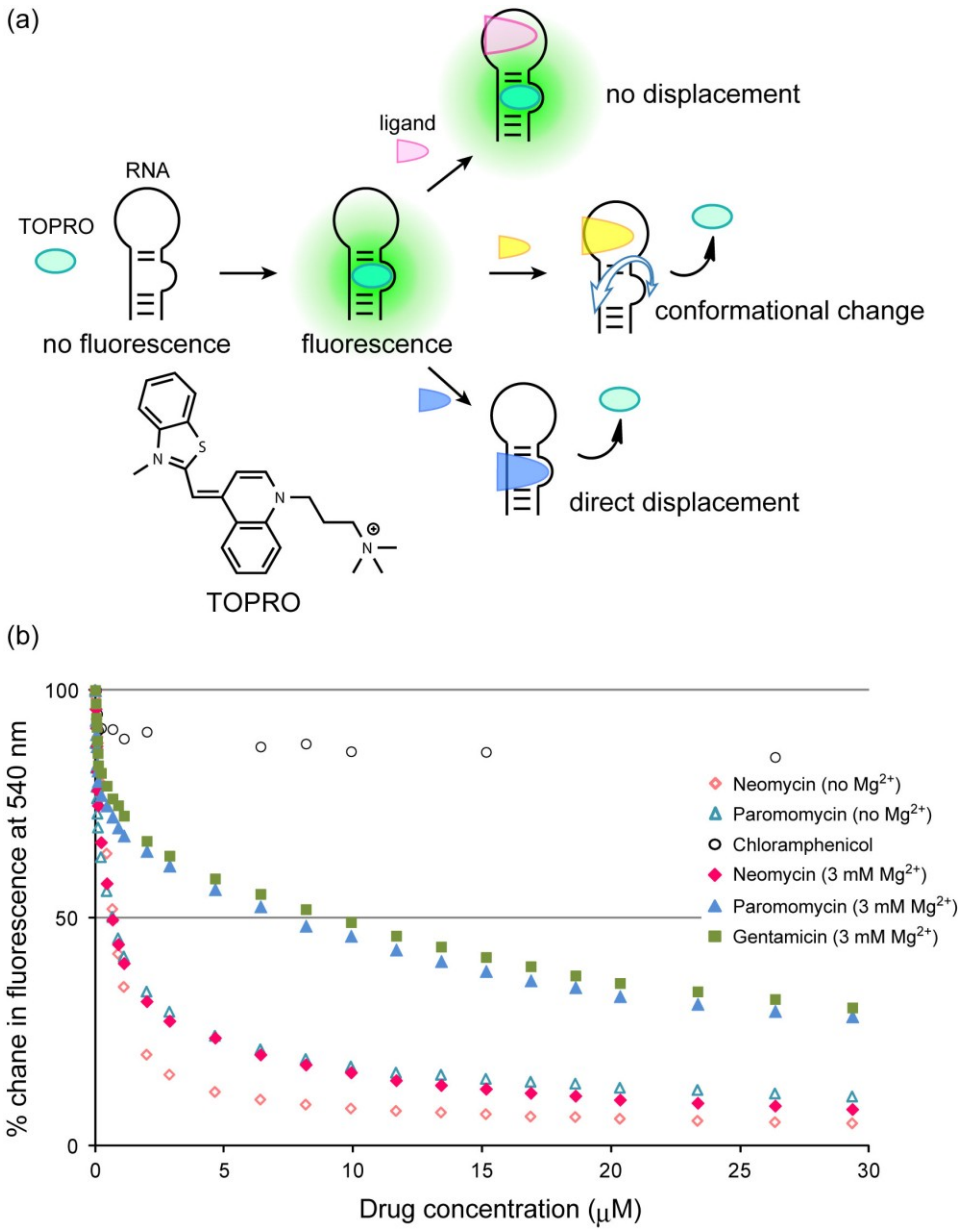

Figure 6.7. (a) A schematic illustration of fluorescence intercalator displacement (FID) is given. Free TOPRO dye does not fluoresce; whereas, it emits fluorescence upon binding to nucleic acid. Three possible observations are shown; no TOPRO displacement due to a different binding site and no conformational change upon binding, TOPRO displacement due to an RNA conformational change upon binding, and direct TOPRO displacement upon binding. (b) The results of FID for H68-aminoglycoside binding are shown. TOPRO dye was excited at 510 nm and fluorescence emission was measured at 540 nm. Changes in fluorescence at each drug concentration were determined with respect to fluorescence without drug and then converted into % change in fluorescence relative to the starting fluorescence intensity.

50S subunits and this change is influenced by magnesium concentration and temperature. The position A1900, identified by DMS, is likely to be a functionally important site in the ribosome, because only point mutations around A1900 give lethal phenotypes. The detailed molecular basis of these effects is unclear, such that further research regarding H68 will certainly be interesting, particularly for drug discovery. Ligands that can bind and inhibit H68 function could cause strong bactericidal activity like the point mutations around A1900. For such purposes, it would be important to analyze H68 by splitting it into several segments because H68 itself is a relatively long stem-loop structure. Thus, H68 is an interesting target not only for drug discovery but also for RNA structural studies.

H68 is conformationally dynamic, as predicted from cryo-EM and crystal structures [98, 224]. FID analyses with a model H68 RNA shows similar trends. Further investigation of H68 conformational states in the presence of magnesium ions and aminoglycoside antibiotics will be significant for understanding the function of H68 in the ribosome and developing it as a new target site for novel therapeutics.

6.5. Materials and methods

6.5.1. Preparation of 5'-end ^{32}P-labeled H68 RNA

The 5'-end ^{32}P-labeled H68 RNA was prepared by *in vitro* transcription as follows. The DNA template for H68 RNA was prepared by polymerase chain reaction (PCR) of a plasmid DNA containing the 23S rRNA gene (pWK1-23S rRNA, a kind gift from Dr. Cunningham in Wayne State University) by using forward (5'–AAATTAATACGACTCACTATAGGCCCGGTGCCGGAAGGTT–3', and reverse (5'–CGACAAGGAATTTCGCTACC–3') DNA primers. The forward primer contains the T7 promoter sequence for T7 RNA polymerase binding (underlined). The reverse primer starts from H69 rather than H68 because of by-products produced if a primer targeting H68 is used. PCR reaction conditions were (1) 95 °C for 3 min, (2) 57 °C for 30 sec, (3) 72 °C for 1 min, (4) 95 °C for 1 min and 30 cycles from (2) to (4), and then 72 °C for 10 min. PCR products were diluted into ddH_2O and used for the next PCR to generate DNA template for RNA transcription by using T7 promoter

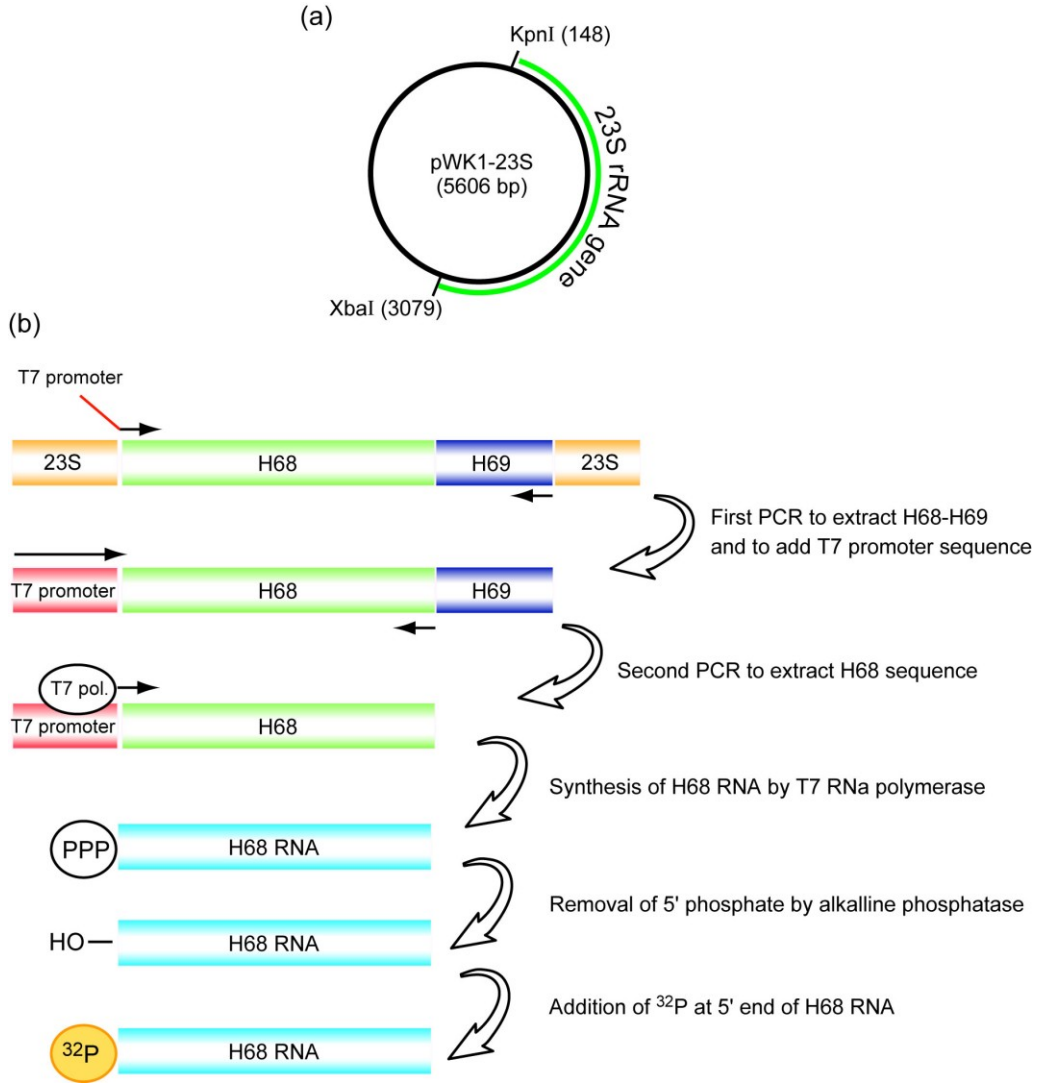

Figure 6.8. (a) A map of pWK1-23S is shown. (b) A schematic illustration of how H68 RNA was generated. H68 DNA template for *in vitro* transcription was prepared by two sequential PCR reactions. In the first reaction, the H68-H69 DNA sequence was extracted from pWK1-23S and a T7 promoter sequence was added. In the second reaction, the T7 promoter-H68 DNA sequence was extracted from the first PCR product. The second PCR product was purified and used for *in vitro* transcription with T7 RNA polymerase. Transcribed RNA was gel purified and used for FID experiments or further treated to label the 5'-end with ^{32}P.

sequence (5'–AAATTAATACGACTCACTATAGG–3') and H68 reverse (5'–CGACAAGGAATTTCGCTACC–3') DNA primers. The second PCR conditions were the same as the first. PCR products were purified with a PCR purification kit (Qiagen) and DNA concentration was determined. It should be noted that the concentration of the first PCR products affected the second PCR reaction, so had to be optimized. *In vitro* transcription was performed in the presence of ~0.1 μM template DNA, 2.5 mM each NTP, 8% PEG8000, 0.02 mg/ml T7 RNA polymerase (produced by expression from a plasmid obtained from Dr. Cunningham at Wayne State University). Buffer was purchased from NEB. The transcription mixture was incubated at 37 °C for 4 hours and ethanol precipitated. The RNA pellet was dissolved in ddH_2O and purified by 10% denaturing PAGE followed by soaking gel pieces corresponding to H68 RNA in soaking buffer (10 mM Tris-HCl pH 7.5, 250 mM NaCl, 1 mM EDTA) at 4 °C overnight. The extracted H68 RNA was ethanol precipitated and dissolved in ddH_2O. The purified H68 RNA was treated with alkaline phosphatase at 50 °C for 20 min followed by additional incubation at 37 °C for 30 min to remove the 5' phosphate group. After dephosphorylation, the 5'-OH H68 RNA was treated with phenol-chloroform to remove alkaline phosphatase, followed by ethanol precipitation. The 5'-OH H68 RNA was labeled by γ-^{32}P ATP and T4 polynucleotide kinase (37 °C for 45 min). The RNA solution was passed through a Sephadex G-25 spin column to remove extra γ-^{32}P ATP and loaded onto a 10% denaturing gel for further purification of the labeled H68 RNA. The corresponding band was visualized by UV shadow and extracted by the soaking method. Extracted 5'-end ^{32}P-labeled H68 RNA was ethanol precipitated and dissolved into ddH_2O and the ^{32}P intensity was measured by Scintillation counting. It should be mentioned that the designed H68 RNA in this experiment contains an extra G-C base pair at the end of the H68 stem because T7 RNA polymerase requires the GG dinucleotide sequence for efficient transcription start.

6.5.2. In-line probing

The 5'-end ^{32}P-labeled H68 was dissolved in refolding buffer (20 mM HEPES, 50 mM KCl, 0.5 mM EDTA, pH 7.3) and denatured at 80 °C for 3 min followed by slow cooling down to room temperature. The refolded RNA solution was mixed with 2x in-line probing buffer (100 m Tris-HCl,

160 mM KCl, pH 8.3) and the Mg^{2+} concentration was adjusted followed by incubation at room temperature for at least 15 min. Aminoglycosides were added, except for the controls, and the solution was incubated for 40 hours at room temperature in the dark. The reaction was stopped by adding loading dye and analyzed directly by 10% denaturing PAGE.

6.5.3. Fluorescent intercalator displacement (FID) assay

FID assay was conducted as follows. The purified H68 RNA (after *in vitro* transcription as above) was dissolved in 20 mM HEPES, 70 mM NH_4Cl, 30 mM KCl, pH 7.3 at room temperature and, concentration was adjusted to 0.1 µM in 400 µl. The RNA solution was incubated at 70 °C for 2 min and then cooled down to room temperature slowly to refold H68 RNA. The Mg^{2+} concentration was adjusted to 3 mM, if necessary. Heating H68 RNA in the presence of Mg^{2+} ion resulted in non-specific degradation of H68. This RNA sample solution was used in FID assays.

Before starting FID, a near saturation concentration of TOPRO dye was determined by titrating TOPRO dye to H68 RNA prepared as above. TOPRO dye was excited at 510 nm and emitted fluorescence of TOPRO dye as a result of binding to RNA was monitored from 520 to 550 nm. The maximum fluorescence intensity at 540 nm was measured. The TOPRO dye concentration required for FID analysis of H68 was 0.45 µM in the absence of Mg^{2+} and 4.5 µM in the presence of 3 mM Mg^{2+}. Displacement of TOPRO dye upon drug binding was observed by titrating 0.5 µl aminoglycoside aliquots into the sample solution in the presence of these TOPRO dye concentrations. Aminoglycoside solutions were prepared by dissolving into the same buffer as the sample solution. Data correction was performed along with volume change, although no change was observed because of small volume change (12 µl max) relative to the total volume (400 µl).

Chapter 7
Conclusions and future directions

1) Probing H69 conformational states in the presence of translation-associated factors, such as mRNA, P- and/or A-site tRNA, RF, and RRF

During my thesis studies, I observed dynamic conformational rearrangements in the loop region of H69 upon subunit association, which were not observed/predicted previously in crystal structures. Subsequent studies revealed that these rearrangements are enhanced by Ψ modifications, which render the well-ordered loop structure to H69. The next question that will be interesting to address is what conformational changes in the H69 loop occur upon introduction of ribosome translation-associated factors such as mRNA, tRNA, RFs, and RRF. In crystal structures of the ribosome with these factors, H69 occupies different positions with different factors, suggesting that H69 plays an important role in sensing factor binding to the ribosome in order to fine tune translation; however, it is unclear whether H69 in solution is really undergoing such conformational rearrangements.

Particularly, probing conformational states of H69 upon installing ribosomes on mRNA in the presence or absence of an initiator $tRNA^{fMet}$ would be the best target. One main reason is that ribosome installation on mRNA does not seem to affect the conformation of H69 based on crystal structures; however, $tRNA^{fMet}$ could influence this conformation because the P-site tRNA interacts with the H69 stem region. Although elongator tRNAs prefer to occupy the hybrid P/E-tRNA configuration (depending on the tRNAs), $tRNA^{fMet}$ prefers to occupy the classical P/P-tRNA configuration and $tRNA^{fMet}$ is the only tRNA that is not delivered as a ternary complex such that it is easy to prepare samples. If a different conformational state of H69 is observed upon P-site tRNA loading, it will provide further concrete evidence that H69 senses ribosome states to regulate translation.

In contrast, it will be challenging to probe H69 conformational states in the presence of other factors, particularly the H69 loop region, because factor binding could simply protect specific nucleotides and mask them from revealing unique conformational states induced by these factors.

However, careful, well-designed probing methods and conditions could potentially provide important information about direct molecular contacts between H69 and translation-associated factors and unpredicted conformational states around the H69 stem and/or loop region. These experiments could perhaps be complemented with spectroscopic methods if site-specific labels can be incorporated at or new H69 within the ribosome.

2) Probing the mutation-introduced H69 conformational state in the ribosome

One of the big questions that has not been addressed yet is whether mutation-induced deleterious phenotypes are associated with changes in conformation or base type. As mentioned in Chapter 1, many mutations in H69 give rise to altered biological functions. Therefore, it will certainly be significant to study mutant H69 conformational states in the ribosome. Interesting mutations include A1913U, ΔA1916, A1912G, and other loop-related mutations. The effects of these mutations on the H69 loop conformation could be analyzed by the conventional methods (SHAPE, DMS, DEPC) used in my dissertation work.

For probing experiments with mutant ribosomes, the most important step is to obtain homogeneous mutant ribosomes; however, some mutations are lethal and it is technically not easy to set up a system in which cells express ribosomes only from an exogeneous DNA plasmid encoding mutant rRNA. To overcome problems about mutant ribosome purification, it would be useful to introduce an MS2-binding sequence or biotin-binding aptamer sequence on the ribosomes, and purify mutant ribsomes from mixtures with wild-type ribosomes by affinity purification.

3) Footprinting study of H69 ligands in ribosomes resistant to drugs

In Chapter 5, I showed that the aminoglycoside class antibiotics neomycin, paromomycin, and gentamicin interact with H69 in the 70S ribosome. In footprinting studies using RluD(–) ribosomes, these drugs were shown to bind H69 but with weaker affinity than with wild-type ribosomes, probably because of the lack of Ψ modifications in H69; however, their binding pattern to h44 of the 30S subunit did not change. Therefore, it should be addressed whether or not the

binding pattern of aminoglycoside antibiotics changes at H69 on mutant 70S ribosomes that are resistant to aminoglycoside antibiotics, such as those containing an A1408G mutation. If the interaction between H69 and aminoglycoside antibiotics on the mutant is not observed, it would suggest that there is a conformational change and communication between h44 and H69 to facilitate aminoglycoside binding to H69 along with h44. One possibility is that a conformational change in h44 induced by the aminoglycoside interaction results in a long-range conformational change in H69 that enhances the H69-aminoglycoside interaction. Because some h44 mutations contribute strongly to drug resistant strains, communication between H69 and h44 is highly likely. Alternatively, if binding to H69 is still observed, it would suggest that this activity is not relevant with respect to targeting.

4) Probing studies of detailed H69 stem conformational state/environment under various situations by cisplatin with direct primer extension

As mentioned in Chapter 1, adenine is the best target base for chemical probing studies because it is possible to analyze the Watson-Crick face, Hoogsteen face, sugar edge (minor-groove) face, and specific base-stacking interactions by employing a series of chemical probing reactions. Guanine is also a good target, but more limited compared to adenine. During footprinting analysis of H69, I found that (1) aminoglycoside antibiotics bind to the H69 stem in solution; this binding was detected by aniline-induced cleavage, but was undetectable by other methods, and (2) H69 conformational changes upon subunit association influence the major groove environment of the H69 stem and its conformations are different in Ψ-deficient ribosomes. G1906 is protected by aminoglycosides, and G1910 is more accessible in RluD(–) ribosomes. Although G1907 accessibility is unclear in wild-type ribosomes, this site is very accessible in RluD(–) ribosomes as well as G1906. Thus, comparisons of data between wild-type and RluD(–) ribosomes indicate an extended or more open major-groove conformation in the H69 stem region in Ψ-deficient ribosomes; however, further detailed analysis, as performed in Chapters 2 and 3, was not possible due to low resolution data after the 1915 position. A leading cause of low resolution data should be non-specific RNA degradation during the process of aniline-catalyzed

rRNA strand scission, particularly since Ψ-deficient, loosely organized 23S rRNA is likely to be more sensitive to RNA degradation compared to wild-type 23S rRNA. An alternative method, therefore, must be used in order to complete analysis of the H69 stem region in the 70S and 50S ribosomes in solution.

One interesting method is cisplatin-based probing with direct primer extension analysis. H69 stem is a G-rich sequence and the accessibility of the H69 stem can be assumed by analyzing the reactivity of N7 of these G, such that cisplatin may be the best alternative method. However, one of the serious issues in this probing method is the limited reaction conditions, since cisplatin reactivity is inhibited by the presence of chloride and ammonium ions. However, cisplatin reacts preferentially with rRNA and other RNA molecules over DNA in yeast cells. This result indicates that it might be possible to use cisplatin under the cellular-like conditions (100 mM NH_4Cl or 150 mM KCl and 6 mM $MgCl_2$.to keep 70S ribosome formation and ribosome activity). Cisplatin probing could provide complementary information to traditional organic probes.

5) Possible additional conformational variety in the presence of polyamines

Historically, the buffer containing 100 mM NH_4Cl and 10 mM $MgCl_2$ or more has been used to maintain active ribosomes *in vitro*. However, some evidence suggests that high Mg^{2+} concentration causes low-fidelity ribosomes, such that the high-fidelity buffer system that contains low Mg^{2+} concentration (3.5 mM) was developed for ribosome activity studies. However, such low Mg^{2+} conditions cannot maintain 70S ribosomes *in vitro*. At least 6 mM Mg^{2+} concentration is required to maintain active 70S ribosomes and I employed this condition in my thesis studies. Recent studies pointed out the importance of polyamines on ribosome activity, particularly on maintaining 70S formation even under low Mg^{2+} buffer conditions. Indeed, polyamines are used for the high-fidelity buffer. In my probing studies, Mg^{2+} concentration considerably influences H69 conformational states, particularly in 70S ribosomes, and we proposed one possibility that such conformational changes could influence tRNA selection (see Chapter 3). Although it is unclear whether these conformational changes are because of direct interactions between Mg^{2+} and H69 or ribosome-induced conformational changes or both, it would be interesting to address the H69

conformational state of 70S ribosomes under the high-fidelity buffer condition and look at differences between the low- and high-fidelity conditions.

In addition, I found H68 conformational changes in the presence of neomycin under lower Mg^{2+} and temperature conditions. The conformational changes induced by neomycin was suppressed by increasing the Mg^{2+} concentration. Because all experiments regarding the footprinting analysis of aminoglycoside-H69 interaction were performed in 6 mM Mg^{2+}, I did not observe any change in H68 conformation. However, if probing conditions could be improved by using polyamines and lowering the Mg^{2+} concentration, more dynamic conformational changes in both H69 and H68 could be observed as a consequence of aminoglycoside or translation- factor binding to ribosomes. Such lower Mg^{2+} conditions may also suppress A1913 flexibility as shown in Chapters 3 and 4; however, factor binding, such as $tRNA^{fMet}$ which favors the classical ribosome configuration, would in turn enhance A1913 flexibility that may not be observed under high Mg^{2+} conditions. Because lower Mg^{2+} conditions are not suitable for single-molecule experiments due to low time resolution but higher molecular motions, chemical probing could be a suitable method to understand ribosome conformational changes under such high-fidelity conditions.

6) Understanding the function of pseudouridine modifications of H69 in ribosome translation activity

The observation that *E. coli* B strain lacking Ψ synthase showed a wild-type phenotype casts doubt on the function of Ψ modifications in H69. Although it has been proposed that Ψ-deficient ribosomes lack 70S ribosome formation, I did not observe any major difference between wild-type and Ψ-deficient ribosome profiles after sucrose density gradient during 70S ribosome isolation (see Chapter 1). Therefore, it will be necessary to address the function of Ψ modifications by employing an *in vitro* translation system and comparing translation efficiency and fidelity under the various system conditions to the chemical probing data.

7) Structural approach to understand the function of 2'-OH modification at C1920 of H69

As mentioned in Chapter 1, the peptide antibiotic capreomycin is a clinically important class of antibiotics; however, the underlying basis of antibacterial activity is unclear, even though crystal structures of ribosomes with capreomycin and viomycin were solved [143]. One big enigma of this class is why they show strong antibacterial activity against *Mycobacterium tuberculosis* but not enterobacteria, such as *Escherichia coli* [88]. Recent studies gave a clue by showing that methyl modification at the 2'-OH of C1920 in H69 changes drug sensitivity and this modification is naturally absent in *E. coli.* By expressing TlyA in *E. coli*, which is responsible for the 2'-OH methylation of C1920 in H69 and C1409 in h44, the susceptibility of *E. coli* to capreomycin was increased, indicating the importance of the 2'-OH methylation of H69 and/or h44. In contrast, no change in susceptibility was observed by deleting the *tlyA* gene in *Thermus thermophilus* (see Chapter 1, section 1.3). In addition, drug resistance studies revealed that a ΔA1916 mutant of H69 is resistant to capreomycin and viomycin in *M. tuberculosis* [88] even though ΔA1916 mutation is lethal to *E. coli* (See Chapter 1). These observations indicate the possible importance of H69 structure and/or B2a intersubunit conformation and different H69 structures between different bacterial species probably due to different RNA sequence or RNA modification levels; therefore, it is important to study the conformational states of H69 containing 2'-OH methyl modification at 1920 and ΔA1916 in order to understand the molecular basis of these clinically important capreomycin-type antibiotics.

8) Drug discovery by using a dual monitoring 2AP-H69 system

By using 2-aminopurine-containing H69 RNA, I demonstrated that 2AP-H69 would be a powerful tool for drug discovery. This system requires relatively low sample amounts and limited time for analysis. In addition, by employing a dual-monitoring system, it is possible to detect simple molecular binding of a candidate ligand, as well as the impact of binding to H69 structure.

It will also be interesting to use H69 containing 2AP at the 1916 or 1918 positions instead of 1913. Based on probing studies in Chapters 2 and 3, A1916 and A1918 were found to have different local conformational states. Although DEPC probing patterns did not change much for

A1918, A1916 was strongly protected from DEPC in the wild-type ribosomes but not in the RluD(–) ribosomes; therefore, 2AP1916 fluorescence would likely be quenched due to base-stacking interactions with neighboring bases in modified H69 RNA. In addition, the position 1916 is likely to be essential for normal ribosome activity (see Table 1.3 in Chapter 1). If a ligand disrupts the local conformation of position 1916 as a result of binding to H69, it could also be a good drug candidate.

9) Single-molecule 2AP experiment

In Chapter 4, I demonstrated that 2AP in H69 provides an interesting fluorescent probe for different loop conformational states. All fluorescent probe experiments were performed in bulk solution; however, the H69 loop state is likely to be dynamic, and analyzing the molecular motions of the this loop would be interesting. In Prof. David Rueda's lab, a single-molecule experiment using 2AP has been developed. By using their single-molecule system, it will be possible to analyze the dynamic nature of the H69 loop and its conformational states at the single-molecule level with higher time resolution. Furthermore, although it is technically challenging, it would be highly interesting to use a re-constituted 50S subunit containing 2AP-incorporated H69 in single-molecule experiments. One of the great advantages for single-molecule experiments is that only small amounts of labeled sample are needed for a well-set-up system. Therefore, engineering 23S rRNA to introduce 2AP-H69, and subsequent re-construction of 50S subunits would be an interesting future topic in this field.

10) Study of aminoglycoside modification and its binding affinity for H69

As stated in Chapter 1, one of the major mechanisms of antibiotic resistance is the inactivation of aminoglycosides by enzymatic modification. It is well known that the modified aminoglycosides have considerably reduced binding affinity for h44 in the 30S subunit; whereas, it is totally unclear whether they are also worse binders for H69 in the 50S subunit. it is important to address this question to understand the binding mechanism, because a strategic modification of aminoglycosides at specific position to disrupt recognition by the modification enzymes while

still allowing binding to H69 could help to combat antibiotic-resistant pathogens. For this purpose, the 2AP-H69 system will be a powerful tool to study these modified aminoglycosides quickly and easily and provide us with important insight in combination with other methods.

11) Summary

Throughout my dissertation research, I carried out various chemical probing analyses of H69 in ribosomes. These studies revealed that H69 undergoes dynamic structural rearrangements upon subunit association, which was not even predicted by crystal structural studies. Also, I demonstrated that results obtained from *in vitro* model studies using small hairpin RNA corresponding to H69 are highly consistent with ribosome probing results. This correlation indicates that the model H69 structure might mimic the functional H69 structure in the ribosome. Importantly, my results also indicate that *in vitro* studies to understand the function of pseudouridine in H69 can be linked to H69 in the ribosome, even though it is technically impossible to study a positional effect of each pseudouridine modification in the H69 loop.

Besides H69 structural analysis, I developed a tool to monitor H69 loop conformational states quickly and efficiently by using structural information obtained by chemical probing. By using this tool, I demonstrated the different binding activity of neomycin compared with other aminoglycosides with a very similar chemical structures. The different binding effect of neomycin was also observed in H69 within ribosomes, as revealed by chemical probing. These conformational differences, induced by aminoglycosides, were not observed in crystal structures. Importantly, such tendencies are in good agreement with single-molecule and toeprinting studies previously reported by other groups. These data indicate the power of fluorescent probes in H69 research and the importance of solution studies. Moreover, information from chemical and fluorescent probing of H69 provides various future directions that should be addressed to further understand H69 structure and function as stated in this chapter.

REFERENCES

1. F. Crick, Central dogma of molecular biology. *Nature* **1970,** *227* (5258), 561.
2. V. Ramakrishnan, P. B. Moore, Atomic structures at last: the ribosome in 2000. *Curr. Opin. Struct. Biol.* **2001,** *11* (2), 144.
3. D. N. Wilson, G. Blaha, S. R. Connell, P. V. Ivanov, H. Jenke, U. Stelzl, Y. Teraoka, K. H. Nierhaus, Protein synthesis at atomic resolution: mechanistics of translation in the light of highly resolved structures for the ribosome. *Curr. Protein. Pept. Sci.* **2002,** *3* (1), 1.
4. D. N. Wilson, K. H. Nierhaus, The ribosome through the looking glass. *Angew. Chem. Int. Ed. Engl.* **2003,** *42* (30), 3464.
5. B. S. Schuwirth, M. A. Borovinskaya, C. W. Hau, W. Zhang, A. Vila-Sanjurjo, J. M. Holton, J. H. Cate, Structures of the bacterial ribosome at 3.5 Å resolution. *Science* **2005,** *310* (5749), 827.
6. K. B. Gromadski, M. V. Rodnina, Kinetic determinants of high-fidelity tRNA discrimination on the ribosome. *Mol. Cell.* **2004,** *13* (2), 191.
7. J. M. Ogle, V. Ramakrishnan, Structural insights into translational fidelity. *Annu. Rev. Biochem.* **2005,** *74*, 129.
8. J. M. Ogle, D. E. Brodersen, W. M. Clemons, Jr., M. J. Tarry, A. P. Carter, V. Ramakrishnan, Recognition of cognate transfer RNA by the 30S ribosomal subunit. *Science* **2001,** *292* (5518), 897.
9. S. Yoshizawa, D. Fourmy, J. D. Puglisi, Recognition of the codon-anticodon helix by ribosomal RNA. *Science* **1999,** *285* (5434), 1722.
10. J. M. Ogle, F. V. Murphy, M. J. Tarry, V. Ramakrishnan, Selection of tRNA by the ribosome requires a transition from an open to a closed form. *Cell* **2002,** *111* (5), 721.
11. E. Villa, J. Sengupta, L. G. Trabuco, J. LeBarron, W. T. Baxter, T. R. Shaikh, R. A. Grassucci, P. Nissen, M. Ehrenberg, K. Schulten, J. Frank, Ribosome-induced changes in elongation factor Tu conformation control GTP hydrolysis. *Proc. Natl. Acad. Sci. U.S.A.* **2009,** *106* (4), 1063.

12. M. Valle, A. Zavialov, W. Li, S. M. Stagg, J. Sengupta, R. C. Nielsen, P. Nissen, S. C. Harvey, M. Ehrenberg, J. Frank, Incorporation of aminoacyl-tRNA into the ribosome as seen by cryo-electron microscopy. *Nat. Struct. Biol.* **2003,** *10* (11), 899.

13. J. C. Schuette, F. V. t. Murphy, A. C. Kelley, J. R. Weir, J. Giesebrecht, S. R. Connell, J. Loerke, T. Mielke, W. Zhang, P. A. Penczek, V. Ramakrishnan, C. M. Spahn, GTPase activation of elongation factor EF-Tu by the ribosome during decoding. *EMBO J.* **2009,** *28* (6), 755.

14. T. M. Schmeing, R. M. Voorhees, A. C. Kelley, Y. G. Gao, F. V. t. Murphy, J. R. Weir, V. Ramakrishnan, The crystal structure of the ribosome bound to EF-Tu and aminoacyl-tRNA. *Science* **2009,** *326* (5953), 688.

15. O. Piepenburg, T. Pape, J. A. Pleiss, W. Wintermeyer, O. C. Uhlenbeck, M. V. Rodnina, Intact aminoacyl-tRNA is required to trigger GTP hydrolysis by elongation factor Tu on the ribosome. *Biochemistry* **2000,** *39* (7), 1734.

16. L. Cochella, R. Green, An active role for tRNA in decoding beyond codon:anticodon pairing. *Science* **2005,** *308* (5725), 1178.

17. S. Ledoux, M. Olejniczak, O. C. Uhlenbeck, A sequence element that tunes *Escherichia coli* tRNA(Ala)(GGC) to ensure accurate decoding. *Nat. Struct. Mol. Biol.* **2009,** *16* (4), 359.

18. H. Murakami, A. Ohta, H. Suga, Bases in the anticodon loop of tRNA(Ala)(GGC) prevent misreading. *Nat. Struct. Mol. Biol.* **2009,** *16* (4), 353.

19. J. Frank, R. L. Gonzalez, Jr., Structure and dynamics of a processive Brownian motor: the translating ribosome. *Annu. Rev. Biochem.* **2010,** *79*, 381.

20. M. V. Rodnina, W. Wintermeyer, Fidelity of aminoacyl-tRNA selection on the ribosome: kinetic and structural mechanisms. *Annu. Rev. Biochem.* **2001,** *70*, 415.

21. M. Yarus, M. Valle, J. Frank, A twisted tRNA intermediate sets the threshold for decoding. *RNA* **2003,** *9* (4), 384.

22. J. L. Brunelle, E. M. Youngman, D. Sharma, R. Green, The interaction between C75 of tRNA and the A loop of the ribosome stimulates peptidyl transferase activity. *RNA* **2006,** *12* (1), 33.

23. J. S. Weinger, K. M. Parnell, S. Dorner, R. Green, S. A. Strobel, Substrate-assisted catalysis of peptide bond formation by the ribosome. *Nat. Struct. Mol. Biol.* **2004,** *11* (11), 1101.

24. E. M. Youngman, J. L. Brunelle, A. B. Kochaniak, R. Green, The active site of the ribosome is composed of two layers of conserved nucleotides with distinct roles in peptide bond formation and peptide release. *Cell* **2004,** *117* (5), 589.

25. T. M. Schmeing, A. C. Seila, J. L. Hansen, B. Freeborn, J. K. Soukup, S. A. Scaringe, S. A. Strobel, P. B. Moore, T. A. Steitz, A pre-translocational intermediate in protein synthesis observed in crystals of enzymatically active 50S subunits. *Nat. Struct. Biol.* **2002,** *9* (3), 225.

26. M. Koch, Y. Huang, M. Sprinzl, Peptide-bond synthesis on the ribosome: no free vicinal hydroxy group required on the terminal ribose residue of peptidyl-tRNA. *Angew. Chem. Int. Ed. Engl.* **2008,** *47* (38), 7242.

27. Y. Huang, M. Sprinzl, Peptide bond formation on the ribosome: the role of the 2'-OH group on the terminal adenosine of peptidyl-tRNA and of the length of nascent peptide chain. *Angew. Chem. Int. Ed. Engl.* **2011,** *50* (32), 7287.

28. V. I. Katunin, A. Savelsbergh, M. V. Rodnina, W. Wintermeyer, Coupling of GTP hydrolysis by elongation factor G to translocation and factor recycling on the ribosome. *Biochemistry* **2002,** *41* (42), 12806.

29. D. Moazed, H. F. Noller, Intermediate states in the movement of transfer RNA in the ribosome. *Nature* **1989,** *342* (6246), 142.

30. J. B. Munro, R. B. Altman, N. O'Connor, S. C. Blanchard, Identification of two distinct hybrid state intermediates on the ribosome. *Mol. Cell.* **2007,** *25* (4), 505.

31. J. Fei, P. Kosuri, D. D. MacDougall, R. L. Gonzalez, Jr., Coupling of ribosomal L1 stalk and tRNA dynamics during translation elongation. *Mol. Cell.* **2008,** *30* (3), 348.

32. J. R. Williamson, Induced fit in RNA-protein recognition. *Nat. Struct. Biol.* **2000,** *7* (10), 834.

33. S. C. Blanchard, H. D. Kim, R. L. Gonzalez, Jr., J. D. Puglisi, S. Chu, tRNA dynamics on the ribosome during translation. *Proc. Natl. Acad. Sci. U.S.A.* **2004,** *101* (35), 12893.

34. A. Korostelev, D. N. Ermolenko, H. F. Noller, Structural dynamics of the ribosome. *Curr. Opin. Cell Biol.* **2008,** *12* (6), 674.

35. P. V. Cornish, D. N. Ermolenko, H. F. Noller, T. Ha, Spontaneous intersubunit rotation in single ribosomes. *Mol. Cell.* **2008,** *30* (5), 578.

36. D. N. Ermolenko, Z. K. Majumdar, R. P. Hickerson, P. C. Spiegel, R. M. Clegg, H. F. Noller, Observation of intersubunit movement of the ribosome in solution using FRET. *J. Mol. Biol.* **2007,** *370* (3), 530.

37. D. N. Ermolenko, P. C. Spiegel, Z. K. Majumdar, R. P. Hickerson, R. M. Clegg, H. F. Noller, The antibiotic viomycin traps the ribosome in an intermediate state of translocation. *Nat. Struct. Mol. Biol.* **2007,** *14* (6), 493.

38. X. Agirrezabala, J. Lei, J. L. Brunelle, R. F. Ortiz-Meoz, R. Green, J. Frank, Visualization of the hybrid state of tRNA binding promoted by spontaneous ratcheting of the ribosome. *Mol. Cell.* **2008,** *32* (2), 190.

39. M. Valle, A. Zavialov, J. Sengupta, U. Rawat, M. Ehrenberg, J. Frank, Locking and unlocking of ribosomal motions. *Cell* **2003,** *114* (1), 123.

40. G. Blaha, R. E. Stanley, T. A. Steitz, Formation of the first peptide bond: the structure of EF-P bound to the 70S ribosome. *Science* **2009,** *325* (5943), 966.

41. F. Tama, O. Miyashita, C. L. Brooks, 3rd, Normal mode based flexible fitting of high-resolution structure into low-resolution experimental data from cryo-EM. *J. Struct. Biol.* **2004,** *147* (3), 315.

42. S. R. Connell, C. Takemoto, D. N. Wilson, H. Wang, K. Murayama, T. Terada, M. Shirouzu, M. Rost, M. Schuler, J. Giesebrecht, M. Dabrowski, T. Mielke, P. Fucini, S. Yokoyama, C. M. Spahn, Structural basis for interaction of the ribosome with the switch regions of GTP-bound elongation factors. *Mol. Cell.* **2007,** *25* (5), 751.

43. V. Berk, W. Zhang, R. D. Pai, J. H. Cate, Structural basis for mRNA and tRNA positioning on the ribosome. *Proc. Natl. Acad. Sci. U.S.A.* **2006,** *103* (43), 15830.

44. Y. Wang, A. J. Rader, I. Bahar, R. L. Jernigan, Global ribosome motions revealed with elastic network model. *J. Struct. Biol.* **2004,** *147* (3), 302.

45. J. Harms, F. Schluenzen, R. Zarivach, A. Bashan, S. Gat, I. Agmon, H. Bartels, F. Franceschi, A. Yonath, High resolution structure of the large ribosomal subunit from a mesophilic eubacterium. *Cell* **2001,** *107* (5), 679.

46. M. M. Yusupov, G. Z. Yusupova, A. Baucom, K. Lieberman, T. N. Earnest, J. H. Cate, H. F. Noller, Crystal structure of the ribosome at 5.5 Å resolution. *Science* **2001,** *292* (5518), 883.

47. M. Selmer, C. M. Dunham, F. V. t. Murphy, A. Weixlbaumer, S. Petry, A. C. Kelley, J. R. Weir, V. Ramakrishnan, Structure of the 70S ribosome complexed with mRNA and tRNA. *Science* **2006,** *313* (5795), 1935.

48. A. Korostelev, S. Trakhanov, M. Laurberg, H. F. Noller, Crystal structure of a 70S ribosome-tRNA complex reveals functional interactions and rearrangements. *Cell* **2006,** *126* (6), 1065.

49. P. V. Cornish, D. N. Ermolenko, D. W. Staple, L. Hoang, R. P. Hickerson, H. F. Noller, T. Ha, Following movement of the L1 stalk between three functional states in single ribosomes. *Proc. Natl. Acad. Sci. U.S.A.* **2009,** *106* (8), 2571.

50. J. Fei, J. E. Bronson, J. M. Hofman, R. L. Srinivas, C. H. Wiggins, R. L. Gonzalez, Jr., Allosteric collaboration between elongation factor G and the ribosomal L1 stalk directs tRNA movements during translation. *Proc. Natl. Acad. Sci. U.S.A.* **2009,** *106* (37), 15702.

51. L. Wang, R. B. Altman, S. C. Blanchard, Insights into the molecular determinants of EF-G catalyzed translocation. *RNA* **2011,** *17* (12), 2189.

52. J. B. Munro, R. B. Altman, C. S. Tung, J. H. Cate, K. Y. Sanbonmatsu, S. C. Blanchard, Spontaneous formation of the unlocked state of the ribosome is a multistep process. *Proc. Natl. Acad. Sci. U.S.A.* **2010,** *107* (2), 709.

53. A. H. Ratje, J. Loerke, A. Mikolajka, M. Brunner, P. W. Hildebrand, A. L. Starosta, A. Donhofer, S. R. Connell, P. Fucini, T. Mielke, P. C. Whitford, J. N. Onuchic, Y. Yu, K. Y. Sanbonmatsu, R. K. Hartmann, P. A. Penczek, D. N. Wilson, C. M. Spahn, Head swivel on the ribosome facilitates translocation by means of intra-subunit tRNA hybrid sites. *Nature* **2010,** *468* (7324), 713.

54. R. K. Agrawal, A. B. Heagle, P. Penczek, R. A. Grassucci, J. Frank, EF-G-dependent GTP hydrolysis induces translocation accompanied by large conformational changes in the 70S ribosome. *Nat. Struct. Biol.* **1999,** *6* (7), 643.

55. D. J. Taylor, J. Nilsson, A. R. Merrill, G. R. Andersen, P. Nissen, J. Frank, Structures of modified eEF2 80S ribosome complexes reveal the role of GTP hydrolysis in translocation. *EMBO J.* **2007,** *26* (9), 2421.

56. L. Kisselev, M. Ehrenberg, L. Frolova, Termination of translation: interplay of mRNA, rRNAs and release factors? *EMBO J.* **2003,** *22* (2), 175.

57. Y. Nakamura, K. Ito, Making sense of mimic in translation termination. *Trends. Biochem. Sci.* **2003,** *28* (2), 99.

58. K. Ito, M. Uno, Y. Nakamura, A tripeptide 'anticodon' deciphers stop codons in messenger RNA. *Nature* **2000,** *403* (6770), 680.

59. A. Korostelev, J. Zhu, H. Asahara, H. F. Noller, Recognition of the amber UAG stop codon by release factor RF1. *EMBO J.* **2010,** *29* (15), 2577.

60. M. Laurberg, H. Asahara, A. Korostelev, J. Zhu, S. Trakhanov, H. F. Noller, Structural basis for translation termination on the 70S ribosome. *Nature* **2008,** *454* (7206), 852.

61. A. Weixlbaumer, H. Jin, C. Neubauer, R. M. Voorhees, S. Petry, A. C. Kelley, V. Ramakrishnan, Insights into translational termination from the structure of RF2 bound to the ribosome. *Science* **2008,** *322* (5903), 953.

62. A. V. Zavialov, L. Mora, R. H. Buckingham, M. Ehrenberg, Release of peptide promoted by the GGQ motif of class 1 release factors regulates the GTPase activity of RF3. *Mol. Cell.* **2002,** *10* (4), 789.

63. J. J. Shaw, R. Green, Two distinct components of release factor function uncovered by nucleophile partitioning analysis. *Mol. Cell.* **2007,** *28* (3), 458.

64. M. Y. Pavlov, D. V. Freistroffer, J. MacDougall, R. H. Buckingham, M. Ehrenberg, Fast recycling of *Escherichia coli* ribosomes requires both ribosome recycling factor (RRF) and release factor RF3. *EMBO J.* **1997,** *16* (13), 4134.

65. D. V. Freistroffer, M. Y. Pavlov, J. MacDougall, R. H. Buckingham, M. Ehrenberg, Release factor RF3 in *E.coli* accelerates the dissociation of release factors RF1 and RF2 from the ribosome in a GTP-dependent manner. *EMBO J.* **1997,** *16* (13), 4126.

66. H. S. Zaher, R. Green, Quality control by the ribosome following peptide bond formation. *Nature* **2009,** *457* (7226), 161.

67. R. E. Monro, K. A. Marcker, Ribosome-catalysed reaction of puromycin with a formylmethionine-containing oligonucleotide. *J. Mol. Biol.* **1967,** *25* (2), 347.

68. H. F. Noller, V. Hoffarth, L. Zimniak, Unusual resistance of peptidyl transferase to protein extraction procedures. *Science* **1992,** *256* (5062), 1416.

69. J. J. Cannone, S. Subramanian, M. N. Schnare, J. R. Collett, L. M. D'Souza, Y. Du, B. Feng, N. Lin, L. V. Madabusi, K. M. Muller, N. Pande, Z. Shang, N. Yu, R. R. Gutell, The comparative RNA web (CRW) site: an online database of comparative sequence and structure information for ribosomal, intron, and other RNAs. *BMC Bioinformatics* **2002,** *3*, 2.

70. C. R. Woese, L. J. Magrum, R. Gupta, R. B. Siegel, D. A. Stahl, J. Kop, N. Crawford, J. Brosius, R. Gutell, J. J. Hogan, H. F. Noller, Secondary structure model for bacterial 16S ribosomal RNA: phylogenetic, enzymatic and chemical evidence. *Nucleic Acids Res.* **1980,** *8* (10), 2275.

71. R. R. Gutell, J. C. Lee, J. J. Cannone, The accuracy of ribosomal RNA comparative structure models. *Curr. Opin. Struct. Biol.* **2002,** *12* (3), 301.

72. C. S. Chow, T. N. Lamichhane, S. K. Mahto, Expanding the nucleotide repertoire of the ribosome with post-transcriptional modifications. *ACS Chem. Biol.* **2007,** *2* (9), 610.

73. W. A. Decatur, M. J. Fournier, rRNA modifications and ribosome function. *Trends. Biochem. Sci.* **2002,** *27* (7), 344.

74. J. Rozenski, P. F. Crain, J. A. McCloskey, The RNA Modification Database: 1999 update. *Nucleic Acids Res.* **1999,** *27* (1), 196.

75. R. Green, H. F. Noller, In vitro complementation analysis localizes 23S rRNA posttranscriptional modifications that are required for *Escherichia coli* 50S ribosomal subunit assembly and function. *RNA* **1996,** *2* (10), 1011.

76. K. R. Noon, E. Bruenger, J. A. McCloskey, Posttranscriptional modifications in 16S and 23S rRNAs of the archaeal hyperthermophile *Sulfolobus solfataricus*. *J. Bacteriol.* **1998,** *180* (11), 2883.

77. D. R. Davis, Stabilization of RNA stacking by pseudouridine. *Nucleic Acids Res.* **1995,** *23* (24), 5020.

78. R. Guymon, S. C. Pomerantz, P. F. Crain, J. A. McCloskey, Influence of phylogeny on posttranscriptional modification of rRNA in thermophilic prokaryotes: the complete modification map of 16S rRNA of *Thermus thermophilus*. *Biochemistry* **2006,** *45* (15), 4888.

79. S. Hur, R. M. Stroud, J. Finer-Moore, Substrate recognition by RNA 5-methyluridine methyltransferases and pseudouridine synthases: a structural perspective. *J. Biol. Chem.* **2006,** *281* (51), 38969.

80. Z. Kiss-Laszlo, Y. Henry, T. Kiss, Sequence and structural elements of methylation guide snoRNAs essential for site-specific ribose methylation of pre-rRNA. *EMBO J.* **1998,** *17* (3), 797.

81. D. Tollervey, T. Kiss, Function and synthesis of small nucleolar RNAs. *Curr. Opin. Cell Biol.* **1997,** *9* (3), 337.

82. S. L. Reichow, T. Hamma, A. R. Ferre-D'Amare, G. Varani, The structure and function of small nucleolar ribonucleoproteins. *Nucleic Acids Res.* **2007,** *35* (5), 1452.

83. S. Raychaudhuri, J. Conrad, B. G. Hall, J. Ofengand, A pseudouridine synthase required for the formation of two universally conserved pseudouridines in ribosomal RNA is essential for normal growth of *Escherichia coli*. *RNA* **1998,** *4* (11), 1407.

84. P. V. Sergiev, D. V. Lesnyak, A. A. Bogdanov, O. A. Dontsova, Identification of *Escherichia coli* m2G methyltransferases: II. The ygjO gene encodes a methyltransferase specific for G1835 of the 23 S rRNA. *J. Mol. Biol.* **2006,** *364* (1), 26.

85. D. V. Lesnyak, P. V. Sergiev, A. A. Bogdanov, O. A. Dontsova, Identification of *Escherichia coli* m2G methyltransferases: I. the ycbY gene encodes a methyltransferase specific for G2445 of the 23 S rRNA. *J. Mol. Biol.* **2006,** *364* (1), 20.

86. I. A. Osterman, P. V. Sergiev, P. O. Tsvetkov, A. A. Makarov, A. A. Bogdanov, O. A. Dontsova, Methylated 23S rRNA nucleotide m2G1835 of *Escherichia coli* ribosome facilitates subunit association. *Biochimie* **2011,** *93* (4), 725.

87. P. V. Sergiev, A. A. Bogdanov, O. A. Dontsova, Ribosomal RNA guanine-(N2)-methyltransferases and their targets. *Nucleic Acids Res.* **2007,** *35* (7), 2295.

88. S. K. Johansen, C. E. Maus, B. B. Plikaytis, S. Douthwaite, Capreomycin binds across the ribosomal subunit interface using tlyA-encoded 2'-O-methylations in 16S and 23S rRNAs. *Mol. Cell.* **2006,** *23* (2), 173.

89. T. Monshupanee, S. T. Gregory, S. Douthwaite, W. Chungjatupornchai, A. E. Dahlberg, Mutations in conserved helix 69 of 23S rRNA of *Thermus thermophilus* that affect capreomycin resistance but not posttranscriptional modifications. *J. Bacteriol.* **2008,** *190* (23), 7754.

90. C. P. van Buul, P. H. van Knippenberg, Nucleotide sequence of the ksgA gene of *Escherichia coli*: comparison of methyltransferases effecting dimethylation of adenosine in ribosomal RNA. *Gene* **1985,** *38* (1-3), 65.

91. K. Inoue, S. Basu, M. Inouye, Dissection of 16S rRNA methyltransferase (KsgA) function in *Escherichia coli*. *J. Bacteriol.* **2007,** *189* (23), 8510.

92. J. Frank, A. Verschoor, Y. Li, J. Zhu, R. K. Lata, M. Radermacher, P. Penczek, R. Grassucci, R. K. Agrawal, S. Srivastava, A model of the translational apparatus based on

a three-dimensional reconstruction of the *Escherichia coli* ribosome. *Biochem. Cell Biol.* **1995,** *73* (11-12), 757.

93. I. S. Gabashvili, R. K. Agrawal, C. M. Spahn, R. A. Grassucci, D. I. Svergun, J. Frank, P. Penczek, Solution structure of the *E. coli* 70S ribosome at 11.5 Å resolution. *Cell* **2000,** *100* (5), 537.

94. K. Kipper, C. Hetényi, S. Sild, J. Remme, A. Liiv, Ribosomal intersubunit bridge B2a is involved in factor-dependent translation initiation and translational processivity. *J. Mol. Biol.* **2009,** *385* (2), 405.

95. M. O'Connor, A. E. Dahlberg, The involvement of two distinct regions of 23 S ribosomal RNA in tRNA selection. *J. Mol. Biol.* **1995,** *254* (5), 838.

96. M. O'Connor, Helix 69 in 23S rRNA modulates decoding by wild type and suppressor tRNAs. *Mol. Genet. Genomics* **2009,** *282* (4), 371.

97. J. Frank, R. K. Agrawal, A ratchet-like inter-subunit reorganization of the ribosome during translocation. *Nature* **2000,** *406* (6793), 318.

98. J. A. Dunkle, L. Wang, M. B. Feldman, A. Pulk, V. B. Chen, G. J. Kapral, J. Noeske, J. S. Richardson, S. C. Blanchard, J. H. Cate, Structures of the bacterial ribosome in classical and hybrid states of tRNA binding. *Science* **2011,** *332* (6032), 981.

99. R. K. Agrawal, M. R. Sharma, M. C. Kiel, G. Hirokawa, T. M. Booth, C. M. Spahn, R. A. Grassucci, A. Kaji, J. Frank, Visualization of ribosome-recycling factor on the *Escherichia coli* 70S ribosome: functional implications. *Proc. Natl. Acad. Sci. U.S.A.* **2004,** *101* (24), 8900.

100. R. F. Ortiz-Meoz, R. Green, Helix 69 is key for uniformity during substrate selection on the ribosome. *J. Biol. Chem.* **2011,** *286* (29), 25604.

101. D. Hirsh, Tryptophan transfer RNA as the UGA suppressor. *J. Mol. Biol.* **1971,** *58* (2), 439.

102. R. F. Ortiz-Meoz, R. Green, Functional elucidation of a key contact between tRNA and the large ribosomal subunit rRNA during decoding. *RNA* **2010,** *16* (10), 2002.

103. I. K. Ali, L. Lancaster, J. Feinberg, S. Joseph, H. F. Noller, Deletion of a conserved, central ribosomal intersubunit RNA bridge. *Mol. Cell.* **2006,** *23* (6), 865.

104. E. M. Youngman, S. L. He, L. J. Nikstad, R. Green, Stop codon recognition by release factors induces structural rearrangement of the ribosomal decoding center that is productive for peptide release. *Mol. Cell.* **2007,** *28* (4), 533.

105. C. Branlant, A. Krol, M. A. Machatt, J. Pouyet, J. P. Ebel, K. Edwards, H. Kossel, Primary and secondary structures of *Escherichia coli* MRE 600 23S ribosomal RNA. Comparison with models of secondary structure for maize chloroplast 23S rRNA and for large portions of mouse and human 16S mitochondrial rRNAs. *Nucleic Acids Res.* **1981,** *9* (17), 4303.

106. J. A. Kowalak, E. Bruenger, T. Hashizume, J. M. Peltier, J. Ofengand, J. A. McCloskey, Structural characterization of U*-1915 in domain IV from *Escherichia coli* 23S ribosomal RNA as 3-methylpseudouridine. *Nucleic Acids Res.* **1996,** *24* (4), 688.

107. M. Ejby, M. A. Sørensen, S. Pedersen, Pseudouridylation of helix 69 of 23S rRNA is necessary for an effective translation termination. *Proc. Natl. Acad. Sci. U.S.A.* **2007,** *104* (49), 19410.

108. M. O'Connor, S. T. Gregory, Inactivation of the RluD pseudouridine synthase has minimal effects on growth and ribosome function in wild-type *Escherichia coli* and *Salmonella enterica*. *J. Bacteriol.* **2011,** *193* (1), 154.

109. S. C. Abeysirigunawardena, C. S. Chow, pH-Dependent structural changes of helix 69 from *Escherichia coli* 23S ribosomal RNA. *RNA* **2008,** *14* (4), 782.

110. J. P. Desaulniers, Y. C. Chang, R. Aduri, S. C. Abeysirigunawardena, J. SantaLucia, Jr., C. S. Chow, Pseudouridines in rRNA helix 69 play a role in loop stacking interactions. *Org. Biomol. Chem.* **2008,** *6* (21), 3892.

111. G. Taubes, The bacteria fight back. *Science* **2008,** *321* (5887), 356.

112. H. C. Neu, The crisis in antibiotic resistance. *Science* **1992,** *257* (5073), 1064.

113. A. Ben-Shem, L. Jenner, G. Yusupova, M. Yusupov, Crystal structure of the eukaryotic ribosome. *Science* **2010,** *330* (6008), 1203.

114. M. Dryden, K. Hand, P. Davey, Antibiotics for community-acquired pneumonia. *J. Antimicrob. Chemother.* **2009,** *64* (6), 1123.

115. I. Chopra, Chemotherapy of mycobacterial infections: molecular action of established drugs and investigational agents. *Expert. Opin. Investig. Drugs* **1998,** *7* (2), 253.

116. T. Hermann, Drugs targeting the ribosome. *Curr. Opin. Struct. Biol.* **2005,** *15* (3), 355.

117. J. Poehlsgaard, S. Douthwaite, The bacterial ribosome as a target for antibiotics. *Nat. Rev. Microbiol.* **2005,** *3* (11), 870.

118. R. Berisio, F. Schluenzen, J. Harms, A. Bashan, T. Auerbach, D. Baram, A. Yonath, Structural insight into the role of the ribosomal tunnel in cellular regulation. *Nat. Struct. Biol.* **2003,** *10* (5), 366.

119. R. Berisio, J. Harms, F. Schluenzen, R. Zarivach, H. A. Hansen, P. Fucini, A. Yonath, Structural insight into the antibiotic action of telithromycin against resistant mutants. *J. Bacteriol.* **2003,** *185* (14), 4276.

120. F. Schlunzen, J. M. Harms, F. Franceschi, H. A. Hansen, H. Bartels, R. Zarivach, A. Yonath, Structural basis for the antibiotic activity of ketolides and azalides. *Structure* **2003,** *11* (3), 329.

121. J. L. Hansen, J. A. Ippolito, N. Ban, P. Nissen, P. B. Moore, T. A. Steitz, The structures of four macrolide antibiotics bound to the large ribosomal subunit. *Mol. Cell.* **2002,** *10* (1), 117.

122. F. Schlunzen, R. Zarivach, J. Harms, A. Bashan, A. Tocilj, R. Albrecht, A. Yonath, F. Franceschi, Structural basis for the interaction of antibiotics with the peptidyl transferase centre in *eubacteria*. *Nature* **2001,** *413* (6858), 814.

123. T. Tenson, M. Lovmar, M. Ehrenberg, The mechanism of action of macrolides, lincosamides and streptogramin B reveals the nascent peptide exit path in the ribosome. *J. Mol. Biol.* **2003,** *330* (5), 1005.

124. J. R. Menninger, D. P. Otto, Erythromycin, carbomycin, and spiramycin inhibit protein synthesis by stimulating the dissociation of peptidyl-tRNA from ribosomes. *Antimicrob. Agents Chemother.* **1982,** *21* (5), 811.

125. T. Otaka, A. Kaji, Release of (oligo) peptidyl-tRNA from ribosomes by erythromycin A. *Proc. Natl. Acad. Sci. U.S.A.* **1975,** *72* (7), 2649.

126. T. Tenson, J. V. Herrera, P. Kloss, G. Guarneros, A. S. Mankin, Inhibition of translation and cell growth by minigene expression. *J. Bacteriol.* **1999,** *181* (5), 1617.

127. V. Heurgue-Hamard, L. Mora, G. Guarneros, R. H. Buckingham, The growth defect in *Escherichia coli* deficient in peptidyl-tRNA hydrolase is due to starvation for Lys-tRNA(Lys). *EMBO J.* **1996,** *15* (11), 2826.

128. V. Heurgue-Hamard, V. Dincbas, R. H. Buckingham, M. Ehrenberg, Origins of minigene-dependent growth inhibition in bacterial cells. *EMBO J.* **2000,** *19* (11), 2701.

129. J. Davies, L. Gorini, B. D. Davis, Misreading of RNA codewords induced by aminoglycoside antibiotics. *Mol. Pharmacol.* **1965,** *1* (1), 93.

130. P. Edelmann, J. Gallant, Mistranslation in *E. coli*. *Cell* **1977,** *10* (1), 131.

131. G. Hirokawa, M. C. Kiel, A. Muto, M. Selmer, V. S. Raj, A. Liljas, K. Igarashi, H. Kaji, A. Kaji, Post-termination complex disassembly by ribosome recycling factor, a functional tRNA mimic. *EMBO J.* **2002,** *21* (9), 2272.

132. D. Moazed, H. F. Noller, Interaction of antibiotics with functional sites in 16S ribosomal RNA. *Nature* **1987,** *327* (6121), 389.

133. D. Fourmy, M. I. Recht, S. C. Blanchard, J. D. Puglisi, Structure of the A site of *Escherichia coli* 16S ribosomal RNA complexed with an aminoglycoside antibiotic. *Science* **1996,** *274* (5291), 1367.

134. S. Yoshizawa, D. Fourmy, J. D. Puglisi, Structural origins of gentamicin antibiotic action. *EMBO J.* **1998,** *17* (22), 6437.

135. A. P. Carter, W. M. Clemons, D. E. Brodersen, R. J. Morgan-Warren, B. T. Wimberly, V. Ramakrishnan, Functional insights from the structure of the 30S ribosomal subunit and its interactions with antibiotics. *Nature* **2000,** *407* (6802), 340.

136. Q. Vicens, E. Westhof, Crystal structure of paromomycin docked into the eubacterial ribosomal decoding A site. *Structure* **2001,** *9* (8), 647.

137. Q. Vicens, E. Westhof, Crystal structure of geneticin bound to a bacterial 16S ribosomal RNA A site oligonucleotide. *J. Mol. Biol.* **2003,** *326* (4), 1175.

138. M. A. Borovinskaya, R. D. Pai, W. Zhang, B. S. Schuwirth, J. M. Holton, G. Hirokawa, H. Kaji, A. Kaji, J. H. Cate, Structural basis for aminoglycoside inhibition of bacterial ribosome recycling. *Nat. Struct. Mol. Biol.* **2007,** *14* (8), 727.

139. G. Hirokawa, N. Demeshkina, N. Iwakura, H. Kaji, A. Kaji, The ribosome-recycling step: consensus or controversy? *Trends. Biochem. Sci.* **2006,** *31* (3), 143.

140. F. Peske, M. V. Rodnina, W. Wintermeyer, Sequence of steps in ribosome recycling as defined by kinetic analysis. *Mol. Cell.* **2005,** *18* (4), 403.

141. N. Gao, A. V. Zavialov, W. Li, J. Sengupta, M. Valle, R. P. Gursky, M. Ehrenberg, J. Frank, Mechanism for the disassembly of the posttermination complex inferred from cryo-EM studies. *Mol. Cell.* **2005,** *18* (6), 663.

142. A. V. Zavialov, V. V. Hauryliuk, M. Ehrenberg, Splitting of the posttermination ribosome into subunits by the concerted action of RRF and EF-G. *Mol. Cell.* **2005,** *18* (6), 675.

143. R. E. Stanley, G. Blaha, R. L. Grodzicki, M. D. Strickler, T. A. Steitz, The structures of the anti-tuberculosis antibiotics viomycin and capreomycin bound to the 70S ribosome. *Nat. Struct. Mol. Biol.* **2010,** *17* (3), 289.

144. J. Modolell, Vazquez, The inhibition of ribosomal translocation by viomycin. *Eur. J. Biochem.* **1977,** *81* (3), 491.

145. F. Peske, A. Savelsbergh, V. I. Katunin, M. V. Rodnina, W. Wintermeyer, Conformational changes of the small ribosomal subunit during elongation factor G-dependent tRNA-mRNA translocation. *J. Mol. Biol.* **2004,** *343* (5), 1183.

146. P. C. Ryan, M. Lu, D. E. Draper, Recognition of the highly conserved GTPase center of 23 S ribosomal RNA by ribosomal protein L11 and the antibiotic thiostrepton. *J. Mol. Biol.* **1991,** *221* (4), 1257.

147. G. Rosendahl, S. Douthwaite, The antibiotics micrococcin and thiostrepton interact directly with 23S rRNA nucleotides 1067A and 1095A. *Nucleic Acids Res.* **1994,** *22* (3), 357.

148. Y. Xing, D. E. Draper, Cooperative interactions of RNA and thiostrepton antibiotic with two domains of ribosomal protein L11. *Biochemistry* **1996,** *35* (5), 1581.

149. M. V. Rodnina, A. Savelsbergh, N. B. Matassova, V. I. Katunin, Y. P. Semenkov, W. Wintermeyer, Thiostrepton inhibits the turnover but not the GTPase of elongation factor G on the ribosome. *Proc. Natl. Acad. Sci. U.S.A.* **1999,** *96* (17), 9586.

150. L. Brandi, S. Marzi, A. Fabbretti, C. Fleischer, W. E. Hill, C. O. Gualerzi, J. Stephen Lodmell, The translation initiation functions of IF2: targets for thiostrepton inhibition. *J. Mol. Biol.* **2004,** *335* (4), 881.

151. D. M. Cameron, J. Thompson, P. E. March, A. E. Dahlberg, Initiation factor IF2, thiostrepton and micrococcin prevent the binding of elongation factor G to the *Escherichia coli* ribosome. *J. Mol. Biol.* **2002,** *319* (1), 27.

152. Y. G. Gao, M. Selmer, C. M. Dunham, A. Weixlbaumer, A. C. Kelley, V. Ramakrishnan, The structure of the ribosome with elongation factor G trapped in the posttranslocational state. *Science* **2009,** *326* (5953), 694.

153. J. W. Bodley, F. J. Zieve, L. Lin, Studies on translocation. IV. The hydrolysis of a single round of guanosine triphosphate in the presence of fusidic acid. *J. Biol. Chem.* **1970,** *245* (21), 5662.

154. K. Lee, S. Varma, J. SantaLucia, Jr., P. R. Cunningham, In vivo determination of RNA structure-function relationships: analysis of the 790 loop in ribosomal RNA. *J. Mol. Biol.* **1997,** *269* (5), 732.

155. F. C. Tenover, Mechanisms of antimicrobial resistance in bacteria. *Am. J. Infect. Control* **2006,** *34* (5 Suppl 1), S3.

156. K. Bush, Antibacterial drug discovery in the 21st century. *Clin. Microbiol. Infect.* **2004,** *10 Suppl 4*, 10.

157. E. V. Koonin, K. S. Makarova, L. Aravind, Horizontal gene transfer in prokaryotes: quantification and classification. *Annu. Rev. Microbiol.* **2001,** *55*, 709.

158. C. Walsh, Molecular mechanisms that confer antibacterial drug resistance. *Nature* **2000,** *406* (6797), 775.

159. I. T. Paulsen, M. H. Brown, R. A. Skurray, Proton-dependent multidrug efflux systems. *Microbiol. Rev.* **1996,** *60* (4), 575.

160. S. B. Levy, Active efflux mechanisms for antimicrobial resistance. *Antimicrob. Agents Chemother.* **1992,** *36* (4), 695.

161. A. Philippon, R. Labia, G. Jacoby, Extended-spectrum beta-lactamases. *Antimicrob. Agents Chemother.* **1989,** *33* (8), 1131.

162. K. J. Shaw, P. N. Rather, R. S. Hare, G. H. Miller, Molecular genetics of aminoglycoside resistance genes and familial relationships of the aminoglycoside-modifying enzymes. *Microbiol. Rev.* **1993,** *57* (1), 138.

163. B. Llano-Sotelo, E. F. Azucena, Jr., L. P. Kotra, S. Mobashery, C. S. Chow, Aminoglycosides modified by resistance enzymes display diminished binding to the bacterial ribosomal aminoacyl-tRNA site. *Chem. Biol.* **2002,** *9* (4), 455.

164. B. Weisblum, Erythromycin resistance by ribosome modification. *Antimicrob. Agents Chemother.* **1995,** *39* (3), 577.

165. A. A. Beauclerk, E. Cundliffe, Sites of action of two ribosomal RNA methylases responsible for resistance to aminoglycosides. *J. Mol. Biol.* **1987,** *193* (4), 661.

166. J. Thompson, P. A. Skeggs, E. Cundliffe, Methylation of 16S ribosomal RNA and resistance to the aminoglycoside antibiotics gentamicin and kanamycin determined by DNA from the gentamicin-producer, *Micromonospora purpurea*. *Mol. Gen. Genet.* **1985,** *201* (2), 168.

167. P. Sander, T. Prammananan, E. C. Bottger, Introducing mutations into a chromosomal rRNA gene using a genetically modified eubacterial host with a single rRNA operon. *Mol. Microbiol.* **1996,** *22* (5), 841.

168. M. I. Recht, J. D. Puglisi, Aminoglycoside resistance with homogeneous and heterogeneous populations of antibiotic-resistant ribosomes. *Antimicrob. Agents Chemother.* **2001,** *45* (9), 2414.

169. M. I. Recht, S. Douthwaite, K. D. Dahlquist, J. D. Puglisi, Effect of mutations in the A site of 16 S rRNA on aminoglycoside antibiotic-ribosome interaction. *J. Mol. Biol.* **1999,** *286* (1), 33.

170. T. Prammananan, P. Sander, B. A. Brown, K. Frischkorn, G. O. Onyi, Y. Zhang, E. C. Bottger, R. J. Wallace, Jr., A single 16S ribosomal RNA substitution is responsible for resistance to amikacin and other 2-deoxystreptamine aminoglycosides in M*ycobacterium abscessus* and *Mycobacterium chelonae*. *J. Infect. Dis.* **1998,** *177* (6), 1573.

171. M. I. Recht, S. Douthwaite, J. D. Puglisi, Basis for prokaryotic specificity of action of aminoglycoside antibiotics. *EMBO J.* **1999,** *18* (11), 3133.

172. P. Pfister, S. Hobbie, Q. Vicens, E. C. Bottger, E. Westhof, The molecular basis for A-site mutations conferring aminoglycoside resistance: relationship between ribosomal susceptibility and X-ray crystal structures. *Chembiochem* **2003,** *4* (10), 1078.

173. A. Bakin, J. Ofengand, Four newly located pseudouridylate residues in *Escherichia coli* 23S ribosomal RNA are all at the peptidyltransferase center: analysis by the application of a new sequencing technique. *Biochemistry* **1993,** *32* (37), 9754.

174. U. Maiväli, J. Remme, Definition of bases in 23S rRNA essential for ribosomal subunit association. *RNA* **2004,** *10* (4), 600.

175. N. Hirabayashi, N. S. Sato, T. Suzuki, Conserved loop sequence of helix 69 in *Escherichia coli* 23 S rRNA is involved in A-site tRNA binding and translational fidelity. *J. Biol. Chem.* **2006,** *281* (25), 17203.

176. D. N. Wilson, F. Schluenzen, J. M. Harms, T. Yoshida, T. Ohkubo, R. Albrecht, J. Buerger, Y. Kobayashi, P. Fucini, X-ray crystallography study on ribosome recycling: the mechanism of binding and action of RRF on the 50S ribosomal subunit. *EMBO J.* **2005,** *24* (2), 251.

177. A. Bashan, I. Agmon, R. Zarivach, F. Schluenzen, J. Harms, R. Berisio, H. Bartels, F. Franceschi, T. Auerbach, H. A. Hansen, E. Kossoy, M. Kessler, A. Yonath, Structural basis of the ribosomal machinery for peptide bond formation, translocation, and nascent chain progression. *Mol. Cell.* **2003,** *11* (1), 91.

178. W. Zhang, J. A. Dunkle, J. H. Cate, Structures of the ribosome in intermediate states of ratcheting. *Science* **2009,** *325* (5943), 1014.

179. G. W. Muth, L. Ortoleva-Donnelly, S. A. Strobel, A single adenosine with a neutral pKa in the ribosomal peptidyl transferase center. *Science* **2000,** *289* (5481), 947.

180. M. A. Bayfield, A. E. Dahlberg, U. Schulmeister, S. Dorner, A. Barta, A conformational change in the ribosomal peptidyl transferase center upon active/inactive transition. *Proc. Natl. Acad. Sci. U.S.A.* **2001,** *98* (18), 10096.

181. S. C. Abeysirigunawardena, Biophysical investigations of structural and stability changes in helix 69 of *Escherichia Coli* 23S RRNA. *Wayne State University: Detroit, MI* **2008**.

182. A. Liiv, D. Karitkina, U. Maiväli, J. Remme, Analysis of the function of *E. coli* 23S rRNA helix-loop 69 by mutagenesis. *BMC Mol. Biol.* **2005,** *6*, 18.

183. R. Ero, L. Peil, A. Liiv, J. Remme, Identification of pseudouridine methyltransferase in *Escherichia coli*. *RNA* **2008,** *14* (10), 2223.

184. Y. Sakakibara, C. S. Chow, Probing conformational states of modified helix 69 in 50S ribosomes. *J. Am. Chem. Soc.* **2011,** *133* (22), 8396.

185. G. Blaha, U. Stelzl, C. M. Spahn, R. K. Agrawal, J. Frank, K. H. Nierhaus, Preparation of functional ribosomal complexes and effect of buffer conditions on tRNA positions observed by cryoelectron microscopy. *Methods Enzymol.* **2000,** *317*, 292.

186. P. Spitnik-Elson, A. Atsmon, Detachment of ribosomal proteins by salt. I. Effect of conditions on the amount of protein detached. *J. Mol. Biol.* **1969,** *45* (1), 113.

187. R. Miskin, A. Zamir, D. Elson, Inactivation and reactivation of ribosomal subunits: the peptidyl transferase activity of the 50 s subunit of *Escherihia coli*. *J. Mol. Biol.* **1970,** *54* (2), 355.

188. I. Behm-Ansmant, M. Helm, Y. Motorin, Use of specific chemical reagents for detection of modified nucleotides in RNA. *J. Nucleic. Acids* **2011,** *2011*, 408053.

189. D. A. Peattie, W. Gilbert, Chemical probes for higher-order structure in RNA. *Proc. Natl. Acad. Sci. U.S.A.* **1980,** *77* (8), 4679.

190. D. A. Peattie, Direct chemical method for sequencing RNA. *Proc. Natl. Acad. Sci. U.S.A.* **1979,** *76* (4), 1760.

191. D. Moazed, H. F. Noller, Transfer RNA shields specific nucleotides in 16S ribosomal RNA from attack by chemical probes. *Cell* **1986,** *47* (6), 985.

192. D. Moazed, H. F. Noller, Interaction of tRNA with 23S rRNA in the ribosomal A, P, and E sites. *Cell* **1989,** *57* (4), 585.

193. Y. Motorin, S. Muller, I. Behm-Ansmant, C. Branlant, Identification of modified residues in RNAs by reverse transcription-based methods. *Methods Enzymol.* **2007,** *425*, 21.

194. N. W. Ho, P. T. Gilham, Reaction of pseudouridine and inosine with *N*-cyclohexyl-*N*'-beta-(4-methylmorpholinium)ethylcarbodiimide. *Biochemistry* **1971,** *10* (20), 3651.

195. E. E. Regulski, R. R. Breaker, In-line probing analysis of riboswitches. *Methods Mol. Biol.* **2008,** *419*, 53.

196. E. J. Merino, K. A. Wilkinson, J. L. Coughlan, K. M. Weeks, RNA structure analysis at single nucleotide resolution by selective 2'-hydroxyl acylation and primer extension (SHAPE). *J. Am. Chem. Soc.* **2005,** *127* (12), 4223.

197. L. Cochella, J. L. Brunelle, R. Green, Mutational analysis reveals two independent molecular requirements during transfer RNA selection on the ribosome. *Nat. Struct. Mol. Biol.* **2007,** *14* (1), 30.

198. P. Khaitovich, A. S. Mankin, R. Green, L. Lancaster, H. F. Noller, Characterization of functionally active subribosomal particles from *Thermus aquaticus*. *Proc. Natl. Acad. Sci. U.S.A.* **1999,** *96* (1), 85.

199. P. Nissen, J. Hansen, N. Ban, P. B. Moore, T. A. Steitz, The structural basis of ribosome activity in peptide bond synthesis. *Science* **2000,** *289* (5481), 920.

200. T. M. Schmeing, P. B. Moore, T. A. Steitz, Structures of deacylated tRNA mimics bound to the E site of the large ribosomal subunit. *RNA* **2003,** *9* (11), 1345.

201. A. E. Scheunemann, W. D. Graham, F. A. Vendeix, P. F. Agris, Binding of aminoglycoside antibiotics to helix 69 of 23S rRNA. *Nucleic Acids Res.* **2010,** *38* (9), 3094.

202. C. Merryman, D. Moazed, G. Daubresse, H. F. Noller, Nucleotides in 23S rRNA protected by the association of 30S and 50S ribosomal subunits. *J. Mol. Biol.* **1999,** *285* (1), 107.

203. L. Jenner, N. Demeshkina, G. Yusupova, M. Yusupov, Structural rearrangements of the ribosome at the tRNA proofreading step. *Nat. Struct. Mol. Biol.* **2010,** *17* (9), 1072.

204. H. Jin, A. C. Kelley, V. Ramakrishnan, Crystal structure of the hybrid state of ribosome in complex with the guanosine triphosphatase release factor 3. *Proc. Natl. Acad. Sci. U.S.A.* **2011,** *108* (38), 15798.

205. M. Selmer, C. M. Dunham, F. t. Murphy, A. Weixlbaumer, S. Petry, A. C. Kelley, J. R. Weir, V. Ramakrishnan, Structure of the 70S ribosome complexed with mRNA and tRNA. *Science* **2006,** *313* (5795), 1935.

206. Y. Sakakibara, C. S. Chow, The Role of Pseudouridine in Structural Rearrangements of Helix 69 During Ribosome Assembly. *ACS Chem. Biol.* **2012**.

207. C. R. Guest, R. A. Hochstrasser, L. C. Sowers, D. P. Millar, Dynamics of mismatched base pairs in DNA. *Biochemistry* **1991,** *30* (13), 3271.

208. D. C. Ward, E. Reich, L. Stryer, Fluorescence studies of nucleotides and polynucleotides. I. Formycin, 2-aminopurine riboside, 2,6-diaminopurine riboside, and their derivatives. *J. Biol. Chem.* **1969,** *244* (5), 1228.

209. M. Meroueh, P. J. Grohar, J. Qiu, J. SantaLucia, Jr., S. A. Scaringe, C. S. Chow, Unique structural and stabilizing roles for the individual pseudouridine residues in the 1920 region of *Escherichia coli* 23S rRNA. *Nucleic Acids Res.* **2000,** *28* (10), 2075.

210. P. N. Asare-Okai, C. S. Chow, A modified fluorescent intercalator displacement assay for RNA ligand discovery. *Anal. Biochem.* **2011,** *408* (2), 269.

211. M. B. Feldman, D. S. Terry, R. B. Altman, S. C. Blanchard, Aminoglycoside activity observed on single pre-translocation ribosome complexes. *Nat. Chem. Biol.* **2010,** *6* (1), 54.

212. N. W. Luedtke, P. Carmichael, Y. Tor, Cellular uptake of aminoglycosides, guanidinoglycosides, and poly-arginine. *J. Am. Chem. Soc.* **2003,** *125* (41), 12374.

213. T. J. Baker, N. W. Luedtke, Y. Tor, M. Goodman, Synthesis and anti-HIV activity of guanidinoglycosides. *J. Org. Chem.* **2000,** *65* (26), 9054.

214. A. Pushechnikov, M. M. Lee, J. L. Childs-Disney, K. Sobczak, J. M. French, C. A. Thornton, M. D. Disney, Rational design of ligands targeting triplet repeating transcripts that cause RNA dominant disease: application to myotonic muscular dystrophy type 1 and spinocerebellar ataxia type 3. *J. Am. Chem. Soc.* **2009,** *131* (28), 9767.

215. C. H. Wong, M. Hendrix, E. S. Priestley, W. A. Greenberg, Specificity of aminoglycoside antibiotics for the A-site of the decoding region of ribosomal RNA. *Chem. Biol.* **1998,** *5* (7), 397.

216. Y. Wang, K. Hamasaki, R. R. Rando, Specificity of aminoglycoside binding to RNA constructs derived from the 16S rRNA decoding region and the HIV-RRE activator region. *Biochemistry* **1997,** *36* (4), 768.

217. S. Shoji, S. E. Walker, K. Fredrick, Reverse translocation of tRNA in the ribosome. *Mol. Cell.* **2006,** *24* (6), 931.

218. M. Kaul, C. M. Barbieri, D. S. Pilch, Aminoglycoside-induced reduction in nucleotide mobility at the ribosomal RNA A-site as a potentially key determinant of antibacterial activity. *J. Am. Chem. Soc.* **2006,** *128* (4), 1261.

219. S. M. Dibrov, J. Parsons, T. Hermann, A model for the study of ligand binding to the ribosomal RNA helix h44. *Nucleic Acids Res.* **2010,** *38* (13), 4458.

220. J. S. Feinberg, S. Joseph, Identification of molecular interactions between P-site tRNA and the ribosome essential for translocation. *Proc. Natl. Acad. Sci. U.S.A.* **2001,** *98* (20), 11120.

221. N. Nevskaya, S. Tishchenko, S. Volchkov, V. Kljashtorny, E. Nikonova, O. Nikonov, A. Nikulin, C. Kohrer, W. Piendl, R. Zimmermann, P. Stockley, M. Garber, S. Nikonov, New insights into the interaction of ribosomal protein L1 with RNA. *J. Mol. Biol.* **2006,** *355* (4), 747.

222. M. Osswald, B. Greuer, R. Brimacombe, Localization of a series of RNA-protein cross-link sites in the 23S and 5S ribosomal RNA from *Escherichia coli*, induced by treatment of 50S subunits with three different bifunctional reagents. *Nucleic Acids Res.* **1990,** *18* (23), 6755.

223. M. Osswald, T. Doring, R. Brimacombe, The ribosomal neighbourhood of the central fold of tRNA: cross-links from position 47 of tRNA located at the A, P or E site. *Nucleic Acids Res.* **1995,** *23* (22), 4635.

224. W. Li, J. Frank, Transfer RNA in the hybrid P/E state: correlating molecular dynamics simulations with cryo-EM data. *Proc. Natl. Acad. Sci. U.S.A.* **2007,** *104* (42), 16540.

225. L. G. Trabuco, E. Schreiner, J. Eargle, P. Cornish, T. Ha, Z. Luthey-Schulten, K. Schulten, The role of L1 stalk-tRNA interaction in the ribosome elongation cycle. *J. Mol. Biol.* **2010,** *402* (4), 741.

226. S. M. Studer, J. S. Feinberg, S. Joseph, Rapid kinetic analysis of EF-G-dependent mRNA translocation in the ribosome. *J. Mol. Biol.* **2003,** *327* (2), 369.

227. S. Dorner, J. L. Brunelle, D. Sharma, R. Green, The hybrid state of tRNA binding is an authentic translation elongation intermediate. *Nat. Struct. Mol. Biol.* **2006,** *13* (3), 234.

228. J. Fei, A. C. Richard, J. E. Bronson, R. L. Gonzalez, Jr., Transfer RNA-mediated regulation of ribosome dynamics during protein synthesis. *Nat. Struct. Mol. Biol.* **2011,** *18* (9), 1043.

229. A. Liiv, M. O'Connor, Mutations in the intersubunit bridge regions of 23 S rRNA. *J. Biol. Chem.* **2006,** *281* (40), 29850.

230. T. Komoda, N. S. Sato, S. S. Phelps, N. Namba, S. Joseph, T. Suzuki, The A-site finger in 23 S rRNA acts as a functional attenuator for translocation. *J. Biol. Chem.* **2006,** *281* (43), 32303.

231. T. Alatossava, H. Jutte, A. Kuhn, E. Kellenberger, Manipulation of intracellular magnesium content in polymyxin B nonapeptide-sensitized *Escherichia coli* by ionophore A23187. *J. Bacteriol.* **1985,** *162* (1), 413.

ABSTRACT

EXPLORING CONFORMATIONAL VARIABILITY OF AN RNA DOMAIN IN THE RIBOSOME: FROM STRUCTURE AND FUNCTION TO POTENTIAL ANTIBIOTIC TARGETING

by

YOGO SAKAKIBARA

August 2012

Advisor: Dr. Christine S. Chow

Major: Chemistry

Degree: Doctor of Philosophy

Crystal structures predicted that helix 69 (H69) of the large subunit (50S) could form variable conformational states during ribosome translation, though it is technically difficult to take a snap shot of each conformational state by X-ray crystallography or cryo-EM. Moreover, the solution structure of H69 was unknown. Therefore, a comprehensive analysis was necessary to detect the multiple conformational states in solution and correlate such structures with ribosome function. In the first project, the H69 conformational dynamics in 50S subunits was analyzed in solution by using a chemical probing methodology. Conformational changes of specific base positions were found upon changing pH, Mg^{2+} concentration, and temperature. Importantly, all of the sites that undergo change in conformation or orientation are thought to be involved in normal ribosome function according to genetic studies. Moreover, the influence of a naturally occurring base modification, namely pseudouridine, on H69 conformation was examined by using 50S subunits from a mutant *E. coli* strain lacking the pseudouridine synthase specific for H69. In pseudouridine-deficient 50S subunits, reduced conformational dynamics of H69 relative to wild-type was found, suggesting that the presence of pseudouridines gives conformational flexibility to functionally important sites. This result was further supported by the observation that H69 undergoes dynamic structural rearrangements upon subunit association, and such rearrangements appear to be controlled in part by an organized H69 structure which is modulated

by Ψ modifications of H69. Such structural rearrangements of H69 upon subunit interaction were not predicted previously by high-resolution crystal structures. Chemical probing also showed increased local nucleoside flexibility at a specific position, A1913, with increasing Mg^{2+} concentration, suggesting a molecular basis for how translation fidelity is reduced under high Mg^{2+} conditions.

Besides conformational studies of H69 in the ribosome, the suitability of H69 as a novel antibiotic target was explored, taken advantage of its important structural and functional roles. H69 was found to be bound by aminoglycoside antibiotics and peptide; however, studies on drug-H69 interactions has only recently been launched and little information is available to date. From the standpoint of the outbreak of advanced antibiotic-resistant strains, it is important to elucidate the mechanism and function of antibiotic interactions with H69 and develop unique tools for drug discovery in order to combat such resistant strains. For such purposes, we developed a fluorescent probe of H69 RNA (2AP-H69) to monitor H69 loop conformational states. By using 2AP-H69, neomycin, one major type of aminoglycoside antibiotic was found to bind H69 and induce a H69 loop conformational change. In contrast, closely related aminoglycoside did not show such binding activity, even though they have a similar chemical structures to neomycin. Further analysis employing chemical footprinting of 70S and 50S ribosomes revealed that these aminoglycoside antibiotics interact with the H69 stem of 70S ribosomes, but not to 50S subunits in solution, indicating the ability of aminoglycosides to recognize a specific H69 component. Besides aminoglycoside-H69 interactions, chemical probing studies of the H69 loop revealed that neomycin induces a different loop conformational state compared to other aminoglycosides. This different binding activity of neomycin is consistent with the 2AP-H69 data and previously reported results. Thus, these data clearly indicate the importance of a detailed evaluation of the underlying principles of antibiotic activity such as conformational dynamics. At the same time, these data showed the potential of H69 as a unique antibiotic target site.

AUTOBIOGRAPHICAL STATEMENT

YOGO SAKAKIBARA

ADVISOR: Prof. Christine S. Chow

DISSERTATION TITLE:

Exploring conformational variability of an RNA domain in the ribosome: from structure and function to potential antibiotic targeting.

EDUCATION:

- Ph.D.; Biochemistry, 2012, Wayne State University, Detroit, Michigan, USA
- M.S.; Biochemistry, 2006, Kyoto University, Kyoto, Japan
- B.S.; Applied Chemistry, 2004, Waseda University, Tokyo, Japan

LIST OF PUBLICATIONS:

1. **Sakakibara, Y.**; Mohamed, A.; Chow, C.S., Potential antibiotics binding on helix 68 of 23S rRNA. (Manuscript in preparation)

2. **Sakakibara, Y.**; Chow, C.S., Dual fluorescent probing of H69 RNA for simultaneous monitoring of small molecule binding and induced conformational change. (Manuscript in preparation)

3. **Sakakibara, Y.**; Chow, C.S., Interaction of aminoglycosides with modified H69 structure in 70S ribosomes induces H69 conformational change. (Manuscript in preparation)

4. **Sakakibara, Y.**; Abeysirigunawardena, S.C.; Duc A.C.D.; Chow, C.S., A tool for monitoring small molecule binding to helix 69 RNA. (Manuscript in preparation)

5. **Sakakibara, Y.**; Chow, C.S., Role of pseudouridine in structural rearrangements of helix 69 during bacterial ribosome assembly. *ACS Chem Biol* **2012**, in press.

6. **Sakakibara, Y.**; Chow, C.S., Probing conformational states of modified helix 69 in 50S ribosomes. *J Am Chem Soc* **2011**, 133 (22), 8396-9

7. Shinohara, K.; Bando, T.; Sasaki, S.; **Sakakibara, Y.**; Minoshima, M.; Sugiyama, H., Antitumor activity of sequence-specific alkylating agents: pyrolle-imidazole CBI conjugates with indole linker. *Cancer Sci* **2006**, *97* (3), 219-25.